Université d'Ottawa • University of Ottawa

ISOTOPIC COMPOSITION OF SILURIAN BRACHIOPODS: IMPLICATIONS FOR COEVAL SEAWATER

by

Karem Azmy

A thesis submitted to the School of Graduate Studies and Research in partial fulfilment of the requirements for the Degree of Ph.D. in Earth Sciences

OTTAWA-CARLETON GEOSCIENCE CENTRE

DEPARTMENT OF GEOLOGY

UNIVERSITY OF OTTAWA

OTTAWA, CANADA, 1996

ABSTRACT

Two hundred and thirty six calcitic brachiopod shells, covering the entire Silurian Period (~ 30 Ma), were collected at high temporal resolution from stratotype sections on Anticosti Island (Canada), in Wales (UK), in the Oslo region (Norway), on Gotland (Sweden), and in Podolia (Ukraine), Estonia, Latvia and Lithuania. Data from petrography, scanning electron microscopy (SEM), cathodoluminescence, isotopes and trace elements all confirmed excellent preservation in most shells, thus ensuring retention of primary isotope signals. The only exceptions were samples from the Oslo region. The $\delta^{18}O$ and $\delta^{13}C$ values for the well preserved samples range from -3 to -6.5 ‰ and from -1 to 7.5 ‰ (PDB), respectively. In terms of temporal trends, oxygen- and carbon-isotopes vary in parallel, with an overall decrease with decreasing age of ~ 1 ‰, through the Silurian. Superimposed on these general trends are short-term variations that are negatively correlated with sea-level changes. Three successive positive $\delta^{18}O$ shifts in early Aeronian, latest Aeronian and early Wenlock correlate with sea-level lowstands and with glacial diamictite deposits in the Amazon Basin and in Africa. The $^{87}Sr/^{86}Sr$ values range from 0.707930 ± 0.000011 to 0.708792 ± 0.000017, increasing with decreasing age. This may indicate increasing riverine flux of radiogenic Sr into the ocean from weathering of continental sialic rocks due to progressive global warming. The Sr-isotope curve shows distinct inflexion points in the earliest Wenlock and in mid-Přídolí. These can be used to correlate the Llandovery/Wenlock boundary in the U.K., on Gotland and in Lithuania and for the Kaugatuma/Ohesaare boundary in the Baltic states and Podolia. Partial linear regressions for Sr-isotope data form a pattern that climbs stepwise with decreasing age, with local drops around the Llandovery/Wenlock boundary and in the latest Ludlow. The slopes of the partial regression lines can be used for reliable age estimates with a resolution of about ±2 biozones (~ 1.5 to 2 Ma).

ACKNOWLEDGEMENT

The author wishes to thank Dr. J. Veizer for his supervision at all stages of study, financial support and critical reading and editing of the manuscript; Drs. M. G. Bassett, P. Copper, D. Kaljo, P. Musteikis and M. Rubel for providing and identifying samples; and Dr. V. Gritsenko for assistance in the field. Special thanks are extended to Dr. B. Cousens for his help with Sr-isotope analysis, Mr. G. Mrazek for his help with thin section preparation, Mr. G. St-Jean for his help with oxygen - and carbon-isotope analyses, Mr. J. Loop for help with trace element analysis, and Mrs. Hélène De Gouffe and Mrs. Sylvie Downing for their help in the administrative work. This project was financed by the Natural Sciences and Engineering Research Council of Canada and by ESSO Resources Canada Limited (Imperial Oil).

To my parents **Karam Azmy** and **Elaine Halaka**, and to **Mari Mina** and **Ava Kiryllos**.

TABLE OF CONTENTS

APPENDICES

LIST OF FIGURES

Figure **Page**

Figure **Page**

LIST OF TABLES

INTRODUCTION

Studies of the isotopic composition of Paleozoic seawater have been relying more and more on brachiopod shells (e.g. Popp et al., 1986; Veizer et al., 1986; Wadleigh and Veizer, 1992; Grossman, 1994; Veizer et al., in press) because (1) brachiopods are abundant in marine successions, (2) they precipitate shells composed of low-Mg calcite in apparent isotopic equilibrium with the ambient seawater, and (3) the low-Mg calcite shells tend to resist diagenesis, thus retaining primary isotopic signals. Furthermore, the available petrographic and chemical techniques, such as transmitted light microscopy, cathodoluminescence, SEM and trace element analysis make it possible to evaluate of diagenetic alteration of the shell ultrastructure. (e.g. Wadleigh and Veizer, 1992; Grossman, 1994).

Oxygen and carbon isotope studies may serve as tools for quantitative evaluation of global climatic variations. Oxygen isotopic composition reflects the changes in temperature and salinity of ambient water, whereas the isotopes of carbon reflect changes in organic productivity, oceanic circulation, and perturbations to the global carbon budget.

Previous studies of Paleozoic brachiopods included some Silurian samples, but the coverage was very incomplete. Paleozoic brachiopods are generally depleted in ^{18}O, compared with their Recent counterparts. The importance of this observation is presently hotly debated (cf. Land, 1995; Veizer, 1995) and possible alternative interpretations will be one of the major issues of the present thesis. The $^{87}Sr/^{86}Sr$ ratio of seawater is a function of the balance between inputs of Sr from continental weathering of sialic rocks, from leaching of young volcanic rocks, and from dissolution of carbonates. The long residence time of Sr in the oceans, compared with the short mixing time of ocean water, results in the Sr isotopic composition of seawater being uniform at any given time. When organisms precipitate their shells, they incorporate the $^{87}Sr/^{86}Sr$ ratio of seawater without any

isotopic fractionation. The changing dynamics of Sr sources and sinks is reflected in the isotopic composition of well preserved calcitic and phosphatic shells (e.g. Burke et al., 1982; Bertram et al., 1992). The deciphered temporal oscillations in Sr-isotopic composition of seawater may therefore reflect changing environmental phenomena, such as paleoclimates or intensity of volcanic activity (e.g. Elderfield, 1986; Farrel et al., 1995). Such temporal isotopic trends can also be used as a correlation tool.

This project will discuss variations in the isotopic composition of Silurian brachiopods, hence seawater, sampled at a high resolution (<1 Ma) in stratotype sections. The main objectives of the study are: (1) to construct detailed isotope curves for the entire Silurian Period, (2) to interpret these trends in terms of paleoclimatic and paleoceanographic causes that may have dominated the Silurian budget of Sr, O and C, and (3) to refine the Sr-isotope curve to such a degree that it may be utilized for high resolution isotope stratigraphy and for correlation of sequences from different depositional settings.

CHAPTER I

THE SILURIAN PALEOENVIRONMENT

1.1. PALEOGEOGRAPHY

The first reference to the Silurian System of rocks, named after the Welsh Border tribe, the Silures, was by Murchison (1835). Originally, it included rocks of what are now recognized as the Cambrian and Ordovician systems but later, in 1960, the Silurian was officially and internationally adopted in its present day restricted sense (Harland et al., 1990). The Silurian Period is subdivided, as discussed in detail later in this text, into two subperiods, the Early Silurian (Llandovery and Wenlock) and the Late Silurian (Ludlow and Přídolí).

The paleogeography of the Silurian was characterized by six main paleocontinents, Gondwana, Laurentia, Baltica, Avalonia, Siberia and Kazakhstania (Fig. 1.1). It was dominated by the large Gondwana crustal plate that probably represented more than half of the world land area (Africa, South America, Australia, Antarctica, India and adjacent parts of Asia and Europe). As this plate drifted over the South Pole (South Africa or South America at that time), the area of what is now southern Europe moved to warmer lower paleolatitudes.

In general, subsequent to late Ordovician glaciation, the Silurian Period commenced with cool conditions and low faunal diversity followed by warmer climate with high faunal diversity and abundance. This global warming resulted in deposition of widespread equatorial evaporites during mid- and late Silurian times (Cocks and Scotese, 1991; Ziegler et al., 1977; 1979). Paleogeographic maps reconstructed from paleogeographic, paleomagnetic and lithofacies data (Scotese and McKerrow, 1990) show that in the Ordovician Period (Fig. 1.2), the Iapetus Ocean

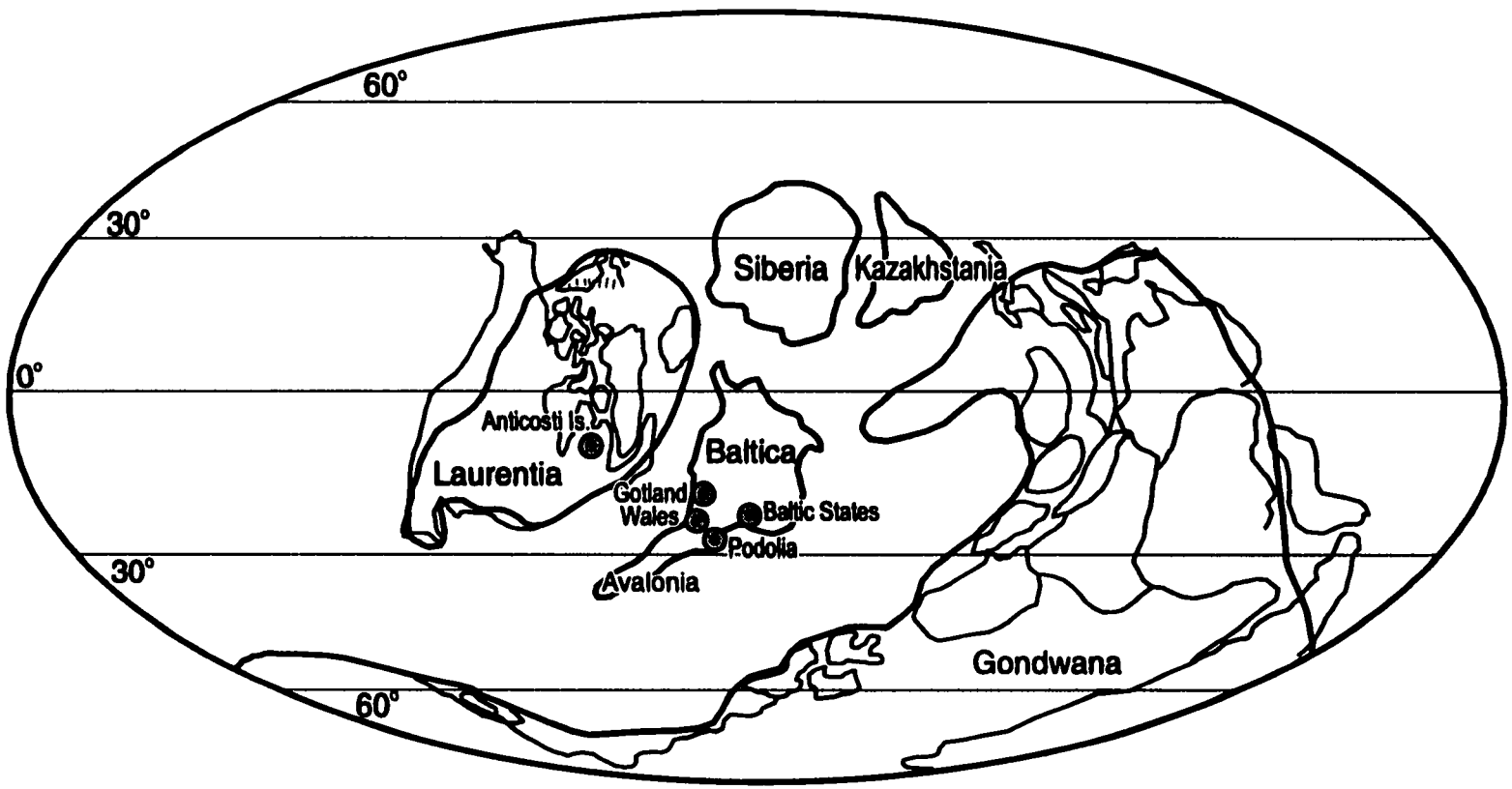

Fig. 1.1. Paleogeographic map of the world during early Silurian (Llandovery), showing relative positions of paleocontinents, and approximate locations of the studied sections (highlighted circles). Modified from Cocks and Scotese (1991).

was bounded by Laurentia to the north, Baltica to the south-east, western Gondwana to the south, and Siberia to the north-east. The Iapetus Ocean is suggested to have opened by about 600 Ma ago in the late Precambrian, possibly as a result of rifting of Baltica or Siberia from Laurentia. During the Ordovician, Avalonia separated from Gondwana, and Baltica moved northward, as did at an even faster rate Avalonia. The resulting collision of Avalonia with Baltica led to the closure of the Tornquist Sea (Fig. 1.1), probably in the Late Ordovician (Ashgill) (McKerrow et al., 1991).

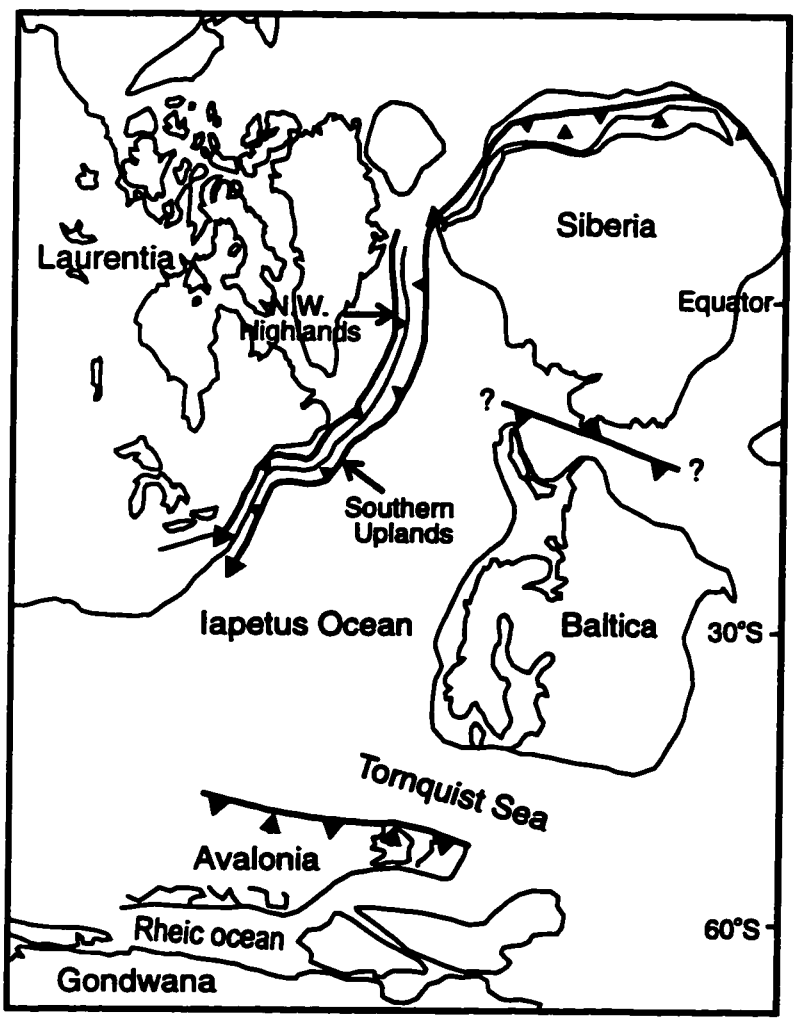

Fig. 1.2. Paleogeographic map of the world during latest Ordovician, showing relative positions and the direction of collisions of paleocontinents (after McKerrow et al., 1991).

By the end of the Llandovery, the distribution of the paleocontinental masses has changed. A subduction zone in north-eastern Greenland suggests a collision with an island arc or a continent. The absence of arc rocks in north Greenland implies that the collision was with a continent, likely Barentsia, that might have been separated from Greenland during late Ordovician or very early Silurian time (McKerrow, 1988). This accretion continued in the southern Uplands until the late Wenlock, with the trench-fill deposits derived from the Mongolian arc of north Siberia, as indicated by the coral *Ceriaster* in the Llandovery turbidites of south-eastern Scotland. This coral was previously known only from Tadzhikistan and China (Scrutton and McCurry, 1987).

The Iapetus Ocean might have commenced its closure by the late Llandovery, followed by three collisions on the eastern margin of Laurentia. These were the collision of Barentsia with north-east Greenland in the late Llandovery, of Baltica with Scotland in the late Wenlock or Ludlow (Scandian Orogeny), and of Avalonia with south-eastern Laurentia by the Early Devonian (Acadian Orogeny) (McKerrow et al., 1991).

1.1.1. Laurentia

During Silurian times, Laurentia was a large continental plate that included what is today north-west Ireland, Scotland, the upper nappes of Norway and western Sweden, Greenland and the bulk of Canada and United States. Florida at that time was part of Gondwana and eastern Newfoundland was part of Avalonia-Baltica. The Silurian sedimentary facies on this paleocontinent include warm water carbonate and evaporitic deposits of the southern tropics (Cocks and Scotese, 1991). Most of the continent was flooded by warm shallow seas (Berry and Boucot, 1970) which left deposits that thicken towards continental margins, such as on Anticosti

Island, Canada, where the thickness of the Llandovery succession reaches 1200 m. The macrofauna, mainly brachiopods, and microfauna, mainly ostracodes and conodonts, reflect tropical conditions of high diversity (Bergström, 1990).

1.1.2. Gondwana

Gondwana was the largest paleocontinent, and included present-day Florida, southern Europe, Turkey, Africa, the Arabian Peninsula, Iran, India, Madagascar, southern China, Tibet and the Shan Thai blocks, New Guinea, New Zealand, Australia and Antarctica. During the Llandovery and Wenlock, the seas covering north Africa and southern Europe were generally characterized by anoxic conditions, as indicated by the pelagic graptolite, bivalve and cephalopod faunal assemblages. The subsequent late Silurian deposits, on the other hand, contain mostly benthic shelly faunas (Berry and Boucot, 1973). During early Silurian times, the Gondwana plate started drifting across the South Pole, located at that time in north Africa. Towards the end of the Silurian and in the early Devonian, the South Pole was in what is now southern Brazil and, as a result, today's southern Europe moved steadily into warmer paleolatitudes. This movement can be traced by two phenomena. First, carbonates became increasingly dominant in the late Silurian of today's Bohemia (Ludlow and Přídolí) and the early Devonian (Lochkovian and Pragian) (Cocks and Scotese, 1991). Second, the eastern side of what is now South America consists of deposits of the Malvinokaffric Province containing *Clarkeia* and other less diverse communities (Isaacson et al., 1976), while the western side deposits contain more diverse assemblages (Laubacher et al., 1982). *Clarkeia* was also found in north-west Africa (Cocks, 1972). This increase in faunal diversity is attributed to the warmer lower paleolatitudes.

The sedimentary records from the Arabian Peninsula, China and Shan Thai block (Burma, Thailand and Malaysia) are not well documented, but they do indicate similar high to low latitude movement during the Silurian Period (Wang et al., 1987; McClure, 1988). No marine deposits of Silurian age have been documented in western Australia, but they are found in Tasmania, Victoria, New South Wales and Queensland, with fossils more abundant and rich in the Ludlow and Přídolí. New Zealand has *Conchidium*-bearing beds of the Llandovery while New Guinea has graptolite-bearing beds.

1.1.3. Baltica and Avalonia

The exact time of merging of these two paleocontinents is unknown and most probably the collision did not occur until earliest Silurian times. Baltica contains the stratotype of the Silurian (Llandovery, Wenlock, Ludlow and Přídolí) in Wales and in the Welsh Borderlands (Siveter et al., 1989), exposures of reference sections on Gotland (Sweden) and in Estonia, as well as subsurface deposits in Lithuania and Latvia (Johnson et al., 1991). Avalonia consisted of the present day Atlantic provinces of Nova Scotia and Newfoundland in Canada (Boucot et al., 1974), south-eastern Ireland and Belgium (McKerrow et al., 1991). The Silurian deposits on this paleocontinent are generally graptolitic shales. The paleocontinent extended also south-eastward to include the Skala Formation of Podolia of the late Silurian (Nikiforova, 1977; Koren et al., 1989).

1.1.4. Siberia

The Siberian paleocontinent comprised mainly today's Siberia, Mongolia and northern China.

It extended northward to the Arctic Ocean, except for Novaya Zemlya which was part of Baltica. The Silurian deposits of Siberia have some cosmopolitan brachiopods in common with those of Baltica, Avalonia and Laurentia (Cocks and Scotese, 1991).

1.1.5. Kazakhstania

The paleocontinent of Kazakhstania included areas of the former USSR east of the Urals, and China south-west of Altai, east of the Urals and north of the Pamirs. The Silurian outcrops on this paleocontinent consist mainly of tropical limestones with corals, indicating that Kazakhstania was located on or close to the paleoequator during the entire Silurian Period. However, the paleogeographic position of Kazakhstania, and of north China and areas between today's Turkey, the Himalayas and south-eastern Asia, are poorly known (Cocks and Scotese, 1991).

1.2. SILURIAN SEA-LEVEL CHANGES

According to Donovan and Jones (1979), the main causes of eustatic sea-level variations are: (1) change in the ocean ridge volume, (2) change in land ice volume, (3) desiccation of isolated seas (minor contribution), and (4) change in global temperature that may change the volume of the water column (Jeppsson, 1990).

The glacioeustatic drop in sea level during the latest Ordovician was followed by a rise during the early Silurian. The occurrence of evaporites in the middle to late Silurian of most paleocontinents that were located near the paleoequator, indicates a relative sea-level drop, but evaporation itself likely had only a trivial effect on Silurian sea levels (Johnson et al., 1991).

The bathymetric models of eustatic sea-level change are based on interpretation of faunal communities and on their associated lithologies (Ziegler, 1965). For example, it is suggested that the *Pentamerus* community lived below wave base (about 30 m depth), that communities dominated by corals and stromatoporoids lived in shallower and warmer environments, and that graptolitic shales were deposited in deep basinal milieus. Johnson et al. (1991) compiled such bathymetric data from different Silurian paleocontinents and used them to construct a composite eustatic sea-level curve (Fig. 1.3) for the Silurian Period. In this compilation, it is suggested that there were four marked eustatic sea-level highstands during the Llandovery. The earliest event, at the Rhuddanian/Aeronian transition, correlates with the *cyphus/gregarius* (= *triangulatus*) Biozone boundary. The next, the Aeronian event, reaches almost the base of the *sedgwickii* Biozone. The third, the early Telychian event, corresponds to the *turriculatus* Biozone. The last, the late Telychian event, correlates with the *crenulata* Biozone. The duration suggested for each of these transgressive-regressive events is about 2.5 Ma (Johnson et al., 1991).

A sea-level highstand occurred in the middle of Wenlock time. This event began approximately in the *riccartonensis* Biozone, lasted until the *ellesae* Biozone, and was followed by a pronounced lowstand in the Homerian.

A significant sea-level fall is recognized also in the mid-Ludlow, probably preceded and followed by sea-level highstands during the early and late Ludlow, respectively. It is suggested that the duration of these events was longer than those of the Llandovery. Data for the Přídolí stage show that sea level varied differently on different paleocontinents, perhaps due to local tectonic movements (Kaljo, 1971).

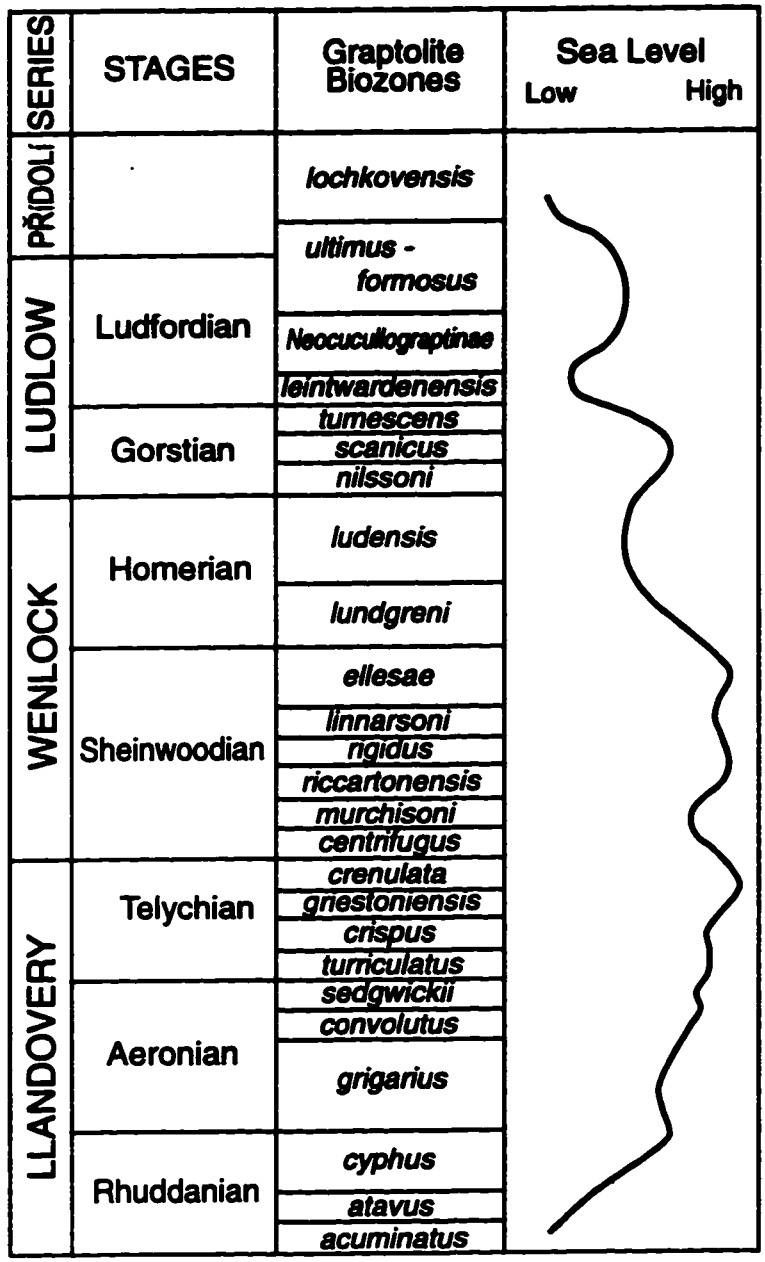

Fig. 1.3. Global Silurian sea-level changes (after Johnson et al., 1991).

1.3. PALEOCLIMATOLOGY

A model of Silurian climate, based on cyclic changes in lithology and conodont diversity, was proposed by Jeppsson (1990). In this model, high conodont diversity was apparently associated with a decline in carbonate deposition on outer platforms, with higher proportion of clayey

deposits in carbonate environments, and with oxic deep shelf sediments. Such times, called P-episodes, were typical of, for example, the *P. amorphognathoides* (Llandovery/Wenlock boundary) and the *P. siluricus* (early Ludfordian) conodont biozones (Fig. 1.4). In contrast, intervals with low conodont diversity, called S-episodes, were coincident with extensive shallow water carbonate reefs and with alum shales in deeper euxinic environments. This was the case in the early Sheinwoodian, the late Homerian and the late Ludfordian. Thus, the P-episodes represent climate that was presumably wetter in low and colder in high latitudes, compared to that of the S-episodes.

Oceanographic circulation patterns generally reflect climatic gradients (Wilde and Berry, 1986). Warm temperatures (>5 °C) at high latitudes cause the densest water to be formed at mid-latitudes, at the cold edge of the salinity maximum. Such sinking waters are oxygen- poor and, as a result, anoxic environments easily develop in the deeper parts of the ocean (S-episodes). In contrast, if high latitudes are cold (<5 °C), it is these that generate the dense waters. Being cold, these waters are well oxygenated and the deep oceans are thus oxic as well (P-episodes). A three-layered ocean may, however, develop if the high-latitude cold water is not dense enough to displace most of the salinity-dense water from the deeper oceanic layers (Wilde and Berry, 1986).

The above climatic cycles are reflected also in weathering processes. Clay transport into oceans increases during the wetter climates of P-episodes due to an increase in chemical weathering and erosion. This was the case during the Wenlock and Ludlow. The high rate of terrestrial weathering also provided nutrients for enhanced organic productivity. As a consequence, planktic fauna would be more abundant during P- than S-episodes.

A model similar to that of Jeppsson (1990) was suggested also by Riding (1993), where the decrease in land area, coincident with sea-level rise, minimizes the weathering input thus diminishing the turbidity of water. As a result, the habitat for shallow water benthos is improved, activating precipitation of carbonates. Conversely, with sea-level fall and increased weathering on land, the increased turbidity inhibits shallow water benthos and reduces carbonate production.

1.4. LITHOFACIES

Sedimentary rocks encrypt environmental records of biological and physical changes through time, and lithofacies therefore reflect paleoceanic conditions in a given time interval. The paleogeographic distribution of Silurian land masses was characterized by three main features: (1) the northern hemisphere was mainly open ocean, (2) most shelf seas were within the tropical zone, and (3) Gondwana, the largest continental mass at that time, was centred over the south pole, but extended northwards into the tropical zone (Cocks and Scotese, 1991; Moore et al., 1993). Brachiopods, in association with crinoids and corals, were dominant among the benthic faunas of tropical shelf seas. Gondwana shorelines were mainly sands that changed laterally into muddy substrates (Berry and Boucot, 1972a,b) with bivalve clams, graptolites and some brachiopods. The presence of clams suggests oxygen-poor benthic environments (Mu et al., 1986). The late Silurian in eastern Australia, in the Urals and in Kazakhstania was characterized by volcanic activity (Talent et al., 1975; Boucot et al., 1968).

In some tropical zones, such as that of Laurentia, the connections to open ocean became restricted so that the central Laurentian platform became a site of accumulation of dolomite and anhydrite (Cocks and Scotese, 1991; Wilde et al., 1991). The land mass of what are now Wales

and Scotland was uplifted, most probably by the Caledonian Orogeny. During the Silurian Period, the shelf margin of that land mass contained marked reef growths (Ziegler et al., 1974; McKerrow, 1978).

Shallowing of the tropical shelf seas and progradation of Gondwana's shorelines had already commenced in the mid-Silurian and became significant by the late Silurian (Fig. 1.3). At the same time, volcanic activity at restricted sites in Gondwana increased markedly. The juxtaposition of these two phenomena may indicate enhanced tectonic activity along oceanic ridges during the late Silurian. By the same token, the juxtaposition of global sea-level rise with the absence of volcanic activity during the early Silurian may indicate tectonic quiescence (Wilde et al., 1991).

In the early Silurian, due to sea-level rise that followed the late Ordovician glaciation, the shelf deposits in temperate zones and the slope and deep shelf deposits in tropical zones were laminated mudrocks with pyrite seams and common graptolites, indicating oxygen-poor or anoxic waters. Some paleoclimatic models suggest that during the Wenlock, most of Gondwana's margins reached warm latitudes where the ocean did not get cold enough to form sea ice. In the absence of sea ice, the water on the outer shelf below the zone of surface turbulence, and in the deeper basins, would have been stagnant and the ocean might have developed a pronounced thermocline. These conditions may have resulted in an oxygen-poor or anoxic bottom layer, due to fast oxygen consumption caused by decomposition of organic matter and due to limited supply of new oxygen (Wilde et al., 1991; Moore et al., 1993).

1.5. STRATIGRAPHY AND TIME RESOLUTION

Based on the sedimentation-time relationship, the stratigraphic section is a record of passage of geologic time during which periods of sedimentation, fluctuating erosion, and non-deposition alternated, resulting in variations in thickness of the accumulated sediments (Sadler, 1981; Tipper, 1983; Crowley, 1984; Anders et al., 1987; Miall, 1994). Thus, sedimentation may vary in rate and have breaks. Such breaks can vary from minutes, for erosion in front of advancing bedforms, up to millions of years, for major regional unconformities caused by tectonic activity. Similarly, the rates of continuous accumulation can vary from few seconds, for grain accumulation on a cross-bed foreset lamina, to thousands of years for slow pelagic fill of an oceanic abyssal plain.

Generally, the mean rates of sedimentation, in both modern and ancient environments, are inversely proportional to the time scale over which they are measured, as shown by Sadler (1981) from compilation of nearly 25,000 rates. This compilation showed a very wide range of sedimentation rates (from 10^{-4} to 10^{7} m/ka), reflecting the increase in the number and duration of sedimentary breaks as the length of the stratigraphic interval increases. Unfortunately, it is difficult to estimate completeness of a stratigraphic section due to factors such as compaction of older sediments, or bioturbation that makes biostratigraphic differences meaningless below a critical mixing thickness (10 to 15 cm), or imprecise radiometric ages (Anders et al., 1987).

The sedimentary breaks within presumably continuous successions may have durations much longer than those suggested by calculations of long-term sedimentation rates and, as a consequence, successions that were deposited during a given time interval may not actually correlate in time (McShea and Raup, 1986; Miall, 1991, 1994). In short, the sedimentary record

may consist of "more gaps than record" (Ager, 1981; Heckel, 1986).

Although in most cases it is hard to estimate the duration of hiatuses, the unconformities themselves were used in the Exxon models (Haq et al., 1987, 1988) as sequence boundaries for conformable successions that were called "correlative conformities". Yet, the diachroneity of sequence boundaries must be taken into consideration. For example, marine transgression-regression cycles may result in sedimentary breaks at different locations within the basin of deposition and at different times. On the open shelf, erosion may occur during regression and starvation during transgression, whereas in marginal-marine environments only the erosion due to regression results in absence of sediments. As a consequence, the sequence boundary unconformities are sometimes offset by as much as a half cycle between the margin and the centre of a depositional basin (Miall, 1994).

Since the Silurian was a quiet period, almost free of major tectonic events (orogenies) (Scotese and McKerrow, 1990), not many regional scale hiatuses developed. They cannot, therefore, serve as a fundamental tool for correlation of sections from different basins. Correlation of the Silurian sections, and estimates of their completeness, cannot be based, therefore, solely on lithostratigraphic criteria and other correlation tools have to be taken into consideration.

1.5.1. Stratotypes

The stratotypes for the Silurian are located in Europe, mainly in Britain (cf. Holland and Bassett, 1989). The Ordovician-Silurian boundary stratotype is well represented at Dobb's Linn in southern Scotland, the Llandovery Series in the Llandovery area, the Wenlock Series in the Wenlock area, the Ludlow Series in the Ludlow area, and the Přídolí Series in the Barrandian

area of Bohemia.

Although these stratotypes are the most complete sections, petrographic features of some suggest a degree of diagenetic alteration that may have compromised the quality of the brachiopod shells needed for the present study. For this reason, alternative reference sections, richer in well preserved brachiopods, were sampled. These include the sections on Anticosti Island (Ordovician-Lower Silurian), in Podolia in the Ukraine (Přídolí), at Kolka in Latvia (Přídolí), in Lithuania (Přídolí), and in the Ohesaare Cliff in Estonia (Přídolí).

The sections selected for this project, although from different depositional basins, were located mainly within the warm climatic zone around the paleoequator. They were chosen on the basis of their completeness, although some contain local minor unconformities.

1.5.2. Biostratigraphy

Correlating and dating stratigraphic sections from different sedimentary basins is not a simple task. It may involve the use not only of lithostratigraphic correlation tools but also of biostratigraphy and other chronostratigraphic methods. This is particularly the case where the sequences cannot be traced by clear physical phenomena, such as regional unconformities or marker beds.

Correlation by macrofossil assemblages provides the underpinning of global stratigraphy, with microfossils, such as foraminiferans and conodonts, contributing to refinement of correlation techniques. Except for some minor work on ostracodes (Siveter et al., 1989), the biostratigraphy of the Silurian Period is based mostly on graptolites, conodonts and brachiopods (Bassett, 1989). Although biocorrelation is a powerful tool, it still has deficiencies that affect its resolution

capability, such as incompleteness of the records or diachroneity. Barriers to dispersal (temperature, geographic or sea-level changes), mass extinction or poor recovery may also result in an incomplete biozone record in the rocks. The temporal ranges of occurrence of many fossils may vary from one location to another, which means that the first appearance datum (FAD) and the last appearance datum (LAD) for the same fossil in different sections can be diachronous (McLeod and Keller, 1991). Such diachroneity in the biostratigraphic record may result in correlation errors. Nevertheless, some species, the "index fossils", are more consistent in their occurrence than others and are therefore preferentially utilized for biostratigraphic correlations.

The subdivision of the Silurian Period takes into consideration the distribution of graptolites, conodonts, brachiopods, chitinozoans, ostracodes, acritarches (phytoplankton), bryozoans, molluscs, trilobites, corals, vertebrates, and some flora in the case of aeolian deposits (cf. Holland and Bassett, 1989). Yet, the most ubiquitous and precise index fossils are the graptolites and, in some cases, the conodonts. The rapid evolution of graptolites and their great diversity during the Silurian Period, as well as their ability to float, enabled them to spread out into all oceans. Their abundance is the reason for the well developed biozonation of the Silurian time scale (Fig. 1.4) and this biostratigraphy is utilized for most of the studied sections. The shelly sequences that do not have a good record of graptolite biozonation, such as the Llandovery of Anticosti Island in Canada or the Přídolí of the Baltic region, are correlated with the help of other fossil groups, such as conodonts and brachiopods. The relative positioning of samples in stratigraphic logs of the studied sections, that is within a given biozone, was provided by field geologists with good experience in the stratigraphy of these sequences (M. G. Bassett, P. Copper, V. Gritsenko, D. Kaljo, and P. Musteikis). Only in the case of the Ukraine (Podolia), it was done

by myself, utilizing marker bentonite beds that were precisely marked in the published profile. In the case of cores (such as Přídolí of Baltic states), their length of core was stated to cover seven biozones by local geologists (D. Kaljo). In this instance, the biozones were assumed to be of equal duration and positioning of samples was based on their depth.

1.5.2.1. The Ordovician-Silurian Boundary

The late Ordovician ice age had its impact on faunal diversity and the subsequent evolutionary high was associated with climatic warming in the course of the Silurian. The base of the Silurian System (Fig. 1.4), and of its basal Rhuddanian Stage, is taken to be at the base of the *acuminatus* Biozone (Bassett, 1985). The latter marks, in most sections, a recognizable widespread marine transgression due to temperature rise (Rickards, 1989). In shelly sections, such as that of Anticosti Island (Canada), where graptolites are scarce, the boundary is taken as the first appearance of the conodont *Ozarkodina oldhamensis* (Barnes, 1989).

1.5.2.2. Rhuddanian Stage

The Rhuddanian Stage includes the *acuminatus* to *cyphus* biozones (Fig. 1.4) and represents an evolutionary buildup toward the *triangulatus* Biozone peak of diversity.

1.5.2.3. Aeronian Stage

The Aeronian Stage begins at the base of the *triangulatus* Biozone (Fig. 1.4), which marks a distinct diversity peak (Rickards, 1989). The triangular monograptids, such as *Monograptus triangulatus*, show the tendency towards isolation and towards triangular thecal profile.

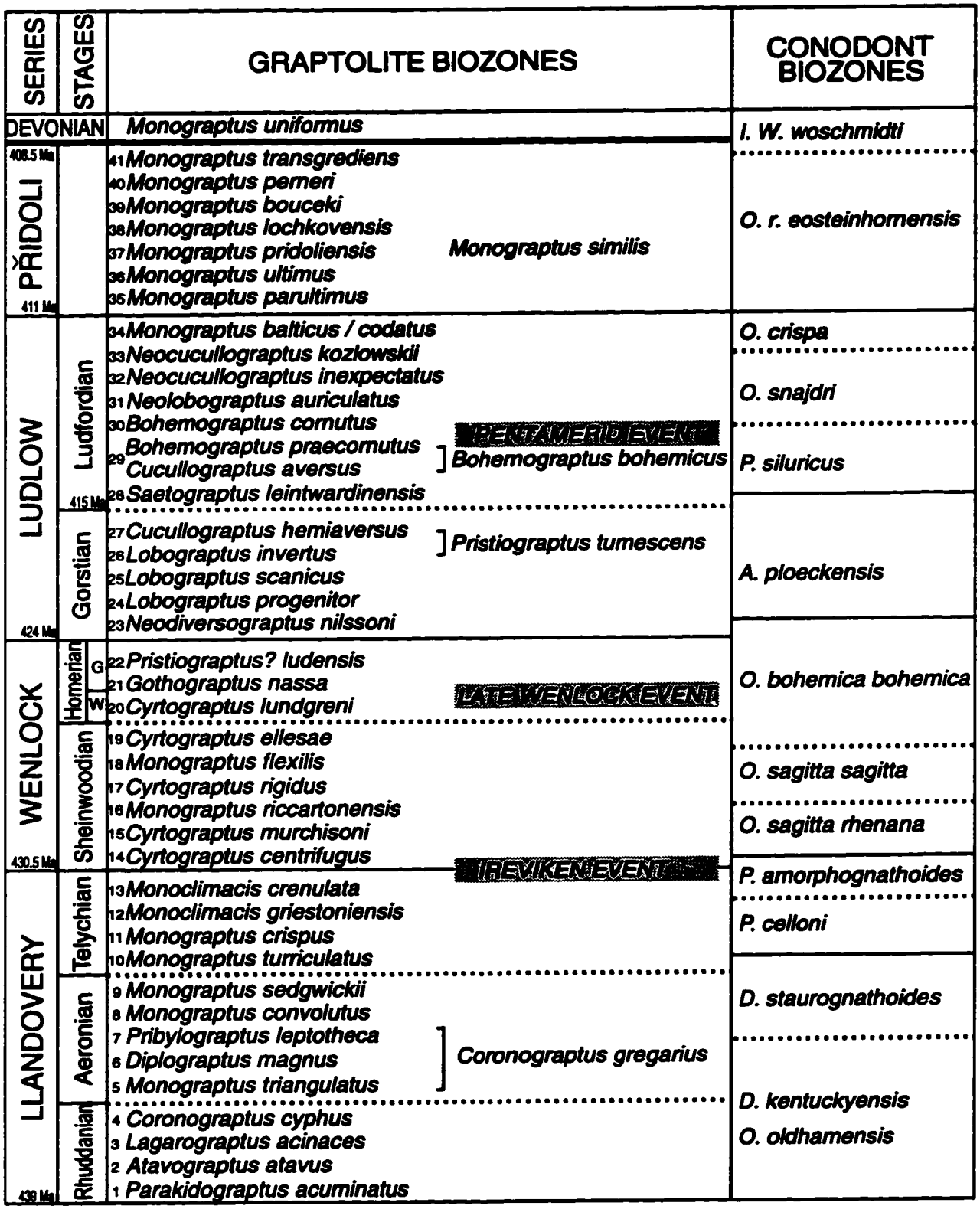

Fig. 1.4. Silurian Series, Stage and Chronozone divisions, including graptolite and conodont biozonation, the estimated numerical ages and the main extinction events. The Whitwell (W) and Gleedon (G) are widely used as informal chronozones (modified from Rickards, 1989; Aldridge and Schönlaub, 1989; Harland et al., 1990; and Talent et al., 1993).

1.5.2.4. Telychian Stage

The Telychian Stage commences at the base of the *turriculatus* Biozone (Fig. 1.4). The monograptids of this stage are commonly large and very long (30 cm), with genus *Monoclimacis* reaching the acme. Coiled rhabdosomes and tiny graptolites with complicated thecae become more common. On the other hand, both the triangulate monograptids and biserial graptolites decline (Rickards, 1989).

1.5.2.5. Sheinwoodian Stage

The Sheinwoodian Stage at the base of the Wenlock begins with the *centrifugus* Biozone (base of the Buildwas Formation in the British stratotype). The Sheinwoodian graptolite biozones are all named after cyrtograptids, except for *Monograptus flexilis* and *M. riccartonensis*.

1.5.2.6. Homerian Stage

The Homerian Stage is subdivided into two informal chronozones, the Whitwell (W) and Gleedon (G) (Fig. 1.4). The top of the stage, also the top of the Wenlock, is the *ludensis* Biozone, while its base is the *lundgreni* Biozone that is equivalent to the Gleedon Chronozone. The *nassa-ludensis* levels have restricted faunal diversity marking a near-extinction evolutionary low (Koren and Rickards, 1980).

1.5.2.7. Gorstian Stage

Following the end of the graptolite decline during the Homerian Stage, the earliest Ludlow records a clear increase in the diversity of species. The base of the Gorstian Stage is the *nilssoni*

Biozone (Fig. 1.4). In the Ludlow Series, monograptids with apertural processes dominate (Rickards, 1989).

1.5.2.8. Ludfordian Stage

The Ludfordian Stage represents another decline in diversity of the graptolite species. Its base is the *S. leintwardinensis* Biozone (Fig. 1.4).

1.5.2.9. Přídolí Series

The Přídolí Series represents another peak of graptolite diversity that followed the decline at the end of the Ludlow (Koren and Rickards, 1980). The base of the stage is the *M. parultimus* Biozone (Fig. 1.4) at the base of the Přídolí Formation in Prague (Ludlow-Přídolí stratotype). The Downtonian is the time equivalent of the Přídolí in the Welsh Borderland sequence, but no graptolites are known from the Downtonian aeolian sandstones. Stages within the Přídolí have not yet been internationally settled, but it comprises about seven graptolite biozones.

1.5.2.10. Other Correlative Biozonations

In some of the studied sections, such as the Přídolí of Podolia (Ukraine) and the Llandovery of Anticosti Island (Canada), graptolite biozonation is not well developed. Faunal biozonations based on conodonts and brachiopods are utilized for correlation purposes.

1.5.3. Marked Extinction Events

Some faunal assemblages, such as brachiopods (pentamerids *Conchidium* and *Kirkidium*), show

a dramatic decrease in diversity at about the beginning of the Wenlock and in the late Ludlow (Talent et al., 1993) and a comparable minimum can also be observed for conodonts at nearly the same time at the end of the *siluricus* Biozone (Ziegler and Lane, 1987). These minimum diversity events are shown in Fig. 1.4 and described below.

The Ireviken Event is a remarkable extinction event that affected conodonts at the *amorphognathoides-ranuliformis* (or *rhenana*) zonal boundary (Fig. 1.4) in the Llandovery-Wenlock transition and is recorded at Ireviken in the Lower Visby Beds of Gotland, Sweden (Jeppsson, 1987, 1990). A moderate decline in brachiopod diversity was documented at about the same stratigraphic level by Talent et al. (1993), but the pentamerid data from the former USSR do not show any clear decline (Sapel'nikov, 1985). **The Late Wenlock Event** consists of several minor extinctions or adaptive radiations. Graptolites were the main species affected. The effect was documented in the *dubius* (or *lundgreni*)- *nassa* biozones (Boucot, 1990). **The Pentamerid Event** was referred to earlier as the *Cardiola* Event (Schönlaub, 1986). It is represented by a dramatic reduction in diversity of pentamerid brachiopods and conodonts. It took place during the late Ludlow at the end of the *siluricus* Biozone (Fig. 1.4) and was documented on a global scale (Jeppsson, 1987). In the **Siluro-Devonian (Přídolí-Lochkovian) Boundary** internal several minor extinction and radiation events have been suggested, but there is no clear evidence for a major extinction (Talent et al., 1993).

1.5.3. Chronostratigraphy

An estimate of the absolute numerical ages, that is, dating of stratigraphic events by radiometric methods, is essential in order to refine regional and global stratigraphic correlations. Most of this

work is based on radiometric bracketing of detrital glauconitic beds or volcanic interbeds. Several attempts were made to date the beginning and the end of the Silurian Period (cf. Harland et al., 1990; Fordham, 1992), but the accuracy and precision varied with the method used. Nevertheless, the geochronometric scale is being steadily refined and the presently accepted duration of the Silurian is about 30 Ma (~439 to ~409 Ma) (Harland et al., 1990; Tucker et al., 1990).

Isotope Dating and Analytical Precision

Several techniques of isotopic dating, using radiogenic isotopes, were utilized to determine absolute ages for the Silurian Period. They included K-Ar, Rb-Sr, Ar-Ar, and fission-track methods and were carried out on a suite of minerals, mainly micas (biotite), K-feldspar, hornblende and zircon (Harland et al., 1990). The precision of a fission-track technique depends on the standard that originates from a rock already dated by other techniques (Gale and Beckinsale, 1983). Consequently, the ages assigned to geologic units have considerable errors.

Errors in Dating the Stage Boundaries

The stage boundaries were dated by different techniques, utilizing age bracketing and chronograms (for more details see Harland et al., 1990). Although these methods were used to minimize the analytical and mathematical errors in age calculations, there are still uncontrollable natural reasons that cause the stage boundary to have a wide range of ages. At times, the estimated error is itself close to the duration of the stage or may even exceed it. The reasons include the following: (1) the data are heterogeneous and include ages determined by different

methods, on different minerals, and in different geological settings; (2) the biostratigraphic stage of a dated mineral may be difficult to establish locally or the correlation of the local biostratigraphic stage with the global stages may be imperfect: sometimes, the chronostratigraphic error from correlating rocks outside the standard section is several times the quoted analytical error; (3) some minerals, such as glauconite, give only minimum ages; and (4) the measured values do not date the stratigraphic unit directly but only bracket its age, with the material dated being stratigraphically distant from the event of interest (Harland et al., 1990; Miall, 1994).

In order to overcome the above problems for the Paleozoic, the tie points method has been employed and the stage boundaries with the tie points assigned numerical ages. The generated chronogram of ages vs. Silurian chrons (graptolite zones) can be thus employed to assign absolute "dates" to the latter by assuming that the chrons between the tie points have equal durations.

Unfortunately, only three tie points are available for the Silurian Period. These are the Ordovician/Silurian (~ 439 ± 7 Ma), the Wenlock/Ludlow (~ 424 ± 4 Ma) and the Silurian/Devonian boundaries (~ 408.5 ± 4 Ma). Note that the error in some cases exceeds the duration of the stage itself. For example, the proposed age for the Llandovery/Wenlock boundary (430.5±9 Ma) has an error that is greater than the estimated duration of the entire Wenlock and almost equal to that of the Llandovery Epoch.

In summary, radiometric dating is an effective chronostratigraphic tool, but a potential error associated with this technique depends on the method used and the stratigraphic situation of the material examined. In some cases the error is large. Absolute ages should therefore be treated

with caution and checked against results based on other correlation techniques. The lack of tie points for the Silurian Period makes it hard to refine the absolute age assignments to the stage level.

1.5.4. Magnetostratigraphy

This method of correlation is based on the retained magnetic imprint that rocks acquired in the geomagnetic field during the time of their formation. Convection currents in the Earth's core cause fluid motion that works as a dynamo and creates a geomagnetic field. These convection currents reverse their direction irregularly, causing reversals in the polarity of the dipole magnetic field. When the polarity is normal, such as at present, the magnetic force lines are directed towards the north magnetic pole and the north-seeking pole of the compass magnetic north-seeking needle points to the north. On reversing polarity, the force lines take the opposite direction and the needle of the compass would point to the south (Harland et al., 1990). Such polarity reversals are retained in rocks and recorded all over the world.

The intervals between these polarity reversals are used as magnetostratigraphic divisions for the correlation of stratigraphic sequences from different basins of deposition (Cox, 1968). The magnetostratigraphic scale is usually calibrated by direct isotope dating (Mankinen and Dalrymple, 1979) or by indirect biostratigraphic correlation (cf. Bralower, 1987).

The paleomagnetic record of the early Paleozoic is poor. The Silurian field was normal. It was preceded by a normal Ordovician field and followed by a reversed Devonian one (Irving and Pullaiah, 1976). Due to the poor record, the magnetostratigraphy of the Silurian did not contribute to the improvement of its temporal resolution.

1.5.5. Isotope Stratigraphy

Variations of the isotopic species (C, O and Sr) in seawater through geologic history are indicative criteria that may reveal the paleoconditions that influenced the evolution of the Earth system. The curves of such variations are used for estimates of paleotemperature and paleoclimatic conditions as well as for stratigraphic correlations (e.g. McArthur, 1994). These topics are the major goals of the present thesis and they will be discussed in detail in Chapters V and VI.

CHAPTER II

GEOLOGICAL SETTING

This study includes samples from diverse basins of deposition and from different continents. Nevertheless, all represent warm paleolatitudes, between 30°N and 30°S. The samples come from Anticosti Island, Québec, Canada (Laurentia), and from England, Norway, Sweden, Estonia, Lithuania and Latvia, and Podolia in the Ukraine (Baltica).

2.1. ANTICOSTI ISLAND, QUÉBEC, CANADA

2.1.1. Location

Anticosti Island is located in the Gulf of St. Lawrence, eastern Canada (49° 04′- 49° 57′N, 64° 32′- 64° 41′W), about 75 km north-east of the Gaspé Peninsula in Québec (Fig. 2.1). The island is about 222 km in length and 56 km at its widest part and is situated on the eastern part of the St. Lawrence platform. The Silurian strata exposed there show no deformation, indicating that they were not significantly affected by the Ordovician Taconic Orogeny (Sami and Desrochers, 1992).

During the early Silurian, the Anticosti basin was located close to the paleoequator, at paleolatitudes 15° to 20° S, on the north-west margin of the Iapetus Ocean (Ziegler et al., 1977, 1979; Scotese et al., 1985). It was part of the Laurentian craton that was covered by shallow epeiric seas and characterized by warm humid climatic conditions (Ziegler et al., 1977).

2.1.2. Lithostratigraphy

Anticosti Island contains one of the best exposed, most continuous and fossil-rich (particularly brachiopods) sedimentary successions in the world. It was therefore considered by the IUGS as a candidate for stratotype for both the Ordovician-Silurian boundary and the lowest series (Llandovery) of the Silurian System.

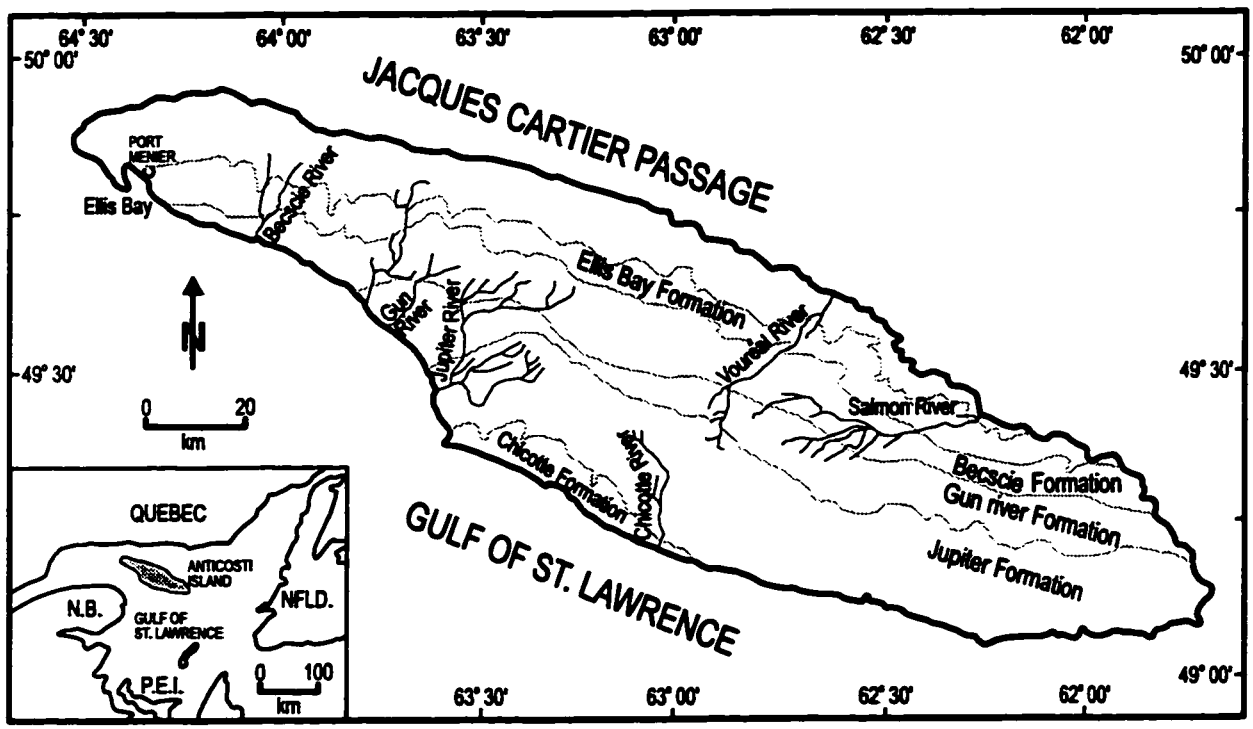

Fig. 2.1. Geological map of Anticosti Island, Québec, Canada (modified from Barnes, 1989).

The Silurian stratigraphy of Anticosti Island (Figs. 2.2a, b) was first studied by Richardson (1857) and Billings (1857), the latter suggesting the term Anticosti Group for the Silurian part of the sequence, including the Ordovician Ellis Bay Formation. Schuchert and Twenhofel (1910) introduced formal formation names and, based on lithostratigraphy, proposed the term Anticostian (Niagaran) Series to the sequence. The Anticosti Group and Anticosti Series were later modified by Twenhofel (1914, 1928) to include only the formations overlying the Ellis Bay

Formation (Becscie, Gun River, Jupiter, and Chicotte), because the Ellis Bay Formation was regarded to be entirely of Ordovician age (Gamachian Stage). The work of Twenhofel was subsequently refined by Bolton (1961, 1970, 1972) and Copeland (1970, 1973, 1974). A detailed lithostratigraphic and basin analysis that led to the readjustment of formational boundaries and subdivisions was carried out by Petryk (1981a,b) and Long and Copper (1987a,b). In extensive study of the Becscie Formation (Fig. 2.2a,b), Copper and Long (1989) assigned its uppermost two members to the newly erected Merrimack Formation.

Prior to their work, only local nomenclature and classification were utilized for the Anticosti sequence. The whole Llandovery sequence (Fig. 2.2) was called the Anticostian Series and it was divided into two stages, the Menierian and the Jumpersian. The Menierian consisted of the Becscie Formation, Gun River Formation, and the lower 10 m of the Jupiter Formation. It included the *acuminatus* through *convolutus* graptolite biozones. The Jumpersian consisted of the rest of the Jupiter and Chicotte formations (Barnes, 1989). Its base was correlated with the base of the *staurognathoides* conodont Biozone (Cooper, 1980) and it included the *sedgwickii* through *crenulata* graptolite biozones. The Jumpersian Stage correlates with the upper Aeronian and Telychian stages of the Llandovery Series (Cocks et al., 1984).

The Llandovery succession on the island is about 525 m thick and is composed of limestones with minor shales and sandstones. The strata dip at $< 2^{\circ}$ south-west and show no deformation or faulting. The colour alteration indices of conodonts are ~ 1, indicating a burial temperature of less than 80° (Barnes, 1989) and thus good preservation of fossils.

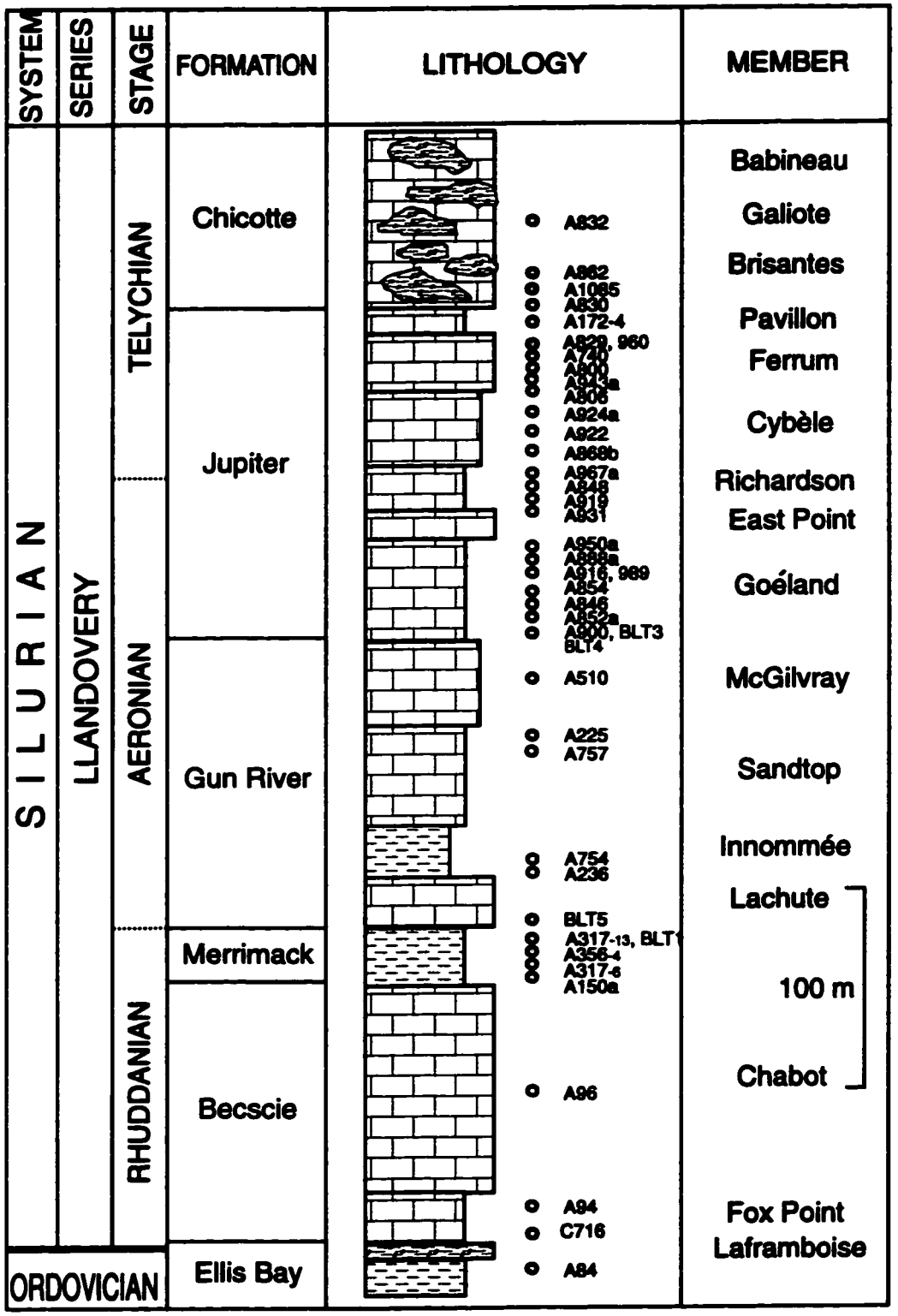

Fig. 2.2a. Lithostratigraphy of the Silurian section on Anticosti Island and the relative positions of samples. Member names are informal (modified from Long and Copper, 1994). For legend, see Fig. 2.2b.

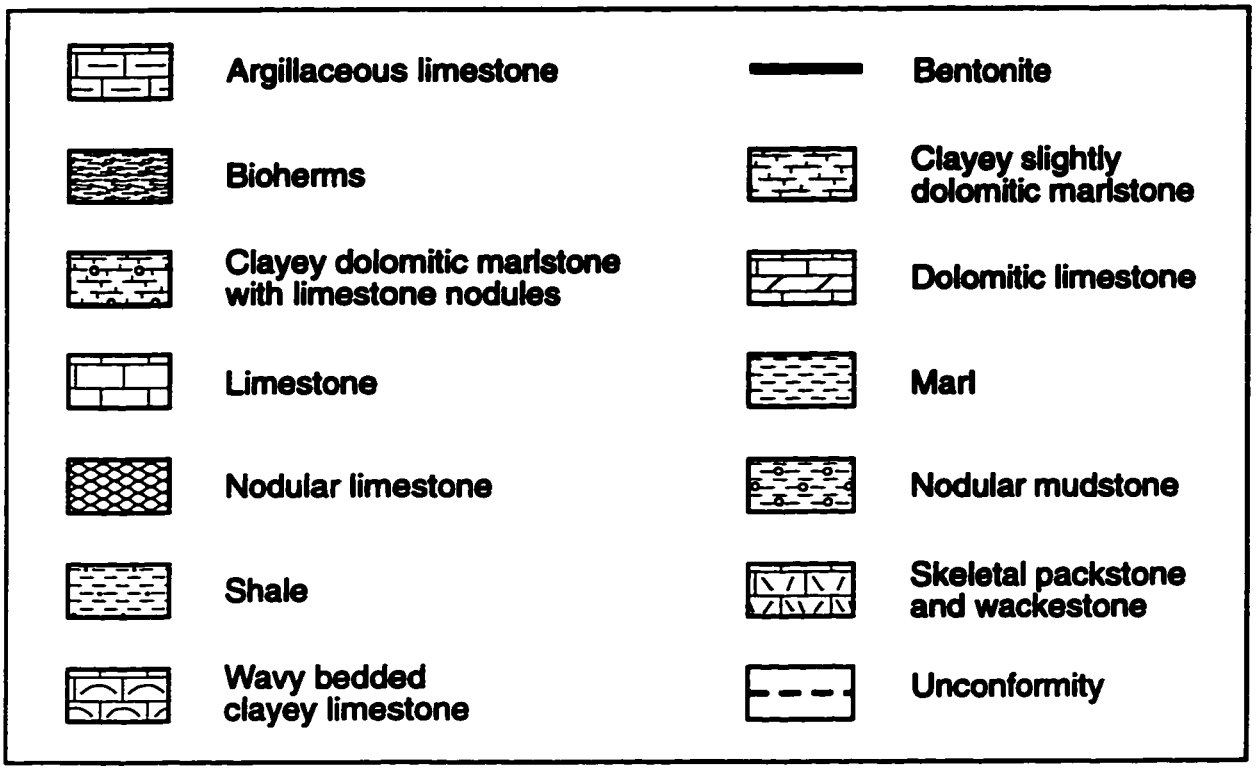

Fig. 2.2b. Legend for all studied outcrops and cores.

The Silurian strata were deposited during the general eustatic sea-level rise that followed the late Ordovician glaciation (Ziegler et al., 1979; Sami and Desrochers, 1992). Sedimentological studies (Petryk, 1979, 1981a) indicate that they were deposited in an open subtidal carbonate platform environment close to the continental margin, but no slope or deep basin sediments have been reported (Sami and Desrochers, 1992). A pattern of sea-level change, based on brachiopod communities, was proposed for the Anticosti sequence by Johnson et al. (1981). Such communities were used later (Jin et al., 1990) to improve the biostratigraphic resolution of the sequence.

As discussed earlier, the lithostratigraphy of the Anticosti sequence (Fig. 2.2a,b) has been progressively refined through many studies (see Long and Copper, 1994 for more details and

references). The Silurian sequence, from bottom to top, consists of the topmost Ellis Bay Formation, and the Becscie, Merrimack, Gun River, Jupiter and Chicotte formations. The Ordovician-Silurian boundary lies possibly at or near the top of the Laframboise Member (a 2.5 m thick biohermal reef patch), the uppermost member in the Ellis Bay Formation (Barnes, 1989; Melchin et al., 1991; Long and Copper, 1994). The boundary was taken as the base of the *oldhamensis* conodont Biozone.

Becscie Formation

The Becscie Formation is about 130 m thick (Petryk, 1981a) and consists of fossiliferous limestone with minor shale interbeds. Brachiopod packstone, rudstone, skeletal wackestone and lime mudstone represent the main lithologies. Highly fossiliferous grainstone and packstone with green shale interbeds constitute the upper 25 m of the sequence (Barnes, 1989). The formation consists of two members (Fig. 2.2a,b), the Fox Point Member and the Chabot Member (Long and Copper, 1994).

Merrimack Formation

The Merrimack Formation consists of up to 25 m of calcareous mudstones, recently separated from the top of the Becscie Formation (Copper and Long, 1989; Sami and Desrochers, 1992).

Gun River Formation

The Gun River Formation is about 145 m thick (Petryk, 1981a) and consists mainly of limestone, typically lime mudstone, packstone and rudstone, with bioherms near the top. It is subdivided, from bottom to top, into 4 members:

Lachute Member: about 14 m of thinly bedded micrite with mudstone interbeds. Brachiopods, gastropods, ostracodes and corals are present.

Innommée Member: about 12-17 m thick, mainly of laminated mudstone at the base, overlain by sandstone with minor carbonate mudstones and micrite (Long and Copper, 1994).

Sandtop Member: up to 44 m of massive micrite with thin beds of calcareous mudstone. Fossils are rare in this member.

McGilvray Member: about 74 m of massive, nodular and laminated micrites with minor mudstones. The sequence is characterized by the first occurrence of the atrypoids *Gotatrypa*, *Jovatrypa* and *Atrypina jupiterensis* (Long and Copper, 1994).

Jupiter Formation

The Jupiter Formation consists of about 171 m of limestone interbedded with minor calcareous shale, lime mudstone, skeletal wackestone and grainstone. Rare sandy siliciclastics and reefal zones are present, mainly near the top (Petryk, 1981c). The formation includes six members (Copper and Long, 1990), from bottom to top:

Goéland Member: about 55 m of calcareous mudstone with minor micritic interbeds. It is rich in brachiopods (*Pentamerus*, *Gotatrypa* and *Triplesia*) but poor in corals and stromatoporoids (Long and Copper, 1994).

East Point Member: 9.8 to 10.4 m thick, consisting of basal calcarenite, overlain by a biohermal massive unit and an upper laminated micritic limestone.

Richardson Member: 25 m thick, consisting mainly of argillaceous limestones in the lower part and micrite and calcarenite in the upper part. The lower strata are characterized by relatively

deeper water, outer shelf, faunal assemblages (rhynchonellids, *Clorinda*), while the upper portion contains shallow water ones (pentamerids).

Cybèle Member: 32-34 m thick and consists of bedded micrite with minor laminated calcareous mudstones. Shelly fossils are uncommon in these layers.

Ferrum Member: a minimum thickness of 32 m of bedded micrite, with calcareous mudstone partings and hardgrounds. Atrypoids (*Gotatrypa*) and rugose corals are common and well preserved.

Pavillon Member: 10 to 12 m thick, mainly calcareous mudstone with interbedded micrite and calcarenite lenses that contain broken brachiopods and abundant crinoids. This member is rich in brachiopods and corals.

Chicotte Formation

The Chicotte formation consists of about 90 m of bedded crinoidal grainstone with patch reefs. The sequence is believed to have been deposited in a shallow wave-agitated setting. It is subdivided, from bottom to top, into three members (Long and Copper, 1994), the Brisantes, Galiote and Babineau (Fig. 2.2a,b).

2.1.3. Chronostatigraphy

The base of the Silurian System is now set by the IUGS (Bassett, 1985) to be coincident with the base of the *Parakidograptus acuminatus* Biozone (Fig. 2.3), but this is difficult to correlate with shelly fossil successions, such as the one on Anticosti Island. Consequently, the base of the Silurian in the Anticosti sequence was taken to be the first appearance of *Ozarkodina*

oldhamensis (Barnes and McCracken, 1981). This species occurs in association with other species, such as *Oulodus hassi*, *Distomodus kentakyensis*, *Icriodella discreta* and *Oulodus? nathani*. *Oulodus? nathani* is considered to mark the base of the Silurian System in the Gaspé

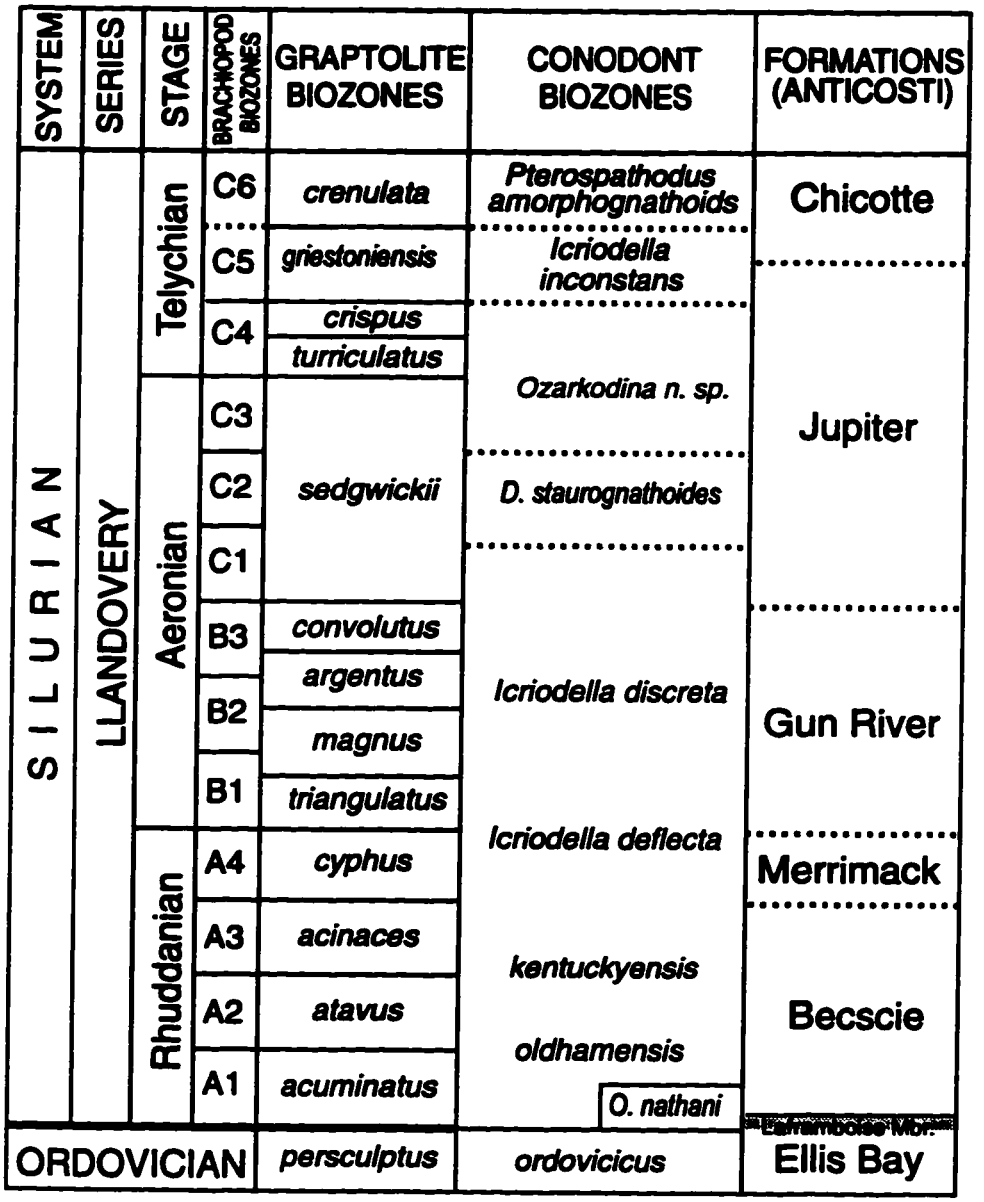

Fig. 2.3. Chronostratigraphy and biostratigraphy of the Silurian succession on Anticosti Island (modified from Barnes, 1989; Jin et al., 1990; and Bassett, pers. comm., 1995). A_1, A_2 etc. refer to brachiopod biozonation.

area (Nowlan, 1983) and in Norway (Aldridge and Mohamed, 1982). The presence of the biozonal species *Icriodella discreta* and *Icriodella deflecta* in the Becscie and Gun River formations allows correlation throughout North America, Britain, the Baltic region and elsewhere. However, in the Ordovician-Silurian boundary section on Cornwallis Island (Arctic Canada), which contains graptolites and conodonts (Melchin et al., 1991), the *nathani* Biozone contains transitional or mixed Ordovician and Silurian fauna. In this section, the base of the overlying *kentuckyensis* Biozone is within the lower *acuminatus* graptolite Biozone.

The Ordovician-Silurian boundary, the base of the *acuminatus* Biozone, is suggested to be at or near the top of the Laframboise Member (Melchin et al., 1991; Long and Copper, 1994). Thus, the Silurian sequence (Fig. 2.3) on Anticosti Island begins with the *oldhamensis* conodont Biozone and includes the uppermost part of the Laframboise Member, the Becscie, Merrimack, Gun River, Jupiter and Chicotte formations. The Chicotte Formation was earlier believed to extend into the Wenlock, but was subsequently shown to be of Telychian (C_5-C_6, Llandovery) age (Copper, 1981; Uyeno and Barnes, 1983; Barnes, 1989). Further correlative studies on Anticosti, and of comparable successions in other basins, are required in order to tie the graptolite and conodont biozones more precisely.

2.2. OSLO REGION, NORWAY

2.2.1. Location

The Oslo region of southeastern Norway (59°- 61° N, 9°- 12° W) lies in a graben with a north-east to south-west trend (Fig. 2.4). During Silurian times, southern Norway was carried by the paleocontinent of Baltica while northern Norway was part of Laurentia. The region has deposits

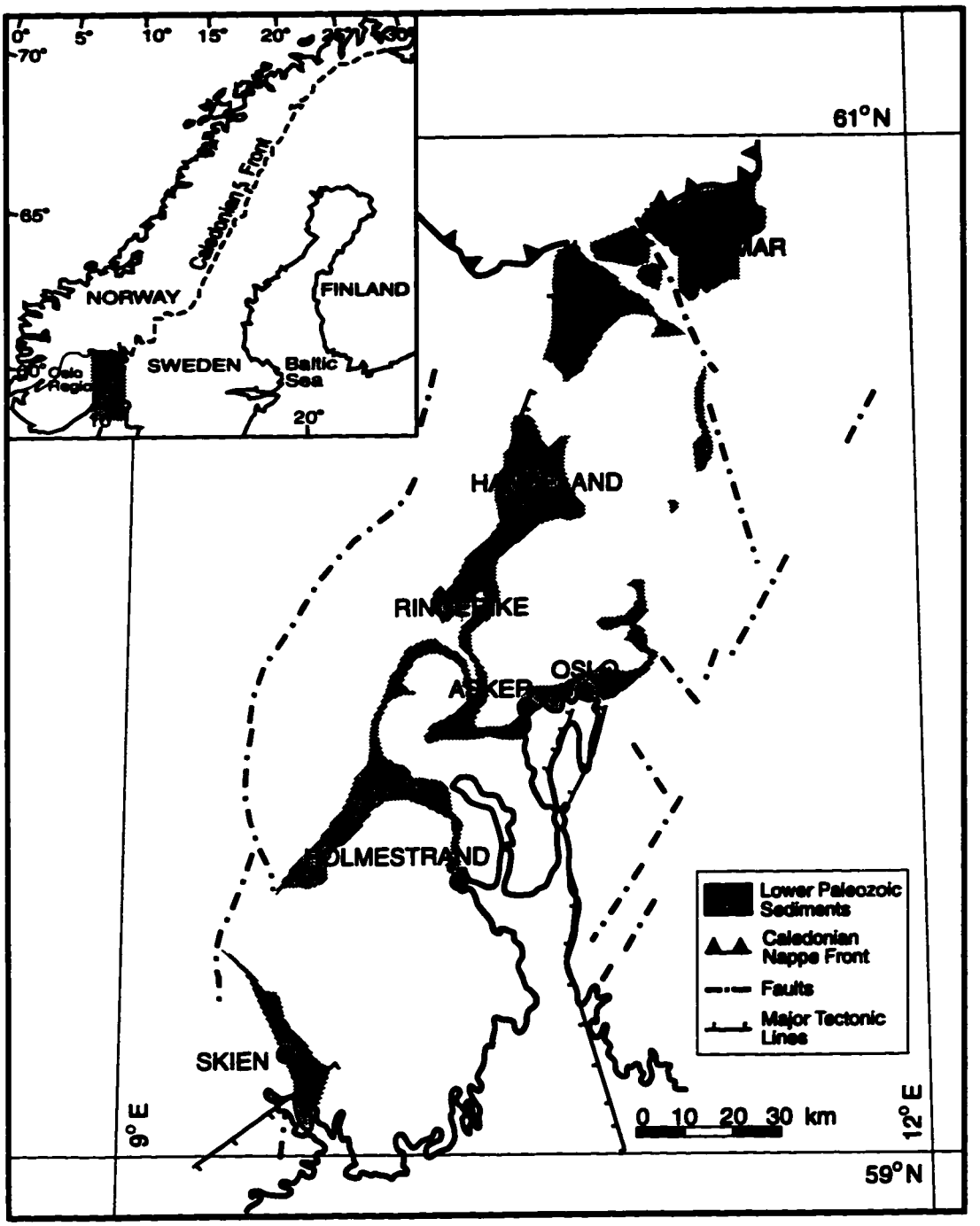

Fig. 2.4. Gelogical map of Oslo region, Norway, showing the Paleozoic outcrops which contain Silurian sediments (modified from Worsley, 1989).

ranging through the entire Paleozoic and it is divided into twelve districts, eight of which contain Silurian sequences of Llandovery to Wenlock age. The entire Silurian succession was deformed during the Scandian Orogeny (sometimes referred to as the Scandian phase of the Caledonian Orogeny) and, subsequently, thermally metamorphosed. The succession was further faulted, forming the Oslo graben during the late Paleozoic (Worsley, 1989).

2.2.2. Lithostratigraphy

The Silurian sediments of the Oslo region were deposited in marine shelf environments that dominated the area. The entire lower Paleozoic sequence in the region was studied by several authors (cf. Kjerulf, 1857; Kiaer, 1908), but a refined lithostratigraphic scheme was proposed only recently by Worsley et al. (1983). The Silurian sequence (Fig. 2.5) is best preserved in the Oslo and Asker districts and it consists of several formations (Worsley et al., 1983; Worsley, 1989) that are briefly described below:

- The **Solvik Formation** is 190 m thick and shale-dominated. It rests with sharp contact on the sandstone of the Ashgillian Langøyene Formation. Its lithofacies characteristics suggest deposition in a storm-influenced open shelf environment. The sharp lithological change that defines the base of the formation indicates an abrupt deepening event that might have resulted from the Gondwana deglaciation at the end of the Ordovician.
- The **Rytteråker Formation** is about 50 m thick and consists of limestones with thin shale interbeds. These limestones are mainly wackestones and packstones as well as patch reefs at the top of the formation. The change from shale-dominated deposits in the subjacent Solvik Formation to limestone-dominated deposits of the Rytteråker Formation

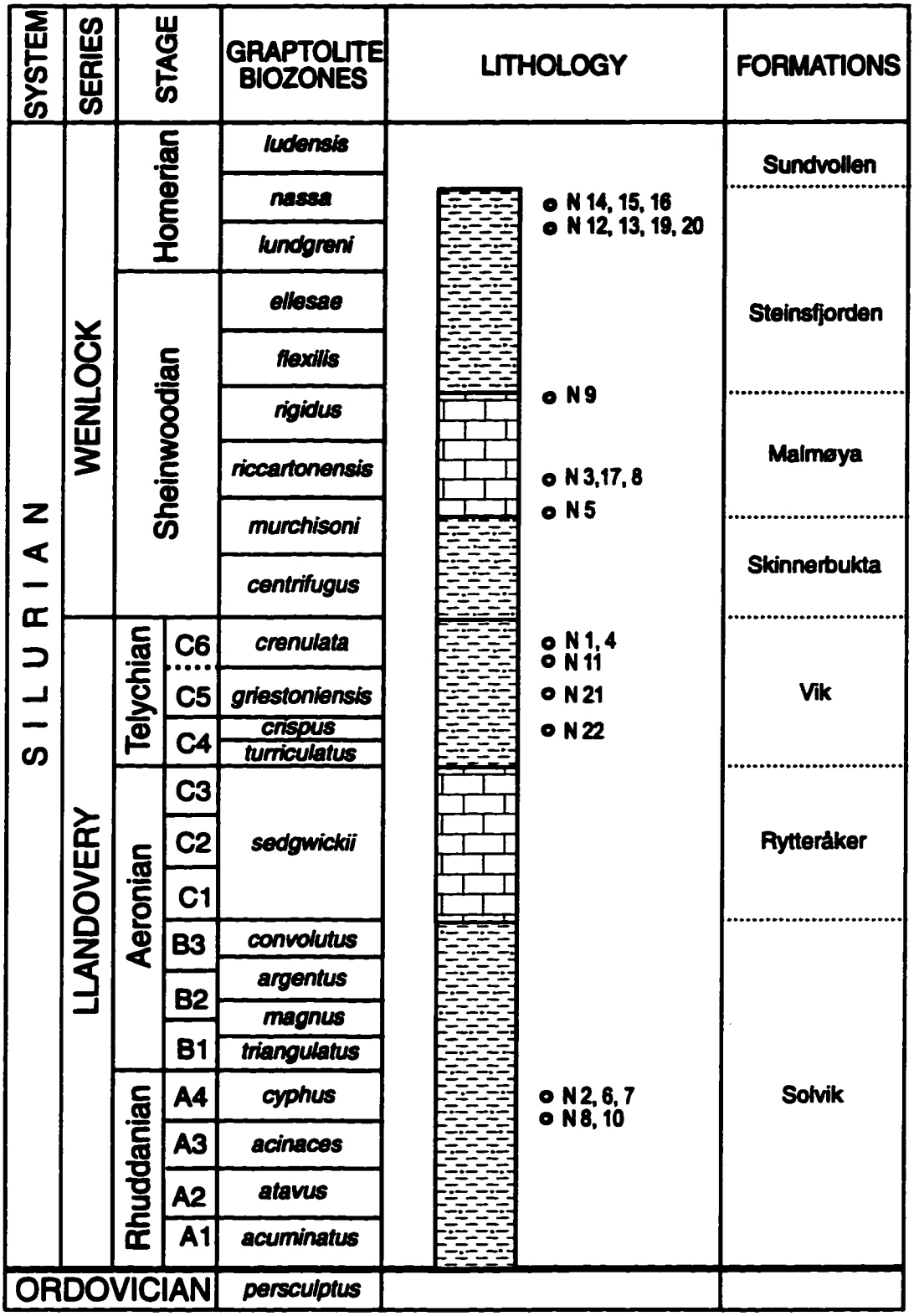

Fig. 2.5. Lithostratigraphy and biostratigraphy of the Oslo Silurian sequence, with the sample positions indicated on the log. Legend as in Figure 2.2b (modified from Worsley et al., 1983 and Worsley, 1989).

suggests upward shallowing .

- The **Vik Formation** is 45 to 80 m thick and consists of shale in the lower- and uppermost parts, with minor nodular limestone in the middle. The change in lithofacies from patch reefs at the top of the underlying Rytteråker Formation to shales in Vik Formation suggests a significant deepening event.
- The **Skinnerbukta Formation** is 80 m thick and consists of graptolitic shale, with ubiquitous limestone interbeds towards the gradational contact with the overlying limestones of the Malmøya Formation. The basal part of the formation spans the Llandovery/Wenlock boundary.
- The **Malmøya Formation** is about 35 m thick, with deposits grading from limestones interbedded with shales at the base to massive bioclastic (stromatoporoid) biostromes in the upper part.
- The **Steinsfjorden Formation** is about 26 m thick and consists of shale, marl, dolomite and limestone. These lithologies reflect small-scale Homerian transgressive-regressive episodes in supratidal to restricted subtidal environments.

2.2.3. Chronostratigraphy

The Silurian succession in the Oslo region is rich in shelly fauna, such as brachiopods, corals, stromatoporoids, and conodonts as well as graptolites. This fossil content facilitated biostratigraphic correlation of the succession with the standard Silurian scale. The biostratigraphy of the Silurian rocks in Oslo region was studied in detail by several authors (cf. Worsley, 1982; 1989) and is briefly discussed below.

The base of the Silurian System in the Oslo and Asker districts (Fig. 2.5) is suggested to be 8 m above the base of the Solvik Formation. This is marked by the appearance of the conodont *Ozarkodina oldhamensis* which was proposed to mark the base of the Silurian on Anticosti Island (Aldridge and Mohamed, 1982; Barnes, 1982). Graptolites have not been recorded yet in the lowermost beds in Asker, but they appear about 11 m above the base of the Solvik Formation. The base of the Aeronian is in the upper part of the Solvik Formation at a level correlated with the base of the *triangulatus* Biozone (Cocks et al., 1984). The Aeronian Stage spans the upper part of the Solvik Formation, the entire Rytteråker Formation and the lower part of the Vik Formation. The base of the Telychian Stage is located in the Vik Formation at a level that correlates approximately with the base of the *turriculatus* Biozone (Cocks and Toghill, 1973). The upper Telychian boundary, which is also the Llandovery/Wenlock boundary, is suggested to be located within the lowermost parts of the Skinnerbukta Formation (shales). This boundary coincides with the base of the *amorphognathoides* Biozone which is equivalent to the base of the *crenulata* Biozone (Worsley, 1989). The Sheinwoodian/Homerian boundary is located in the Steinsfjorden Formation at a level equivalent to the base of the *lundgreni* Biozone (Worsley, 1982).

2.3. WENLOCK EDGE AREA, WALES, BRITAIN (Wenlock Series)

The term Wenlock was first used by Murchison in his description of the Wenlock Limestone, as a major division of strata underlying the Old Red Sandstone of the Welsh Borderland and southern Wales. Subsequent studies and revisions have followed Murchison's nomenclature and recognized the Wenlock rocks in the Wenlock area as a standard succession for that interval of

the Silurian System (Cocks, 1971; Bassett et al., 1975).

2.3.1. Location

Wenlock Edge in Shropshire in west-central England is a limestone escarpment that extends about 25 km south-west and 7 km east of the town Much Wenlock (Fig. 2.6). The Wenlock Series overlies soft rocks of the upper Llandovery, whereas reefal limestones occupy the uppermost part of the series (Bassett, 1989). The sediments are unmetamorphosed, rich in micro- and macrofossils, and dip gently (~ 8° to 10°) towards the south-east. The succession is continuous, with clear facies relationships, minimal faulting and no tectonic complications. Such criteria make the area a good stratotype (Cowe et al., 1986).

It is suggested that during Silurian time, the Wales area was carried by the paleocontinent of Baltica (McKerrow et al., 1991), although some geologists believe that it was a part of the Midland platform (Siveter et al., 1989). Late Llandovery rocks are poorly exposed in some localities of the Wenlock Edge area while other localities have incomplete successions of the Ludlow Series. However, a complete Ludlow Series occurs ideally in the Ludlow anticline and the emphasis is therefore directed to the Wenlock Series in that area.

2.3.2. Lithostratigraphy

Sedimentation of the Silurian deposits in the Wenlock Edge area started with the late Llandovery transgression. The topmost Llandovery formation is a fossiliferous purple shale and mudstone. The boundary between the Llandovery and Wenlock Series is marked by the general change in colour, from purple to grey, and by the occurrence of bands of calcareous nodules

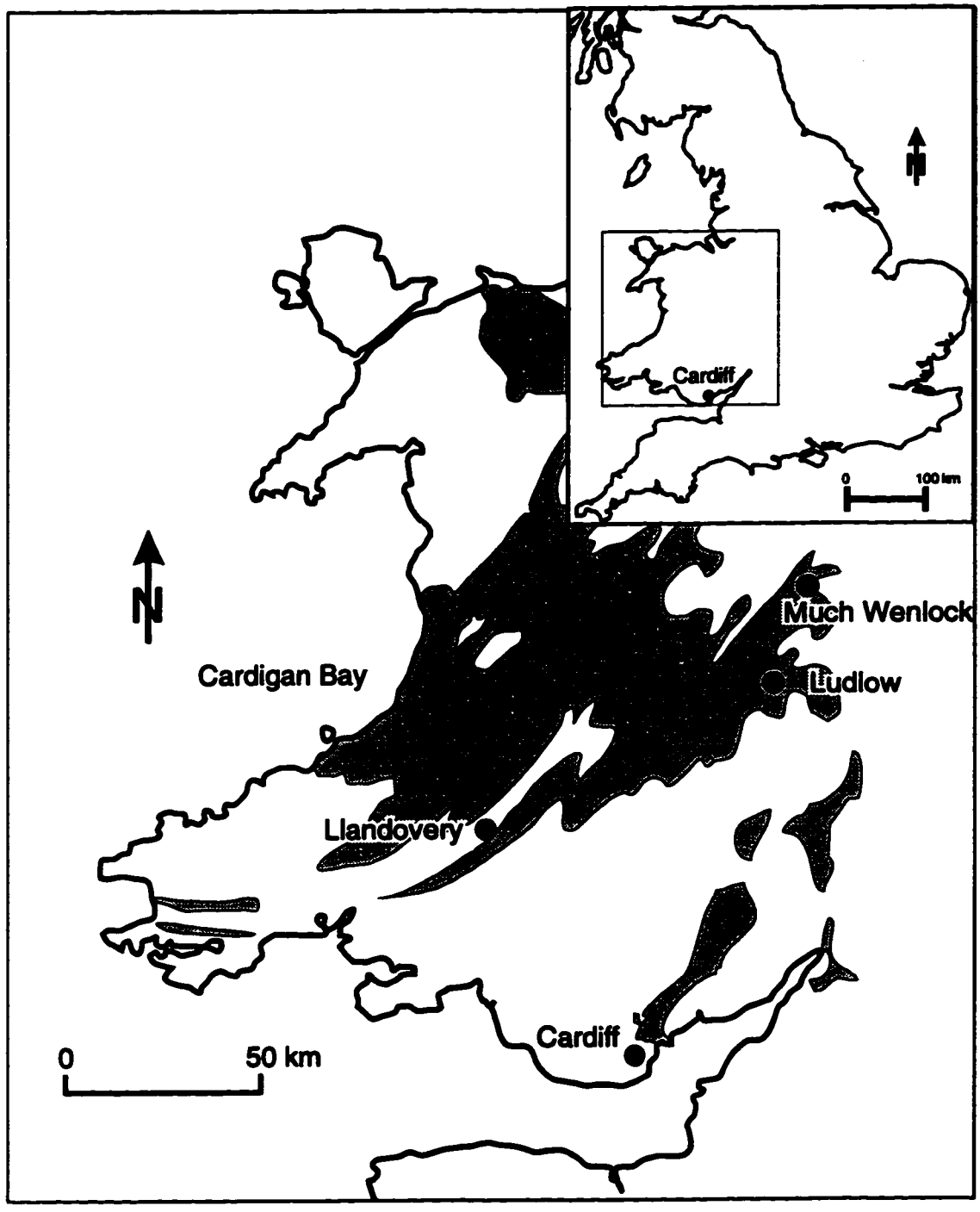

Fig. 2.6. Map of the Silurian outcrops (grey) in Wales and Welsh Borderland of Great Britain (after Cocks et al., 1992).

(Siveter et al., 1989).

The Wenlock Series in the Wenlock Edge area consists of three formations (Fig. 2.7), from bottom to top, the Buildwas, Coalbrookdale, and Much Wenlock Limestone formations (Bassett et al., 1975; Siveter et al., 1989; Bassett, 1989; Cocks et al., 1992). The total thickness of the series in the area ranges between 265 and 330 m.

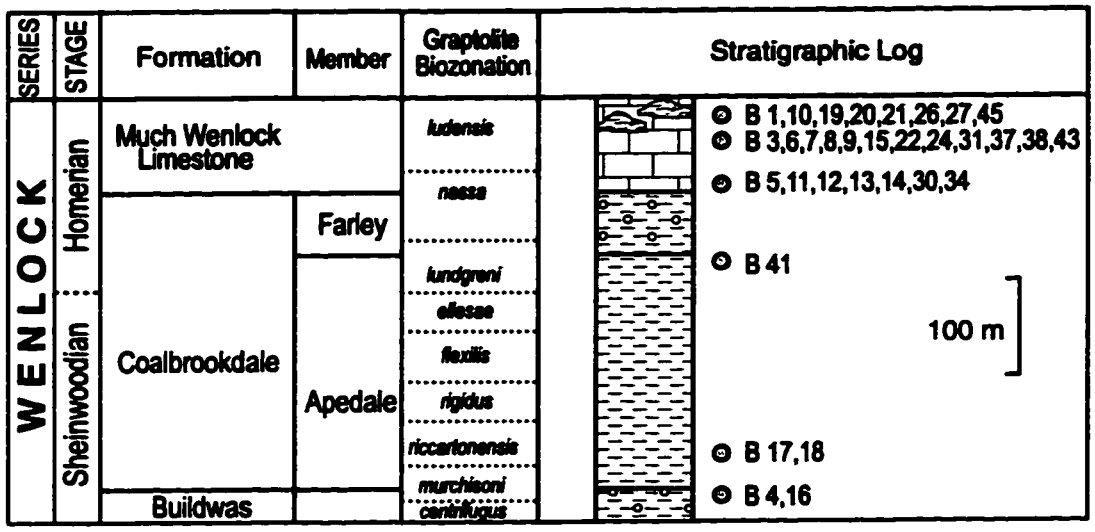

Fig. 2.7. Lithostratigraphy and chronostratigraphy of the Wenlock sequence in Wenlock Edge area (U. K.), with sample positions indicated on the the stratigraphic log. Legend as in Figure 2.2b (modified from Siveter et al., 1989).

Buildwas Formation

The Buildwas Formation constitutes the basal unit of the Wenlock Series in the Wenlock Edge area. It is composed of buff to olive green and grey mudstones with nodular calcareous mudstones and muddy limestones. Bentonite bands, about 15 cm thick, are common. Carbonate nodules are up to 20 cm in diameter, well spaced and ubiquitous in the lowest and uppermost parts of the formation. These nodules, together with bentonite bands, are useful as correlative marks in local mapping. The formation is 27 to 40 m thick. Shell debris is concentrated locally

in bands or pockets but rarely forms a wackestone texture (Siveter et al., 1989; Bassett, 1989).

Shelly fossils are abundant in the whole Wenlock Edge sequence, but are mostly small or fragmentary. Brachiopods are common and include *Atrypa reticularis*, *Atrypa barrandii*, *Dicoelosia biloba*, *Isorthis elegantulina*, *Eoplectodonta duvalii* and *Resserella sabrinae*. The last four species replace other species of the same genera that occur in the underlying Llandovery purple shale. Conodonts, ostracodes, trilobites, foraminifers, chitinozoans and other microflora are also present (Siveter et al., 1989). Graptolites are abundant as well and the Wenlock rocks in the Wenlock Edge area serve therefore as an international standard for the Wenlock Series (Bassett, 1989).

Coalbrookdale Formation

The Coalbrookdale Formation overlies the Buildwas Formation and consists of olive grey to dark blue-grey mudstone beds dipping eastward at 2° to 3° (Siveter et al., 1989). This formation consists of two members: 1) Apedale Member: this lower member rests on the highest Buildwas nodular limestone and contains thin beds of calcareous siltstone and nodular carbonates as well as bentonite bands. Graptolites are the most common macrofossils whereas shelly fossils are rare. 2) Farley Member: this upper member consists mainly of an alternating sequence of grey mudstones and thin nodular blue-grey limestones, the latter mostly wackestones that contain fossil allochems. The calcareous bands and nodules in this member are an indication of upward shallowing. The mudstones are petrographically similar to those of the underlying Apedale Member.

Much Wenlock Limestone Formation

The Much Wenlock Limestone caps the Wenlock Edge escarpment and represents continuation of the upward shallowing indicated in the upper member of the Coalbrookdale Formation. The formation is up to 29 m thick, and thins gradually southwestward to about 21 m. The Much Wenlock Limestone Formation consist mainly of interbedded silty mudstones and impure limestones, but purer limestones of shallow water origin occur at the top.

Organic patch reefs are common (Riding, 1981; Siveter et al., 1989) and, based on their occurrence, the formation is subdivided into two parts:

(1) A Reef tract, which forms the lower part of the formation and rests directly on the Farley Member. It consists of regularly bedded limestones with several bioherms. These limestones are mainly fossiliferous packstones, but rarely coarse packstones are present. The irregular relationship of the bioherms with the limestone interbeds made it difficult to assign a member status to the reef tract (Bassett, 1989).

(2) An Off-reef tract, which has more consistent facies relationship so that a formal nomenclature can be assigned: 1) the Longville Member directly overlies the Farley Member and consists of 12 to 15 m of tabular and bedded limestones interbedded with silty mudstones (Shergold and Bassett, 1970); 2) the Edgton Member in its lower part consists of nodular limestones, and its upper part is pelmatozoan limestone (Bassett, 1989).

2.3.3. Chronostratigraphy

According to the work of the Subcommision on Silurian Stratigraphy of the International Union of Geological Sciences (IUGS), the Wenlock Series of the Wenlock Edge area has two formal

stages, the Sheinwoodian and the Homerian. The series extends from the base of the *centrifugus* Biozone to the top of the *ludensis* Biozone (Fig. 2.7) (Bassett, 1989; Cocks et al., 1992).

The Sheinwoodian Stage embraces the Buildwas Formation and the lower half of the Apedale Member of the Coalbrookdale Formation. In the graptolite biozonation, the Sheinwoodian Stage covers an interval that extends from the base of the *centrifugus* Biozone to the top of the *ellesae* Biozone (Bassett, 1989; Cocks et al., 1992). The base of the Wenlock Series is coincident with that of the Sheinwoodian Stage and correlates with the base of the *centrifugus* Biozone (Fig. 2.7).

The Homerian Stage embraces the upper half of the Apedale Member and the Farley Member of the Coalbrookdale Formation as well as the whole of the Much Wenlock Limestone Formation. It spans a graptolite interval from the base of the *lundgreni* Biozone to the top of the *ludensis* Biozone (Bassett et al., 1975).

Although the subdivision of the Homerian Stage into the Whitwell and Gleedon chronozones was not officially ratified by the International Commission on Stratigraphy, these chronozones are widely used and they are internationally correlatable (Bassett et al., 1975). The **Whitwell Chronozone** (referred to as substage in Harland et al., 1990) embraces the strata within the upper part of Apedale Member and coincides with the graptolite interval of the *lundgreni* Biozone. The overlying **Gleedon Chronozone** spans the strata of the Farley Member and the whole of the Much Wenlock Limestone Formation (Bassett, 1989; Cocks et al., 1992). It correlates with the *nassa* and *ludensis* graptolite biozones (Fig. 2.7).

2.4. GOTLAND, SWEDEN

2.4.1. Location

Gotland is a Swedish island located approximately in the centre of the Baltic Sea (Fig. 2.8) on the European craton. During Silurian times, this island was carried by the paleocontinent of Baltica and was suggested to have been located near the paleoequator.

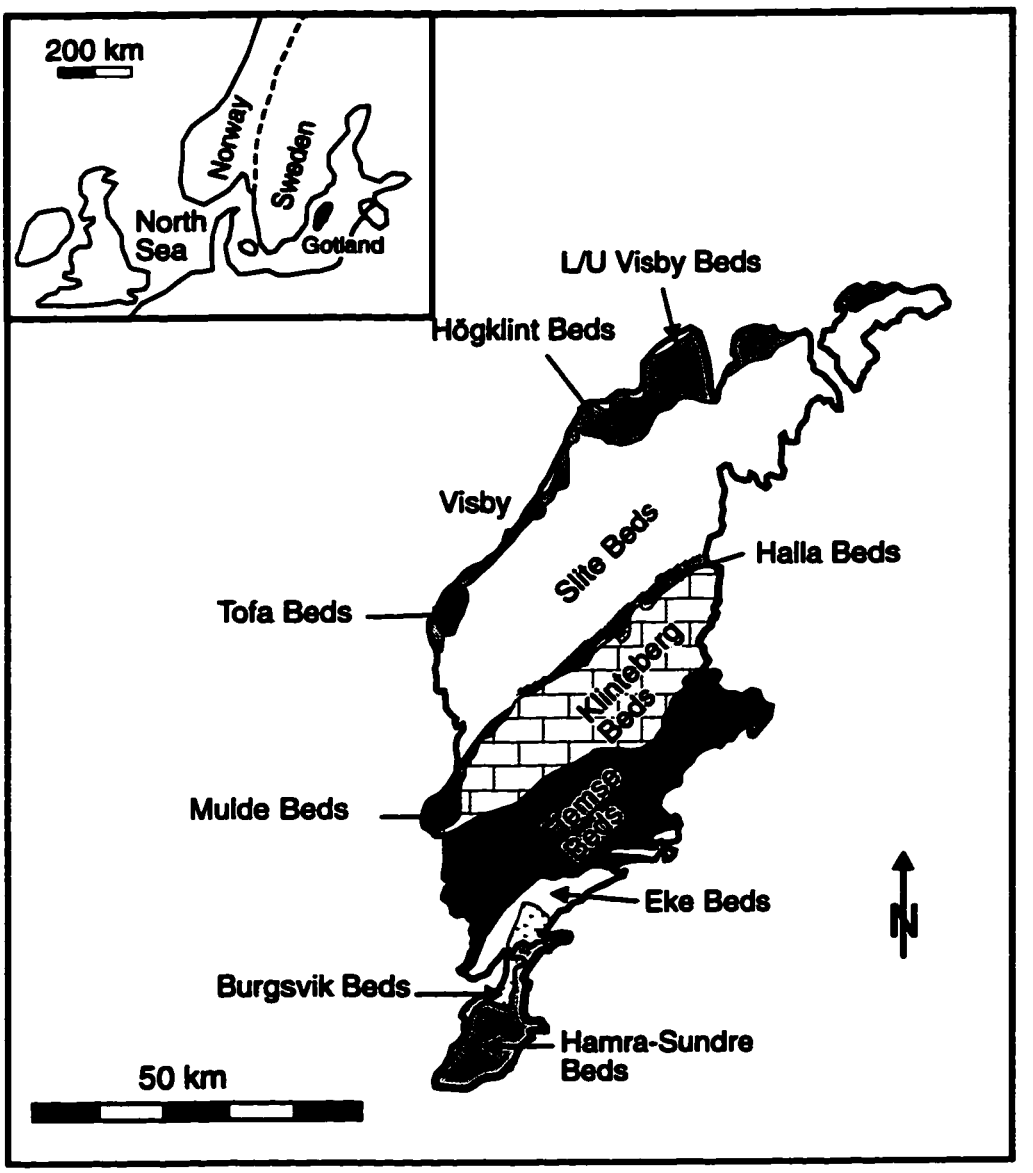

Fig. 2.8. Geological map of Gotland (Sweden) showing the regional distribution of the Silurian outcrops (modified from Bassett et al., 1989).

2.4.2. Lithostratigraphy

The Silurian succession of Gotland is about 500 m thick, with fossiliferous shallow-water deposits (Neuman and Kershaw, 1991) that span the upper Llandovery to upper Ludlow interval. The sediments show a very low grade of diagenesis and excellent preservation of shelly fossils. The burial depth is estimated to have been 2 to 3 km and burial temperature < 100 °C (Frykman, 1986). The strata are undeformed, dipping < 1° towards the southeast.

The litho- and biostratigraphy of the succession were studied earlier by Hede (1960) and refined recently by several authors (for more references see Neuman and Kershaw, 1991). The entire lithostratigraphic framework shows a general shallowing-upward trend and is described briefly from bottom to top as follows:

- The ***Lower Visby Beds*** comprise 11 m of interbedded micritic limestone and marl beds rich in shelly benthic fossils, such as brachiopods and corals.
- The ***Upper Visby Beds*** are about 12 m thick and consist of micritic limestone and marl beds with common packstone and grainstone intercalations in the upper part.
- The ***Hogklint Beds*** consist of cross-bedded crinoidal grainstones and packstones that contain local stromatoporoid bioherms growing together near the top to form a biostromal platform (Neuman and Kershaw, 1991).
- The ***Tofta Limestones*** are 8 m thick, composed of oncolitic limestones and biostromes made of algae and stromatoporoids. The upper surface of this unit contains mud cracks indicating subaerial exposure. Furthermore, the Tofta limestone rests unconformably on the underlying Hogklint beds.

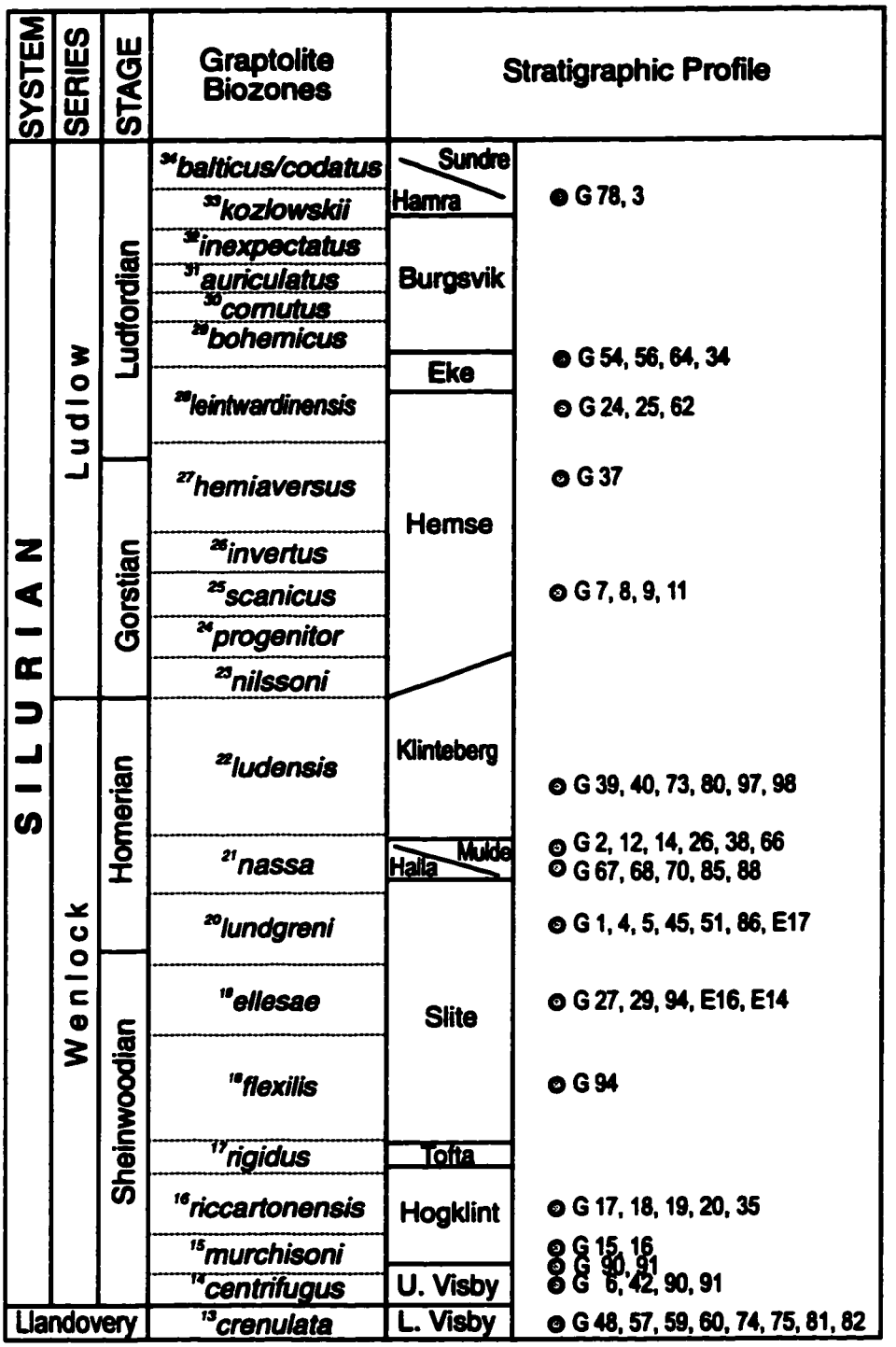

Fig. 2.9. Stratigraphic profile of the Silurian succession on Gotland, with the positions of samples annotated (modified from Bassett et al., 1989).

- The ***Slite Beds*** are about 100 m thick and consist of marine facies. Reef mounds and pelloidal limestones of very shallow water environments occur on the north-eastern part of the island, but they pass south-westward into more argillaceous sediments. The highest 5 m toward the south-west contain a unit of siliciclastic rippled sediments known as the Slite Siltstone.
- The ***Halla Beds*** are approximately 15 m thick and consist of shallow marine deposits, with oolites at the base, overlain by argillaceous limestones indicating a marginal marine to lagoonal environment. The Halla Beds rest disconformably on the Hogklint Beds.
- The ***Mulde Beds*** are the lateral equivalent, toward the west of the Halla beds. The former are about 20 m thick, consist of argillaceous and micritic limestones and marls and indicate undisturbed shelf basin conditions below wave base.
- The ***Klintberg Beds*** encompass 70 m thick reef mounds dominated by stromatoporoids, tabulate corals and bryozoans mantled by thick bedded crinoidal limestones. The mounds pass laterally north-eastward into a complex facies mosaic of bedded limestones rich in oncolitic algae.
- The ***Hemse Beds*** are ~100 m thick, with various carbonate lithologies. On northeastern Gotland, the Hemse Beds are stratified limestones rich in stromatoporoids and bivalve biostromes, whereas in the south they pass into graptolitic marlstones.
- The ***Eke Beds*** are 15 m thick, consisting of argillaceous limestones with marlstone alternations marked by a sharp increase in algae content.
- The ***Burgsvik Beds*** consist of fine grained, thickly bedded, calcareous to argillaceous sandstones with thin interbeds of shale and marl. In some places, the uppermost part

consists of oolitic limestones.

- The ***Hamra Beds*** are 40 m thick consisting of stratified limestones that pass upwards into argillaceous limestones and then into reefal and crinoidal beds. The beds become thinner towards the north-west where stromatoporoids become more dominant.
- The ***Sundre Beds*** are the youngest unit (late Llandovery) in the Silurian succession of Gotland. They consist of about 10 m of crinoidal limestone and stromatoporoid and algal reefs.

2.3.4. Chronostratigraphy

Chronostratigraphic correlation of the Silurian succession of Gotland with the standard Silurian graptolite biozonation scale is summarized in Figure 2.9. The subsurface succession, a mixed terrigenous/carbonate mud facies, extends downward into the Telychian, with the lowest exposed beds of the lower Visby assigned to the *crenulata* Biozone (Fig. 2.9). This dating was based on stricklandiid brachiopods and on the diagnostic coral *Paleocyclus porpita* (Bassett and Cocks, 1974).

The base of the Wenlock Series is correlated with the base of the upper Visby Beds, approximately at the *centrifugus/murchisoni* biozonal level. The Slite siltstones may correlate with the *lundgreni* Biozone. The *nilssoni* Biozone at the base of the Ludlow Series is recognized in the marls of the lower Hemse Beds (Fig. 2.9) (Bassett et al., 1989).

2.4. PODOLIA, UKRAINE

2.4.1. Location

The Dnestr Basin in Podolia (Fig. 2.10), Ukraine, is a site of Silurian-Devonian neritic deposits. It is located in the south-western part of the Russian Platform on the slope of the Ukrainian Shield. The outcrops, particularly those of the Přídolí Epoch, extend along the Dnestr River as accessible and well-exposed complete sections (Nikiforova and Predtechensky, 1968). The Silurian deposits of the Podolian paleobasin are believed to have accumulated in a pericontinental sea that was an integral part of the 800 km long and about 200 km wide Mid-European geosyncline (Koren et al., 1989). Due to the undisturbed nature and completeness of the Podolian sequence, it was proposed as a stratotype for the Silurian-Devonian boundary.

2.4.2. Lithostratigraphy

The earliest stratigraphy of the Podolian Silurian deposits was proposed by Kozlowsky (1929) and was based on brachiopods. A subsequent, brachiopod-based, detailed biostratigraphic study for the entire Silurian succession of Podolia was published by Nikiforova (1948, 1954). Her stratigraphic framework has been progressively refined by a team of geologists from the VSEGEI and other institutions of the former USSR (e.g. Balashov, 1968; Abushik, 1971; Nikiforova et al., 1972; Kaljo et al., 1982; Predtechensky et al., 1983; Koren et al., 1989). This stratigraphic scheme is utilized in the present study (Fig. 2.11).

Samples covering the Přídolí (Rashkov and Dzwinogorod formations) were collected in the field in Podolia and a few additional samples were obtained from the National Museum of Wales, Cardiff. The latter were assigned to graptolite biozones by M. G. Bassett (personal

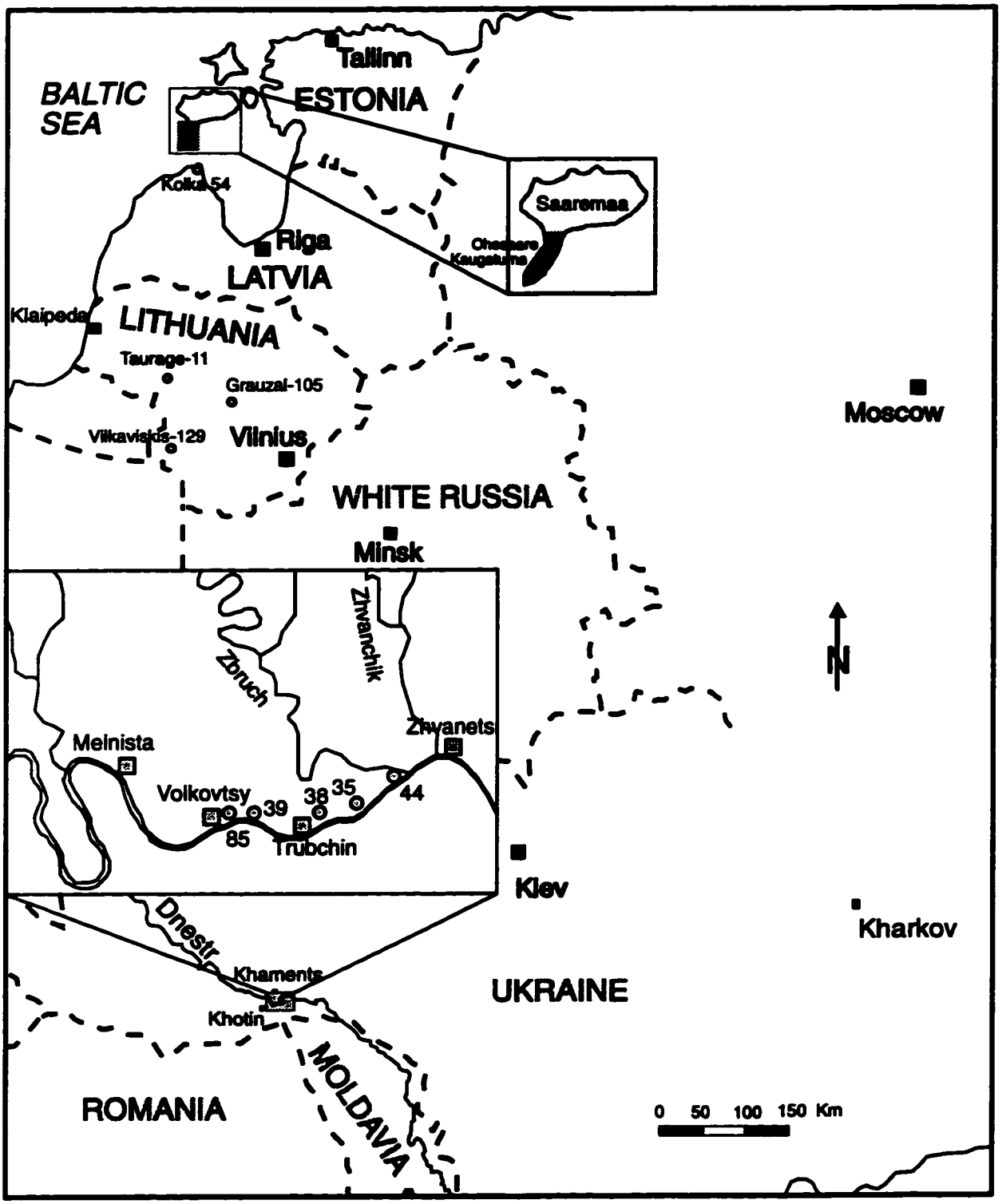

Fig. 2.10. Map of the studied areas in the Baltic states (Estonia, Latvia and Lithuania) and the Ukraine (Podolia) showing the location of sampled successions and subsurface cores (modified from Nikiforova and Predtechensky, 1968; Brazauskas and Musteikis, 1990; and Kaljo, pers. comm., 1994).

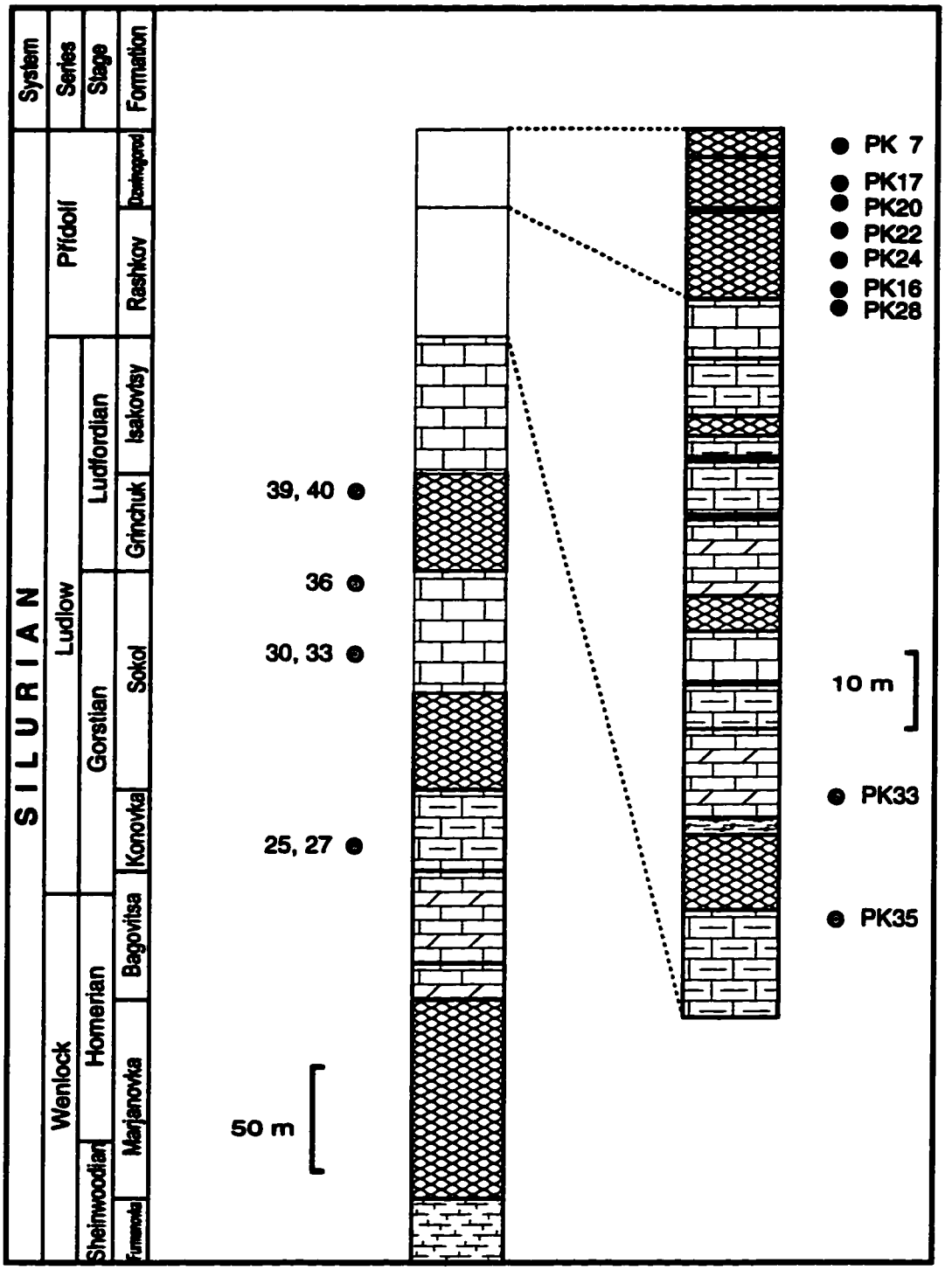

Fig. 2.11. Lithostratigraphy of the Silurian succession in the Podolian basin, with the positions of samples indicated on the stratigraphic log. Legend as in Figure 2.2b (modified from Nikiforova and Predtechensky, 1968 and Koren et al., 1989).

communication, 1995). This sample collection covers the lower Wenlock (*murchisoni* Biozone), lower Ludlow (*nilssoni* Biozone), middle Ludlow (*hemiaversus* and *leintwardinensis* biozones) and upper Ludlow (*auriculatus* Biozone) (Figs. 2.11 and 2.12). The description of the entire succession was reviewed by Koren et al. (1989) and is summarized, from bottom to top, as follows:

- The ***Furmanovka Formation*** (up to 26 m) includes the Restevo (lower) and Demshin (upper) members. The Restevo Member is characterized by fine grained limestones and marls of the outer shelf environments, whereas the Demshin Member consists of shallow water nodular limestones.
- The ***Marjanokova Formation*** (~ 60 m) consists of the Vrublevtsy, Sursha and Cherche Members, all mainly nodular and argillaceous limestones of platform environments. Sediments are rich in fossils and brachiopods are common.
- The ***Bagovitsa Formation*** (up to 54 m) includes the Muksha (lower) and Ustje (upper) members. The lower member is dominated by limestones and marls, whereas the upper member is composed of dolomitic limestones, dolomite and dolomitic marls of lagoonal origin.
- The **Konovka Formation** (up to 31 m) consists of argillaceous limestones of open shelf environments with bioherms of algae and stromatoporoids in the lower part. Dolomite and marls of lagoonal environments occur in some places.
- The ***Sokol Formation*** (~ 40 m), in its lower part consists of nodular limestones of open shelf environments that contain metabentonites, and in the upper part of tabular limestone rich in corals and stromatoporoids.

- The ***Grinchuck Formation*** (up to 24 m) is composed of layered nodular fossiliferous limestones with tempestites of a typical shallow open shelf environments.
- The ***Isakovtsy Formation*** (6 to 9 m) is formed of shoal limestones overlain by lagoonal dolomite.
- The ***Prigorodok Formation*** is typically unfossiliferous lagoonal dolomitic marl with gypsiferous interbeds and stromatolitic beds at the top.
- The ***Rashkov Formation*** (94 to 106 m) is well exposed and well correlated along the Dnestr River (Fig. 2.10) at the Okopy Village (outcrop 44), Belovtsy (outcrop 35), Trobchin (outcrop 38) and Dzwinogorod (outcrop 39) and contains two members: the Varnitsa (lower) Member: (Fig. 2.11) consists of stromatoporoid limestones that alternate with dolomite, dolomitic marl and nodular limestone, and was probably deposited in outer and inner shelf environments. Stromatoporoids, ostracodes and rugose corals are abundant, while brachiopods are less frequent (Nikiforova and Predtechensky, 1968; Koren et al., 1989); the Trobchin (upper) Member is composed mainly of limestone, with ostracodes, stromatoporoids and algae, and some interbedded dolomites. The member contains two bentonite layers (Koren et al., 1989).
- The **Dzwinogorod Formation** (up to 30 m) represents the top unit of the Přídolí Series in Podolia and is composed mainly of carbonate deposits. It is geographically limited to well exposed sections at Dzwinogorod (outcrop 85) and Volkovtsy Village (outcrop 64) (Fig. 2.10). The formation is composed mainly of nodular limestones and marls, with bentonite interbeds that can be seen in the upper part as clay bands (Nikiforova and Predtechensky, 1968). Stromatoporoids, rugose corals, bryozoa, nautiloids, brachiopods

and trilobites are frequent. *Daya navicula bohemica* is one of the fossils that characterize this part of the section (Nikiforova and Predtechensky, 1968; Abushik et al., 1985). The faunal assemblage in the upper part of the Dzwinogorod Formation indicates deeper water conditions (Koren et al., 1989).

2.4.3. Chronostratigraphy

The studied benthic fauna was utilized to correlate the Silurian sequence in Podolia with the standard Silurian stratigraphy (Fig. 2.12). Unit boundaries are based on comparative analysis of fauna including conodonts, brachiopods, tabulate corals, and graptolites where available. The biostratigraphic correlation was discussed in detail by several authors (see Koren et al., 1989 for further references) and is summarized in Fig. 2.12.

2.5. THE BALTIC REGION

The sediment fill in the Baltic basin covers a time span ranging from Cambrian to Mesozoic. The Silurian deposits in this basin indicate relatively shallow marine conditions. The basin rests on a basement of Precambrian continental crust, dipping a few degrees towards the south.

The Silurian rocks crop out mainly in two areas, on Gotland and on the eastern Baltic coast on islands of Estonia (Fig. 2.10), where well exposed, carbonate-dominated successions occur.

An extensive drilling project, started in 1940 throughout the Baltic region, provided a comprehensive picture of the subsurface distribution of Silurian deposits from Estonia to Latvia and Lithuania (see Flodén, 1980 and Bassett et al., 1989 and references therein). This knowledge contributed to the resolution of Silurian stratigraphical problems and to the correlation of

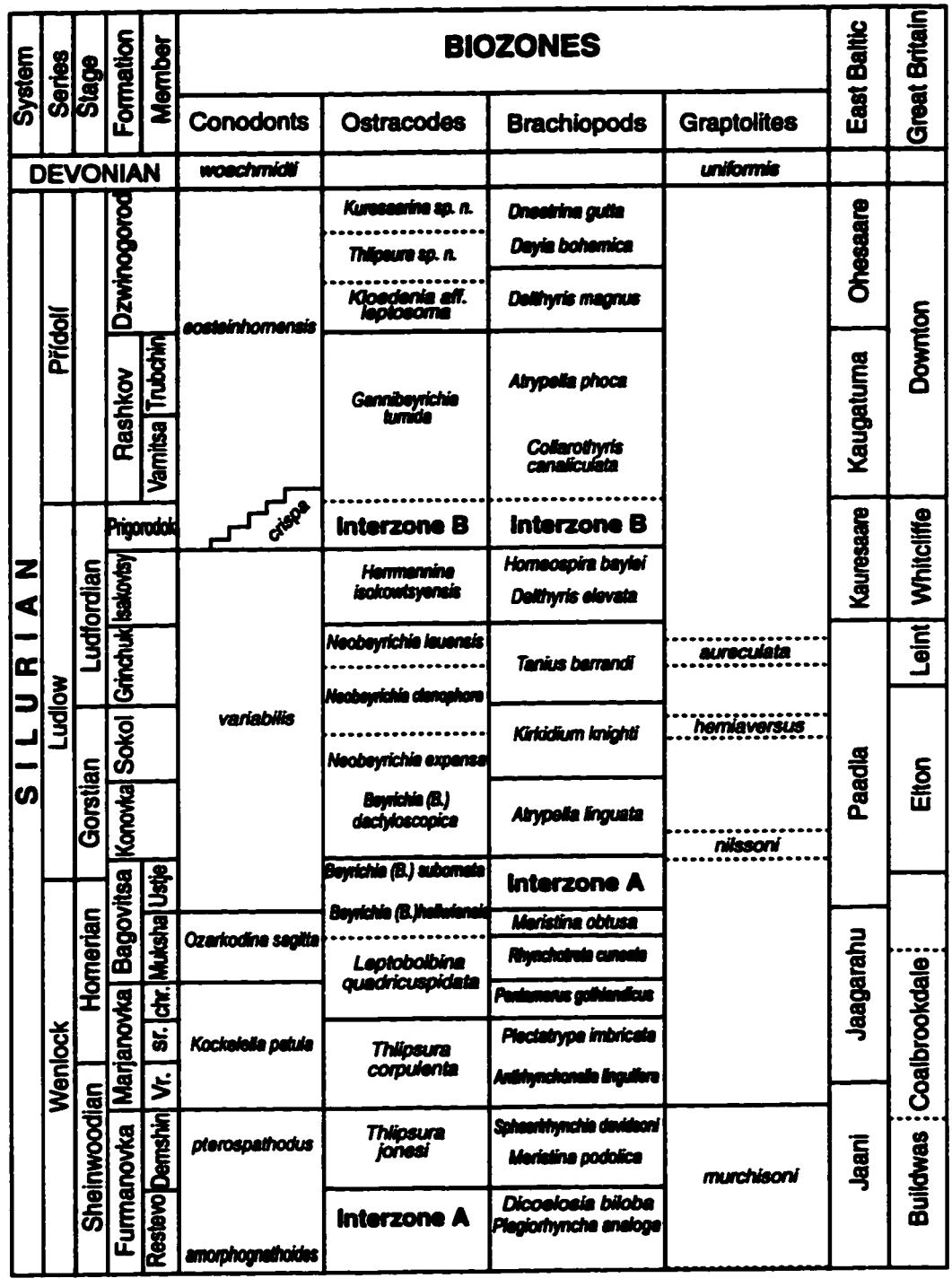

Fig. 2.12. Chronostratigraphy and biostratigraphy of the Silurian section in Podolia and its correlation with the Baltic states and Great Britain (after Bassett et al., 1989 and Koren et al., 1989).

onshore shelly successions of platforms with offshore mud-dominated (graptolite-rich) successions.

Lithostratigraphic classifications of the Silurian successions in the Baltic states have been established independently over many years and this might be the reason for inconsistencies in nomenclature. The detailed stratigraphy is based on paleontological criteria that define the "horizon" of Soviet usage (Grigelis, 1978). These were later regarded to be Regional Stages (Bassett et al., 1989). For instance, the later discussed Minija and Jura stages of the Přídolí in Lithuania are considered to be stages in local usage, but they are not standard chronostratigraphic units. Nevertheless, these non-standard divisions facilitate correlation and interpretation of the regional events in the area.

During the Silurian Period, the Baltic basin was located in the paleocontinental mass of Baltica. Paleogeographic data show that, during early to mid-Silurian times, Baltica was located in southern tropical to equatorial paleolatitudes, moving to the northern tropics by the end of the period (McKerrow et al., 1991). As a result, the climate became relatively more arid. The abundance of carbonates and of fine-grained terrigenous sediments in the Silurian deposits of the Baltic basin indicates extensive coastal plains and low-relief lands.

The selection of cores for examination in this study was made after a discussion with Estonian and Lithuanian paleontologists and was based on the completeness of the succession and the availability of brachiopod samples. They cover the Přídolí Series in Estonia, Lithuania and Latvia and the Wenlock Series in Lithuania.

2.5.1. Sórve Peninsula, Estonia (Přídolí)

2.5.1.1. Location

The Přídolí Series in Estonia is exposed on Sórve Peninsula, Estonia (Fig. 2.10). The Upper Přídolí is exposed at the Ohesaare Cliff, located on the western coast of the peninsula near Ohesaare village. The Ohesaare cliff represents a stratotype for the Ohesaare Stage in the east Baltic area (Pander, 1856; Nestor, 1990). The Lower Přídolí is exposed at the Kaugatuma Cliff, located on the same coast, a few kilometres southward from the neck of the peninsula, about 100 m from the sea.

2.5.1.2. Lithostratigraphy

The stratigraphy of the Ohesaare section (Fig. 2.13) was studied and refined by many authors (cf. Nestor, 1990). Its 3.5 to 4 m high outcrops extend ~ 600 m along the coast. The section is characterized by intercalated thinly bedded limestones and marlstones. Skeletal grainstones constitute the top and the bottom layers of the section, with skeletal packstone in the middle. This packstone includes a few lenses of cross-bedded pelletal grainstone. Dolomitization is noticeable in the upper beds and the uppermost top of the section contains a 0.2 m-thick layer of cross-bedded fissile calcareous siltstone.

Kaugatuma Cliff consists mainly of two units. The lower unit is a 0.5 m thick, and consists of unsorted skeletal wackestone deposited in an open shelf environment. The skeletal debris is mainly fragments of brachiopods, crinoids, ostracodes, trilobites, gastropods and bryozoans. The upper unit is 1.5 m thick and consists of crinoidal grainstone of a forereef environment. Some bedding planes in this unit show erosional features (Einasto, 1990). The sedimentary facies of

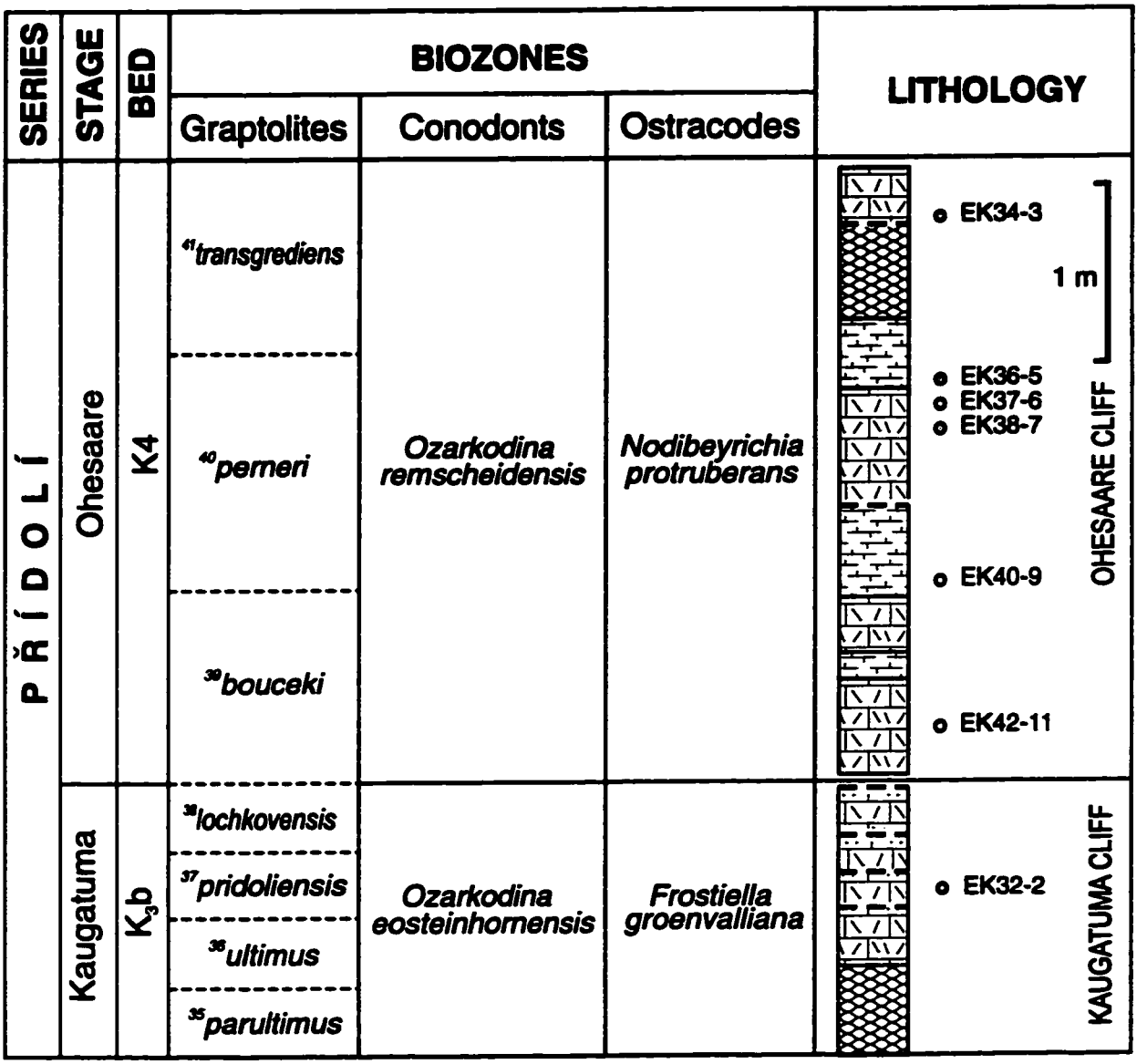

Fig. 2.13. Lithostratigraphy and chronostratigraphy of the Pridolian sequence in Estonia, with positions of samples indicated on the stratigraphic log. Legend as in Figure 2.2b (modified from Bassett et al., 1989 and Kaljo, 1990).

the upper and lower parts of the section (skeletal grainstones) indicate high-energy shoal depositional environments, while the middle part (skeletal packstones and marls) indicate an open shelf setting.

2.5.1.3. Chronostratigraphy

The Ohesaare Cliff section is rich in shelly fauna, such as brachiopods (*Delthyris magna, Delthyris elevata, Hoenoeospira baylei, Isorthis ovalis*), trilobites (*Calymene soervensis*), corals (*Favosites forbesi*), and stromatoporoids (Nestor, 1990). Shelly fauna is common also in the Kaugatuma Cliff section and includes tabulate corals (*Syringopora blanda*) and trilobites (*Calymene schmidti*). Some vertebrate remains are present as well (Einasto, 1990).

The Kaugatuma Stage covers the lower Přídolí (Fig. 2.13). Its base, the Ludlow-Přídolí boundary, is taken as the first appearance of the conodont *Ozarkodina eosteinhornensis*, and the ostracod *Frostiella groenvalliana* (Jeppsson et al., 1994; Kaljo, 1990). The top of this stage, the Kaugatuma-Ohesaare stage boundary, is taken as the first appearance of the conodont *Ozarkodina remscheidensis* and the ostracod *Nodibeyrichia protruberans*. In southeastern Estonia, graptolites (*Monograptus ultimus*) have been recovered only rarely from the basal beds of the Ohesaare Stage (Kaljo, 1990).

2.5.2. Lituania and Latvia

2.5.2.1. Location

Unlike in Estonia, the Přídolí Series is not exposed in either Lithuania or Latvia, but it has been studied in the boreholes Tauragė-11 (Lithuania) and Kolka-54 (Latvia), located in western Lithuania and northern Latvia, respectively (Fig. 2.10). The Wenlock Series of Lithuania is represented by two stages, the Gèluva Stage and the Riga Stage, named locally after the Gèluva and the Riga formations (Lapinskas et al., 1985, as referred to in Paškevičius et al., 1994). These Wenlock stages were covered by sampling two boreholes, Graužai- 105 and Vilkaviškis- 129,

located in central Lithuania (Fig. 2.10). These two cores show no unconformities in the succession which makes them suitable for isotope stratigraphy. In addition, the clayey facies are abundant and they are rich in graptolites and shelly benthic fauna. Despite lateral variations in lithology and problems of nomenclature, the graptolite content makes correlation with the standard Silurian stratigraphic scale easier and reliable.

2.5.2.2. Lithostratigraphy

The lithostratigraphy of the boreholes is described in detail in Paškevičius et al. (1994) but it will be discussed briefly in this text. The Přídolí Series in both Lithuania and Latvia includes two formations, referred to as stages in local nomenclature. The sequence is represented by open marine clayey facies with limestones rich in shelly fossils, such as brachiopods, bivalves, gastropods, ostracodes, conodonts, trilobites and vertebrates.

Riga Stage

The Wenlock Riga Stage (Fig. 2.15) is mainly represented by clayey, slightly dolomitic marlstones with interbeds or nodules of limestone. No significant lateral change is reported.

Gèluva Stage

The lithology of the Wenlock Gèluva Stage rocks (Fig. 2.15) varies laterally. In central Lithuania, this stage is represented by the Siesartis Formation (Gèluva Formation equivalent), mainly dark grey to black thinly-laminated argillite with limestone nodules in the middle part. Laminated marl and microcrystalline clayey limestone occur in the lower part of the formation.

However, in southern Lithuania, the upper part changes into grey marl and the middle part into skeletal clayey limestone. The lower part varies from nodular grey marl to dolomitic marl in the east to sandy limestone in the west of Lithuania (Paškevičius et al., 1994).

Minjia Formation (Stage)

The Minija Formation consists of greenish gray clays with interbeds of microcrystalline and detrital limestones. It may contain some reefal carbonates and rare dolomitic marl layers (Paškevičius et al., 1994). This stage (formation) is correlated with the lower part of the Kaugatuma Stage of Estonia (Fig. 2.14).

Jūra Formation (Stage)

The Přídolí Jūra Formation is represented by clayey open marine facies in the west and carbonaceous clayey lagoonal facies with some dolomitization in eastern and northern Lithuania. Lithologically, the rocks are generally greenish grey clays with microcrystalline limestone interbeds. Their carbonate content increases upwards (Paškevičius et al., 1994). The Jūra Formation commenced with a transgressive cycle, indicated by the high clay content, but ended with a regressive cycle characterized by a lesser clay but a higher carbonate content.

2.5.2.3. Chronostratigraphy

The lower boundary of the Minija Formation (Fig. 2.14) is taken as the first appearance of the *parultimus* graptolite Biozone which occupies a narrow vertical interval in the succession. This makes it a good datum. In addition, in many sections, the lower boundary of the Minija

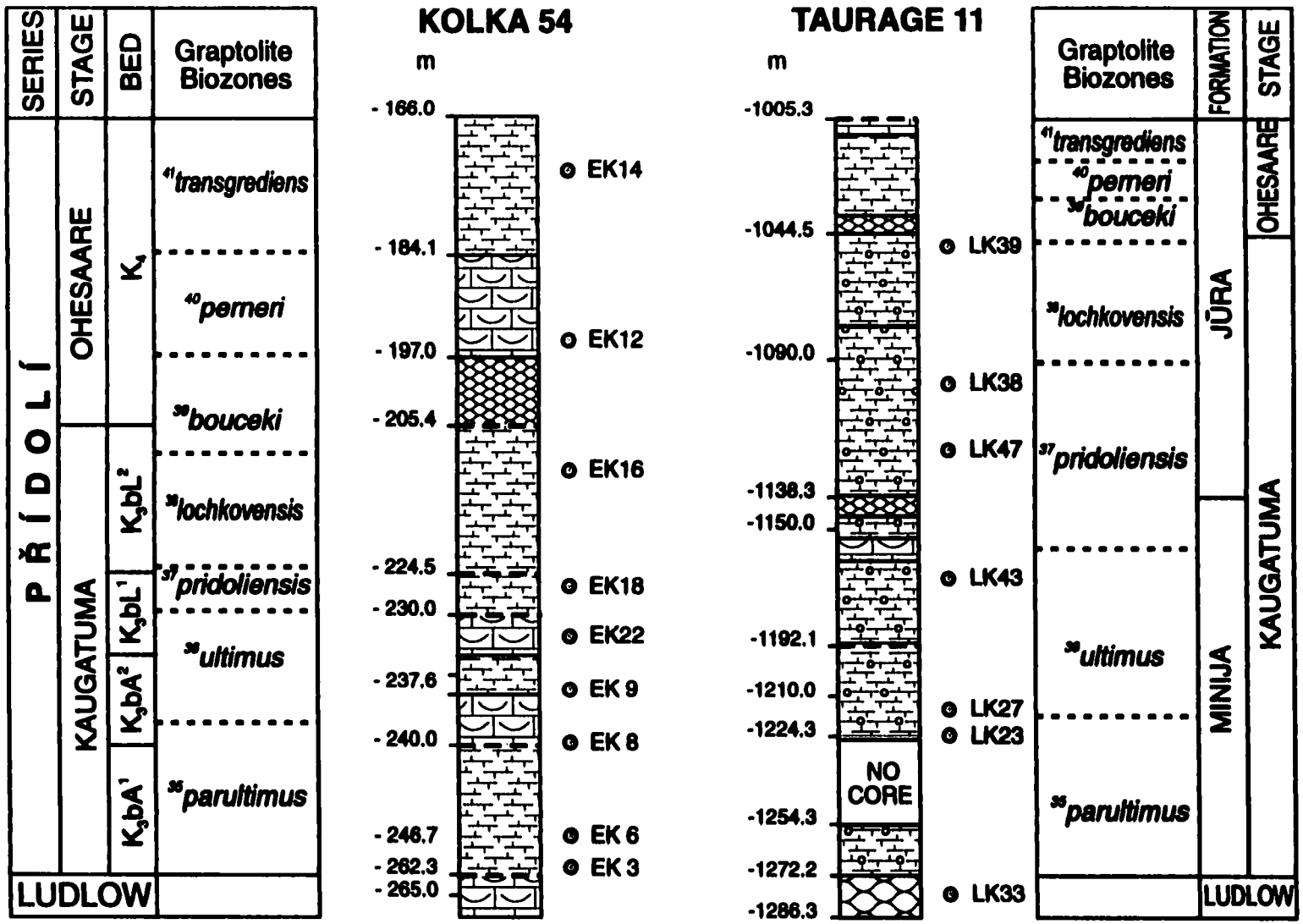

Fig. 2.14. Stratigraphic subdivisions of the Přídolí Series in Latvia (core Kolka 54) and Lithuania (core Taurage 11) showing the relative positions of samples. Legend as in Figure 2.2b. Location of cores is shown in Figure 2.10 (modified from Kaminskas and Musteikis, 1994 and Kaljo, pers. comm., 1994).

Formation coincides with the base of the *eosteinhornensis* conodont Biozone.

The lower boundary of the Jūra Formation is marked by the *latviensis* ostracode Biozone and the vertebrate *punctatus* Biozone. Its upper boundary, also the Přídolí/Devonian boundary, is marked by the appearance of characteristic Devonian vertebrates, such as *Turinia pagei* (Paškevičius et al., 1994).

The Minija Stage (Formation) is correlated with the lower part of the Kaugatuma Stage and the Ohesaare Stage of Saarema Island (Fig. 2.13) in Estonia (Bassett et al., 1989, Paškevičius et al., 1994).

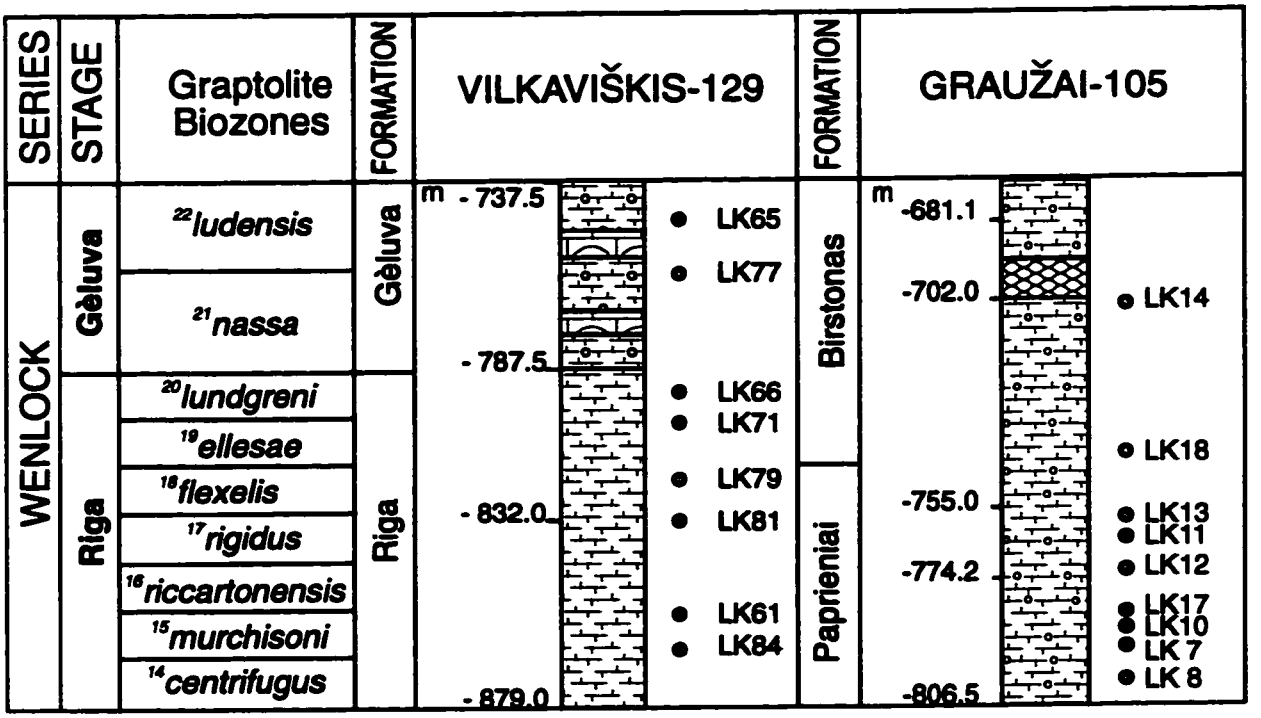

Fig. 2.15. Lithostratigraphy and chronostratigraphy of the Wenlock Series in Lithuania with the positions of samples indicated on the cores Vilkaviškis-129 and Graužai-105 in Lithuania. Core locations are shown in Figure 2.10. Legend as in Figure 2.2b (modified from Kaminskas and Musteikis, 1994).

The graptolite content of the rocks shows that the Gèluva Stage includes the *nassa* and *ludensis* biozones (Fig. 2.15) and its lower boundary, which is also the upper boundary of the Riga Stage, coincides with the base of the former biozone (Paškevičius, 1979 in Paškevičius et al., 1994). This stage may correspond to the British Gleedonian Chron of the upper Homerian Stage. The lower boundary of the Riga Stage is taken as the base of the *centrifugus* Biozone (Bassett et al., 1989).

CHAPTER III

BRACHIOPODS AND THEIR SHELLS

3.1. BRACHIOPOD CALCITE SHELLS

Inorganic and biogenic carbonate components, calcareous shells and cements, all have been utilized for reconstruction of ancient marine isotopic signatures and these, in turn, served as constraints for development of paleoceanographic scenarios (e.g. Brenchley et al., 1995). Paleozoic brachiopod shells have been emerging as particularly suitable material for the above purposes (e.g. Lohmann, 1983; Popp et al., 1986) for several reasons:

3.1.1. Spatial and Environmental Distribution

Brachiopods are common in most carbonate sequences through the Paleozoic where they have been used as bathymetric and environmental indicators (e.g. Ziegler 1965; Ziegler et al., 1968). Paleozoic brachiopods lived in most shelf environments, but they were more abundant in shallow warm waters of carbonate platforms. In contrast, Recent counterparts live at various depths and are more characteristic of temperate climatic zones(Clarkson, 1993).

3.1.2 Shell Thickness

Fossil brachiopod shells are usually thick enough to be sampled easily for geochemical analysis. In this work, a chip of a fossil shell was placed under a binocular microscope, the thin outer primary layer (usually altered) removed, and the thicker well preserved inner secondary layer sampled. The thickness of the shell is usually proportional to the brachiopod size, being thickest (~ 0.5 to 2 mm) around the umbo area. Some species, such as strophomenids, had only thin shells

(~ 0.2 mm) and were hard to sample; these were sampled very carefully in order to avoid contamination from the primary layer or from internal sediment. In contrast to strophomenids, spiriferids (particularly the atrypoids) had the thickest shells of all Silurian brachiopods examined in this study.

Selective sampling of only the well preserved parts of shells is not always possible for fossils of other organism groups, such as foraminifers, because their shells are usually very thin.

3.1.3. Shell Structure

The shells of fossil brachiopods typically have two calcitic layers, a primary granular and a secondary prismatic layer (Williams et al., 1965). The compact pattern of stacking of calcite fibres in the secondary layer may restrict penetration of such fluids, keeping the fibres unaltered.

3.1.4. Shell Mineralogy

Articulate brachiopods build their shells from low-Mg calcite, but some inarticulate ones have phosphatic shells. Recent brachiopod shell calcite contains about 0.5 to 7 mole% $MgCO_3$ (Lowenstam, 1961; Morrison and Brand, 1986) and ancient counterparts had likely a comparable mineralogical composition (cf. Veizer et al., in press). The low-Mg calcite is a relatively stable mineralogical phase that usually, but not always, resists alteration (Popp et al., 1986; Rush and Chafetz, 1990; Qing and Veizer, 1994).

The calcitic brachiopod shells provide suitable material not only for the C- and O-isotope studies but also for Sr-isotope work. Some researchers believed that the phosphatic shells of conodonts should be less susceptible to diagenetic alteration than the low-Mg calcite shells of

brachiopods (e.g. Bertram et al., 1992), but a comparative study based on Devonian specimens (Diener et al., 1996) has shown that the latter retained a better preserved seawater Sr-isotope signal.

3.2. BRACHIOPOD HABITAT

Brachiopods are benthic marine animals whose soft parts are enclosed within a two-valved shell and the shell is fixed to the sea floor by a stalk or pedicle. The internal soft parts include a complex food-trapping mechanism called the lophophore that filters food from the water sucked into the shell. Although modern brachiopods inhabit both warm shallow (New Zealand) and cold deep (British Isles) marine waters (Clarkson, 1993), Paleozoic brachiopods inhabited mainly warm shallow seas and many are associated with reefs that were characteristic of warm water environments with normal salinity. Despite the fact that brachiopods are typically benthic marine animals that inhabit aerobic environments and normal salinity waters, some Recent brachiopod genera were found inhabiting dysaerobic hypersaline and brackish environments (Bates and Brand, 1991). The two valves of the shell have different sizes but they are symmetrical in shape. The bigger valve carries the pedicle and is called the pedicle valve, whereas the other one is called the brachial valve. Based on the method of attachment of the two valves, the Phylum Brachiopoda is classified into two classes:

(a) Class Inarticulata: in genera such as *Lingula*, the two valves are not hinged by teeth and sockets and the shell is usually chitinophosphatic, but rarely calcitic. Some shells do not have the pedicle and they may fix themselves to the substrate by cementation. The class Inarticulata encompasses four orders of brachiopods.

(b) Class Articulata: the two valves of the shell are hinged by teeth in the pedicle valve and sockets in the brachial valve. The shell is calcareous and the pedicle is made of dead horny material. The articulate brachiopods are more advanced and diverse than the inarticulate ones. Seven orders are categorized under Class Articulata (Clarkson, 1993).

3.3. SHELL MICROSTRUCTURE

The brachiopod shell grows by secreting new material from the mantle at the valve edges and the shape of the shell is therefore a function of the relative growth rates at different valve edges (Rudwick, 1959). In all living articulate brachiopods, three shell layers can be distinguished: an outer non-calcareous periostracum, a middle calcareous primary layer and an inner calcareous secondary layer (Fig. 3.1). The calcareous layers are secreted as low-Mg calcite near or in isotopic equilibrium with ambient sea water (Carpenter and Lohmann, 1995). The primary shell layer beneath the periostracum is formed of fine granular or structureless crystalline calcite, whereas the secondary layer consists of distinctive enlarged regularly stacked calcite fibres (prisms) which are at an angle to the shell surface (McKinnon, 1974).

In fossil brachiopods, the outermost layer (periostracum) is always absent because it is made of organic matter that easily decays. The primary layer is normally no more than a few microns thick and is therefore commonly recrystallized, merging with micrite of the enclosing carbonate matrix. The secondary inner layer is composed of fibrous low-Mg calcite that is usually well preserved and therefore retains the original isotopic signal (Popp et al., 1986; Veizer et al., in press).

This succession, of organic periostracum followed by the mineral primary and secondary layers, is the predominant fabric of articulate brachiopods, but in some pentamerids and spiriferids an additional tertiary prismatic layer is secreted (McKinnon, 1974).

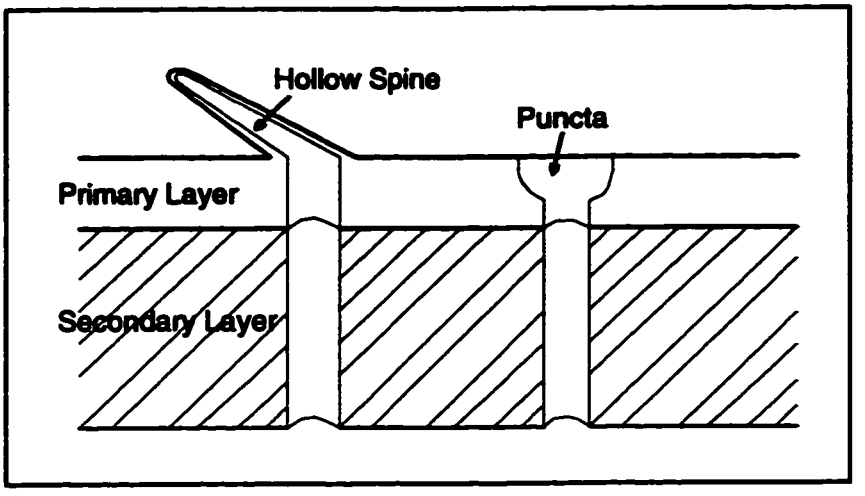

Fig. 3.1. Schematic diagram showing brachiopod shell microstructure.

Shells of some articulate brachiopods are **impunctate,** with no perforations through the shell structure, while others are **endopunctate,** with the shell penetrated by regularly arranged tube-shaped cavities called **punctae**. These punctae - in 0.05 to 0.1 mm intervals - are arranged normal to the shell surface (Fig. 3.1).

In living animals, the punctae contain **caecae** which are tubular overgrowths of the mantle that are formed at the edge of the shell during shell secretion. As the edge grows, the caecae stay in their positions and may switch to a respiratory function.

In fossil brachiopods, the caecae have decomposed and the punctae are filled with secondary minerals (usually calcite). In some shells, angled rods called taleolae penetrate the inner layer of the shell and such shells are called **pseudopunctate**. However, punctation is not the only cause of shell perforation, because some brachiopod species have hollow spines that are continuous

with perforations through the entire shell.

Most orthids, spiriferids and rhynchonellids and all atrypids and pentamerids are impunctate (Williams et al., 1965; Clarkson, 1993). The majority of the Silurian brachiopods analysed in this study were intentionally selected for their impunctate shells in order to avoid post-depositional contamination by secondary calcite. Nevertheless, some punctate shells were examined for comparative purposes.

3.4. SHELL PRESERVATION: MICROSCOPIC ASSESSMENT

Diagenetic alteration of marine carbonates is a major problem for Paleozoic samples, because it distorts the original isotope signal and this may result in inaccurate application of paleothermometry or in false paleoclimatic interpretations. It is therefore necessary to consider the state of shell preservation prior to interpretation of ancient marine environments. Diagenesis of marine carbonates in meteoric, marine or burial environments results generally in trends towards higher Mn and Fe contents and lower Na, Sr, $\delta^{18}O$ and $\delta^{13}C$ values (Veizer, 1983a,b; Popp et al., 1986). To ensure that the studied brachiopod shells were well preserved, the following sequential procedure was applied to the samples:

(1) shell microstructure was examined in thin sections using the standard polarizing microscope, luminoscope (CL) and scanning electron microscope (SEM), in order to detect the evidence of any diagenetic textural changes,

(2) trace element composition of the shells was measured and compared with those of the closest modern counterparts, and

(3) the acquired $\delta^{18}O$ and $\delta^{13}C$ values were compared with other coeval samples.

3.4.1. Transmitted Light Microscopy

Thin sections of the brachiopod shells were studied under the standard polarizing microscope for a preliminary determination of the state of preservation of calcite prisms in the secondary layer. Diagenetic alteration, caused by dissolution-precipitation reactions, usually results in deformation of the crystal structure (Fig. 3.2A,B). This was observed in some shells from successions that show features of some diagenetic alteration, such as the slight dolomitization that affects the Přídolí sequences in Podolia and in the Baltic region. Yet, despite these textural changes, trace element concentrations of the studied brachiopods fall within the range of those for their modern counterparts, suggesting that the recrystallization phenomenon in the shells was either of limited extent and/or that it occurred in a relatively closed diagenetic system.

Disseminated pyrite is common in the studied shells as a secondary mineral, likely resulting from bacterial decomposition. Pyrite occurs in the shell in two patterns: (1) disseminated grains in fibrous calcite of the secondary layer and/or in the internal sediments, and (2) rarely as filling of microcracks (Fig. 3.3A,B).

Micro-structures, such as punctation in the punctate shells, can be seen clearly under the standard microscope, with punctae visible as long tiny tubes filled with secondary calcite that cut through the shell layers (Fig. 3.4A).

3.4.2. Cathodoluminescence Petrography (CL)

Cathodoluminescence can be used for rapid evaluation of the degree of preservation of brachiopod shells (Popp et al., 1986; Rush and Chafetz, 1990). The technical background is discussed in detail in Appendix 1. The theoretical principles of the technique are based on

observation that the presence of high Mn^{2+} concentrations in the carbonate lattice activates the luminescence, whereas Fe^{2+} has the opposite effect. As a result, the luminescence of the sample is not simply a reflection of its Mn^{2+} or Fe^{2+} concentration, but also of Mn^{2+}/Fe^{2+} ratio, of other elements in the lattice, and of the rate of precipitation (Machel 1985; Bruhn et al., 1994).

However, non-luminescence and low Mn and Fe concentrations of calcite are not definitive proof of good preservation of the fossil shell in terms of chemical attributes. Diagenetic fluids of high pH may have low Mn and Fe contents and can cause shell alteration without adding any of these elements to the secondary calcite lattice. Such fluids can even precipitate non-luminescent, Mn- and Fe-poor, secondary cements. This may be an explanation for observations of Rush and Chafetz (1990) who noticed depleted $\delta^{18}O$ and $\delta^{13}C$ signals in Devonian non-luminescent brachiopod shells, with values decreasing upsection towards an exposure surface, suggesting an alteration caused by Mn-poor fluids. A similar relationship was observed also by Plocher et al. (1992).

As a result, some brachiopods with destroyed microstructure appear non-luminescent under the luminoscope. On the other hand, shells originating in a low Eh and pH environment might incorporate high concentrations of Mn into the primary calcite lattice that causes the shell to exhibit bright luminescence. In summary, non-luminescence alone is not a proof of good preservation, but in combination with other tests, such as the SEM and trace element analysis, it is helpful in evaluation of shell preservation.

Under the luminoscope, the primary layer of fossil brachiopod shells, if present, usually appears brightly luminescent due to its alteration and this is the case also for the internal sediments, matrix and cements (Figs. 3.3B, 3.5). During separation of brachiopods from the enclosing rocks,

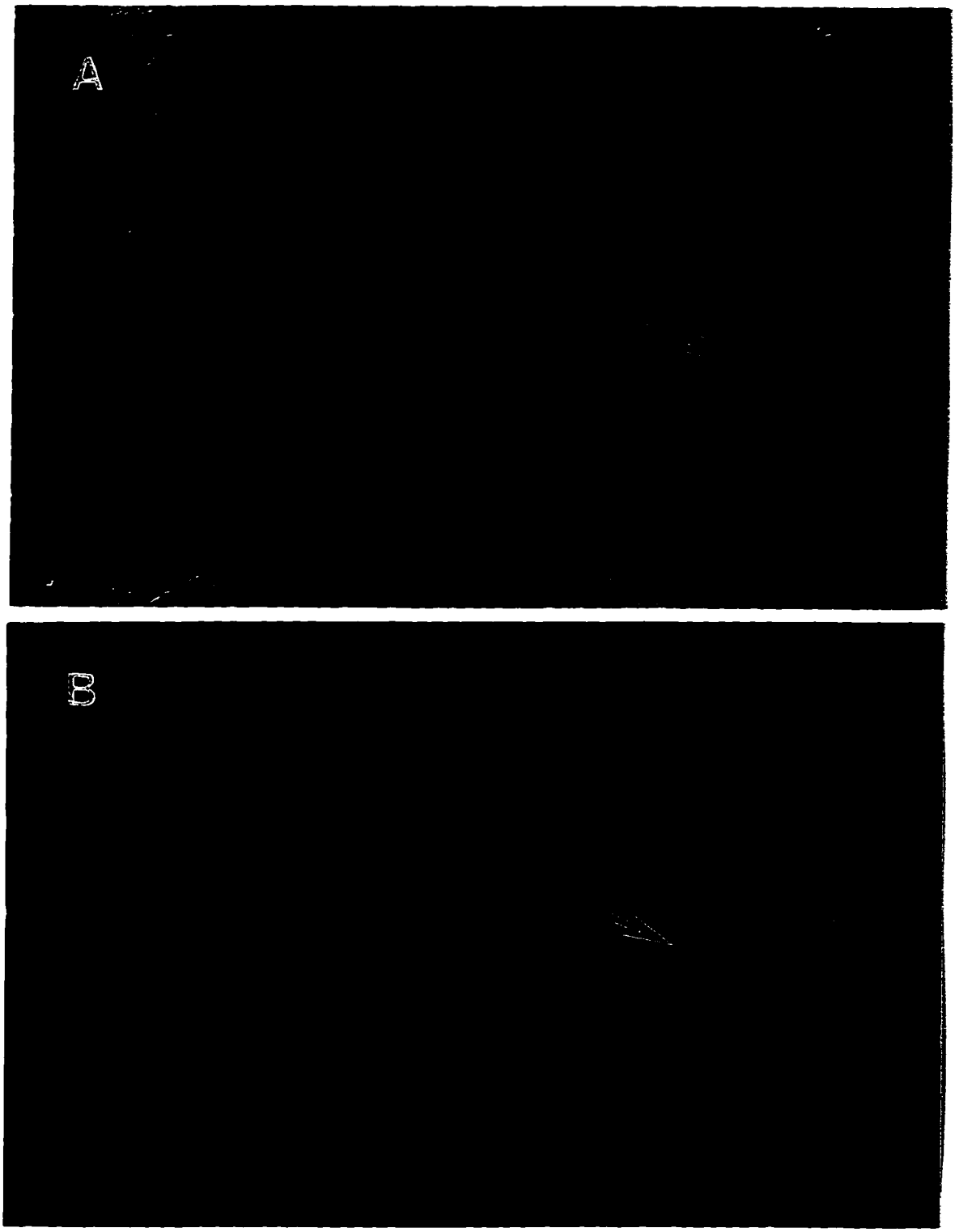

Fig. 3.2. Photomicrographs of secondary layer in shell of *Atrypa* sp. (sample PK22). (A) Calcite fibres (arrow) are partially deformed by alteration (to right) and (B) the altered fibres exhibit bright luminescence while the preserved ones (to left) are dull. Field of view is 1 mm across.

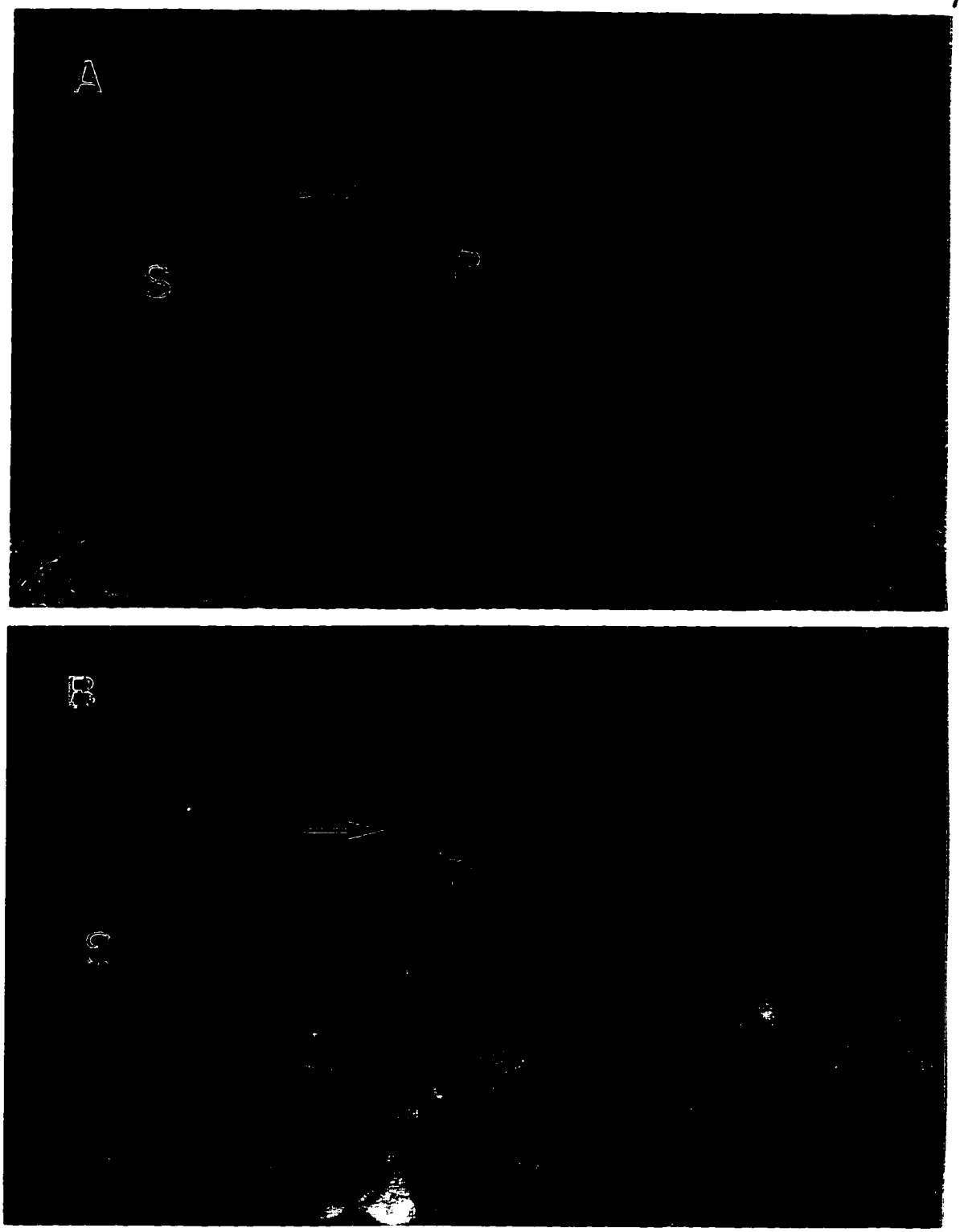

Fig. 3.3. Photomicrographs of a thin section of the secondary layer (S) in a shell of *Atrypa* sp. (sample LK65). (A) Disseminated pyrite (P) appears as black dots along microcracks (arrows) running through preserved calcite fibres, and (B) the same secondary layer exhibiting dull luminescence, compared to the bright luminescence internal sediments. Field of view is 1 mm across.

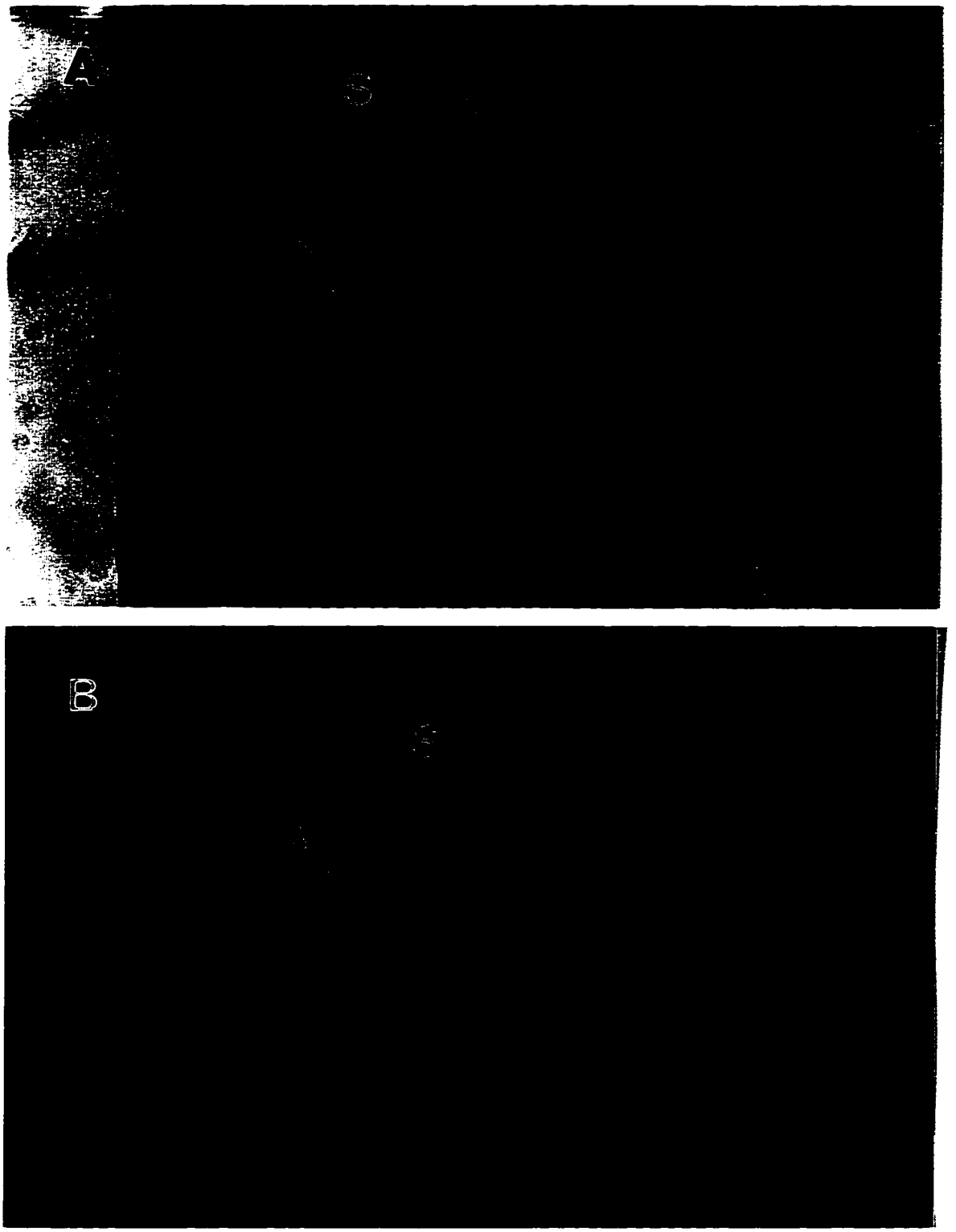

Fig. 3.4. Photomicrographs of a thin section of the secondary layer (S) in a punctate shell of *Isorthis* sp. (sample LK33). (A) Punctae (arrow) penetrate the preserved shell, and (B) secondary calcite (arrow) filling the punctae exhibit bright luminescence. Field of view is 1 mm across.

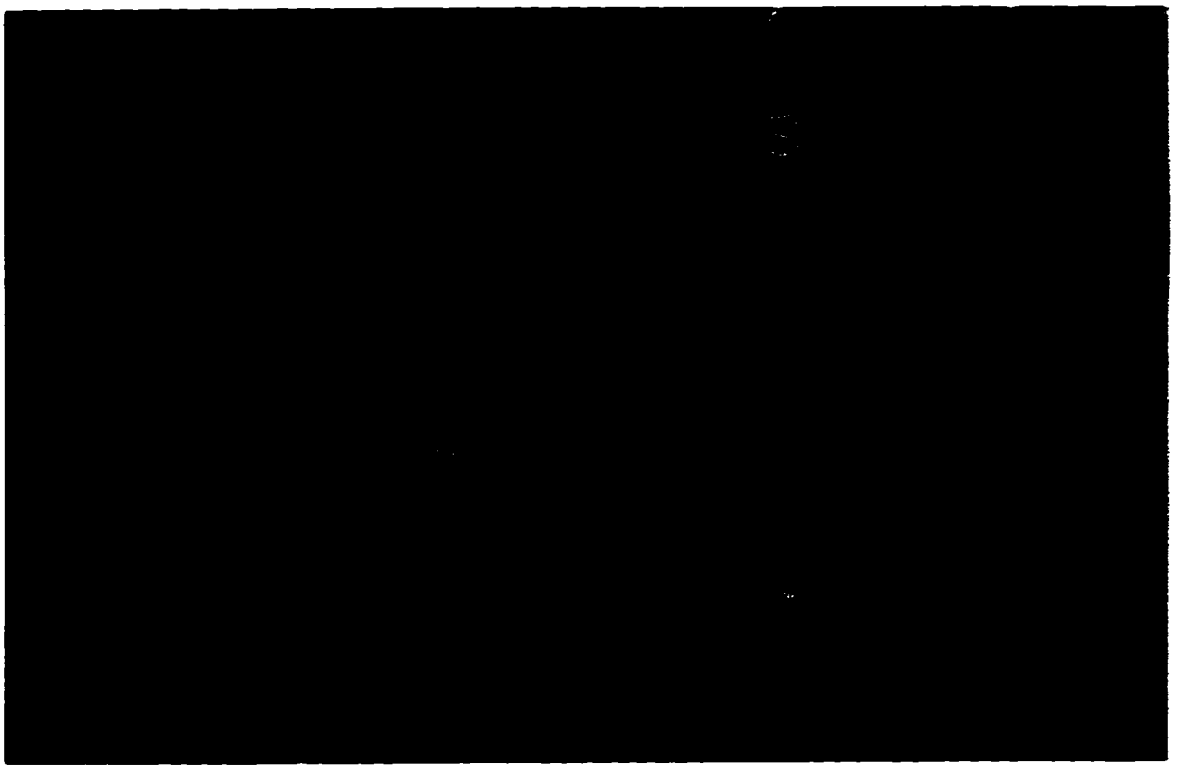

Fig. 3.5. Photomicrograph of a thin section of well preserved non-luminescent secondary layer (S) in a shell of *Gotatrypa* sp. (sample A800) interspersed with brightly luminescent veinlets (arrow). Field of view is 1 mm across.

a portion of, or the entire, primary layer usually adheres to the enclosing rock, whereas the secondary layer spalls along its contact with the primary one. This may explain the absence of the primary layer from many of the examined brachiopods. The secondary layers of the studied Silurian brachiopod shells exhibited all types of luminescence, but most were non-luminescent (Fig. 3.5) or dull (e.g. Fig. 3.3B). In particular, the Llandovery brachiopods from Anticosti Island, Canada, showed exceptionally well preserved microstructure and were non-luminescent. The tight stacking of calcite fibres in the secondary layer may have minimized fluid penetration. Nevertheless, diagenetic fluids often do penetrate the interior through microcracks that develop along calcite fibres. These appear under the luminoscope as brightly luminescent microveins (veinlets) or streaks within the secondary layer (Fig. 3.5). Yet, these regular parallel brightly

luminescent bands in the secondary layer must not always be the consequence of alteration, particularly if there is no evidence of textural disruption, since such bands were observed also in specimens of modern brachiopods (Barbin and Gaspard, 1995) where they were equated with periods of slow growth (winter seasons) and with variations in environmental conditions.

In some of the examined brachiopods, alteration affected only one of the two valves, or only specific spots in the shell and only these parts exhibited bright luminescence, whereas the rest of the shell appeared dull to non-luminescent. Such spots were avoided during sampling. The shells that exhibited entirely bright luminescence or severe textural diagenetic features were discarded.

In species with punctate shells, the punctae were usually filled with secondary calcite that appeared brightly luminescent under the luminoscope (Fig. 3.4B).

3.4.3 Scanning Electron Microscopy (SEM)

The scanning electron microscope has such a high magnification power that the ultrastructure of the brachiopod shell can be studied in detail (Williams 1970a,b) and this allows individual calcite fibres in the secondary layer to be scanned for dissolution features and cement inclusions. Alteration of the shell usually causes clear deformation of the shapes of calcite prisms and the degree of deformation is proportional to the degree of dissolution-precipitation that affected the shell.

Most of the examined brachiopod shells had excellent preservation and showed regularly stacked calcite prisms with smooth clean straight boundaries (Figs. 3.6A, B). Shells that had good overall preservation but suffered from minor alterations showed preserved calcite fibres

with minor dissolution features, commonly at crystal boundaries (Fig. 3.6C). Shells that were considerably altered, although infrequent in our sample population, exhibited clear dissolution features, but the calcite prisms kept the general crystal form (Fig. 3.6D).

Despite the fact that low-Mg calcite is a relatively stable phase that resists diagenetic alteration, some shells were entirely altered and the shapes of the calcite prisms were totally destroyed (Fig. 3.6E). It appears, from SEM images, that the diagenetic dissolution progressed sequentially. It commenced at crystal boundaries and proceeded into the crystal interior with increasing degree of alteration.

Several studied brachiopods had punctae in their shells. Their abundance in the shell was usually < 5% and they were filled with secondary calcite. Although the punctae may have acted as conduits for diagenetic fluids, activating the process of shell alteration, many punctate shells exhibited good preservation of the prisms (Fig. 3.6F), with sharp boundaries to the secondary fill in the punctae. Similar observations were documented also by optical and PIXE studies by Bruhn et al. (1994). For this study, mainly impunctate shells were selected in order to avoid post-depositional contamination from the secondary calcite within the punctae.

In summary, the retention of primary ultrastructural features observed in the Silurian brachiopod shells, such as undeformed calcite crystals with smooth and clean boundaries, shell foliation and stacked calcite fibres, are strong evidence for high degree of preservation of the shells.

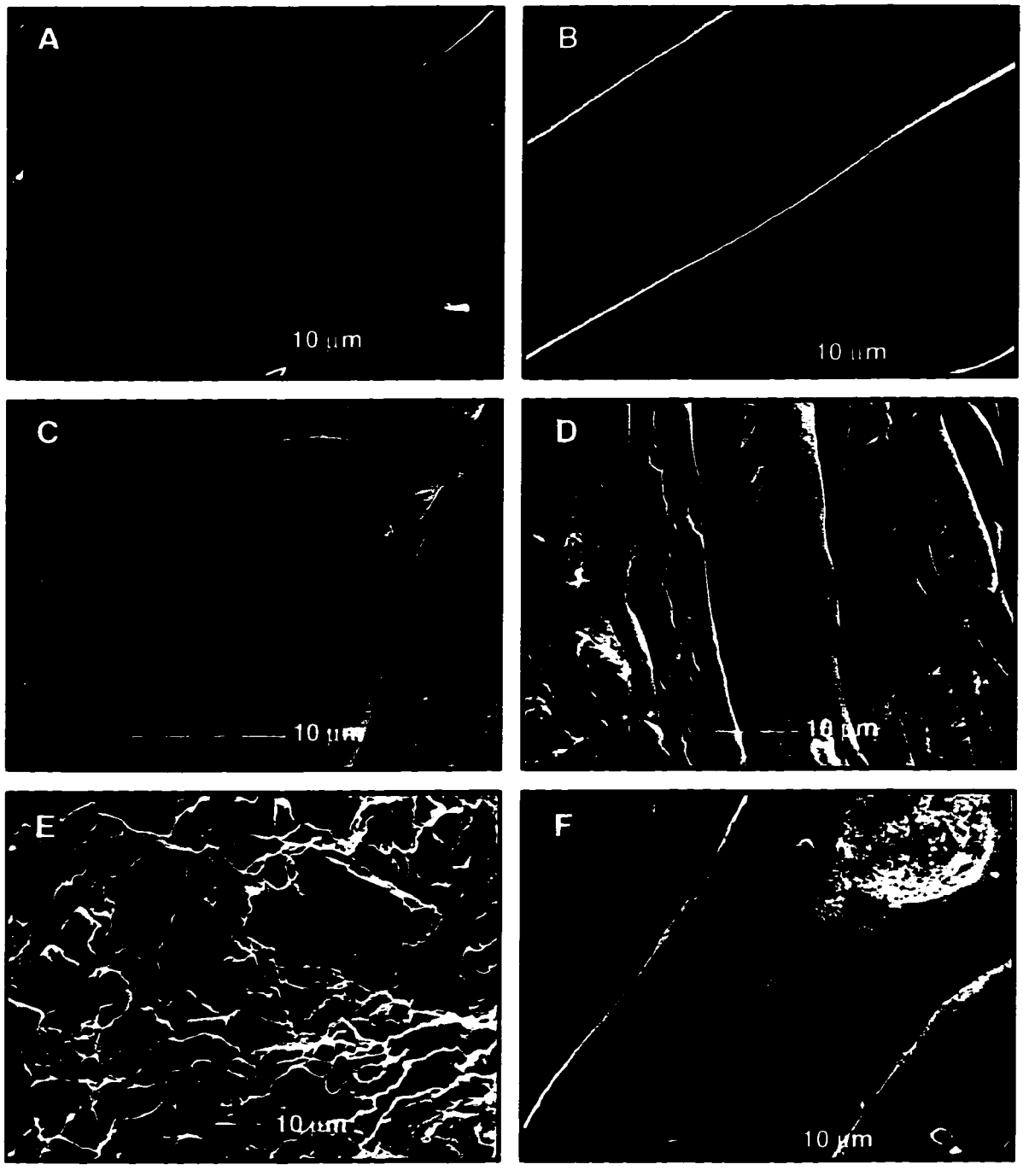

Fig. 3.6. SEM photomicrographs of clean brachiopod shell fragments of the secondary layer showing: (A) excellent preservation and clean crystal boundaries (sample A916). (B) a closeup of (A). (C) good preservation with minnor dissolution features at the crystal boundaries (sample A806). (D) fair preservation with dissolution features extended to the crystal interiors (sample PK22). (E) total recrystallization (sample G19). and (F) well preserved secondary layer containing a diagenetic cement filled puncta (sample EK3).

3.4.4. Distribution of Diagenetic Fabrics in Brachiopod Orders

3.4.4.1. Order Orthida

Brachiopods of this order were collected mainly in Wales (Britain) and Gotland (Sweden), and some from the Baltic region. They included the following genera: *Daljina*, *Dolerorthis*, *Isorthis* and *Resserella*. The anterior to posterior length of the shells varied between 6 and 15 mm. The maximum shell thickness around the umbo was between 0.4 mm (*Isorthis* sp.) and 0.8 mm (*Resserella* sp.), with the smallest specimens generally from the Baltic states. Order Orthida is considered to include the most primitive articulate brachiopods (Williams, 1968).

The primary shell layer was poorly developed and could not be identified in the studied specimens. Except for *Resserella* sp., all orthid shells studied were punctate. Nevertheless , despite this punctation, the CL and SEM images indicate good preservation of the secondary layer of the shells. Brightly luminescent veinlets can, at times, be seen in the secondary layer under the luminoscope.

3.4.4.2 Order Pentamerida

Only 9 pentamerid shells were examined in this study and they included the genera *Anastrophia*, *Hercotrema* and *Parastrophonella*. The shell length ranged between 10 mm (*Hercotrema* sp.) and 14 mm (*Anastrophia* sp.) and the maximum shell thickness around the umbo was between 0.2 and 0.3 mm.

The shell structure of the pentamerids is similar to that of the rhynchonellids and spiriferids and very close to that of the orthids. The primary layer may be present as a recrystallized remnant on the secondary layer. The secondary layer consists of a series of stacked calcite fibres with a

lineation at a shallow angle to the shell surface. Some shells contained disseminated pyrite in the secondary layer as well as some cracks, but no punctae were observed.

The remains of the primary layer exhibit bright luminescence under the luminscope, while the secondary layer is mostly non- to dull luminescent, indicating good preservation. In some specimens, lamellar and patchy bright luminescence parallel to calcite fibres suggests penetration by diagenetic fluids. Overall, the SEM images confirm good preservation of the secondary layer of the shells.

3.4.4.3 Order Rhynchonellida

Twenty three samples of rhynchonellids were examined, including the genera *Ancillotoechia*, *Fenestrirostra*, *Microsphaeridiorhynchus*, *Morinrhynchus*, *Plagiorhynchia*, *Rhynchia*, *Rhynchotrema*, *Sphaerirhynchia* and *Stegerhynchia*. Shell length in these samples ranged from 27 mm (*Rhynchtrema fringilla*) to 8 mm (*Microsphaeridiorhynchus* sp.) and shell thickness near the umbo was between 0.8 and 0.3 mm.

The primary layer was rarely present and the preserved secondary layer was similar to that of the pentamerids. Under the luminoscope, the secondary layer exhibits non- to dull luminescence with a few fine bright luminescent lines along the intercrystalline boundaries. The SEM images reveal minor dissolution features along those boundaries.

3.4.4.4 Order Strophomenida

The examined strophomenids (15 samples) were represented by the genera *Leptaena*, *Eoplectodonta*, *Fardenia* and *Iridistrophia*. The average shell length was about 20 mm and the

shell thickness near the umbo about 1.2 mm, but the shells from this order were generally thinner than those of the other orders, and particularly so for *Leptaena*.

The strophomenids are considered to have a highly evolved shell structure, with the periostracum followed directly by the fibrous calcite layer. The primary layer does not exist and it was suggested that it has been replaced by angled calcite rods, or taleolae, which cut through the secondary layer deflecting the shell fabrics. This structure makes the shell appear as if truly punctate (Clarkson, 1993), as demonstrated by *Leptaena* (Fig. 3.7). However, the shells of *Iridistrophia* have a regular fibrous secondary layer similar to that of the orthids and rhynchonellids, without the punctate appearance.

Fig. 3.7. Photomicrograph of well preserved secondary layer in a shell of *Leptaena depressa* (sample G12) showing taleolae, indicated by arrows. Field of view is 2 mm across.

Under the luminoscope, the lamellar penetrative luminescence is more frequent in the shells of this order, particularly in *Leptaena*, but such bright CL lamellar fabrics are mostly not so dense that they would preclude acceptance of the shells for the present research.

3.4.4.5 Order Spiriferida

Spiriferids, particularly the atrypoids (*Atrypa reticularis*), represent the majority of the shells examined in this study. They include the genera *Atrypa*, *Cyrtia*, *Delthyris*, *Eospirifer*, *Eospirigerina*, *Gotatrypa*, *Joviatrypa*, *Hesperorthis* and *Meristina*. The length of the shell reached up to 25 mm and the thickness near the umbo was up to 2 mm. However, the samples from the Baltic states were considerably smaller (< 8 mm long) and with thinner (~ 0.2 mm) shells. Some spiriferid shells contained the primary layer which exhibited bright red CL. Brightly CL veinlets extended parallel to, or across, calcite fibres of the secondary layer but less so in strophomenids. The SEM images showed good preservation of the secondary layer.

In summary, diagenetic features, such as bright CL veinlets, disseminated pyrite or patchy CL areas, were found in the secondary shell layers of most of the studied genera. The strophomenids, particularly *Leptaena*, were, however, more often altered than brachiopods from the other orders. Nevertheless, in most of the studied shells such diagenetic alteration fabrics were only subordinate phenomena, rendering the samples suitable for the isotopic study.

CHAPTER IV

TRACE ELEMENT CONTENTS OF THE SHELLS

4.1. INTRODUCTION AND THEORETICAL CONCEPT

Taking into account that brachiopod calcite shells are utilized as carriers of the isotopic signals, it is important to examine whether they preserve the primary signals acquired from seawater or only the diagenetically altered ones. Comparison of trace element chemistry of fossil brachiopods with that of their modern counterparts may serve as one of the distinguishing criteria (e.g. Veizer et al., 1986).

Alteration of the original carbonate phase, precipitated in equilibrium with seawater, by action of pore water involves a dissolution-precipitation process that mixes the trace elements in carbonates with those in pore waters. This reaction results in repartitioning of minor (e.g. Sr and Mg) and trace (e.g. Na, Fe and Mn) elements into the carbonate lattice (Veizer, 1983a,b). Incorporation of trace elements into carbonate minerals may occur by different ways such as (1) substitution for Ca in the $CaCO_3$ lattice, (2) emplacement in interstitial sites between lattice planes, (3) occupation of free positions formed by lattice defects, (4) adsorption due to remnant ionic charges, or (5) presence in non-carbonate inclusions. Many elements can substitute for Ca in the $CaCO_3$ lattice, but Mg, Sr, Mn and Fe are the most common and thus most frequently utilized in evaluation of carbonate diagenesis.

Generally speaking, when marine carbonates undergo dissolution-precipitation reaction, the metastable phases, such as high-Mg calcite (HMC) and aragonite (A), are stabilized into diagenetic low-Mg calcite (dLMC). Since brachiopod shells are formed of LMC, the stable phase of calcite, they should resist diagenesis and the process of alteration is expected to involve only the

precipitation of cements. Nevertheless, even the primary LMC of brachiopods may suffer from some diagenetic alteration effects (e.g. Al-Aasm and Veizer, 1986a,b).

The trace element composition of the secondary calcite differs from that of the original carbonate and the distribution of trace elements between the solid phase ($CaCO_3$) and the liquid phase (diagenetic fluids) can be expressed as (Pingitore, 1978; Veizer, 1983a)

$$(m_{Me}/m_{Ca})_s = D\,(m_{Me}/m_{Ca})_w$$

where m is the molar concentration, Me stands for trace element, s and w signify the solid ($CaCO_3$) and the diagenetic fluid (liquid phase), and D is the partition coefficient for a given element. The magnitude of the positive or negative deviation of the partition coefficient (D) from unity determines the degree of enrichment or depletion of a particular trace element in the solid phase, relative to the parent liquid phase. When D>1 (such as in the case of Fe and Mn), the precipitated solid phase will contain, relative to calcium, higher Me concentration than the liquid phase. On the other hand, when D<1 (such as in case of Sr and Na), the opposite effect occurs. If D=1, the trace element is incorporated in similar amounts in both solid and liquid phases. Veizer (1983a, Table 3-1) summarized the approximate D values for carbonate minerals.

If water changes its composition in the course of precipitation, the trace element concentration within the solid phase would follow the Doerner-Hoskins heterogeneous distribution law (Gordon et al., 1959, Chapter 9), expressed as follows:

$$\log (m_{Me}{}^{o}/m_{Me}{}^{f}) = \lambda \log (m_{Ca}{}^{o}/m_{Ca}{}^{f})$$

where o and f indicate initial and final concentrations of trace elements and Ca in solution.

Despite the uncertainties in the D values (Bathurst, 1975; p. 265; Lorens, 1981), these estimates help us to understand the general chemical trends and the trace element behaviour during diagenesis

(Veizer, 1983a). The post-depositional repartitioning of trace elements between marine A and HMC and their successor dLMC is controlled by the following factors (Pingitore, 1978; Brand and Veizer, 1980; Veizer, 1983a; Banner and Hanson, 1990; Morse and Bender, 1990):

(1) The precursor mineralogy (A, HMC and LMC) that determines the original trace element concentration and subsequently contributes to the diagenetic solutions;

(2) The water/rock ratio that reflects the openness of the system;

(3) The molar difference in trace element concentration of the diagenetic solution relative to the water of the sedimentary environment;

(4) Biological fractionation, because some organisms precipitate their skeletons in inorganic equilibrium with their ambient seawater while others do not. This may cause enhancement or suppression of some elements in the shell;

(5) The activity coefficient of the trace cations that changes during precipitation due to change of the solution composition;

(6) Heterogeneity in solid phase composition caused by the recrystallization of the solid phase ($CaCO_3$) during precipitation;

(7) Rate of precipitation of the solid phase (O'Hara and Reid, 1973; Lorens, 1981); and

(8) Temperature and pressure prevalent during precipitation.

In open systems (high water/rock ratio), the amount of solid is small compared to liquid. The dissolution of the pre-existing solid phase will thus cause only a minor change in the liquid composition and in the cement precipitated from it. On the other hand, in closed systems (low water/rock ratio), the amount of solid is larger and its dissolution will cause a significant change in the composition of the diagenetic fluid and the precipitated cement. Hydrology, as a function of

porosity and lithology, thus plays a significant role in the process of diagenesis.

Repartitioning of trace elements and isotopes during diagenesis follows two general trends, with some elemental concentrations enhanced with increasing degree of stabilization (e.g. Fe and Mn) and others declining (e.g. Sr, Na) (Veizer, 1983a).

4.2. OBJECTIVES OF TRACE ELEMENTS STUDY

The emphasis in this discussion will be on (1) evaluation of the degree of preservation of the brachiopod shells as carriers of the primary geochemical signals, and (2) evaluation of the controls on the incorporation of trace elements into calcite forming the shell.

4.3. TRACE ELEMENTS AND CHEMICAL PRESERVATION

Comparison of trace element content of fossil brachiopod shells with that of their modern counterparts has frequently been utilized for evaluating their degree of preservation (e.g. Popp et al., 1986; Morrison and Brand, 1986). Unfortunately, the studies of trace element composition of modern brachiopods are rare (Lowenstam, 1961; Lepzeltzer et al., 1983) and they do not cover the entire range of ecosystems. As a result, the ranges of concentrations for different elements in the shells vary considerably from one author to another. For example, the Mn contents of modern articulate brachiopod shells were reported to be less than < 180 ppm by Lepzeltzer et al. (1983), whereas Dittmar and Vogel (1968) reported 120 to 1530 ppm and Morrison and Brand (1986) 4 to 460 ppm. With such high Mn contents (>300 ppm), modern brachiopods can exhibit pronounced bright luminescence under the luminoscope (cf. Barbin and Gaspard, 1995). Despite the above uncertainties, trace element contents of modern brachiopod shells still provide the base reference

with which the fossil brachiopods can be compared. Recent brachiopod shells usually have Sr contents ranging from 800 to 2000 ppm, Na 500 to 3700 ppm, Fe 20 to 700 (Lowenstam, 1961; Morrison and Brand, 1986), and Mn 4 to 300 (Frank et al., 1982; Grossman, 1994).

The bulk of the studied Silurian brachiopods has Sr and Mn contents (Appendix 2) similar to those of Recent brachiopods (Fig. 4.1). Except for the few samples with higher Sr contents (~ 2500 ppm), and some with Mn contents of up to about 500 ppm, the majority of samples (~90%) are within the 1000 to 2000 ppm Sr and 10 to 200 ppm Mn ranges. If the Mn limits are extended to 500 ppm (cf. Morrison and Brand,1986), all samples plot within the modern range. Note also that the scatter diagram (Fig. 4.1) shows no correlation between these two elements, reflecting the excellent preservation and variability of the original signals.

Compared to values in brachiopod shells, the Sr and Mn contents of cement and matrix plot clearly outside the ranges of Recent brachiopods, with significantly higher Mn and lower Sr contents (Fig. 4.1). This indicates that the sampled shells contain no matrix contamination and minimal or no inclusions of cements.

Unfortunately, despite caution taken during experimental work, the results for Na and Fe cannot be utilized for confirmation of the above conclusion due to contamination. This was caused by two factors. First, many of the analysed shells contain disseminated pyrite within the secondary layer, probably deposited by bacterial action, with a resulting increase in the measured content of Fe. Second, Na was likely leached out from the reaction vessels during acid extraction of the CO_2 as Pyrex glass contains 4% Na_2O, mainly in the surface layer. Since the quantity of sample used for analysis was very small (3 to 4 mg), a blank correction was difficult to apply.

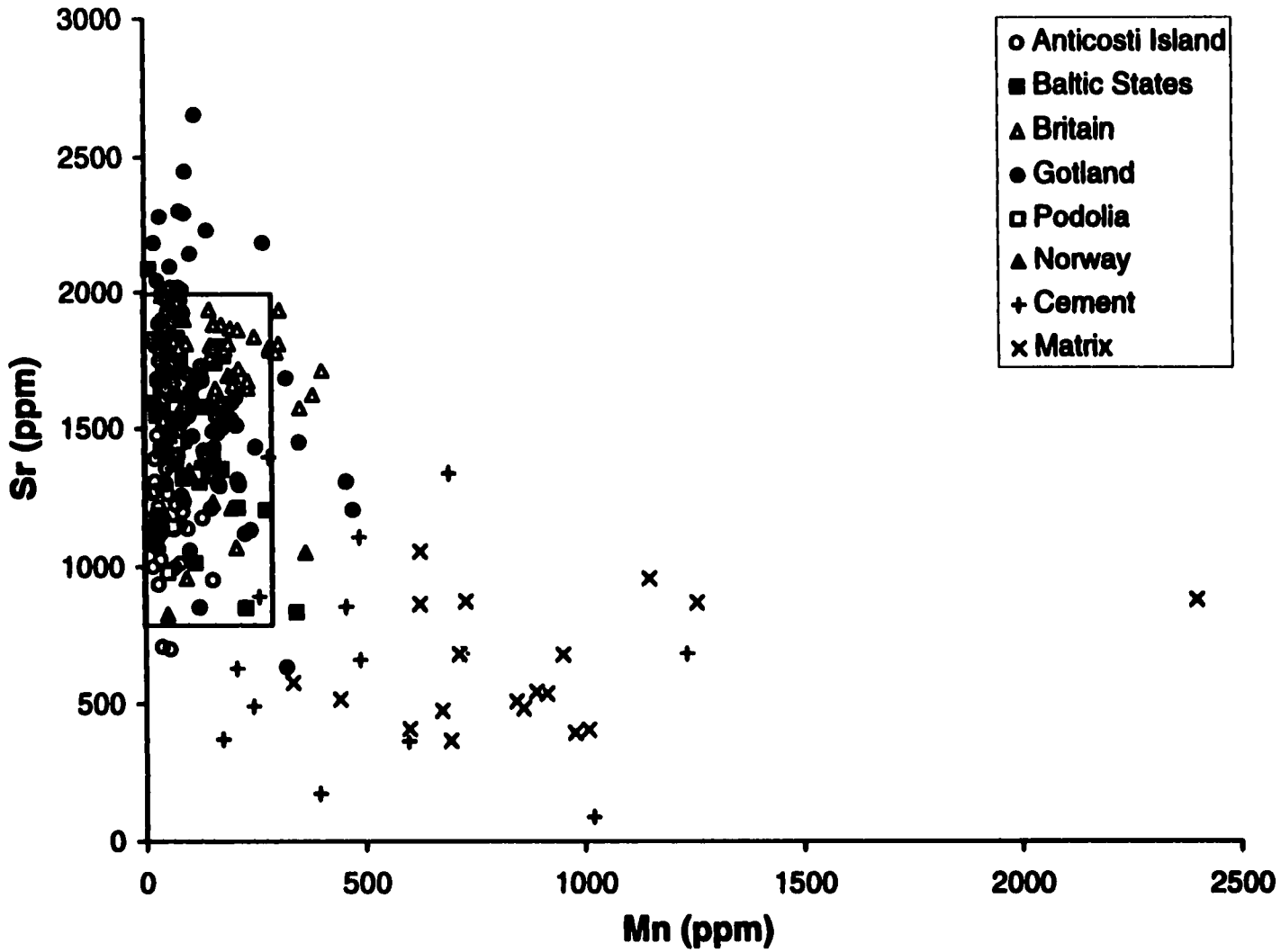

Fig. 4.1. Scatter diagram of Mn vs. Sr for all studied samples; brachiopod shells, cement and matrix. The box represents the trace element ranges for Recent brachiopods.

4.3.1. Vital Effect

The distributions of Mn and Sr concentrations in the studied Silurian brachiopods are illustrated by orders in Figure 4.2 and by localities and mean values in Table 4.1. Most of the brachiopod orders (Orthida, Pentamerida, Rhynchonellida, Spiriferida and Strophomenida) have concentrations of Mn and Sr within the ranges suggested for Recent brachiopods (~ 4 to 300 ppm for Mn, ~ 800 to 2000 ppm for Sr). Some strophomenids as well as few spiriferids have Sr contents which are slightly higher than 2000 ppm. This is likely an original feature, because alteration should decrease the Sr content ($D_{Sr}<1$). This, and the residual differences in Sr contents among different orders, may be a result of varying growth rates (cf. Nicolas and Brand, 1991). In a similar manner, a few spiriferids show a slightly higher content of Mn, up to 500 ppm. As discussed earlier, these samples did not show any clear evidence of alteration and the higher Mn content may therefore be a primary feature as well. Note also that, despite the risk of contamination increasing with thin shells, the strophomenids still exhibit Mn and Sr contents typical of well preserved shells, attesting to clean and efficient experimental work.

4.3.2. Depth control

It was suggested that Silurian rhynchonellids inhabited mainly shallow subtidal waters, while the spiriferids and pentamerids were common in deeper waters, as deep as 1500 m (Hancock et al., 1974). The orthids and strophomenids were scattered across the entire depth spectrum (Fürsich and Hurst, 1974). It could be argued that this could explain the higher Mn contents of some of the spiriferids (Fig. 4.2). Yet, most samples in this study originate from carbonate formations with reef associations and not from shales and thus all are from relatively shallow waters. The similarity of

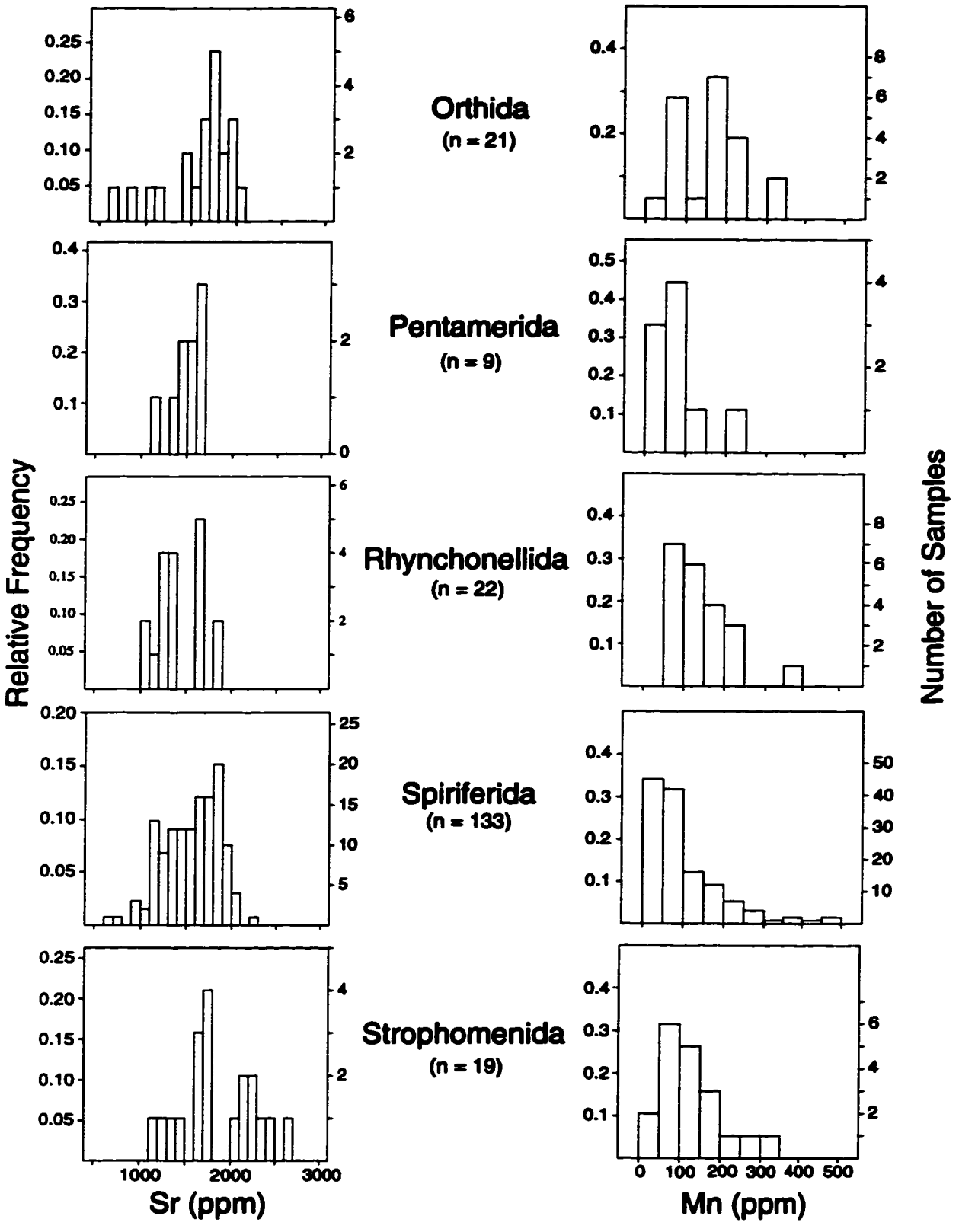

Fig. 4.2. Histograms of Sr and Mn values for brachiopod orders. Mean values and standard deviations are given in Table 4.1a.

(a)

Order	Orthida				Pentamerida				Rhynchonellida				Spiriferida				Strophomenida			
Element	Mn	Sr	$\delta^{18}O$	$\delta^{13}C$	Mn	Sr	$\delta^{18}O$	$\delta^{13}C$	Mn	Sr	$\delta^{18}O$	$\delta^{13}C$	Mn	Sr	$\delta^{18}O$	$\delta^{13}C$	Mn	Sr	$\delta^{18}O$	$\delta^{13}C$
No. of Samples	21	21	21	21	9	9	9	9	22	22	22	22	133	133	133	133	19	19	14	14
Minimum	36	632	-6.1	-0.9	22	1137	-5.1	1.5	51	1014	-6.6	5.4	9	435	-6.4	1.1	33	1134	-5.7	-0.5
Maximum	321	2007	-3.6	4.4	234	1686	-2.7	-0.6	352	1836	-3.9	-0.2	472	2281	-2.0	6.4	322	2651	-4.2	4.9
Mean	153	1599	-5.2	1.5	81	1502	-4.5	0.7	143	1446	-5.1	1.5	103	1552	-5.0	1.2	134	1870	-5.0	1.5
Std. Deviation	79	373	0.8	1.7	63	173	0.7	0.7	70	243	0.7	1.8	92	322	0.8	0.6	75	422	0.6	1.7

(b)

Location	Anticosti Island				England				Gotland				Baltic States				Podolia			
Element	Mn	Sr	$\delta^{18}O$	$\delta^{13}C$	Mn	Sr	$\delta^{18}O$	$\delta^{13}C$	Mn	Sr	$\delta^{18}O$	$\delta^{13}C$	Mn	Sr	$\delta^{18}O$	$\delta^{13}C$	Mn	Sr	$\delta^{18}O$	$\delta^{13}C$
No. of Atrypoids	19	19	20	20	19	19	19	19	33	33	31	30	14	14	14	14	5	5	5	5
Minimum	9	435	-6.0	-0.2	39	1672	-5.9	-0.3	25	1206	-6.0	0.8	11	1119	-5.9	-1.0	36	978	-6.1	-0.4
Maximum	154	1408	-4.4	2.1	402	1988	-1.9	2.4	472	2281	-3.5	4.4	155	1828	-3.4	4.2	85	1577	-5.3	0.2
Mean	37	1139	-5.1	0.9	173	1809	-4.9	1.0	96	1717	-4.7	1.4	74	1474	-4.5	0.6	63	1381	-5.8	0.0
Std. Deviation	34	197	0.4	0.6	99	94.6	0.7	0.9	97	263	0.8	1.4	42	215	0.8	1.6	19	233	0.3	0.3

Table 4.1. Mn, Sr, $\delta^{18}O$ and $\delta^{13}C$ statistics for brachiopod orders (a) and atrypoids (b) from all studied areas.

$\delta^{18}O$ values for all orders (Table 4.1a) also argues against such an environmental scenario.

4.3.3. Basinal Control

Since the atrypoids represent more than half of the studied brachiopod population in this project, it is interesting to examine the effect of location on the distribution of trace elements in their shells. The distributions of Mn and Sr in the shells are summarized in Table 4.1b and Fig. 4.3. The atrypoids from the Anticosti basin have the lowest Sr and Mn contents (1139 ±197 and 37 ± 34 ppm, respectively), the samples from the Baltic states and Podolia are intermediate, and those from England and Gotland have the highest Sr and Mn contents. The reasons for these differences are not yet clear, but both environmental and biological factors may have played a role.

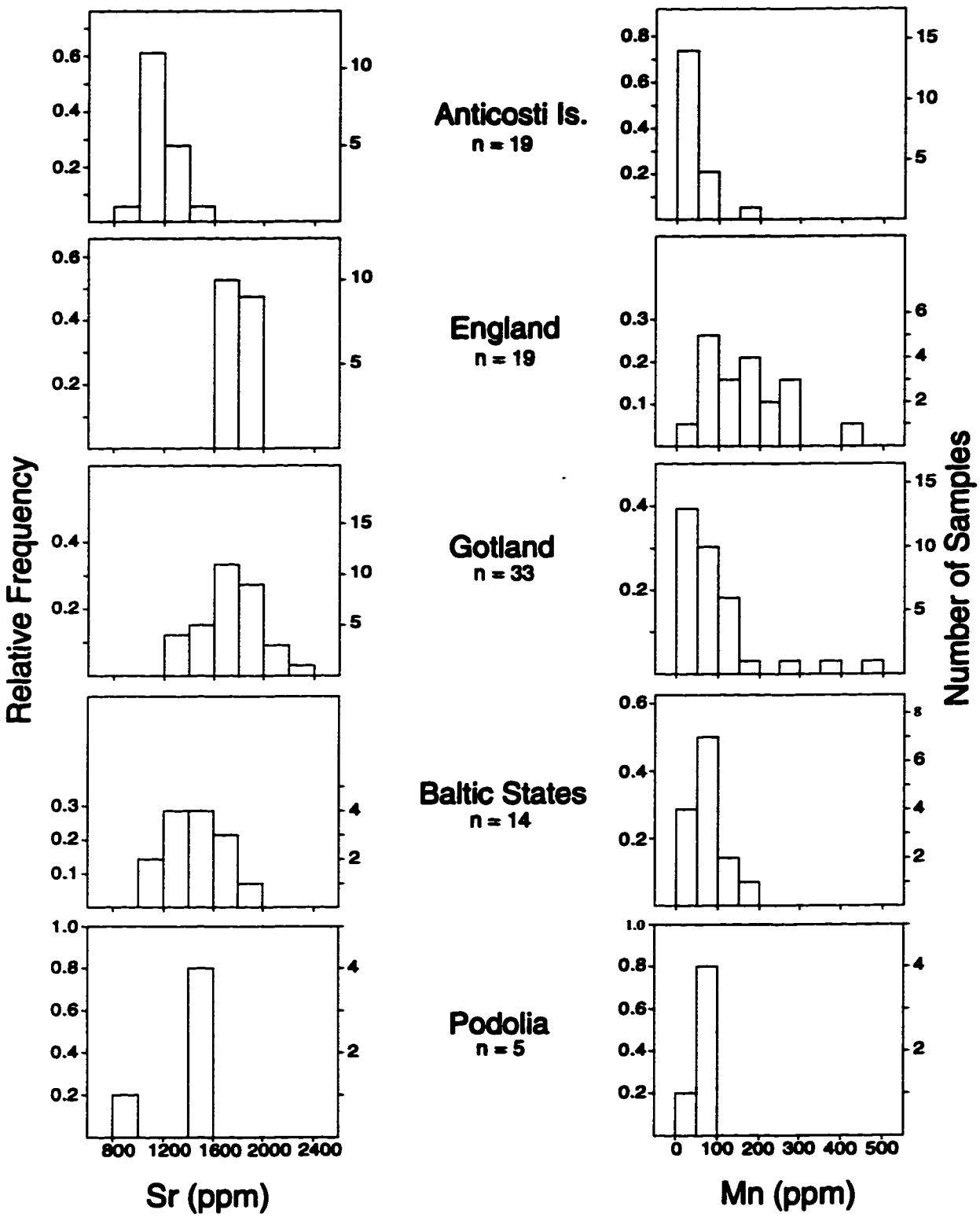

Fig. 4.3. Histograms of Sr and Mn for atrypoids from all sections. Mean values and standard deviations are shown in Table 4.1b. The Norwegian samples are not included because of their unusual $\delta^{18}O$ signal discussed in the subsequent chapter

CHAPTER V

CARBON AND OXYGEN ISOTOPE GEOCHEMISTRY

5.1. INTRODUCTION AND THEORETICAL CONCEPT

The brachiopod shell incorporates, in addition to trace elements, oxygen and carbon isotopes into the lattice of calcite and the ratios of such isotopes may reflect the temperature and the isotopic composition of the ambient seawater (Anderson and Arthur, 1983). The main reservoirs of oxygen and carbon isotopes are carbonate sediments, but carbon is also present in organic matter (Hoefs, 1980, 1982) while the main additional reservoir of oxygen is water (Lohmann, 1983).

Diagenetic alteration, by dissolution-precipitation reactions, causes the isotopic composition of marine carbonates to equilibrate with the intervening diagenetic water (Bathurst, 1975 Chapter 8), resulting in repartitioning of stable isotopes, as well as in redistribution of trace elements (Veizer and Fritz, 1976; Brand and Veizer, 1981; Lohmann, 1983; Veizer, 1983b; Banner and Hanson, 1990). This interaction with diagenetic (e.g. meteoric) fluids usually leads to the enrichment of ^{12}C and ^{16}O isotopes in the stabilized dLMC and the reaction can be expressed by the following equation:

$$^{13}C^{18}O_3^{2-} + H_2{}^{16}O + {}^{12}CO_2 \rightleftharpoons {}^{12}C^{16}O_3^{2-} + H_2{}^{18}O + {}^{13}CO_2$$

The isotopic composition of a sample is measured relative to a known ratio of a standard, and usually reported in δ-notation values in per mil (‰) (Faure, 1986). This relationship is defined as:

$$\delta^{18}O = 1000 \left((^{18}O/^{16}O)_{sample} - (^{18}O/^{16}O)_{standard} \right) / (^{18}O/^{16}O)_{standard}$$

Calcite values are usually reported relative to PDB standard (specimen of *Belemnitella americana* from the Peedee Formation of South Carolina), whereas water is referred to the SMOW standard (Standard Mean Ocean Water).

The diagenetic alteration is traced through the variation in $\delta^{18}O$ and $\delta^{13}C$ values of the carbonate phase (Meyers and Lohmann, 1985). The redistribution of O and C isotopes is controlled by the following factors (see Brand and Veizer, 1981; Anderson and Arthur, 1983; Banner and Hanson, 1990):

(1) Isotopic composition of calcite and the intervening diagenetic water;

(2) Temperature and salinity of seawater and the intervening diagenetic pore water, where the increase in temperature decreases the isotopic fractionation (Friedman and O'Neil, 1977). As a consequence, oxygen isotopes can be utilized for thermometry (Epstein et al., 1953);

(3) Altitude, latitude and seasonal variations, resulting in change in the $\delta^{18}O$ of the intervening pore waters of meteoric origin, with the $\delta^{18}O$ values becoming more depleted at high latitudes and altitudes;

(4) Secular variations in $\delta^{18}O$ and $\delta^{13}C$ of seawater. These variations can be explained in term of three causes (cf. Veizer, 1983a):

(a) post-depositional alteration,

(b) variations in $\delta^{18}O$ of seawater, and

(c) increase in seawater temperature;

(5) Biochemical fractionation of isotopes. Some organisms secrete their shell material at isotopic equilibrium with seawater, such as molluscs (Brand, 1982), foraminifera (Emiliani, 1955) and brachiopods (Lowenstam, 1961; Carpenter and Lohmann, 1995), while others, such as corals and

algae (Keith and Weber, 1964) as well as crinoids (Weber and Raup, 1968) do not;

(6) Openness of the diagenetic system, with the isotopic composition of carbonates affected by the water/rock ratio of the environment (Land, 1986; Banner and Hanson, 1990; Morse and McKenzie, 1990, Chapter 7);

(7) Other factors, such as the original mineralogy of the carbonate sediments or the shell formation rate, the latter having an inverse relationship with the degree of isotopic fractionation (Turner, 1982).

5.2. OBJECTIVES OF STABLE ISOTOPE STUDY

The main objectives for a study of isotopic composition of Silurian brachiopod shells are the following: (1) reconstruction of the isotopic composition of Silurian oceans, (2) reconstruction of relationships to paleoclimatic changes, including coeval sea-level stands, and (3) reconstruction of paleoceanographic phenomena for the Silurian seas.

5.3. PREVIOUS WORK

Most of the earlier oxygen and carbon isotope studies aimed to track the general trend of $\delta^{13}C$ and $\delta^{18}O$ variations through the entire Phanerozoic. The mean values of 194 measurements of $\delta^{13}C$ and $\delta^{18}O$ from Silurian brachiopod shells (Appendix 3), published by Veizer et al. (1986), Popp et al. (1986) and Wadleigh and Veizer (1992), are reproduced here (Fig. 5.1) in an attempt to reconstruct the pattern of isotopic variations during the Silurian Period. Unfortunately, these samples do not provide temporal resolution that would permit delineation of detailed trends and most of them are from one continent, namely North America. Such data show parallel $\delta^{13}C$ and

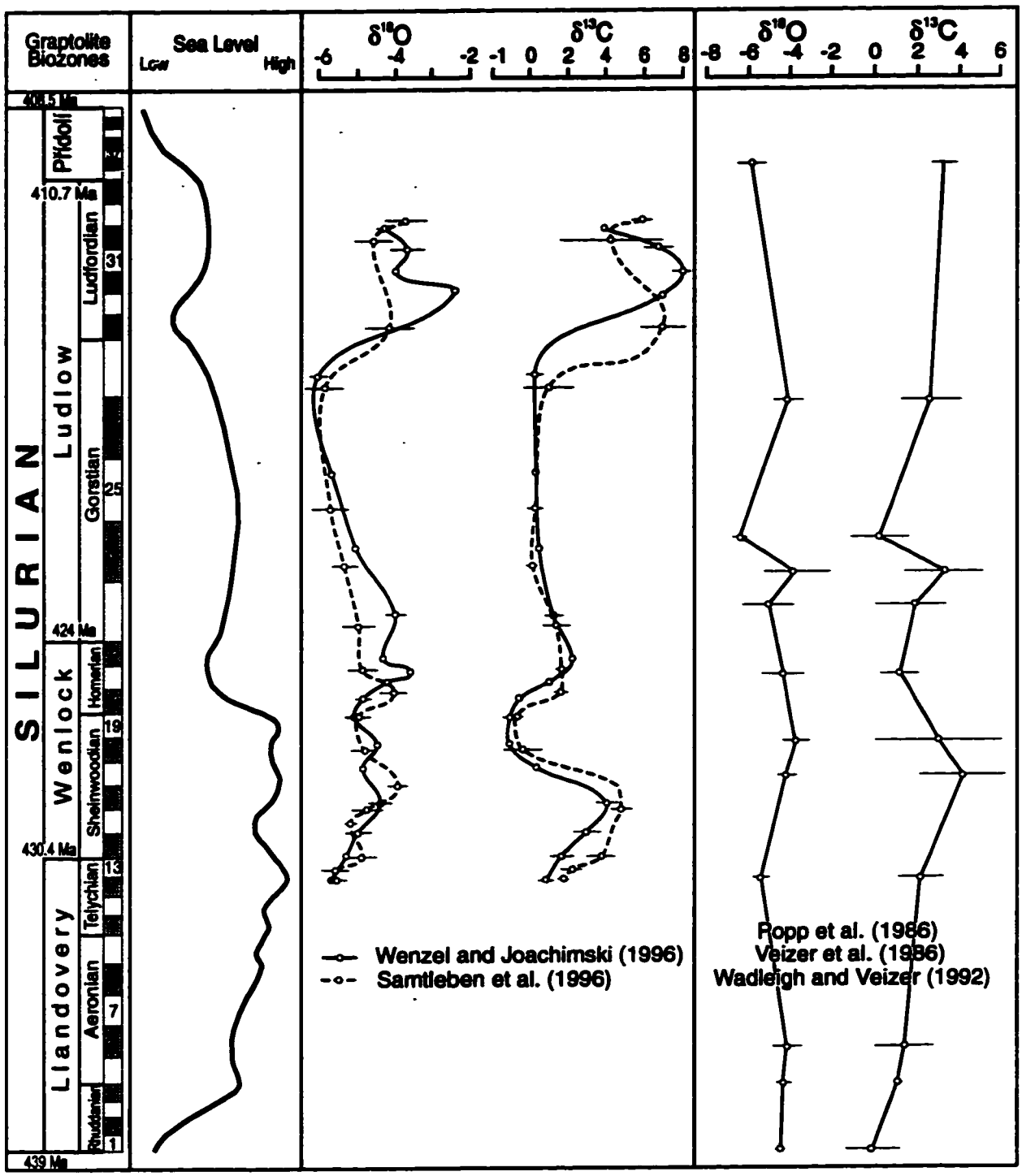

Fig. 5.1. Variations in $\delta^{18}O$ and $\delta^{13}C$ values (in ‰ PDB) of Silurian brachiopods in relation to inferred sea-level changes (after Johnson et al., 1991). Bars represent 2σ values. The estimated absolute ages follow the scale of Harland et al. (1990) and the numbers in the biozonation bar refer to the graptolite biozones in Figure 1.4.

$\delta^{18}O$ trends, with a minimum in the early Ludlow. A comparison of these isotopic patterns with the Silurian eustatic sea-level curve of Johnson et al. (1991) shows no clear relationship.

Recent work by Wenzel and Joachimski (1996) and Samtleben et al. (1996) on Silurian brachiopods from Gotland provided much better resolved temporal trends (Fig. 5.1), with clear positive isotope shifts in $\delta^{13}C$ and $\delta^{18}O$ during the early and late Wenlock and particularly in the late Ludlow. These curves hint at reciprocal relationship with sea-level stands.

Correlative isotope measurements exist also for whole-rock samples. Although these do not represent the original signals, because of diagenetic alteration, they may retain general features of isotopic variations through time. Such data from the Anglo-Welsh area (Corfield et al., 1992) reveal a recognizable negative shift in $\delta^{13}C$ values (~ 2‰ PDB) around the Wenlock/Ludlow boundary (*[21]nassa/[22]ludensis* biozones) that coincides with a sea-level fall (Johnson et al., 1991) and with a decline in pelagic graptolite diversity (Koren and Rickards, 1980; Kemp, 1991). Similarly, the whole-rock data from Estonia (Kaljo et al., 1994) show positive $\delta^{13}C$ shifts for early and late Wenlock times, at the *[16]riccartonensis* and *[21]nassa* biozones, with magnitudes of 4.2 ‰ and 4.6 ‰ (PDB), respectively. A very large increase in $\delta^{13}C$ values, with a magnitude of 12 ‰, was recorded in the upper Ludlow rocks at the Brocker River section in Queensland, Australia (Andrew et al., 1994a,b) and these authors documented also a minor ^{13}C enrichment across the Llandovery/Wenlock boundary.

5.4. TOTAL DATA SET AND PRESERVATION OF SIGNAL

The $\delta^{18}O$ and $\delta^{13}C$ signals (Appendix 2) for all studied Silurian brachiopod shells (237 samples) are plotted in Figure 5.2. Except for the Norwegian samples, they range from -6.4 to -2 ‰ and

from -1 to 7.5 ‰ (PDB), respectively. Compared with modern brachiopods ($\delta^{18}O$= -3 to 3.5 ‰ and $\delta^{13}C$= -1.5 to 4.5 ‰; Carpenter and Lohmann, 1995), the Silurian brachiopods are consistently depleted in ^{18}O but slightly enriched in ^{13}C. They also have a narrower range of $\delta^{18}O$ (~ 4.5 ‰) and a wider range of $\delta^{13}C$. The narrow spread of $\delta^{18}O$ values may be attributed to the limited paleolatitudinal range of Silurian brachiopods, because they all originate from low latitude (30°N and 30°S) warm shallow waters, frequently with reef associations. In contrast, their modern counterparts cover a wider range of latitudes and depths.

The total population shows only an indistinct positive correlation ($R^2 = 0.16$) between $\delta^{18}O$ and $\delta^{13}C$, indicating that the samples reflect an original scatter that is not strongly affected by post-depositional resetting. This is true even if samples for every locality are considered independently. Note also that there is no correlation between $\delta^{18}O$ and Mn or Sr in the studied brachiopod shells (Figs. 5.3 and 5.4). As for stable isotopes, this is the case even if samples are subdivided into populations based on localities. The above observations support the results of optical studies that suggested a high degree of preservation of the analysed shells.

Despite the general good preservation of samples, some anomalies do exist, as discussed in the following text. The samples from Norway (Oslo region) have Sr and Mn contents similar to Recent brachiopods (Fig. 4.1). Yet, their $\delta^{18}O$ signals are highly depleted, as low as -20.7 ‰ (Appendix 2). These samples plot entirely outside the cluster of the well preserved shells (Fig. 5.2), indicating a greater degree of alteration, as confirmed by the SEM images that showed strongly deformed shell microstructure. Such discrepancy between trace element and oxygen isotope data is difficult to understand. An explanation can perhaps be based on differing water/rock ratios with respect to trace elements and oxygen in the respective diagenetic systems.

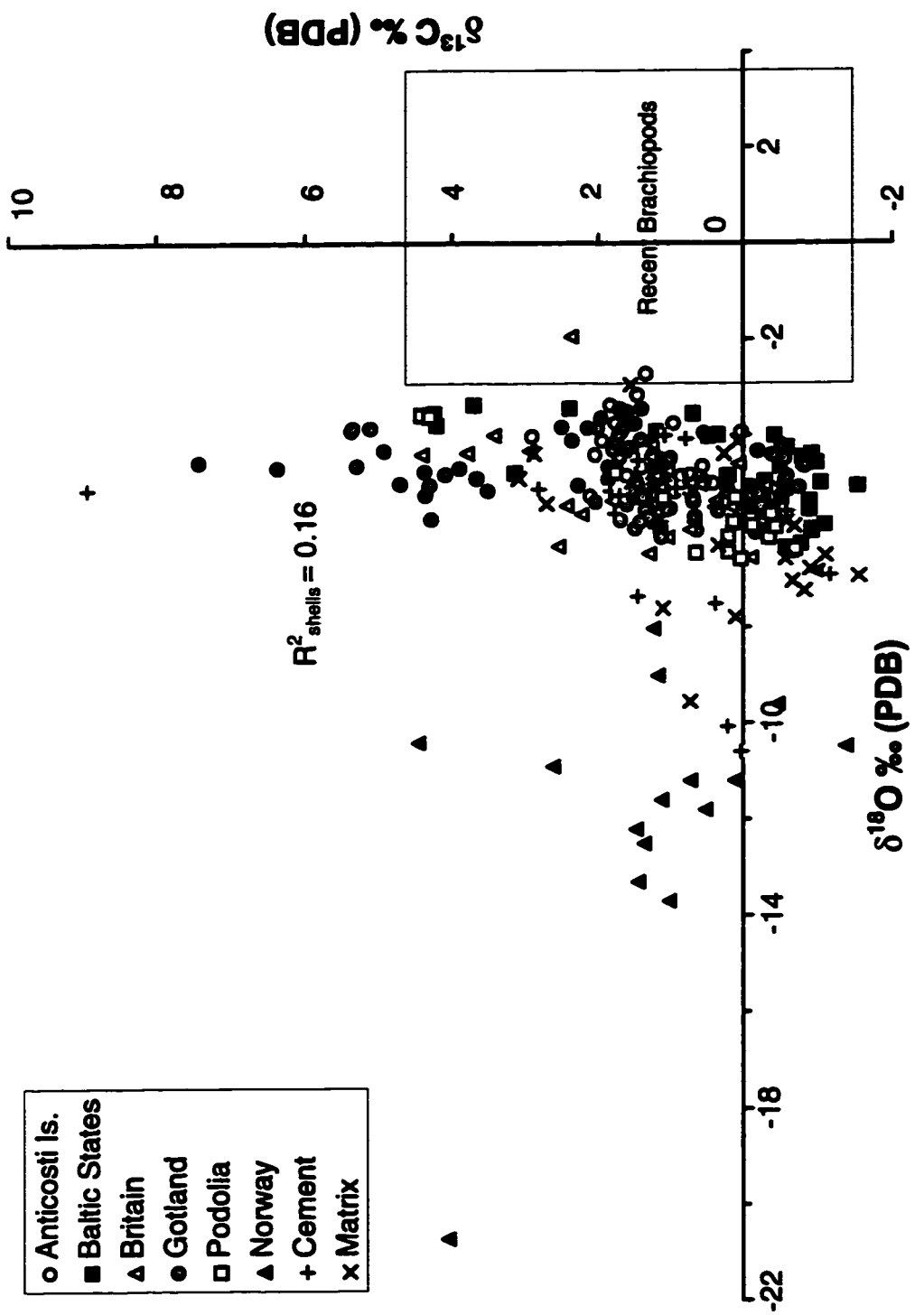

Fig. 5.2. Scatter diagram of $\delta^{18}O$ vs. $\delta^{13}C$ for all studied Silurian brachiopods as well as cements and matrix from different localities. The box represents the range of isotopic compositions for Recent brachiopods.

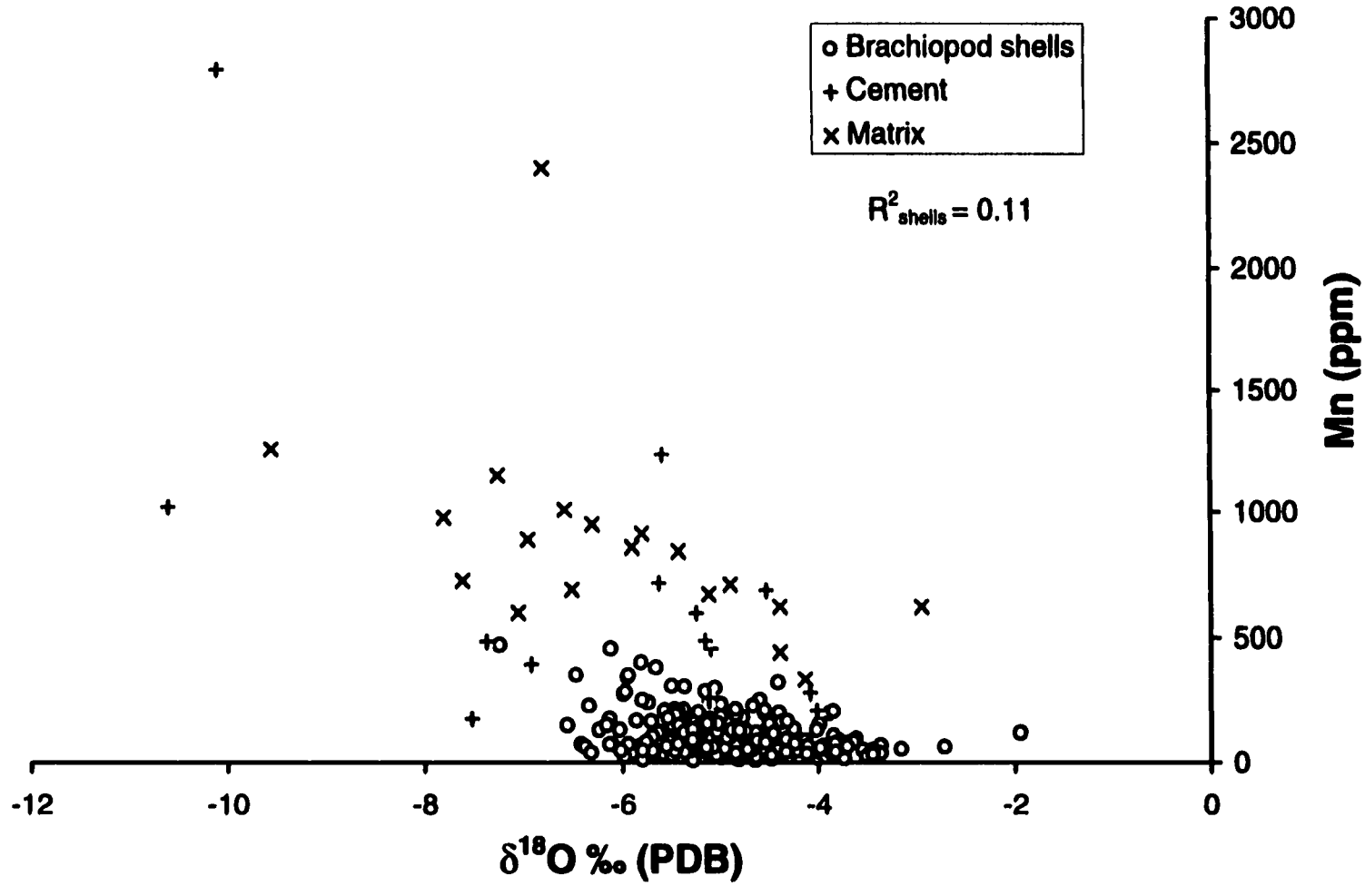

Fig. 5.3. Scatter diagram of $\delta^{18}O$ vs. Mn for all studied samples (brachiopod shells, cement and matrix). Oslo data are not included.

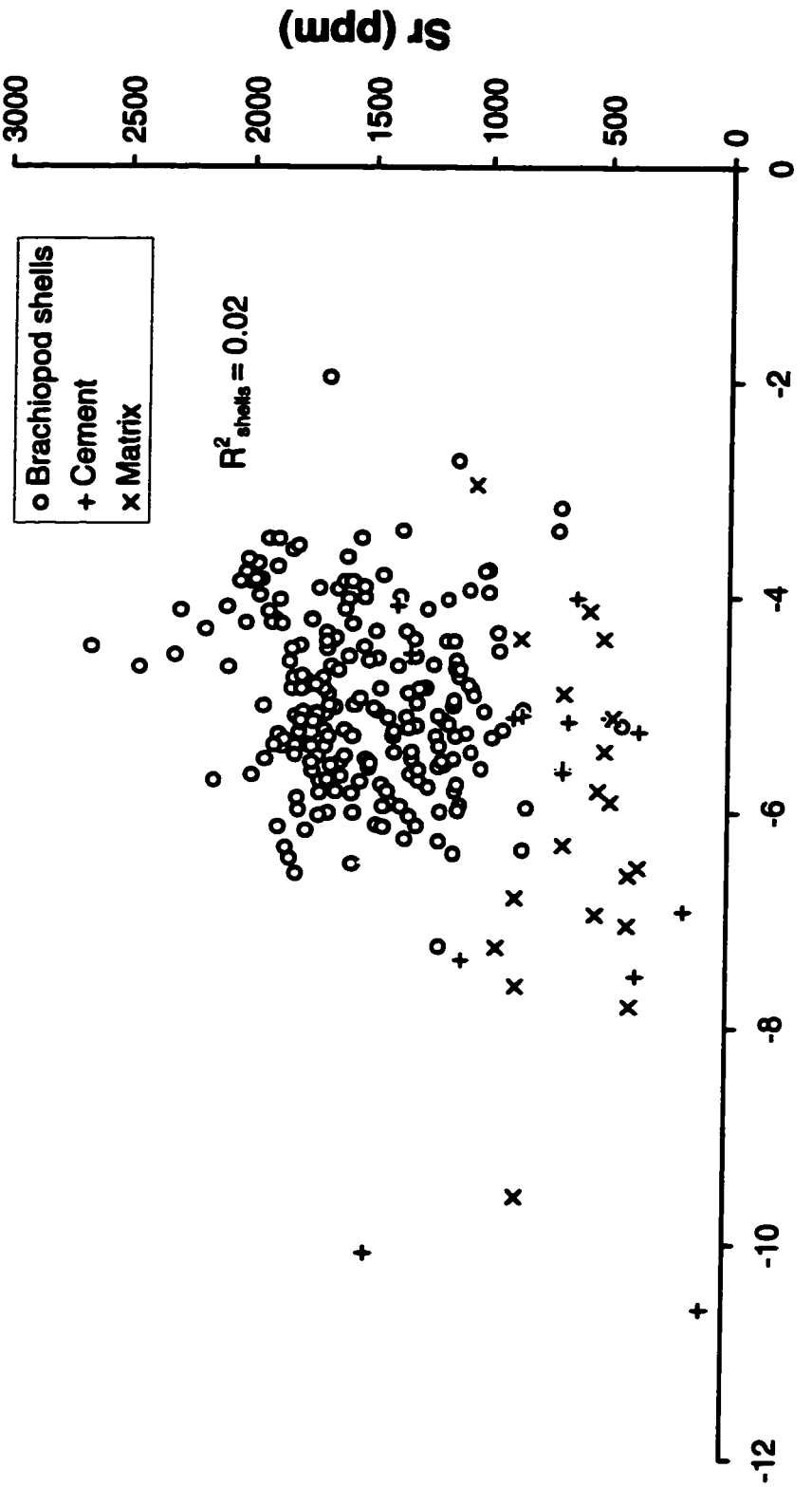

Fig. 5.4. Scatter diagram of $\delta^{18}O$ vs. Sr for all studied samples (brachiopod shells, cement and matrix). Oslo data are not included.

Differences in water/rock ratios among diagenetic systems of sampled localities could perhaps also explain why most of the matrix and cements show clear post-depositional repartitioning trends for $\delta^{18}O$, Mn and Sr, yet a few have isotopic signatures similar to those of the preserved shells (Fig. 5.3), particularly where the matrix was made of reworked shell fragments of other shells or when the cements were of marine origin. Among such isotopically "near-marine" cements and matrix (particularly those from Gotland and Britain), some have bright red luminescence and they also have Sr and Mn contents typical of the altered samples (Fig. 4.1). An interpretation that could explain the above observations can perhaps be based on the general rule that most carbonate diagenesis is an early post-depositional phenomenon, with diagenetic fluids having a high seawater component. In that case, recrystallization in a rock dominated system may yield altered trace element patterns, while isotope ratios may still remain seawater-like.

Isotope Signals and Preservation of Ultrastructure

Most samples in this project show petrographic and chemical criteria that support their good textural preservation. It is therefore not surprising that the results for single samples are in accord with the average values for all samples in their biozones (Table 5.1). Yet, this is frequently the case also for somewhat altered (e.g. PK 22) or entirely recrystallized (e.g. G19) samples. This would suggest that, in many instances, recrystallization of the shell was either accomplished during very early diagenesis when the isotopic and chemical properties of diagenetic solutions still retained the vestiges of seawater composition, and/or that the recrystallization was attained in successive small steps in a closed rock-dominated system.

Sample ID	$\delta^{18}O_{shell}$	$\delta^{18}O_{biozone} \pm 1\sigma$	$\delta^{13}C_{shell}$	$\delta^{13}C_{biozone} \pm 1\sigma$	SEM	CL
A916	-5.29	-5.30 ± 0.14	0.69	1.14 ± 0.38	excellent	none
A806	-5.01	-4.93 ± 0.57	0.68	1.03 ± 0.87	good	dull to none
EK3	-5.38	-5.30 ± 0.35	-0.52	-0.28 ± 0.35	good	dull to none
PK22	-6.11	-5.76 ± 0.41	0.20	-0.30 ± 0.29	fair to poor	dull
G19	-4.75	-4.70 ± 0.68	4.37	4.15 ± 0.82	altered	N/A

Table 5.1. Correlation of the isotopic composition of brachiopod shells with different degrees of ultrastructure preservation and their comparison with the average isotopic signal for correlative biozones.

5.5. VITAL CONTROLS

5.5.1. Inter-species and Intra-species Isotopic Variations

Many marine organisms exhibit disequilibrium fractionation of O and C isotopes during shell calcification (cf. Wefer and Berger, 1991). In contrast, brachiopods are among the few organisms that tend to precipitate their shells near or in equilibrium with the isotopic composition of ambient seawater (cf. Lowenstam 1961; Bates and Brand, 1991; Carpenter and Lohmann, 1995). Table 5.2 shows the variations in the $\delta^{18}O$ and $\delta^{13}C$ mean values of samples for different brachiopod orders from the same graptolite biozone (*M. ludensis*). The slight, ± 0.3 ‰, variations between the orders for both isotopes imply that these brachiopod shells do not possess any significant **inter-species** vital isotope fractionation effect (cf. also Bates and Brand, 1991; Wadleigh and Veizer, 1992; Qing and Veizer, 1994). Comparable modern brachiopods, from latitudes less than 40°, display similar small $\delta^{18}O$ variations of up to ± 1 ‰ (Carpenter and Lohmann, 1995).

In order to test for **intra-species** isotope variations, 12 samples of *Atrypa reticularis* from the same formation (Much Wenlock, Britain) and the same biozone were analysed. Their $\delta^{18}O$ and

$\delta^{13}C$ values (-5.11 ± 0.47 and 1.00 ± 0.44 ‰, respectively) show less than ± 0.5 ‰ deviations. This is comparable to the 0.5 ‰ range reported for intra-specimen variations in modern brachiopods (cf. Carpenter and Lohmann, 1995).

Order	n	$\delta^{18}O \pm 1\sigma$	$\delta^{13}C \pm 1\sigma$
Orthida	3	-5.70 ± 0.37	1.29 ± 1.05
Rhynchonellida	3	-5.61 ± 0.85	0.71 ± 1.03
Pentamerida	2	-5.05 ± 0.04	0.86 ± 0.39
Spiriferida	14	-5.04 ± 0.54	1.23 ± 0.67
Biozone	22	-5.35 ± 0.34	1.02 ± 0.31

Table 5.2. Mean $\delta^{18}O$ and $\delta^{13}C$ values of brachiopod samples from the *M. ludensis* Biozone, n= number of samples.

5.5.2. Intra-specimen Variations

The posterior (umbo) and anterior parts of the individual shell were sampled in different specimens, including *Atrypa reticularis* (spiriferid), *Hesperorthis* sp. (orthid) and *Leptaena depressa* (strophomenid). Their $\delta^{18}O$ and $\delta^{13}C$ values (Table 5.3) display no clear pattern, but the differences within the same shell were always less than 0.5 ‰ for both isotopes. Again, this is similar to variations observed in modern brachiopods (Carpenter and Lohmann, 1995).

In conclusion, the isotope signals recorded from the examined Silurian brachiopods show no evidence of significant influence by vital controls.

Sample ID	Formation	Genus	$\delta^{18}O$	$\delta^{13}C$
G12p	Mulde	*Leptaena depressa*	-4.65	1.86
G12a			-4.46	1.70
G38p	Mulde	*Atrypa reticularis*	-3.45	1.40
G38a			-3.76	1.49
G59p	L. Visby	*Hesperorthis sp.*	-6.12	1.13
G59a			-5.71	1.30
G60p	L. Visby	*Atrypa reticularis*	-5.29	1.38
G60a			-5.94	1.49
G66p	Mulde	*Atrypa reticularis*	-3.91	1.68
G66a			-3.98	1.71
G74p	L. Visby	*Atrypa reticularis*	-5.29	1.38
G74a			-5.80	1.42
G85p	Mulde	*Atrypa reticularis*	-3.51	1.60
G85a			-3.45	1.70
G86p	Slite	*Atrypa reticularis*	-5.08	-0.76
G86a			-5.47	-0.25

Table 5.3. Variations in $\delta^{18}O$ and $\delta^{13}C$ values of the posterior (p) and anterior (a) parts of brachiopod shells from the Silurian succession in Gotland.

5.6. FACTORS CONTROLLING ISOTOPIC COMPOSITION OF SILURIAN BRACHIOPODS

The full spectrum of the newly accumulated $\delta^{18}O$ and $\delta^{13}C$ data for Silurian brachiopods is presented in Figure 5.5 (see also Appendices 2 and 4). The overall Silurian trends show frequent oscillations that correlate with sea-level changes, with $\delta^{18}O$ likely reflecting temperature and salinity of the Silurian seawater and $\delta^{13}C$ indicating changes in the dissolved inorganic carbon (DIC) content. All these factors are discussed in depth in the subsequent text.

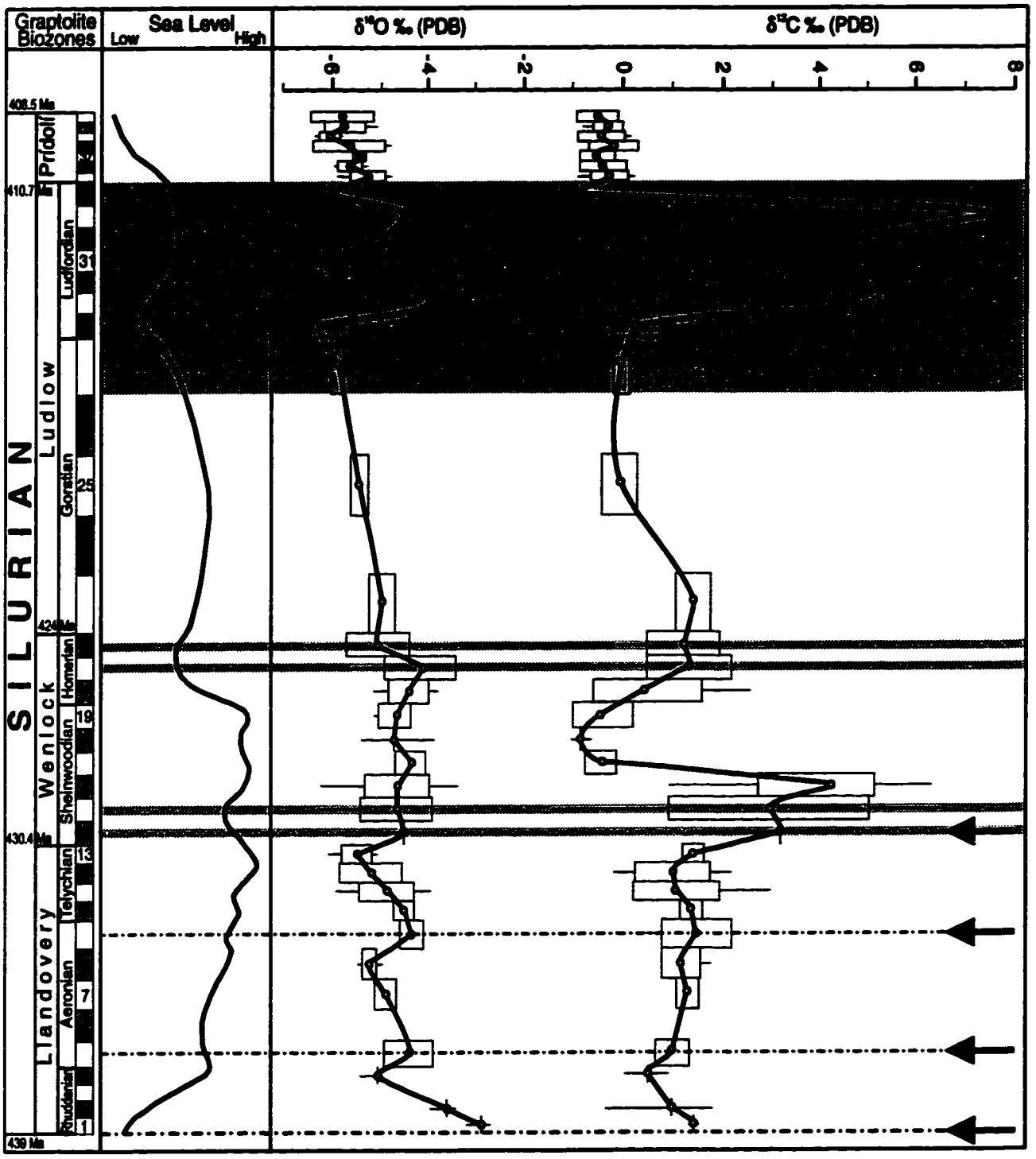

Fig. 5.5. Silurian isotope curves showing the variations in $\delta^{18}O$ and $\delta^{13}C$ values of brachiopods and of sea-level changes, the latter after Johnson et al. (1991). The black lines connect the means for each graptolite biozone. Boxes represent 2 σ ranges and bars refer to the maximum and minimum values. The estimated absolute ages follow the scale suggested by Harland et al. (1990). The highlighted bands represent ventilation episodes, as suggested for the Wenlock by Kemp (1991) and for the Ludlow by Jaeger (1976). Arrows refer to glacial episodes, as suggested by Grahn and Caputo (1992).The numbers on the biozonation bar refer to graptolite biozones in Fig. 1.4. The samples from Norway are excluded. The full list of data is in Appendix 2.

5.6.1. Oxygen Isotopes

5.6.1.1. Temperature

Determination of paleotemperature using $\delta^{18}O$ values of fossil carbonates relies on the fact that fractionation of $^{18}O/^{16}O$ between seawater and precipitated calcite depends on temperature as well as the isotope composition of seawater from which the carbonate was precipitated. This relationship can be expressed by the equation (Hays and Grossman, 1991):

$$T\,(^{\circ}C) = 15.7 - 4.36\,(\delta_c - \delta_w) + 0.12\,(\delta_c - \delta_w)^2$$

where δ_c stands for the $\delta^{18}O$ value of calcite (brachiopod shell) in PDB, δ_w is the $\delta^{18}O$ value of seawater in SMOW and T is the ambient temperature in °C. An increase in temperature results in proportionally less incorporation of ^{18}O in the precipitated calcite, whereas a decrease results in the opposite effect. The knowledge of δ_w is one of the chief limitations on the use of $\delta^{18}O$ variations for calculation of paleotemperatures, because the $\delta^{18}O$ of seawater can vary due to glaciation, evaporation, or to dilution by freshwater in near-shore areas.

In modern environments, the temperature of tropical seawater ranges between 23 and 27 °C, the optimum condition for reef growth (Milliman, 1974). Protein molecules cannot withstand unbroken temperatures in excess of 37°C (Brand, 1989). Since the sampled successions (Anticosti, Wales, Gotland, Baltic states and Podolia) were all located between paleolatitudes 30°N and 30°S (cf. Scotese and McKerrow, 1990; McKerrow et al., 1991) and they were all associated with reefal facies, a comparable range of temperatures is to be expected also for the tropical Silurian seas. Assuming that the $\delta^{18}O$ of seawater was constant during geologic history, at about -1 ‰ SMOW (Karhu and Epstein, 1986), the calculated temperatures for Silurian seawater would have ranged between 20.18 °C and 42.7°C, not a realistic scenario. Assuming

a $\delta^{18}O$ for Silurian seawater of 0 ‰ SMOW, as today, would only compound the difficulty by increasing the temperatures by about 5°C. Furthermore, such a large range of temperatures (22 °C) is atypical for the equatorial zone, where even the post-glacial increase in temperature was estimated to be no more than about 5 to 6 °C (Crowley, 1994; Guilderson et al., 1994). The consequences of these observations will be discussed later in the text.

5.6.1.2. Salinity

Salinity (S), as a function of evaporation or freshwater dilution, contributes to the factors controlling the $\delta^{18}O$ variations in surface ocean water. The increase in the rate of evaporation causes an enrichment in ^{18}O of surface water, whereas mixing with ^{18}O-depleted meltwater or river runoff has the opposite effect.

Modern open ocean waters range in salinity between 33 and 37 ppt (‰) and in $\delta^{18}O$ SMOW between -0.5 and 1.1 ‰, with $\Delta\delta^{18}O/\Delta S = 0.15$ (GEOSECS, 1987). Evaporation may increase the seawater $\delta^{18}O$ by 0.3 to 0.4 ‰ per ppt salinity increase (Railsback et al., 1990), whereas mixing with runoff, depending on the source, may decrease it by 0.1 to ~ 0.6 ‰ per ppt salinity decrease (Craig and Gordon, 1965). For comparison, Carpenter and Lohmann (1995) suggested an average $\Delta\delta^{18}O/\Delta S$ gradient of about 0.5. Yet, the $\Delta\delta^{18}O/\Delta S$ ratio does appear to vary with latitude and longitude because every oceanic domain has a different salinity value (cf. Faure, 1986; Carpenter and Lohmann 1995). For equatorial seawater, Mii and Grossman (1994) proposed a $\Delta\delta^{18}O/\Delta S$ gradient of 0.1. Assuming that the Silurian salinity patterns were similar to the present ones, the $\Delta\delta^{18}O/\Delta S$ value of 0.1 will be applied here.

If salinity were assumed to be the sole factor controlling the $\delta^{18}O_{shell}$, the expected range of

$\delta^{18}O$ variations would only be ~ 0.4 ‰ for a salinity range of ~ 33 to 37 ppt, and ~ 0.6 ‰ for a 32 to 37 ppt range (cf. Carpenter and Lohmann, 1995). In such a scenario, the observed *[29]nassa-bohemicus* Biozone (zone 29 in Fig. 5.5) shift of ~ 2 ‰ would require a salinity change of approximately 20 ppt. This is an unrealistic alternative since the brachiopods, and the associated fossils (e.g. corals), are a stenohaline fauna that cannot tolerate such large salinity variations.

5.6.1.3. Paleodepth

The association of reefs with the studied successions is a significant indication of shallow environmental conditions. Comparison of $\delta^{18}O$ values for shells from such successions with those from successions without reef associations may therefore provide a clue about the paleodepth control on the $\delta^{18}O$ values. Figure 5.6 compares $\delta^{18}O_{shell}$, commonly spiriferids, from Gotland and Britain (reef-associated) with those from Lithuania (non reef-associated) during Wenlock times. The $\delta^{18}O$ values of shells from Lithuania (-4.1 ± 0.4 ‰ PDB) are consistently heavier than those from Gotland (-4.8 ± 0.5 ‰ PDB) and Britain (-4.9 ± 0.4 ‰ PDB). The difference, on average about 0.8 ‰, may reflect a temperature gradient of about 4 °C, with the deeper water being somewhat cooler. Pursuing this argument further, one could expect that for Lithuania there may exist also an ^{18}O enrichment gradient westwards with increasing paleodepth (cf. Paškevičius et al., 1994). This, however, is not the case, with the $\delta^{18}O$ signal from the core Graužai-105 in the east being comparable to the one from the core Vilkaviškis-129 in the southwest (Fig. 2.10). Nonetheless, the consistently heavier $\delta^{18}O$ of deeper water brachiopods, relative to their reef-associated counterparts, strongly supports the previously advocated proposition that the measured $\delta^{18}O$ values reflect the primary seawater signal.

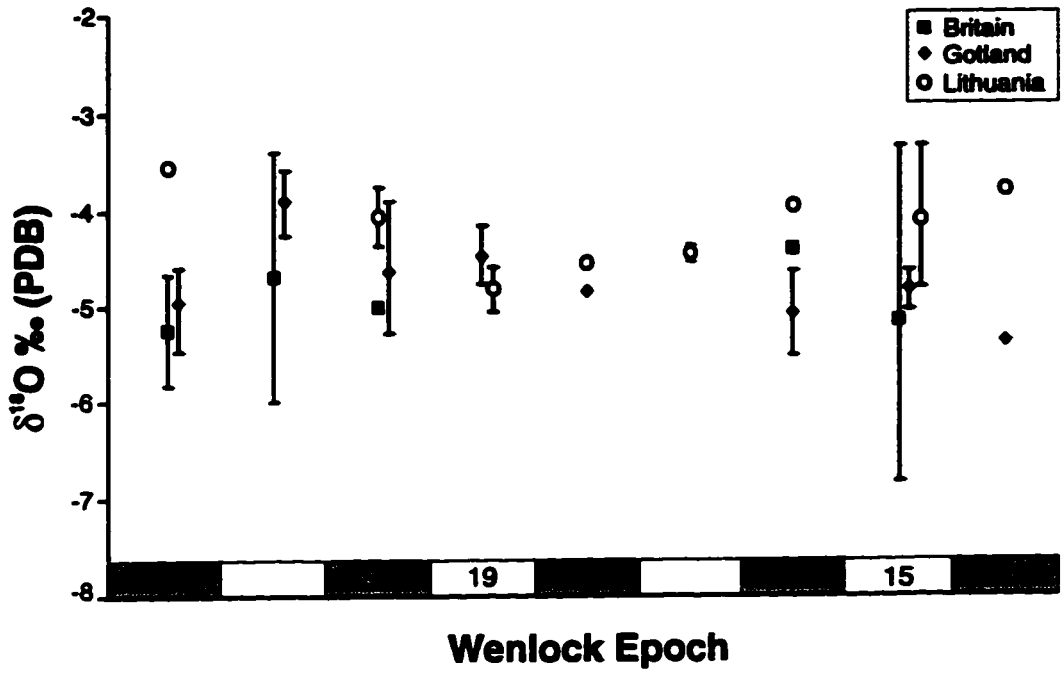

Fig. 5.6. Correlation of average $\delta^{18}O$ values of Wenlock brachiopods from different depositional settings. Numbers on the x-axis refer to the graptolite biozones as in Figure 1.4. Error bars represent 2σ values.

5.6.1.4. Change of Seawater $\delta^{18}O$

(a) Long-Term Secular Changes:

The isotope record of marine chemical sediments shows a general trend of decreasing $\delta^{18}O$ values with increasing age. This trend has been observed in carbonates (Keith and Weber, 1964; Weber, 1965; Perry and Tan, 1972; Schidlowski et al., 1975; Veizer and Hoefs, 1976; Popp et al., 1986; Veizer et al., 1986; Wadleigh and Veizer, 1992; Qing and Veizer, 1994), cherts (Degens and Epstein, 1962; Perry and Tan, 1972; Knauth and Epstein, 1976; Knauth and Lowe, 1978) and glauconites (Keppens and O'Neil, 1985). In accord with this, all $\delta^{18}O$ values for the Silurian are strongly depleted in ^{18}O (Figs. 5.1 and 5.5).

The overall $\delta^{18}O$ depletion of Silurian brachiopods is some 4 to 5 ‰, if compared with their Recent counterparts. As already discussed (section 5.6.1.1), the assumption that the $\delta^{18}O$ of Silurian seawater was similar to the Quaternary one (0 to -1 ‰ SMOW) would result in paleotemperature of ~ 20 to 48 °C, unrealistically high if compared to those of the modern environments.

The brachiopod $\delta^{18}O$ signals reflect mainly the temperature of summer seasons during which the rate of shell precipitation is at optimum. Assuming that the temperature of the Silurian tropical surface seawater during warm episodes was about 20 to 30 °C, similar to that of modern environments in summer (Skinner and Porter, 1987), the most depleted brachiopod signals (-4.5 to -6.4 ‰ PDB) would indicate a seawater $\delta^{18}O$ of about -3.5 ‰ SMOW (Fig. 5.7). During glacial times, with seawater $\delta^{18}O$ suggested to have been heavier by ~ 1 ‰ (cf. Guilderson et al., 1994; Crowley, 1994; Railsback, 1990), the heaviest brachiopod signals (-2.9 to -4 ‰ PDB), would correspond to temperatures range of 14 to 23 °C (Fig. 5.7), comparable to tropical temperatures of 14 to 28 °C during the latest Quaternary glaciation (Skinner and Porter, 1987). The above temperature ranges are reasonable estimates and they are also consistent with the frequent association of the studied brachiopods with coral reefs.

In conclusion, the Silurian surface seawater is suggested to have had $\delta^{18}O$ composition of -2.5 to -3.5 ‰ SMOW. The lowest $\delta^{18}O$ value of -6.4 ‰, from the Ludfordian of Podolia, was not duplicated by the isotope records from the other basins, such as Gotland (cf. Wenzel and Joachimski, 1996). This suggests that the observed minimum is of local rather than of global significance.

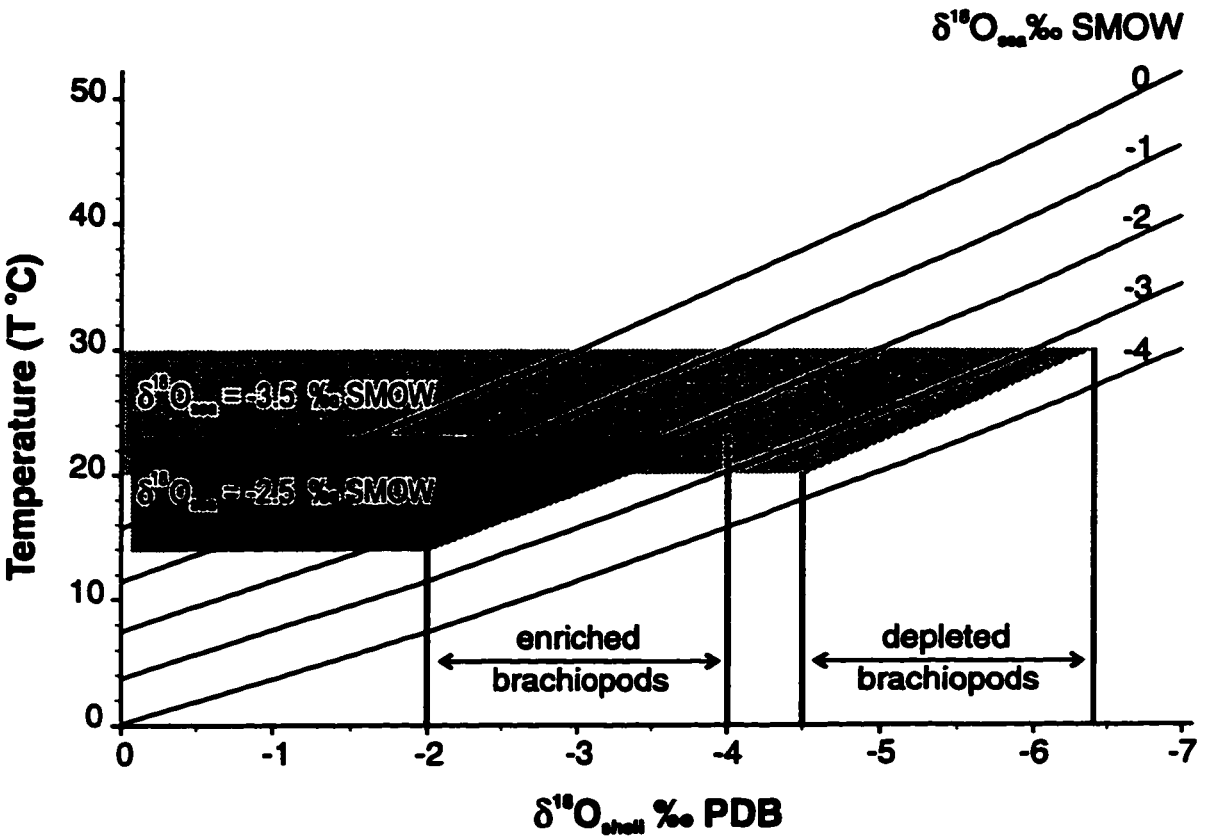

Fig. 5.7. $\delta^{18}O_{shell}$ vs. temperature for various $\delta^{18}O_{seawater}$ values. The vertical bars indicate the $\delta^{18}O_{shell}$ ranges for the most enriched and depleted Silurian brachiopods and shaded areas mark the preferred temperature ranges. For more details, see text.

The problem is how to generate the advocated -3 ± 0.5 ‰ isotopic shift in view of the large reservoir of ocean water. The interpretation may be based on an assumption of a changing magnitude of water/silicate interaction at mid-ocean ridges (Holland, 1984). The interaction of water with basalts in high temperature hydrothermal systems results in preferential enrichment of ^{18}O in seawater, whereas the low temperature submarine weathering causes an opposite effect. The overall Silurian $\delta^{18}O$ gradient of about -1 ‰ per 30 Ma could still be easily accommodated within the varying water/silicate regime, since the required adjustments to the model in favour of the low temperature processes would have to be relatively minor. The progressive increase in $^{87}Sr/^{86}Sr$ value with decreasing age (Burke et al., 1982; Bertram et al., 1992, Chapter VI in this study) could also be consistent with the suggestion of declining volcanic activity in the course of the Silurian, at least until the late Ludlow. However, the general global warming that followed the late Ordovician glaciation (e.g. Frakes et al., 1992) was a more plausible reason for both the overall slightly decreasing Silurian $\delta^{18}O_{shell}$ values and the increased input of radiogenic Sr from the continents due to increased weathering.

On the other hand, the relative budgets of seawater/silicate interactions at high to low temperatures suggest that they may have balanced each other, thus keeping the $\delta^{18}O$ values of oceans around 0 ‰ SMOW (Muehlenbachs, 1986). In such a scenario, large scale changes in $\delta^{18}O$ of seawater are not permissible (Gregory, 1991). The observed downward shift of the entire $\delta^{18}O$ data set, by some 4 to 5 ‰, is therefore difficult to reconcile with the existing models of oceanic water/rock interactions, providing the models indeed reflect the natural system. At this stage, the explanation for the large ^{18}O depletion of Paleozoic samples remains enigmatic.

(b) Short-Term Secular Changes:

The Silurian $\delta^{18}O$ spectrum (Fig. 5.5) shows a relative depletion of ~ 1 ‰ PDB with decreasing age, opposite to the trend for the entire Paleozoic. Assuming that the $\delta^{18}O$ of Silurian seawater did indeed differ from its Quaternary counterpart, the 1 ‰ depletion is consistent with the general global warming trend during the Silurian that followed the late Ordovician glaciation (cf. Middleton et al., 1991; Long, 1993). Superimposed on this long-term trend are short-term oscillations of up to 2 ‰ that may have various causes.

Glaciation, one of the suggested mechanisms for generation of short-term $\delta^{18}O$ oscillations in seawater composition, results in the storage of ^{16}O in polar ice caps, leaving the seawater enriched in ^{18}O (Anderson and Arthur, 1983). In addition, advances of ice sheets can enhance the albedo effect and reduce the CO_2 content of the atmosphere, due to inhibited weathering, thus leading to a drop in temperature of the terrestrial atmosphere.

The equatorial seawater temperature rise following the latest glacial maximum was ~ 6 °C (cf. Guilderson et al., 1994; Crowley, 1994). This temperature oscillation alone could account for $\delta^{18}O_{shell}$ variations of ~ 1 ‰ and the simultaneous waning and waxing of ice sheets could have strengthened the signal by a similar amount. Comparable short-term $\delta^{18}O$ fluctuations have been observed also during the Silurian (Fig. 5.5) and the lower Silurian ^{18}O enrichments indeed coincide, within the uncertainty limits of one biozone, with the proposed glacial episodes and with the drops in sea level. The coincidence of lower temperatures with sea-level drops is to be expected even in the absence of polar ice caps, since variations in seawater temperature also result in corresponding changes in the volume of the water mass. An increase in seawater temperature from 0 to 12 °C, for a water column of 3.44 km, may lead to a sea-level rise of

about 3 m in shelf areas (Cotter, 1988).

Following the large late Ordovician glaciation, three successive glacial phases, indicated by diamictites, have been recognized in the Amazon Basin (Grahn and Caputo, 1992). These were in the early middle Llandovery (early Aeronian, *gregarius* Biozone), the middle Llandovery (latest Aeronian) and the earliest Wenlock. Comparable glacial phases were documented also in the Silurian deposits of north and south Africa (Grahn and Caputo, 1992). The estimated duration of each glacial phase is about 2.5 Ma (Johnson et al., 1991; Cotter, 1988), comparable to the third order cycles of eustatic sea-level changes (Plint et al., 1992). The earliest Wenlock positive $\delta^{18}O$ shift was documented also by Wenzel and Joachimski (1996) in Gotland, but they assigned it upward by two graptolite biozones, possibly due to minor correlation mismatch.

No Silurian glacial deposits, or evidence of cool climatic conditions younger than the earliest Wenlock, are as yet known from Gondwana and it is, therefore, difficult to assign the observed younger ^{18}O enrichments to such a cause. It is still possible that the glacial record has been eradicated by erosion or by subduction, but such a scenario is not very plausible in view of the generally warm climate that dominated the later Silurian (Frakes et al., 1992).

Except for the earliest Wenlock glacial episodes, that may conceivably have coincided with the Ireviken Event, none of these glacial phases coincided with extinction events. Global changes in temperature were therefore not the sole driving force for the sharp faunal changes. This is similar to the Quaternary, where large eustatic sea-level changes did not result in significant extinctions in marine biota (cf. Eckert, 1988).

(c) Stratified Oceans:

Wilde et al. (1991) and Cotter (1988) claimed that the mudrock clam assemblages of Gondwana's shelf seas indicate oxygen-poor environments, perhaps implying a salinity stratification of the ocean (cf. Railsback, 1990; Railsback et al., 1990). The latter authors invoked such a model in order to explain those negative $\delta^{18}O$ shifts that correlate with sea-level highstands. The existence of strongly stratified oceans could also be consistent with assumed lower oxygen levels in the Silurian atmosphere (30 to 50 % of modern; Kemp, 1991) that was supposedly a consequence of lesser terrestrial plant cover. All this may have resulted in an anoxic water body below about 100 m, that is below the photic zone (cf. Wilde et al., 1991). If so, the scenario may also be invoked as the explanation for the bacterial pyrite in many Silurian brachiopod shells.

Regardless of the validity of the above assupmtions, the distribution of Silurian paleocontinents and lithofacies (McKerrow et al., 1991; Cocks and Scotese, 1991) suggests the existence of expanded epeiric seas with restricted connection to the open ocean as indicated by dolomitic facies, particularly in the tropical zones. During warm episodes and sea-level highstands, evaporation would have been enhanced in shelf environments, generating dense warm saline ^{18}O-rich waters. Such water would circulate down slope, feeding the warm saline deep water (WSDW) and leaving the surface water less saline and enriched in ^{16}O (Fig. 5.8). Formation of warm saline water would have been terminated during sea-level lowstands, with cold water from polar zones flushing the ^{18}O-rich saline waters from deep oceans and establishing a prevailing thermohaline circulation (Fig. 5.8).

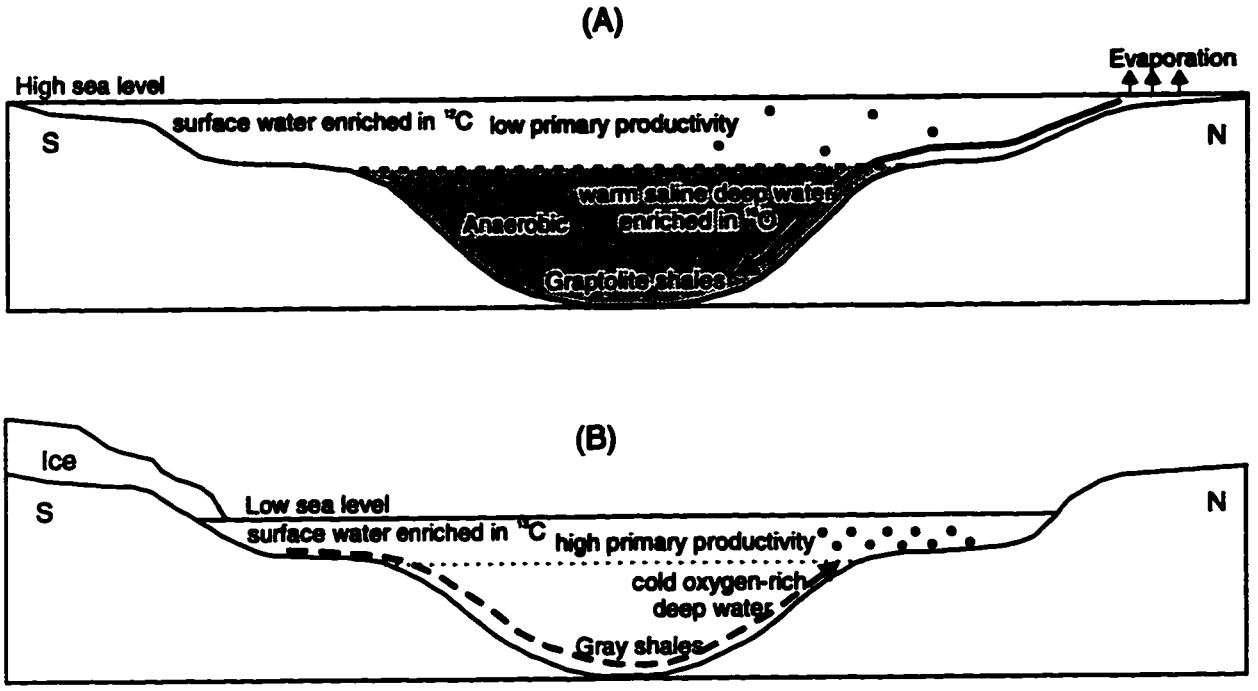

Fig. 5.8. Models of Silurian ocean during (A) sea- level highstands and (B) sea-level lowstands.

The drop in $\delta^{18}O$ signals for surface water caused by WSDW circulation is estimated to be about 0.5 to 1.5 ‰ SMOW, whereas enrichment caused by glaciation should account for 0.5 to 1.2 ‰ SMOW (cf. Railsback, 1990). These magnitudes are comparable to the $\delta^{18}O$ oscillations exhibited by the Silurian oxygen-isotope curve (Fig. 5.5).

In summary, all indications are that the $\delta^{18}O$ signal of Silurian brachiopods is a primary feature of the geologic record, although the reason for overall ^{18}O depletion relative to its modern counterpart remains somewhat enigmatic. In contrast, the shorter term fluctuations of smaller magnitude can well be a consequence of waning and waxing of ice caps and/or changes in deep ocean circulation.

5.6.2. Carbon Isotopes

Carbon isotope variations during the Phanerozoic form the experimental base for modelling of variations in partitioning of carbon among global carbon reservoirs (e.g. Magaritz, 1991). The sizes of reservoirs are controlled by inputs from riverine influx of organic and inorganic carbon, from exchange with atmospheric CO_2 , from submarine volcanic CO_2 degassing, and from oxidation of organic matter. The outputs include deposition of marine carbonates and burial of organic matter (Anderson and Arthur, 1983).

The overall trend of Silurian $\delta^{13}C$ shows a depletion of about 1 ‰ with decreasing age (Fig. 5.5), with several remarkable short-term shifts, of 3 to 8 ‰ magnitude, superimposed on this general trend during the early and late Wenlock and the early Ludlow. A similar heavy $\delta^{13}C$ spike has previously been observed also during the late Ordovician, a glacial interval marked by sea-level lowstand (Middleton et al., 1991; Frakes et al., 1992; Brenchley et al., 1995). In the Ordovician, the spike likely reflects a high organic productivity (cf. Holser, 1994). In the Silurian, the spikes also correlate with sea-level lowstands and with positive $\delta^{18}O$ shifts, that is with episodes with vigorous circulation and highly oxygenated deep ocean water. Such conditions are amenable to high oxidation and dispersal of $C_{organic}$. It is therefore unlikely that enhanced $C_{organic}$ burial was the cause of the positive $\delta^{13}C$ spikes. More likely, as in the Ordovician, it was the increased productivity, perhaps due to nutrients supplied by upwellings, and/or by enhanced influx of organic matter from land sources during sea-level lowstands (cf. Schidlowski and Aharon, 1992) that could have been the causative factors. Yet, the Silurian record shows no clear evidence of anomalously high productivity, such as the Cenozoic plankton blooms, that could be made accountable for a large global scale $\delta^{13}C$ shift of up to ~ 8 ‰ in the

Ludfordian (Fig. 5.5). It is therefore possible that this large excursion is only a local feature of the Gotland basin.

Jaeger (1976) and Kemp (1991) proposed a Silurian paleoceanographic ventilation model along the lines of above scenario, suggesting that the black shales were deposited beyond the outer shelf under anoxic to anaerobic conditions during sea-level highstands. During ventilation periods, that indeed appear to have coincided with sea-level lowstands (Fig. 5.5) during the early and late Wenlock and late Ludlow (Ludfordian) (Johnson et al., 1991), the black shale deposition was retarded. Note, however, that the reverse is not always true because the Llandovery black shales do not correlate with sea-level highstands (Kemp, 1991).

Summarizing the discussion for stable isotopes, I propose that the slight overall depletion of ~ 1 ‰ PDB in $\delta^{18}O$ during the Silurian may reflect a slight increase in global temperature during a tectonically inactive period. The $\delta^{18}O$ and $\delta^{13}C$ trends are parallel and correlate negatively with sea-level stands of Johnson et al. (1991). The glacial phases, documented for the early Silurian by Grahn and Caputo (1992), correlate with the positive $\delta^{18}O$ shifts in the Silurian isotope curve and with low sea levels, but other $\delta^{18}O$ shifts have no known glacial correlatives. The Přídolí was generally a warm episode with sea-level highstands, punctuated by apparent minor sea-level oscillations that were most probably caused by local tectonism (Kaljo, 1971). The overall light oxygen isotope values of Silurian brachiopods, in contrast to the superimposed variations, cannot be explained conclusively by any single causative factor. It appears that scenarios which involve a differing mode and/or magnitude of seawater/silicate interaction in the global tectonic cycle as well as temperature and salinity variations must all be taken into account. The remarkable $\delta^{13}C$ shifts shown by the Silurian isotope trend are not accompanied by any clear evidence of

high rate of $C_{organic}$ burial. An alternative explanation, that they may have been caused by variations in organic productivity, needs confirmation by additional evidence.

CHAPTER VI

STRONTIUM ISOTOPE GEOCHEMISTRY

6.1. INTRODUCTION AND THEORETICAL CONCEPT

Variations in seawater $^{87}Sr/^{86}Sr$ over geologic time, particularly for the Phanerozoic, have proven to be a useful tool for reconstruction of the evolutionary history of ancient seawater (Veizer and Compston, 1974; Burke et al., 1982; Veizer, 1989; McArthur, 1994; and references therein), for understanding of continental weathering processes and of mid-ocean ridge hydrothermal circulation (cf. Hodell et al., 1990; Richter et al., 1992; Farrell et al., 1995), and for correlation and dating of marine sedimentary rocks (e.g. Elderfield, 1986; Quinn et al., 1991; McArthur, 1994). The dominant driving forces causing the changes in seawater isotopic ratios are: (1) the continental runoff and groundwater runout, which supply radiogenic strontium to the oceans, and (2) the seawater-oceanic crust interaction, particularly the hydrothermal rift-related activities supplying the less radiogenic strontium (Palmer and Elderfield, 1985). Other factors, such as diagenetic flux and carbonate recycling, may account for a minor contribution (Elderfield, 1986; Veizer, 1989).

When biogenic marine carbonate forms, the $^{87}Sr/^{86}Sr$ of ocean water is incorporated into its structure with no fractionation. The oceanic uniformity of $^{87}Sr/^{86}Sr$ at any given time is to be expected, because the residence time of Sr in the oceans (~ 10^6 yrs.) is much longer than the time it takes for currents to mix the oceans (Faure, 1986). However, for highly stratified oceans, the response may be different due to possible mixing rates of bottom waters approaching the residence times for Sr in seawater (McArthur, 1994).

The seawater Sr-isotope composition is usually expressed as $^{87}Sr/^{86}Sr \pm 2\sigma$, where σ is the standard deviation, but some authors convert the $^{87}Sr/^{86}Sr$ into δ-notation, where:

$$\delta^{87}Sr = \left\{\left(\left(^{87}Sr/^{86}Sr\right)_{sample}/\left(^{87}Sr/^{86}Sr\right)_{standard}\right) - 1\right\} * 10^5$$

Others (Dia et al., 1992) use $\Delta^{87}Sr$ notation, where:

$$\Delta^{87}Sr = \left(\left(^{87}Sr/^{86}Sr\right)_{sample} - \left(^{87}Sr/^{86}Sr\right)_{standard}\right) * 10^5$$

The accuracy and precision of the isotopic data are evaluated by repeated measurements of Sr isotope standards. The National Bureau of Standards (NBS) Standard Reference Material 987 (SRM 987) is the most frequently used (Thirwall, 1991), but the USGS Tridacna carbonate standard (EN-1), prepared from a modern clam from Enewetak Atoll, and the Eimer and Amend Standard (E & A) are also utilized, the latter only rarely.

The decay of ^{87}Rb to ^{87}Sr, which alters the $^{87}Sr/^{86}Sr$ value, is usually adjusted for by Rb-correction, but for carbonates that usually have Sr concentrations exceeding those of Rb by orders of magnitude, this is mostly negligible (cf. McArthur, 1994).

Variations in $^{87}Sr/^{86}Sr$ composition of past seawater, resolvable on a short-time scale of 10^7 to 10^6 yrs., may be utilized for high-resolution stratigraphic correlations with an accuracy comparable to, and perhaps higher than, that of biostratigraphy, the latter usually 1 to 5 Ma, providing the temporal $^{87}Sr/^{86}Sr$ variations are characterized by steep slopes. This was the case for several intervals of the Phanerozoic, and particularly for the Cenozoic (e.g. Mead and Hodell, 1995).

6.2. OBJECTIVES OF STRONTIUM ISOTOPE STUDY

The main objectives of this study are: (1) refinement of the Sr-isotope curve for Silurian

seawater, (2) utilization of such a refined curve for high resolution stratigraphic correlation, and (3) improved understanding of geochemical cycling of Sr during the Silurian, particularly with a view to constraining coeval paleoclimatic patterns.

6.3. PREVIOUS WORK

Significant temporal oscillations in Sr isotopic composition of Phanerozoic seawater were outlined by Burke et al. (1982), but their work was based mostly on whole-rock samples. Due to possible distortion of the original $^{87}Sr/^{86}Sr$ signal by diagenetic alteration, other materials have been suggested for development of a seawater curve, including biogenic carbonates, marine barite, apatite (conodonts, fish teeth and bones), and marine carbonate cements (Burke et al., 1982; Bertram et al., 1992; Ruppel et al., 1996).

For the Silurian, only the data of Bertram et al. (1992) and Ruppel et al. (1996), based on phosphatic fossil conodonts, are presently available. These data have less scatter and they also fall closer to the lower limit of the Burke et al. trend, with Ruppel et al. measurements generally having the least radiogenic values (Fig. 6.1). The observed scatter in the published data may be attributed to either partial diagenetic alteration of the analysed samples or to uncertainties in their age assignment. The incorporated impurities may also contribute to the distortion of the $^{87}Sr/^{86}Sr$ values. Ruppel et al. (1996) reported also some cyclic trends but their amplitudes (0.000015) are within the documented $^{87}Sr/^{86}Sr$ intra-specimen variations for conodonts.

The published Silurian data reveal a general trend of increasing $^{87}Sr/^{86}Sr$ values with decreasing age, followed by a decline in the late Ludlow and Přídolí (Fig. 6.1).

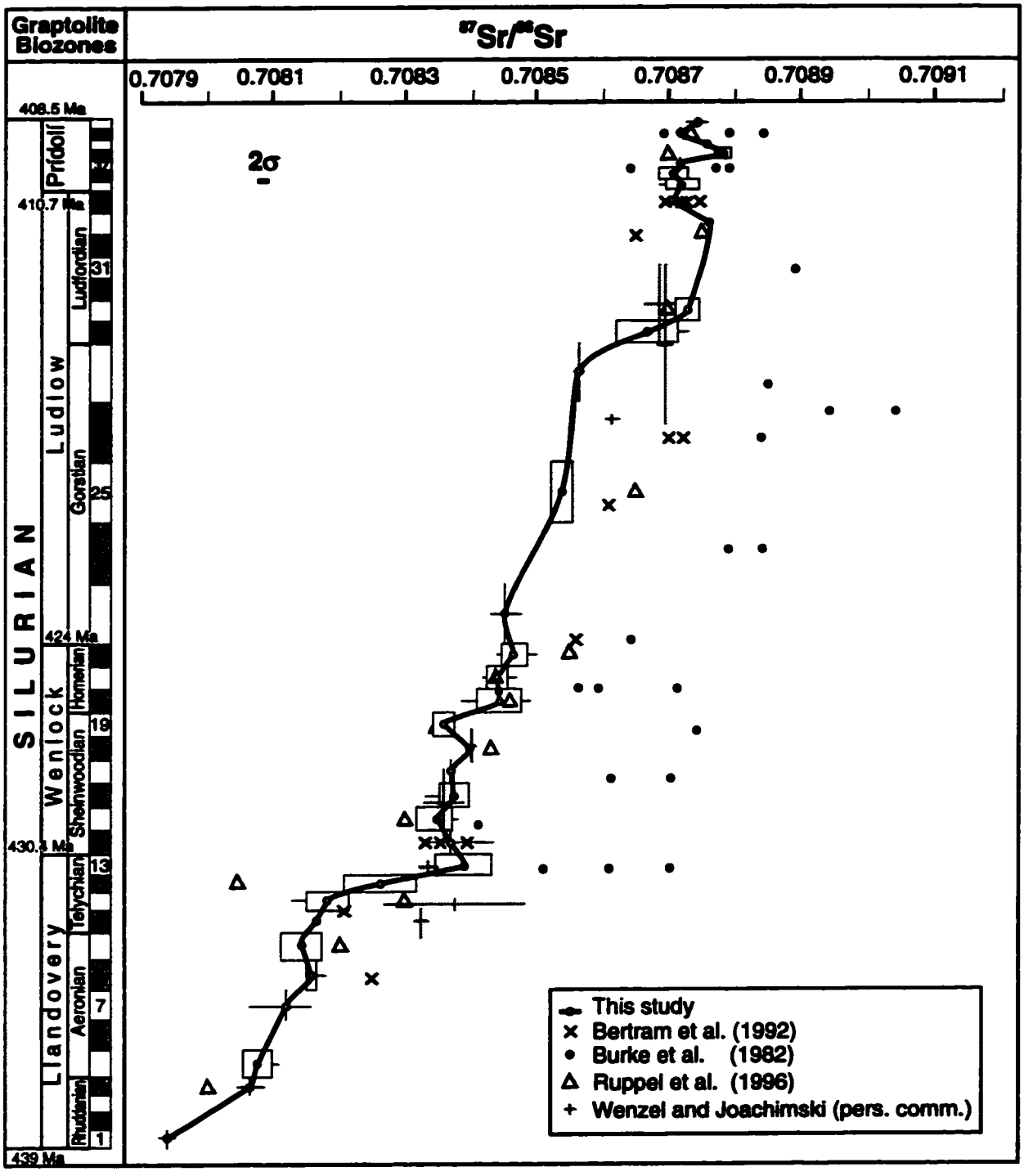

Fig. 6.1. Evolution of $^{87}Sr/^{86}Sr$ ratios throughout the Silurian Period and comparison with the pulished results of Burke et al. (1982), Bertram et al. (1992), Ruppel et al. (1996) and Wenzel and Joachimski (pers. comm., 1996). Boxes represent 2σ values and the bars refer to the ranges of data (see Figure 5.1). The 2σ error bar for the $^{87}Sr/^{86}Sr$ parameter (top left corner) is estimated from the repeated measurements of the NBS 987 standard. Biozonation and numerical ages are as in Figure 5.1. Published $^{87}Sr/^{86}Sr$ data were normalized to 0.710256 for the NBS 987 standard.

6.4. SILURIAN STRONTIUM-ISOTOPE CURVE

The present Sr-isotope curve for the Silurian covers the entire period estimated to be about 30 Ma long, from 439 ± 7 to 408.5 ± 4 (Harland et al., 1990). This time span includes 41 graptolite biozones (Fig. 1.4), each with an estimated duration of less than 1 Ma, except for the Gorstian (early Ludlow) with biozones up to 2 Ma. The curve shows an overall increase in $^{87}Sr/^{86}Sr$ with decreasing age (Fig. 6.1), with abrupt jumps superimposed on the overall trend. The shape of the curve is mainly controlled by: (1) accuracy of the age model used to calibrate the isotope curve, (2) temporal variations in the $^{87}Sr/^{86}Sr$ value of Silurian seawater, (3) post-depositional alteration of brachiopod shells that plays only a subordinate role, and (4) analytical errors (cf. McArthur, 1994).

Point (3) was already discussed in Chapters III and IV and point (4) accounts for only about 0.000015 magnitude (cf. McArthur, 1994). As a result, the data based on brachiopods have less scatter and are usually less radiogenic than published data from coeval whole rocks (Burke et al., 1982) and phosphatic conodonts (Bertram et al., 1992; Ruppel et al., 1996). The present scatter for the majority of biozones is small, with 2σ range mostly less than 0.00003 (Appendix 4).

Taking into account the above clarifications, the curve is considered to reflect mainly temporal changes in Sr-isotopic composition of Silurian seawater, with a proviso that the assigned absolute ages are only somewhat uncertain linear interpolations.

Although most of the previously published data are more radiogenic than the present brachiopod values, some conodont measurements of Ruppel et al. (1996) plot below the brachiopod trends (Fig. 6.1). The reasons for this discrepancy are not clear, but the most likely explanation is a correlation mismatch. Except for the single Telychian sample (Fig. 6.1), all

could be made compatible with the brachiopod curve by a minor temporal adjustment.

6.5. PALEOCLIMATIC AND PALEOCEANOGRAPHIC IMPLICATIONS

Variations in the Sr-isotope composition of seawater are mainly a function of balance between inputs of radiogenic $^{87}Sr/^{86}Sr$ from sialic continental crust and low $^{87}Sr/^{86}Sr$ from hydrothermal sources. The riverine input of weathering products of sialic rocks has higher $^{87}Sr/^{86}Sr$ (0.7119) than that of modern seawater (0.709) (Palmer and Edmond, 1992). Erosion, usually enhanced by uplift and/or glaciation, increases the exposed surface area, enabling radiogenic Sr to be mobilized from K-rich minerals and transported to seawater by river runoff. Conversely, hydrothermal input, through alteration of mid-ocean ridge basalts or weathering of volcanic rocks, has lower $^{87}Sr/^{86}Sr$ (~ 0.703) than that of the seawater. During the Silurian, the hydrothermal input is expected to have been less effective than the continental input due to relatively dormant volcanic activity (cf. Palmer and Elderfield, 1985; Elderfield, 1986; Mead and Hodell, 1995). As already pointed out, in Chapter V, the $^{87}Sr/^{86}Sr$ increase of Silurian seawater (Fig. 6.1) is easier to explain by enhanced mechanical and chemical weathering due to progressive global warming (cf. McKerrow et al., 1991).

6.6. STRONTIUM ISOTOPE STRATIGRAPHY

High resolution strontium isotope stratigraphy is being increasingly utilized as a tool for correlation and dating of marine samples (cf. Hodell, 1994; McArthur, 1994). For this task, the trend of $^{87}Sr/^{86}Sr$ variations can be approximated by regressions that are either linear (e.g. Hodell et al., 1989, 1990; Oslick et al., 1994; Mead and Hodell, 1995) or curvilinear (Miller et al., 1991;

Hodell and Woodruff, 1994; Oslick et al., 1994). In the present set, modelling by simple linear regressions for specific time segments, expressed as $y = ax + b$, fits the $^{87}Sr/^{86}Sr$ data well. Figure 6.2 shows the regression lines, equations and R^2 values calculated for each segment. The Silurian data set contains 6 regression segments. The regression lines I, III and V, of Rhuddanian (*acuminatus* to *cyphus* biozones), Telychian (*crispus* to *crenulata* biozones) and early Ludfordian (*bohemicus* to *auriculatus* biozones) ages have significantly steeper slopes and higher R^2 values (> 0.7) than the other three segments. These steep lines may provide temporal resolution of 1 Ma or better.

Slow rate of sedimentation, condensed sedimentary record or stratigraphic hiatus may theoretically be the main reasons for such steep slopes. The absence of exposure surfaces in the Rhuddanian (segment I) and Telychian (segment III) sediments in the sampled stratotype section at Anticosti Island likely excludes the presence of unconformities, but not of interruptions in sedimentation. The segment V (early Ludfordian of Gotland) nearly correlates with the fluvial sandstones of the Burgsvick Formation (Bassett et al., 1989). The remarkable positive $\delta^{13}C$ shifts, discussed in Chapter V, coincide approximately with the steep segments III and V. This may suggest a significant increase in the rate of continental erosion, but a specific scenario is, at this stage, still enigmatic.

The regression lines depict a general stepwise climb of $^{87}Sr/^{86}Sr$ values with decreasing age, but local drops exist at the commencements of segments IV and VI, the Llandovery/Wenlock boundary and the latest Ludlow, respectively (Fig. 6.2). The early drop coincides with the Barrandian (Rheic) volcanism during the latest Llandovery and the latter one may correlate with the late Ludlow volcanic activity documented in Poland (cf. Neuman and Kershaw, 1991).

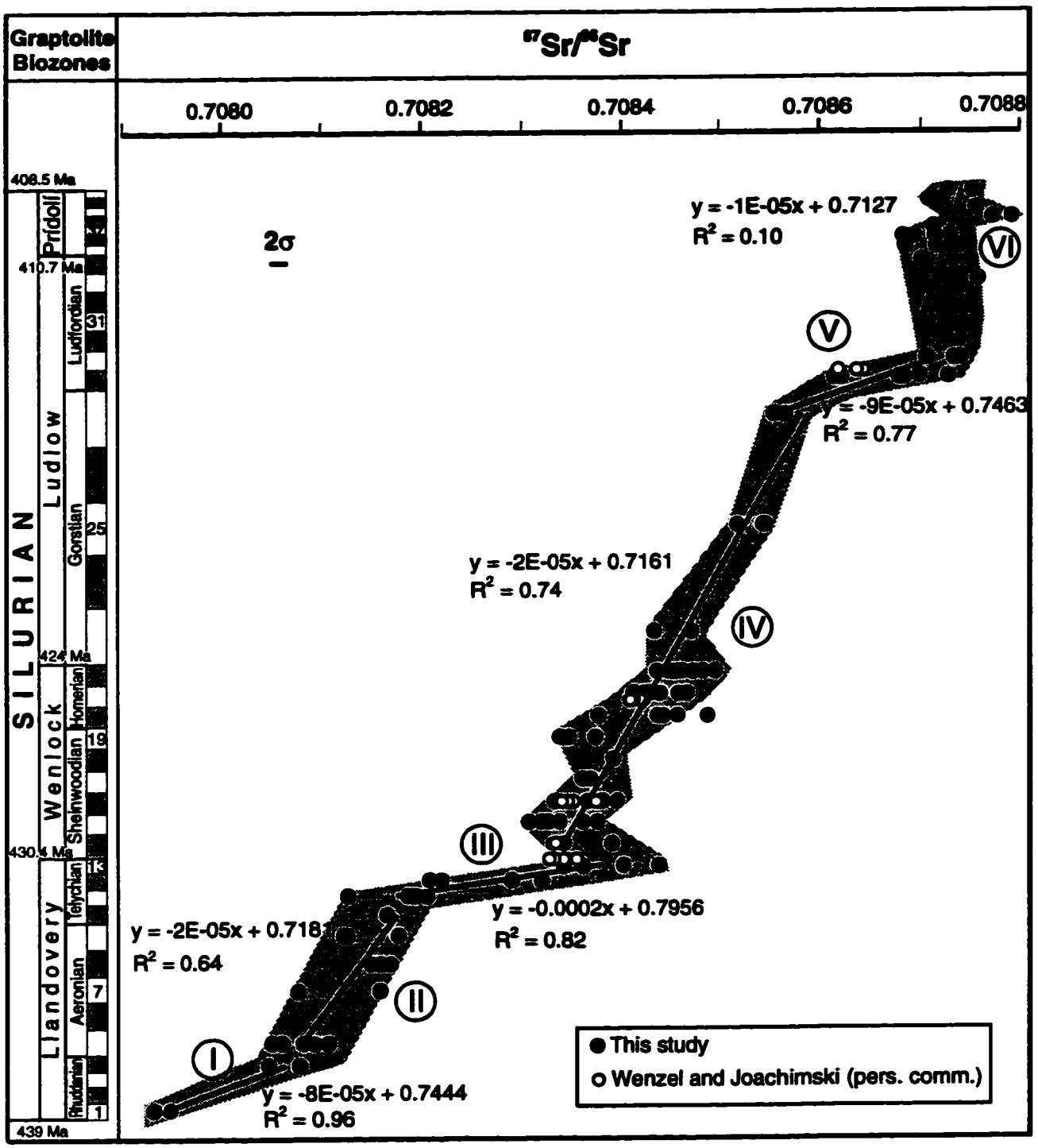

Fig. 6.2. Silurian $^{87}Sr/^{86}Sr$ values vs. age. Heavy lines are the best fit regression lines. (y) and (x) in the regression equations refer to $^{87}Sr/^{86}Sr$ and age (Ma), respectively. The 2σ error bar for the $^{87}Sr/^{86}Sr$ parameter (top left corner) is estimated from repeated measurements of the NBS 987 standard. Biozonation and numerical ages were generated using the same parameters as in Fig. 5.1.

Except for the high slope segments, the regression lines are almost parallel at a similar gentle slope ($a \approx -2x10^{-5}$) indicating a uniformly increasing rate of input of radiogenic Sr, presumably reflecting a similar increase in the riverine runoff. The general low scatter of data points for segments I to V enables one to make reliable "age" estimates. In contrast, the youngest segment VI, of Ludfordian (late Ludlow) to Přídolí ages, has a large scatter and is therefore of doubtful value for chronostratigraphy. This high scatter of data may be due to errors in correlation of biozones, to post-depositional overprinting of $^{87}Sr/^{86}Sr$ values, to non-uniform rate of sedimentation, or to a combination of all the above causes. It is also possible that we are dealing with short-term oscillations in Sr isotopic composition of seawater.

The regression lines can be utilized to estimate the ages for the studied graptolite biozones. The uncertainty for the estimated ages is controlled by the degree of scatter of the data points around the regression lines and by the slope. However, by far the biggest uncertainty for the absolute (numerical) estimate of the age is due to the large error associated with the calibration tie points. For this reason, the numerical values should be viewed only as a relative superposition of the biozones. In that case, the $^{87}Sr/^{86}Sr$ values can be utilized as a correlation tool. The confidence intervals, at the 95 % level , for "ages" in each segment are summarized in Table 6.1. Excluding segment VI where the data scatter is high, the error in estimated ages is equivalent to about ± 2 biozones, but can be as high as ± 4 biozones in the lower part of segment IV (Wenlock), the latter characterized by more scattered data (Fig. 6.2).

Segment	Error (in Ma)	Error (in biozones)	Covered epoch
VI	± 2.1 to 2.2	5	Přídolí
V	± 0.8 to 0.9	2	late Ludlow
IV	± 2.1 to 2.5	2	Ludlow
IV	± 2.1 to 2.5	4	Wenlock
III	± 0.9 to 1.0	2	late Llandovery
II	± 2.3 to 2.5	3	mid-Llandovery
I	± 1.1 to 1.2	2	early Llandovery

Table 6.1. Estimated error in age calculated for each segment of the Silurian regression plot based on confidence interval at the 95% level.

6.6.1. Correlation Using Inflexions

Points of inflexion in the Sr-isotope curve can serve as reliable tie-points that can be used for correlation (cf. McArthur, 1994), particularly when samples are taken at short intervals. Such trends can be generated also by post-depositional alteration but an excellent preservation of the sampled brachiopods is a prerequisite if one is to exclude the possibility of false signals. Stratigraphic hiatuses, when they do not include the inflexion point, usually cause a shift in the position of inflexions (McArthur, 1994) and correlation of such tie points can help to estimate the duration of the hiatus.

The Přídolian sections of Latvia (Kolka 54), Lithuania (Taurage 11) and Ukraine (Podolia) contain minor unconformities, yet their Sr-isotope curves all show three main inflexions (Fig. 6.3) that correlate with the ^{36} *ultimus*, ^{38} *lochkovensis* and ^{40} *permeri* biozones, respectively. The most significant inflexion is the one in the ^{38} *lochkovensis* Biozone, this biozone being characteristic of the Kaugatuma/Ohesaare Stage boundary in the Baltic sections (Latvia and Lithuania) and of the Rashkov/Dzwingorod Formation boundary in the Podolian section.

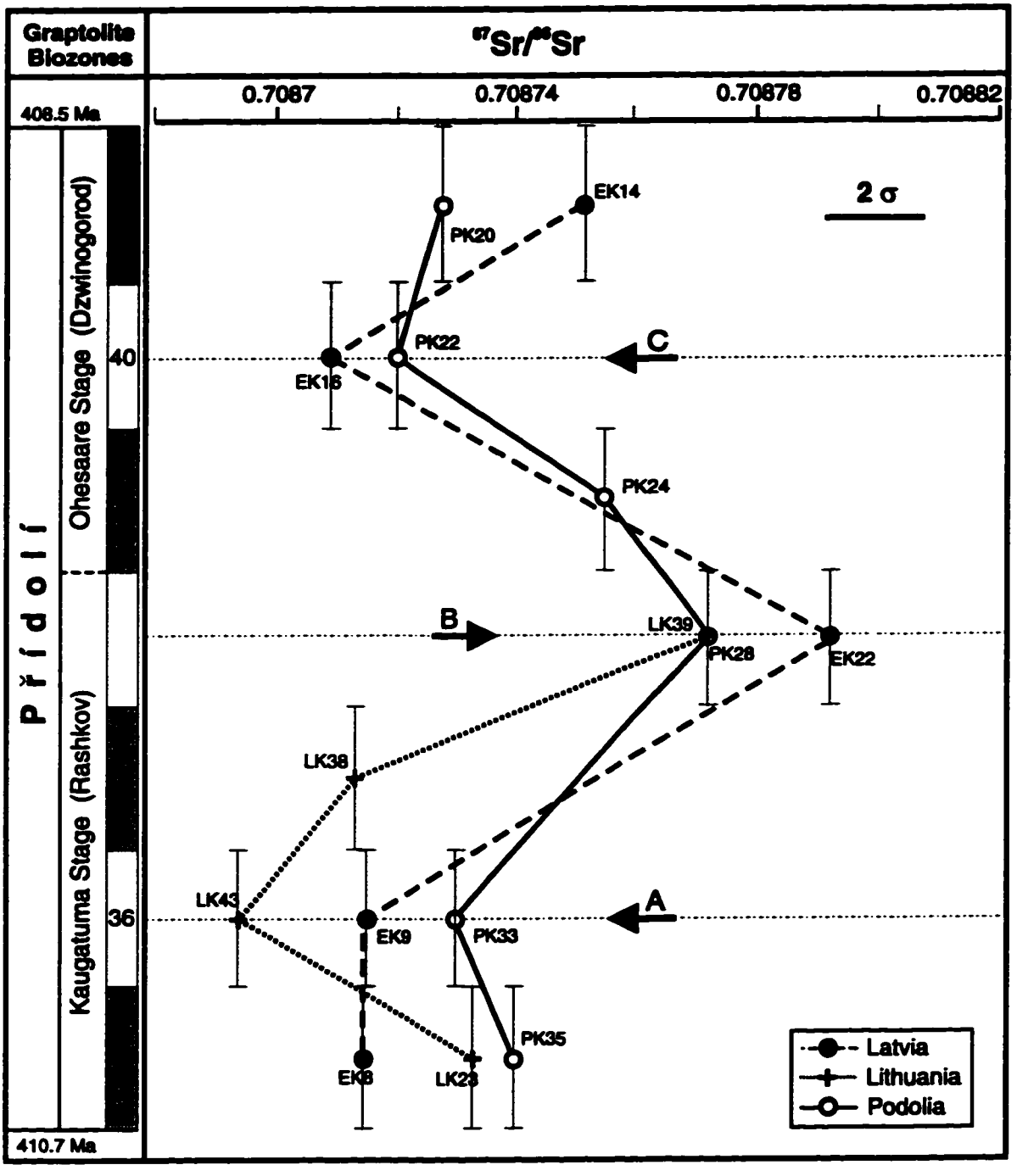

Fig. 6.3. The inflexion points (A, B and C) revealed by comparison of $^{87}Sr/^{86}Sr$ curves of Přídolí for Latvia, Lithuania and Podolia. Age error bars refer to estimated duration of the biozone. The 2 σ error bar for the $^{87}Sr/^{86}Sr$ parameter (top right corner) is estimated from the repeated measurements of the NBS 987 standard. Biozonation and numerical ages were generated using the same parameters as in Fig. 5.1.

This is in agreement with the lithostratigraphic record for the Podolian and Lithuanian sections (Figs. 2.11 and 2.14), but in the Latvian section (Kolka-54) the inflexion lies in the lower portion of the upper Kaugatuma Stage (Figs. 2.14 and 6.3). I suggest that the stratigraphic position of the Kaugatuma/Ohesaare boundary in the Latvian section be shifted downwards to a level of approximately the present K_3bL^1 / K_3bL^2 Bed boundary (Fig. 2.14).

The Wenlockian Sr-isotope curves for Wales (Britain), Gotland (Sweden) and Lithuania follow similar patterns (Fig. 6.4), with a $^{87}Sr/^{86}Sr$ inflexion correlated with the [15] *murchisoni* Biozone, where the decline that commenced in the latest Telychian (Fig. 6.1) is reversed. Samples from Gotland show a considerable drop in the $^{87}Sr/^{86}Sr$ record also towards the [19]*ellesae* Biozone, but in the other sections this could not be confirmed due to lack of samples. The relatively large discrepancy (~ 6 x 10^{-6}) in the [20] *lundgreni* Biozone for the Lithuanian vs. British and Gotland data would require additional work to be resolved.

In conclusion, the use of inflexion points in Sr-isotope stratigraphy is an effective technique for correlation of successions from different basins, particularly when sampling is done at close intervals in a high resolution pattern.

6.6.2. Curve Testing

Externally measured $^{87}Sr/^{86}Sr$ values of 20 samples (from Wenzel and Joachimski, personal communications, 1996) of known ages were applied to the calculated regression plots of this study in order to evaluate their reliability as a correlation tool. Table 6.2 shows the $^{87}Sr/^{86}Sr$ values, their assigned ages and the ages estimated from the regression curves. The estimated correlations fall within ± 1 biozone and in many cases the two ages agree exactly.

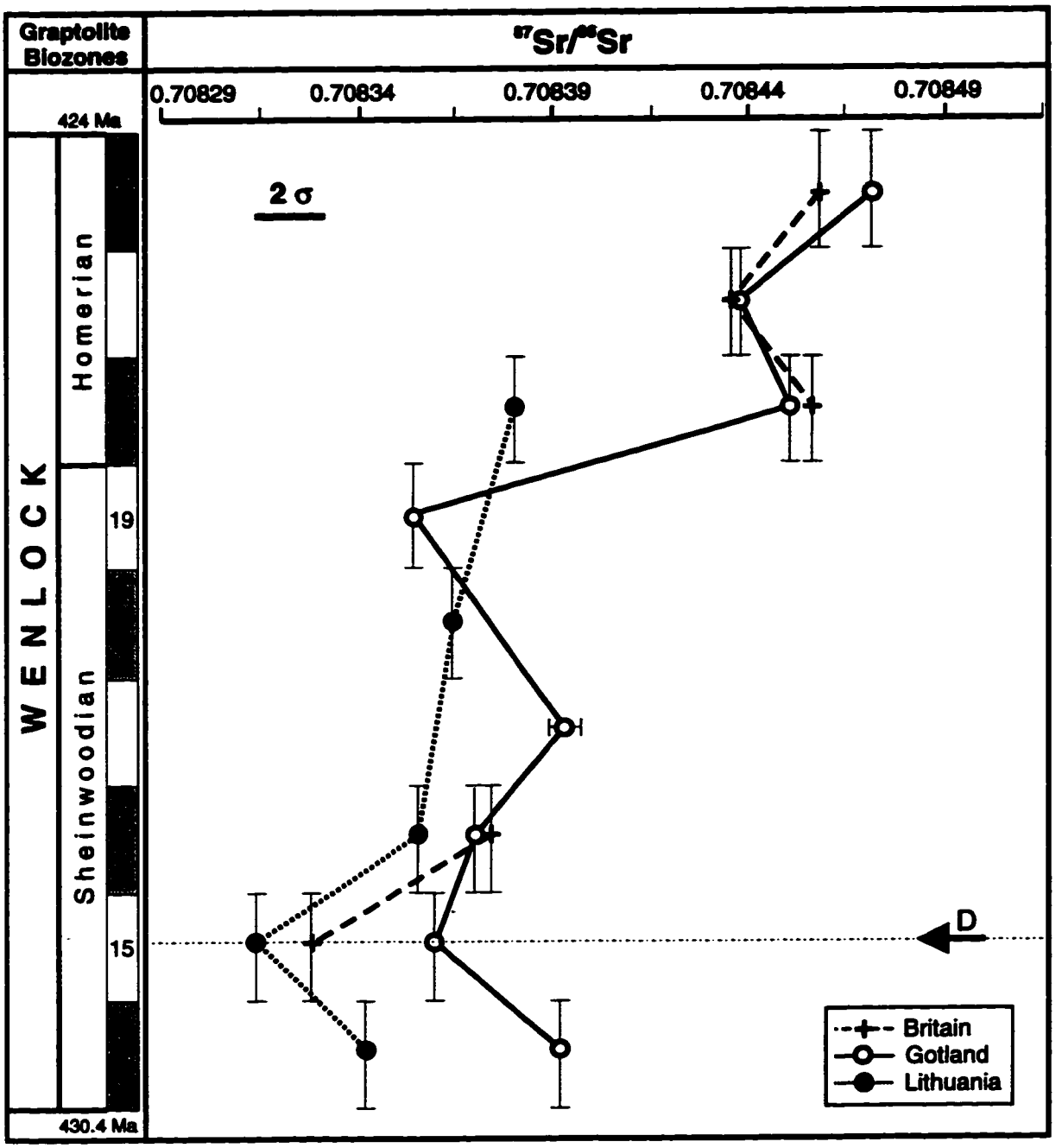

Fig. 6.4. The inflexion point (D, indicated by arrow) revealed by comparison of $^{87}Sr/^{86}Sr$ curves for the Wenlock of Britain (Wales), Gotland and Lithuania. Erorr bars refer to estimated duration of the biozone. The error bar for the $^{87}Sr/^{86}Sr$ (top left corner) is estimated from the repeated measurement of the NBS 987 standard and represents 2σ value. The biozonation bar and numerical ages were generated using the same parameters as in Fig. 5.1.

Sample I.D.	$^{87}Sr/^{86}Sr \pm 2\sigma$	Known age	Estimated age	Error
LV3-1	0.708334 ± 0.000008	uppermost Llandovery	[13] *crenulata*	1 biozone
LV3-2	0.708330 ± 0.000008	uppermost Llandovery	[13] *crenulata*	1 biozone
LV 10	0.708356 ± 0.000008	uppermost Llandovery	[13] *crenulata*	none
LV 14	0.708347 ± 0.000007	uppermost Llandovery	[13] *crenulata*	none
LV 17	0.708344 ± 0.000006	uppermost Llandovery	[13] *crenulata*	none
Y2a	0.708332 ± 0.000007	Llandovery/Wenlock boundary	[14] *centrifugus*	1 biozone
Y2b	0.708332 ± 0.000008	Llandovery/Wenlock boundary	[14] *centrifugus*	1 biozone
V4	0.708375 ± 0.000008	[16] *riccartonensis*	[16] *riccartonensis*	none
V5	0.708352 ± 0.000007	[16] *riccartonensis*	[15] *murchisoni*	1 biozone
V6	0.708342 ± 0.000008	[16] *riccartonensis*	[15] *murchisoni*	2 biozones
V14	0.708349 ± 0.000008	[16] *riccartonensis*	[14] *centrifugus*	2 biozones
M1	0.708411 ± 0.000008	[21] *nassa*	[20] *lundgreni*	1 biozone
M2	0.708423 ± 0.000008	[21] *nassa*	[21] *nassa*	none
M6	0.708416 ± 0.000007	[21] *nassa*	[20] *lundgreni*	1 biozone
M10	0.708419 ± 0.000006	[21] *nassa*	[20] *lundgreni*	1 biozone
M40	0.708420 ± 0.000008	[21] *nassa*	[20] *lundgreni*	1 biozone
H1	0.708637 ± 0.000008	Leintwardinian	[28] *leintwardinesis*	none
H12	0.708642 ± 0.000008	Leintwardinian	[28] *leintwardinesis*	none
H14	0.708618 ± 0.000008	Leintwardinian	[27] *hemiaversus*	1 biozone
H28	0.708638 ± 0.000008	Leintwardinian	[28] *leintwardinesis*	none

Table 6.2. Estimated errors in age determination , expressed in biozones, for the Silurian regression lines. Data from Wenzel and Joachimski (pers. comm., 1996) were used to evaluate the reliability of regressions. The $^{87}Sr/^{86}Sr$ values were corrected to the NBS 987 value of 0.710256 before application to the curve. The superscript numbers, prior to biozones, refer to the same pattern of biozonation as in Figure 6.2.

CHAPTER VII

CONCLUSIONS

1- The low-Mg calcitic brachiopod shells are an outstanding material that usually resists diagenetic alteration and keeps the primary isotopic signal inherited from ambient seawater. The wet chemical data and the SEM observations confirm the good preservation of ultrastructure of the brachiopod shells selected for this study.

2- Brachiopods exerted no vital control on fractionation of oxygen and carbon isotopes during their incorporation into shells.

3- The $\delta^{18}O$ signals of the Silurian Period show a general long-term depletion with decreasing age and superimposed short-term oscillations. These trends were caused by a combination of factors, such as temperature, salinity and the degree of silicate/water interaction, but the general warming trend during the Silurian appears to have been the dominant factor.

4- The short-term oscillations in the Silurian $\delta^{18}O$ values show positive peaks that correlate with glacial episodes as documented in the lower Silurian of Brazil and Africa. The younger observed isotope shifts, however, are not correlatable with any such events.

5- The isotope signals of brachiopods suggest a seawater isotopic composition that varied from - 2.5 ‰ (SMOW) during cold episodes to - 3.5 ‰ (SMOW) during warm episodes. If so, the corresponding estimated temperatures for the tropical zones were likely similar to those of the last glaciation and of the present day, respectively.

6- The Silurian brachiopods of the Wenlockian Lithuanian basin exhibited relatively more enriched $\delta^{18}O$ values than their counterparts from other locations, reflecting the deeper water

conditions of their deposition.

7- The progressive increase in the $^{87}Sr/^{86}Sr$ values of Silurian seawater with decreasing age reflects an enhanced degree of weathering of the continental sialic rocks that may have been associated with the global warming during the Silurian.

8- The $^{87}Sr/^{86}Sr$ values exhibit a stepwise increase with decreasing age, creating a smooth calibration curve that can be used for correlation with an accuracy of about ±2 biozones.

9- The Sr-isotope curve contains several reliable inflexion points in the Wenlock and the Přídolí that can be utilized for correlation of sequences from different depositional settings.

REFERENCES

Abushik, A. F., 1971. Ostracoda from the Silurian-Lower Devonian key sections of Podolia. *In*: A. F. Abushik, E. A. Gusseva and I. E. Zannina (eds.), Palaeozoic ostracodes from key sections in the European part of the USSR, 7-133, pls. 1-46, Nauka, Moscow. (In Russian).

Abushik, A. F., Berger, A. YA., Koren, T. N., Mozdalevskaya, T. L., Nikiforova, O. I. and Predtechensky, N. N., 1985. The fourth series of the Silurian System in Podolia. Lethaia, 18: 125-146.

Ager, D. V., 1981. The nature of the stratigraphical record (second edition): John Wiley, New York, 122 p.

Al-Aasm, I.S. and Veizer, J., 1986a. Diagenetic stabilization of aragonite and low-Mg calcite, 1. trace elements in rudists. J. Sed. Petrol., 56: 138-152.

Al-Aasm, I.S. and Veizer, J., 1986b. Diagenetic stabilization of aragonite and low-Mg calcite, 2. stable isotopes in rudists. J. Sed. Petrol. 56: 763-770.

Aldridge, R. J. and Mohamed, I., 1982. Conodont biostratigraphy of the early Silurian of the Oslo region. *In*: Worsley D. (ed.). Field meeting Oslo Region 1982. IUGS, Subcommission on Silurian Stratigraphy. Palaeont. Contr. Univ. Oslo, 278: 109-120, 2pls.

Aldridge, R. J. and Schönlaub, H. P., 1989. Conodonts. *In*: C. H. Holland and M. G. Bassett (eds.). A global standard for the Silurian System. National Museum of Wales, Cardiff, Geological Series no. 9: 274-279.

Anders, M. H., Krueger, S. W. and Sadler, P. M., 1987. A new look at sedimentation rates and the completeness of the stratigraphic record. J. Geology, 95: 1-14.

Anderson, T. F. and Arthur, M.A., 1983. Stable isotopes of oxygen and carbon and their application to sedimentologic and paleoenvironmental problems. SEPM Short Course, 10: 151 pp.

Andrew, A. S., Hamilton, P. J., Mawson, R. Talent, J. A. and Whitford, D. J., 1994a. Isotopic correlation tools in the Mid-Palaeozoic and their relation to extinction events. Austr. Petrol. Explor. Assoc., 34: 268-277.

Andrew, A. S., Talent, J. A., Mawson, R., Whitford, D. J. and Hamilton, P. J., 1994b. Comparison of carbon isotopic responses associated with Silurian-Devonian mass extinction events. (Abstr.) Final Meet. IGCP Project 293, Erlanger geol. Abh., 122: 4.

Balashov, Z. G. (ed.), 1968. Silurian-Devonian fauna of Podolia, 123 pp. Leningrad University.

Banner, J. L. and Hanson, G. N., 1990. Calculations of simultaneous isotopic and trace element variations during water-rock interaction with application to carbonate diagenesis. Geochim. Cosmochim. Acta, 54: 3123-3138.

Barbin, V. and Gaspard, D., 1995. Cathodoluminescence of Recent articulate brachiopod shells: Implications for growth stages and diagenesis evaluation. J. Geobios, M.S. 18: 39-45.

Barnes, C. R., 1982. The proposed Ordovician-Silurian boundary stratotype, Anticosti Island, Québec. Report Ordovician-Silurian Working Group, 50: 1-10.

Barnes, C. R., 1989. Lower Silurian chronostratigraphy of Anticosti Island, Québec. *In*: C. H. Holland and M. G. Bassett (eds.). A global standard for the Silurian System. National Museum of Wales, Cardiff, Geological Series no. 9: 101-108.

Barnes, C. R. and McCracken, A. D., 1981. Early Silurian chronostratigraphy and a proposed Ordovician-Silurian boundary. Ellis Bay Formation, Anticosti Island, Québec. *In*: P. J. Lespérence (ed.). I.U.G.S. Field meeting, Anticosti-Gaspé, Québec, 1981. Volume II Stratigraphy and paleontology. Départment de géologie, Université de Montréal, 71-80.

Barnes, R. A., 1989. Biogeochemical cycles of carbon and sulfur and their effect on atmospheric oxygen over Phanerozoic times. Palaeogeogr., Palaeoclimatol., Palaeoecol., 75: 97-122.

Bassett, M. G., 1985. Towards a 'Common Language' in stratigraphy. Episodes, 8: 87-92.

Bassett, M. G., 1989. The Wenlock Series in the Wenlock area. *In*: C. H. Holland and M. G. Bassett (eds.). A global standard for the Silurian System. National Museum of Wales, Cardiff, Geological Series no. 9: 51-73.

Bassett, M. G. and Cocks, L. R. M., 1974. A review of Silurian brachiopods from Gotland. Fossils and Strata, 3: 56 pp.

Bassett, M. G., Holland, C. H., Rickards, R. B. and Warren, P. T., 1975. The type Wenlock Series. Institute of Geological Sciences Report, 75/13.

Bassett, M. G., Kaljo, D. and Teller, L., 1989. The Baltic region. *In*: C. H. Holland and M. G. Bassett (eds.). A global standard for the Silurian System. National Museum of Wales, Cardiff, Geological Series no. 9: 158-170.

Bates, N. R. and Brand, U., 1991. Environmental and physiological influences on isotopic and elemental compositions of brachiopod shell calcite: Implications for the isotopic evolution of Paleozoic oceans. Chem. Geol., 94: 67-78.

Bathurst, R. G . C., 1975. Carbonate sediments and their diagenesis; Elsevier, Amsterdam, 685p.

Bergström, S. M., 1990. Relations between conodont provincialism and the changing palaeogeography during the early Palaeozoic. *In*: W. S. McKerrow and C. R. Scotese (eds.). Palaeozoic palaeogeography and biogeography. Geol. Soc. Lond. Mem. 12: 105-121.

Berry, W. B. N. and Boucot, A. J., 1970. Correlation of North American Silurian rocks. Geol. Soc. Amer., Spec. Pap., 102: 1-289.

Berry, W. B. N. and Boucot, A. J. (eds.), 1972a. Correlation of the South American Silurian rocks. Ibid. 133: 1-59.

Berry, W. B. N. and Boucot, A. J., 1972b. Correlation of the southeast Asian and Near Eastern Silurian rocks. Ibid. 137: 1-65.

Berry, W. B. N. and Boucot, A. J., 1973. Correlation of the African Silurian rocks. Geol. Soc. Amer., Spec. Pap., 147: 1-83.

Bertram, C. J., Elderfield, H., Aldridge, R. J. and Morris, S. C., 1992. $^{87}Sr/^{86}Sr$, $^{143}Nd/^{144}Nd$ and REEs in Silurian phosphatic fossils. Earth. Planet. Sci. Lett., 113: 239-249.

Billings, E., 1857. Report for 1856, of E. Billings, Esq., Palaeontologist. Geological Survey of Canada, Report of Progress 1853-1856: 247-345.

Bolton, T. E., 1961. Ordovician and Silurian formations of Anticosti Island, Québec. G. S. C., Pap. 61-26: 18p.

Bolton, T. E., 1970. Subsurface Ordovician fauna, Anticosti Island, Québec. G. S. C., Bull. 187: 31-41.

Bolton, T. E., 1972. Geological map (22H, 12E, F) and notes on the Ordovician and Silurian litho- and biostratigraphy, Anticosti Island, Québec. G. S. C., Pap. 71-19: 45p.

Boucot, A. J., 1990. Silurian and pre-Upper Devonian bioevents. *In*: E. G. Kauffman and O. H. Walliser (eds.). Extinction Events in Earth History. Lecture Notes in Earth Sci., 30: 125-132.

Boucot, A. J., Berry, W. B. N. and Johnson, J. G., 1968. The crust of the Earth from a Lower Palaeozoic point of view. *In*: R. A. Phinney(ed.). The history of the Earth's crust. Princeton University Press, Princeton, N. J., 208-228.

Boucot, A. J., Dewey, J. F., Dineley, D. L., Fletcher, R., Fyson, W. K., Griffin, J. G., Hickox, C. F., McKerrow, W. S. and Ziegler, A .M., 1974. Geology of Arisaig area, Antigonish County, Nova Scotia. Geol. Soc. Amer., Spec Pap., 139: 1-191.

Bralower, T. J., 1987. Valanginian to Aptian calcareous nanofossil stratigraphy and correlation with the upper M-sequence magnetic anomalies. Marine Micropaleontology, 11: 293-310.

Brand, U., 1982. The oxygen and carbon isotope composition of Carboniferous fossil components: Seawater effects. Sedimentol., 29: 139-147.

Brand, U., 1989. Biogeochemistry of late Paleozoic North American brachiopods and secular variation of seawater composition. Biogeochemistry, 7: 159-193.

Brand, U. and Veizer, J., 1980. Chemical diagenesis of a multicomponent carbonate system-1: trace elements. J. Sed. Petrol., 50:1219-1236.

Brand, U. and Veizer, J., 1981. Chemical diagenesis of a multicomponent carbonate system-2: stable isotopes. J. Sed. Petrol., 51: 987-997.

Brazauskas, A. and Musteikis, P., 1990. Brachiopod and conodont distribution at the Wenlock-Ludlow boundary of Lithuania. Estonian Acad. Sci. Geol., 40 (2): 61-68.

Brenchley, P. J., Carden, G. A. F. and Marshall, J. D., 1995. Environmental changes associated with the "first strike" of the late Ordovician mass extinction. Modern Geology, 20: 69-82.

Bruhn, F., Bruckschen, P. Richter, D. K., Meijer, J., Stephan, A. and Veizer, J., 1994. Diagenetic history of sedimentary carbonates: Constraints from combined cathodoluminescence and trace element analyses by micro-PIXE. The 4th. International Conference on Nuclear Microprobe Technology and Applications, Shanghai. Nucl. Inst. Meth. in Physics Res. B, 32: 83-95.

Burke, W. H., Denison, R. E., Hetherington, E. A., Koepnick, R. B., Nelson, H. F. and Otto, J. B., 1982. Variation of seawater $^{87}Sr/^{86}Sr$ throughout Phanerozoic time. Geology, 10: 516-519.

Carpenter, S. J. and Lohmann, K. C., 1995. $\delta^{18}O$ and $\delta^{13}C$ values of modern brachiopods. Geochim. Cosmochim. Acta, 59: 3749-3764.

Choquette, P.W. and James, N.P., 1987. Diagenesis #12 in Limestones-3. The deep burial environment. Geoscience Canada, 14:3-36.

Clarkson, E. N. K., 1993. Invertebrate paleontology and evolution. Chapman and Hall, London, 434 pp.

Cocks, L. R. M., 1971. Facies relationships in the European Lower Silurian. *In*: Colloque Ordovician-Silurian, Brest, 1971. Mém. Bur. Rech. géol. Minièr., 73: 223-227.

Cocks, L. R. M., 1972. The origin of the Silurian *Clarkeia* shelly fauna of South America, and its extension to West Africa. Palaeontology, 15: 623-630.

Cocks L. R. M., Holland, C. H. and Rickards, R. B., 1992. A revised correlation of Silurian rocks in the British Isles. J. Geol. Soc. Lond., Spec. Rep., 21: 1-32.

Cocks, L. R. M. and Scotese, C. R., 1991. The global biogeography of the Silurian Period. Spec. Pap. Palaeontol., 44: 109-122.

Cocks, L. R. M. and Toghill, P., 1973. The biostratigraphy of the Silurian rocks of the Girvan District, Scotland. J. Geol. Soc. Lond., 129: 209-243. Pls. 1-3.

Cocks, L. R. M., Woodcock, N. H., Rickards, R. B., Temple, J. T. and Lane, P. D., 1984. The Llandovery Series of the type area. Bull. Br. Mus. Nat. Hist. (Geol.), 38: 131-182.

Coleman, M. L., Walsh, J. N. and Benmore, R. A., 1989. Determination of both chemical and stable isotope composition in milligram-size carbonate samples. Sediment. Geol., 65: 233-238.

Cooper, B. J., 1980. Toward an improved Silurian conodont biostratigraphy. Lethaia, 13: 209-227.

Copeland, M. J., 1970. Ostracoda from the Vauréal Formation (Upper Ordovician), Anticosti Island, Québec. G. S. C. Bull., 187: 15-29.

Copeland, M. J., 1973. Ostracoda from the Ellis Bay Formation (Ordovician), Anticosti Island, Québec. G. S. C., Pap. 72-43: 1-49

Copeland, M. J., 1974. Silurian Ostracoda from Anticosti Island, Québec. G. S. C. Bull., 241: 73.

Copper, P., 1981. Atrypoid brachiopods and their distribution in the Ordovician-Silurian sequence of Anticosti Island. *In*: P. J. Lespérence (ed.). I.U.G.S. Field meeting, Anticosti-Gaspé, Québec, 1981. Volume II Stratigraphy and paleontology. Département de géologie,

Université de Montréal, 137-142.

Copper, P. and Long, D. G. F., 1989. Stratigraphic revisions of a key Ordovician-Silurian boundary section, Anticosti Island, Canada. Newsletters in Stratigraphy, 21: 59-73.

Copper, P. and Long, D. G. F., 1990. Stratigraphic revision of the Jupiter Formation. Newsletters in Stratigraphy, 23: 11-36.

Corfield, R. M., Siveter, D. J., Cartlidge, J. E. and McKerrow, W. S., 1992. Carbon isotope excursion near the Wenlock-Ludlow (Silurian) boundary in the Anglo-Welsh area. Geology, 20: 371-374.

Cotter, E., 1988. Hierarchy of sea-level cycles in the medial Silurian siliciclastic succession of Pennsylvania. Geology, 16: 242-245.

Cowe, J. W., Ziegler, W., Boucot, A. J., Bassett, M. G. and Remane, J., 1986. Guidelines and statutes of the International Commission on Stratigraphy (ICS). Cour. Forsch.-Instit. Senckenberg, 83: 1-14.

Cox, A. V., 1968. Lengths of geomagnetic polarity intervals. J. Geophys. Res., 73: 3247-3260.

Craig, H., 1957. Isotopic standards for carbon and oxygen and correction factor for mass spectrometric analysis of carbon dioxide. Geochim. Cosmochim. Acta, 12: 133-149.

Craig, H. and Gordon, L. I., 1965. Deuterium and oxygen 18 variations in the ocean and the marine atmosphere. *In*: E. Tongiorgi (ed.). Stable isotopes in oceanographic studies and paleotemperatures. Spoleto, Consiglio Nazionale delle Ricerche, Laboratorio di Geologia Nucleare, Pisa, p. 1-22.

Crowley, K. D., 1984. Filtering of depositional events and the completeness of sedimentary sequences. J. Sediment. Petrol., 54: 127-136.

Crowley, T. J., 1994. Pleistocene temperature changes. Nature, 371: 664.

Degens, E. T. and Epstein, S., 1962. Relationship between $^{18}O/^{16}O$ ratios in coexisting carbonates, cherts and diatomites. AAPG Bull., 46: 534-542.

Dia A. N., Cohen, A. S., O'Nions R. K. and Shakleton, N. J., 1992. Seawater Sr isotope variation over the past 300 kyr and influence of global climate cycles. Nature, 356: 786-788.

Diener, A., Ebneth, S., Veizer, J. and Buhl, D., 1996. Strontium isotope stratigraphy of the Middle Devonian: Brachiopods and conodonts. Geochim. Cosmochim. Acta, 60: 639-652.

Dittmar, H. and Vogel, K., 1968. Die Superenelemente Mangan und Vanadium in Brachiopoden-Schalen in Abhängigkeit vom Biotop. Chem. Geol., 3: 95-110.

Donovan, D. T. and Jones, E. J. W., 1979. Causes of world-wide changes in sea level. J. Geol. Soc. Lond., 136: 187-192.

Eckert, J. D., 1988. Late Ordovician extinction of North America and British crinoids. Lethaia, 21: 147-167.

Einasto, R., 1990. Locality 7:3 Kaugatuma Cliff. *In*: D. Kaljo and H. Nestor (eds.), Field Meeting Estonia 1990. An Excursion Guidebook, p. 174-175.

Elderfield, H., 1986. Strontium isotope stratigraphy. Palaeogeogr. Palaeoclimatol. Palaeoecol., 57: 71-90.

Emiliani, C., 1955. Pleistocene temperature: J. Geol., 63: 538-578.

Epstein, S., Buchsbaum, R., Lowenstam, H. A. and Urey, H. C., 1953. Revised carbonate water isotopic temperature scale. Geol. Soc. Am. Bull., 64: 1315-1326.

Farrell, J. W., Steven, C. C. and Gromet, L. P., 1995. Improved chronostratigraphic reference curve of late Neogene seawater $^{87}Sr/^{86}Sr$. Geology, 23: 403-406.

Faure, G., 1986. Principles of isotope geology, Second edition. John Wiley and Sons, New York, 464 p.

Flodén, T., 1980. Seismic stratigraphy and bedrock geology of the central Baltic. Stockholm Contr. Geol., 35: 1-240.

Fordham, B. G., 1992. Chronometric calibration of mid-Ordovician to Tournaisian conodont zones: A compilation from recent graphic correlation and isotope studies. Geol. Mag., 129: 709-721.

Frakes, L. A., Francis, J. E. and Syktus, J. I., 1992. Climate modes of the Phanerozoic: the history of the earth's climate over the past 600 million years. Cambridge University Press, Cambridge. 274 pp.

Frank, J. R., Carpenter, A. B., and Oglesby, T. W., 1982. Cathodoluminescence and composition of calcite cement in the Taum Sauk Limestone (Upper Cambrian), southeast Missouri. J. Sed. Petrol., 52: 631-638.

Friedman, I. and O'Neil, J. R., 1977. Compilation of stable isotope fractionation factors of geochemical interest: *In*: M. Fleischer(ed.). Data of geochemistry, 6th ed. U.S. Geol. Surv. Prof. Pap., 440 pp.

Frykman, P., 1986. Diagenesis of Silurian bioherms in the Klinteberg Formation, Gotland, Sweden. *In*: J. H. Schroeder and B. Purser (eds.). Reef diagenesis. Springer Heidelberg, p. 399-423.

Fürsich, F. T. and Hurst, J. M., 1974. Environmental factors determining the distribution of brachiopods. Palaeontology, 17/4: 879-900.

Gale, N. H. and Beckinsale, R. D., 1983. Comments on the paper "Fission-track dating of British Ordovician and Silurian stratotype" by R. J. Ross et al. Geol Mag., 120: 295-302.

GEOSECS, 1987. GEOSECS Atlantic, Pacific, and Indian Ocean expeditions. Vol. 7: Shore based data and graphics: Washington, D. C., National Science Foundation, 200 p.

Gordon, L., Salutsky, M. L. and Willard, H. H., 1959. Precipitation from homogeneous solution. John Wiley and Sons, New York, 289 pp.

Grahn, Y. G. and Caputo, M. V., 1992. Early Silurian glaciation in Brazil. Palaeogeogr. Palaeoclimat. Palaeoecol., 99: 9-15.

Gregory, R. T., 1991. Oxygen isotope history of seawater revisited: Composition of seawater. *In*: H. P. Taylor Jr. et al. Stable isotope geochemistry: A tribute to Samuel Epstein. Geochem. Soc. Spec. Publ., 3: 65-76.

Grigelis, A. A., 1978. Regional stratigraphic scheme for the Silurian deposits of the east Baltic. *In*: Interdepartmental Stratigraphical Committee of the USSR. Decisions of the Interdepartmental Regional Stratigraphical Conference on the Production of Unified Stratigraphical Schemes for the Baltic Republics in 1976; with Unified Stratigraphical Correlation Tables, 85 pp. Ministry of Geology of the USSR, Leningrad. (In Russian)

Grossman, E. L., 1994. The carbon and oxygen isotope record during the evolution of Pangea: Carboniferous to Triassic. Geol. Soc. Amer. Spec. Pap., 288: 207-228.

Grossman, E. L., Mii, H. and Yancey, T. E., 1993. Stable isotopes in Late Pennsylvanian brachiopods from the United States: Implications for Carboniferous paleoceanography.

Geol. Soc. Amer. Bull., 105: 1284-1296.

Grossman, E. L., Zhang, C. and Yancey, T. E., 1991. Stable-isotope stratigraphy of brachiopods from Pennsylvanian shales in Texas. Geol. Soc. Amer. Bull., 103: 953-965.

Guilderson, T. P., Fairbanks, R. G. and Rubenstone, J. L., 1994. Tropical temperature variations since 20,000 years ago: Modelling interhemispheric climate change. Science, 236: 663-665.

Hancock, N. J., Hurst, J. M. and Fürisch, F. T., 1974. Depths inhabited by Silurian brachiopod communities. J. Geol. Soc. Lond., 130: 151-156.

Haq, B. U., Hardenbol, J. and Vail, P. R., 1987. Chronology of fluctuating sea levels since the Triassic (250 million years ago to present). Science, 235: 1156-1167.

Haq, B. U., Hardenbol, J. and Vail, P. R., 1988. Mesozoic and Cenozoic chronostratigraphy and eustatic cycles. *In*: C. K. Wilgus et al. (eds.). Sea level research - An integrated approach. SEPM, Spec. Pub., 42: 71-108

Harland, W. B., Armstrong, R. L., Cox, A. V., Craig, L. E., Smith, A. G. and Smith, D. G., 1990. A geologic time scale. Cambridge University Press, 263 pp.

Hays, P. D. and Grossman, E. L., 1991. Oxygen isotopes in meteoric calcite cements as indicators of continental paleoclimate. Geology, 19: 441-444.

Heckel, P. H., 1986. Sea-level curve for Pennsylvanian eustatic marine transgressive-regressive depositional cycles along midcontinent outcrop belt, North America. Geology, 14: 330-334.

Hede, J. E., 1960. The Silurian of Gotland. Guide to excursions A22 and C17. 21st Internat Geol Congress Copenhagen: 4489.

Hodell, D. A., 1994. Progress and paradox in strontium isotope stratigraphy. Paleoceanography, 9 (3): 395-398.

Hodell, D. A., Mead, G. A. and Müller, P. A., 1990. Variation in the strontium isotopic composition of seawater (8 Ma to present): Implications for the chemical weathering rates and dissolved fluxes to the oceans. Chem. Geol., 80: 291-307.

Hodell, D. A., Müller, P. A., McKenzie, J. A. and Mead, G. A., 1989. Strontium isotope stratigraphy and geochemistry of the late Neogene ocean. Earth Planet. Sci. Lett., 92: 165-178.

Hodell, D. A. and Woodruff, F., 1994. Variations in the strontium isotopic ratio of seawater during the Miocene: Stratigraphic and geochemical implications. Paleoceanography, 9 (3): 405-426.

Hoefs, J., 1980. Stable isotope geochemistry (2nd edition), Springer-Verlag, 1208 pp.

Hoefs, J., 1982. Isotope geochemistry of carbon. *In*: H. L. Schmidt, H. Forstel, K. Keizinger (eds.). Stable isotopes. Elsevier Scient. Publ. Co., Amsterdam, p. 103-113.

Holland, H. D., 1984. The chemical evolution of the atmosphere and oceans. Princeton, New Jersey, Princeton University Press, 582 p.

Holland, C. H. and Bassett, M. G. (eds.), 1989. A global standard for the Silurian System. National Museum of Wales, Cardiff, Geological Series no. 9: 325 pp.

Holser, W. T., 1994. Geochemical events in inorganic carbon isotopes. *In*: W. Buggisch (ed.). Geochemical event markers in the Phanerozoic. IGCP Project 293, Abstracts and Guidebook, Erlanger Geologische Abhandlungen, 122: 29-30.

Irving, E. and Pullaiah, G., 1976. Reversals of geomagnetic field, magnetostratigraphy and relative magnitude of paleosecular variation in Phanerozoic. Earth Science Reviews, 12: 35-64.

Isaacson, P. E., Antelo, B. and Boucot, A. J., 1976. Implications of a Llandovery (Early Silurian) brachiopod fauna from Salta Province, Argentina. J. Paleontology, 50: 1103-1112, pl. 1.

Jaeger, H., 1976. Das Silur und Unterdevon vom thüringischen Typ in Sardinien und seine regionalgeologische Bedeutung. Nova Acta Leopoldina, Neue Folge, 45: 263-299.

Jeppsson, L., 1987. Lithological and conodont distributional evidence for episodes of anomalous oceanic conditions during the Silurian. *In*: R. J. Aldridge (ed.). Palaeobiology of conodonts. Br. Micropalaeontol. Soc. Ser., p. 129-145.

Jeppsson, L., 1990. An oceanic model for lithological and faunal changes tested on the Silurian record. J. Geol. Soc. London, 147: 663-674.

Jeppsson, L., Viira, V. and Männik, P., 1994. Silurian conodont-based correlations between Gotland (Sweden) and Saaremaa (Estonia). Geol. Mag. 131: 201-218.

Jin, J., Caldwell, W. G. E., and Copper, P., 1990. Evolution of the early Silurian rhynchonellid brachiopod *Fenestrirostra* in the Anticosti Basin of Québec. J. Paleont. 64: 214-222.

Johnson, M. E., Cocks L. R. M. and Copper, P., 1981. Late Ordovician-Early Silurian fluctuations in sea level from eastern Anticosti Island, Québec. Lethaia 14:73-82.

Johnson, M. E., Kaljo, D. and Rong, J.-Y., 1991. Silurian eustasy. Spec. Pap. Paleontol., 44: 145-163.

Kaljo, D., 1971. The tectonic factor in the geological history of the east Baltic Basin during the Silurian. Colloque Ordovician-Silurian, Brest, September 1971. Mémoire du Bureau de

Recherches Géologiques et Minières, 73: 275-279.

Kaljo, D., 1990. The Silurian of Estonia. *In*: D. Kaljo and H. Nestor (eds.), Field Meeting Estonia 1990. An Excursion Guidebook, p. 21-26.

Kaljo, D., Kiipli, T. and Martma, T., 1994. Geochemical and isotope ($\delta^{13}C$) event markers through the Wenlock-Přídolí sequence in Ohesaare (Estonia) (Abstr.). Erlanger Geol. Abh., 122: 36.

Kaljo, D. L., Koren, T. N., Modzalevskaya, T. L., Nestor, KH. E., Predtechensky, N. N. and Einasto, R. W., 1982. Peculiarities of Silurian sedimentation evolution of communities in marginal seas in Podolia and East Baltic. *In*: Theory and usage of ecostratigraphy, 39-40. Tallin.

Kaminskas, D. and Musteikis, P., 1994. Quantitative evaluation of carbonate and terrigenous material influence on brachiopod distribution. Geologija, 17: 96-105.

Karhu, J. and Epstein, S., 1986. The implication of oxygen isotope records in coexisting cherts and phosphates. Geochim. Cosmochim. Acta, 50: 1745-1756.

Keith, M. L. and Weber, J. N., 1964. Carbon and oxygen isotopic composition of selected limestones and fossils. Geochim. Cosmochim. Acta, 28: 1787-1816.

Kemp, A. E. S., 1991. Mid-Silurian pelagic and hemipelagic sedimentation and palaeoceanography. Spec. Pap. Palaeont., 44: 261-299.

Keppens, E. and O'Neil, J. R., 1985. Isotope geochemistry of glauconitic sediments: II-Stable isotopes. *In*: Isotopes in the sedimentary cycle. Abstr. (Obernai, France).

Kiaer, J., 1908. Etage 5 I Asker (English Summary). Nor. Geol. Unders., 34: 111 pp.

Kjerulf, T., 1857. Ueber die Geologie des südlichen Norwegens. Nyt. Mag. Naturvid, 9: 193-333.

Knauth, L. P. and Epstein, S., 1976. Hydrogen and oxygen isotope ratios in nodular and bedded cherts. Geochim. Cosmochim. Acta, 40: 1095-1108.

Knauth, L. P. and Lowe, D. R., 1978. Oxygen isotope geochemistry of cherts from the Onverwacht Group (3.4 Billion years), Transvaal. South Africa, with implications for secular variations in the isotopic composition of cherts. Earth Planet. Sci. Lett., 64: 398-404.

Koren, T. N., Abushik, A. F., Modzalevskaya, T. L. and Predtechensky, N. N., 1989. Podolia, *In*: C. H. Holland and M. G. Bassett (eds.). A global standard for the Silurian System. National Museum of Wales, Cardiff, Geological Series no. 9: 141-149.

Koren T. N. and Rickards, R. B., 1980. Extinction of graptolites. *In*: A. L. Harris, C. H. Holland and C. E. Leake (eds.). The Caledonides of the British Isles-reviewed. Geol Soc. Lond., Spec. Publ., 8: 457-466 (for 1979).

Kozlowsky, R., 1929. Les Brachiopodes Gothlandiens de la Podolie Polonaise. Palaeont. pol. 1: 1-254.

Land, L.S., 1986. Diagenesis of metastable skeletal carbonates: Unpublished Ph.D. thesis, Lehigh University, 141 p.

Land, L. S., 1995. Comment on "Oxygen and carbon isotopic composition of Ordovician brachiopods: Implications for coeval seawater" by H. Qing and J. Veizer. Geochim. Cosmochim. Acta, 59: 2843-2844.

Laubacher, G., Boucot, A. J. and Gray, J., 1982. Additions to Silurian stratigraphy, lithofacies, biogeography and palaeontology of Bolivia and southern Peru. J. Paleontology, 56: 1138-1170, pls. 1-5.

Lepzeltzer, C. G, Anderson, T. F. and Sandberg, P. A., 1983. Stable isotope variation in modern articulate brachiopods (Abstr.): AAPG Bul., 67: 500-501.

Lohmann, K.C., 1983. Unravelling the diagenetic history of carbonate reservoirs: Integration of petrographic and gechemical techniques. AAPG Short Course, Section V, p. 1-41.

Long, D. G. F., 1993. Oxygen and carbon isotopes and event stratigraphy near the Ordovician-Silurian boundary, Anticosti Island Québec. Palaeogeogr., Palaeoclimatol., Palaeoecol., 104: 49-59.

Long, D. G. F. and Copper, P. 1987a. Stratigraphy of the Upper Ordovician Vauréal and Ellis Bay Formations, eastern Anticosti Island. Can. J. Earth Sci., 24: 1807-1820.

Long, D. G. F. and Copper, P. 1987b. Late Ordovician sand-wave complexes on Anticosti Island, Québec: a marine tidal embayment? Can. J. Earth Sci., 24: 1820-1832.

Long, D. G. F. and Copper, P., 1994. The Late Ordovician-Early Silurian carbonate tract of Anticosti Island, Gulf of St. Lawrence, eastern Canada. GAC, MAC, Joint Annual Meeting, Waterloo 1994, Field trip B4: Guidebook, 69 p.

Lorens, R.B., 1981. Sr, Cd, Mn and Co distribution coefficient in calcite as a function of calcite precipitation role. Geochim. Cosmochim. Acta, 45: 553-561.

Lowenstam, H. A., 1961. Mineralogy, $^{18}O/^{13}C$ ratios, and strontium and magnesium contents of recent and fossil brachiopods and their bearing on the history of oceans. J. Geol., 69: 241-260.

Machel, H. G., 1985. Cathodoluminescence in calcite and dolomite and its chemical interpretation. Geosci. Canada, 12: 139-147.

Machel, H. G. and Burton, E. A., 1991. Factors governing cathodoluminescence in calcite and dolomite, and their implications for studies of carbonate diagenesis. *In*: Luminescence microscopy and spectroscopy, qualitative and quantitative applications, SEPM Short Course, 25: 37-57.

Machel, H. G., Mason, R. A., Mariano, A. N. and Mucci, A., 1991. Causes and emission of luminescence in calcite and dolomite. *In*: Luminescence microscopy and spectroscopy, quantitative and qualitative applications, SEPM Short Course, 25: 9-25.

Magaritz, M., 1991. Carbon isotopes, time boundaries and evolution. Terra Nova, 3: 251-256.

Mankinen, E. A. and Dalrymple, G. B., 1979. Revised geomagnetic polarity time scale for the interval 0-5 m.y. BP. J. Geophys. Res., 84: 615-626.

McArthur, J. M., 1994. Recent trends in strontium isotope stratigraphy. Terra Nova, 6: 331-358.

McClure, H. A., 1988. The Ordovician-Silurian boundary in Saudia Arabia. Bulletin of the British Museum (Natural History) (Geology), 43: 155-163.

McCrea, J. M., 1950. On the isotopic chemistry of carbonates and paleothermometer scale. J. Chem. Phys., 18: 849-857.

McKerrow, W. S., 1978. The ecology of fossils. MIT Press, Cambridge, Mass., 3844 pp.

McKerrow, W. S., 1988. The development of the Iapetus ocean from the Arenig to the Wenlock, p. 405-412. *In*: A. L. Harris and D. J. Fettes (eds.). The Caledonian-Appalachian Orogeny. J. Geol. Soc. Lond., Spec. Pub., 38: 643 pp.

McKerrow, W. S., Dewey, J. F. and Scotese, C. R., 1991. The Ordovician and Silurian development of the Iapetus ocean. Spec. Pap. Palaeont., 44: 165-178.

McKinnon, D. I., 1974. The shell structure of spiriferid Brachiopoda. Bull. British Museum, 25: 187-261.

McLeod, N. and Keller, G., 1991. How complete are Cretaceous/Tertiary boundary sections? A chronostratigraphic estimate based on graphic correlation: Geol. Soc. Amer., 103: 1439-1457.

McShea, D. W. and Raup, D. M., 1986. Completeness of the geological record. J. Geology, 94: 569-574.

Mead, G. A. and Hodell, D. A., 1995. Controls on the $^{87}Sr/^{86}Sr$ composition of seawater from the middle Eocene to Oligocene: Hole 689B, Maud Rise, Antarctica. Paleoceanography, 10 (2): 327-346.

Melchin, M. J., McCracken, A. D. and Oliff, F. J., 1991. The Ordovician-Silurian boundary on Cornwallis and Truro Islands, Arctic Canada: preliminary data. Can. J. Earth Sci., 28: 1854-1862.

Meyers, W.J. and Lohmann, K.C., 1985. Isotope geochemistry of regionally extensive calcite cement zones and marine components in Mississippian Limestones, New Mexico. *In*: N. Schneidermann and P.M. Harris(eds.). Carbonate cements. Spec. Publ. SEPM 36: 223-239.

Miall, A. D., 1991. Hierarchies of architectural units in terrigenous clastic rocks, and their relationship to sedimentation rate. *In*: A.D. Miall and N. Tyler (eds.). The three dimensional facies architecture of terrigenous clastic sediments and its implications for

hydrocarbon discovery and recovery. SEPM, Concepts in sedimentology and paleontology, 3: 6-12.

Miall, A. D., 1994. Sequence stratigraphy and chronostratigraphy: problems of definition and precision in correlation and their implications for global eustasy. Geoscience Canada, 21: 1-26.

Middleton, P. D., Marshall, J. D. and Brenchley, P. J., 1991. Evidence for isotopic changes associated with late Ordovician glaciation from brachiopods and marine cements of central Sweden. Geol. Surv. Canada. Pap. 90-9, pp. 313-321.

Mii, H. S. and Grossman, E. L., 1994. Late Pennsylvanian seasonality reflected in the ^{18}O and elemental composition of the brachiopod shell. Geology, 22: 661-664.

Miller, J., 1988. Cathodoluminescence microscopy. *In*: Tucker, M.E. (ed.). Techniques in sedimentology. Oxford, Blackwell Sci. Publ., p. 86-107.

Miller, K. G., Feigenson, M. D., Wright, J. D. and Clement, B. M., 1991. Miocene isotope reference section, Deep Sea Drilling Project Site 608: An evaluation of isotope and biostratigraphic resolution. Paleoceanography, 6 (1): 33-52.

Milliman, J. D., 1974. Marine carbonates. Springer-Verlag, New York, 375 pp.

Moore, G. T., Hayashida, D. N. and Ross, C. A., 1993. Late Early Silurian (Wenlockian) general circulation model-generated upwelling, graptolitic black shales, and organic-rich source rocks- An accident of plate tectonics? Geology, 21: 17-20.

Morrison, O. J. and Brand, U., 1986. Paleocene No. 5: Geochemistry of recent marine invertebrates. Geosci. Canada, 13: 237-254.

Morse J. W. and Bender, M. L., 1990. Partition coefficient in calcite: Examination of factors influencing the validity of the experimental results and their applications to natural systems. Chem. Geol., 82: 265-277.

Morse, J. W. and McKenzie, F. T., 1990. Geochemistry of sedimentary carbonates, Chapter 7. Developments in sedimentology 48, Sci. Publ. Elsevier, Amsterdam, 707 p.

Mu, E. Z., Boucot, A. J., Chen, X. and Rong, J. Y., 1986. Correlation of the Silurian rocks of China. Spec. Pap., Geol. Soc. Amer., 202: 1-80.

Muehlenbachs, K., 1986. Alteration of the oceanic crust and the ^{18}O history of seawater. *In*: J. W. Valley, H. P. Jr. Taylor and R. R. O'Neil (eds.). Stable isotopes in high temperature geological processes. Review in Mineralogy, 16: 425-444.

Murchison, R. I., 1835. On the Silurian System of rocks. Lond. Edinb. Phil. Mag. 7: 46-52.

Nestor, H., 1990. Locality 7:4 Ohesaare Cliff. *In*: D. Kaljo and H. Nestor (eds.), Field Meeting Estonia 1990. An Excursion Guidebook, p. 175-178.

Neuman, B. E. E. and Kershaw, S., 1991. VI International symposium on Fossil Cnidaria including Archaeocyatha and Porifera. Presymposium excursion A1 Gotland/Sweden Silurian reefs and coral bearing strata. Excursion Guide-Book. 111 pp. Bergen.

Nicholas, R. B. and Brand, U., 1991. Environmental and physiological influences on isotopic and elemental compositions of brachiopod shell calcite: Implications for the isotopic evolution of Paleozoic oceans. Chem. Geol., 94: 67-78.

Nickel, E., 1978. The present status of cathode luminescence as a tool in sedimentology. Miner. Sci. Engng., 10: 73-100.

Nikiforova, O. I., 1948. Stratigraphical chart of the Upper Silurian of Podolia. Materialy VSEGEI, Obsch. ser. 8: 43-54 (In Russian).

Nikiforova, O. I., 1954. Stratigraphy and brachiopods of the Silurian deposits of Podolia. Trudy vses. nauchno-issled. geol Inst. (VSEGEI), 1-218 (In Russian).

Nikiforova, O. I., 1977. Podolia. *In*: A. Martinsson (ed.). The Silurian-Devonian boundary, 52-64. IUGS Series A, No. 5. E. Schweizarbart'sche Velargsbuchhandlung, Stuttgart.

Nikiforova, O. I., Abushik, A. F., Ignatovich, M. M., Modzalevskaya, T. L., Berger, A. YA., Novoselova, L. S. and Burkov, Y. K., 1972. Silurian and Lower Devonian key section of Podolia. Nauka SSSR, Ministerstvo Geologii SSSR, Mezhvedomstvennyi Stratigraficheskii Komitet SSSR, 5: 1-262, Nauka, Leningrad (In Russian).

Nikiforova, O. I. and Predtechensky, N. N., 1968. A guide to the geological excursion on Silurian and Lower Devonian deposits of Podolia (Middle Dnestr River), 58 pp. Third international symposium on Silurian-Devonian boundary and Lower and Middle Devonian stratigraphy. Ministry of Geology of the USSR, All-Union Scientific-Research Geological Scientific Research Institute (VSEGEI), Leningrad.

Nowlan, G. S. 1983. Early Silurian conodonts of eastern canada. Fossils and Strata 15: 95-110.

O'Hara, M. and Reid, R.C., 1973. Modelling crystal growth rates from solution. Prentice-Hall, Englewood Cliffs, N.J., 272 p.

Oslick, J. S., Miller, K. G. and Feigenson, M. D., 1994. Oligocene-Miocene strontium isotopes: Stratigraphic revisions and correlation to an inferred glacioeustatic record. Paleoceanography, 9: 427-443.

Palmer, M. R. and Edmond, J. M., 1992. Controls over the strontium isotope composition of river water. Geochim. Cosmochim. Acta, 56: 2099-2111.

Palmer, M. R. and Elderfield, H., 1985. Sr isotope composition of seawater over the past 75 Myr. Nature, 314 (6011): 526-528.

Pander, C. H., 1856. Monographie der fossilen Fische des Silurischen Systems der Russich-Baltischen Gouvernements. St. Petersburg, 1-91.

Paškevičius, J., Lapinskas, P., Brazauskas, A., Musteikis, P. and Jacyna, J., 1994. Stratigraphic revision of the Upper Silurian part in the Baltic basin. Geologija, 17: 64-87.

Perry, E. C. and Tan, F. C., 1972. Significance of oxygen and carbon isotope variations in early Precambrian cherts and carbonate rocks of southern Africa. Geol. Soc. Amer. Bull., 83: 647-664.

Petryk, A. A., 1979. Stratigraphie revisée de l'île d'Anticosti. Ministère de l'Energie et des Resources du Québec. DPV 711, 24 p.

Petryk, A. A., 1981a. Géologie de la partie ouest de l'île d'Anticosti. Ministère de l'Energie et des Resources du Québec. DPV 815, 25 p., and Map at scale 1: 100,000.

Petryk, A. A., 1981b. Carte Géologique de l'île d'Anticosti. Ministère de l'Energie et des Resources du Québec. DPV 823, scale 1: 100,000.

Petryk, A. A., 1981c. Stratigraphy, sedimentology and paleogeography of the Upper Ordovician-Lower Silurian of Anticosti Island, Québec. *In*: P. J. Lespérence (ed.). I.U.G.S. Field meeting, Anticosti-Gaspé, Québec, 1981. Volume II, Stratigraphy and paleontology. Départment de géologie, Université de Montréal, p. 11-39.

Pingitore, N. E., 1978. The behaviour of Zn^{2+} and Mn^{2+} during carbonate diagenesis: theory and applications. J. Sed. Petrol., 48: 799-814.

Plint, A. G., Eyles, N. and Walker, R. G., 1992. Control of sea level change. *In*: R. G. Walker and N. P. James (eds.), Facies models: Response to sea level change. Geological Association of Canada, p. 15-25.

Plocher, O. W., Ludvigson, G. A., Witzke, B. J., González, L. A., and Day, J. E., 1992. Stable isotopic systematics of the Coralville T-R cycle, *In*: J. Day and J. B. Bunker (eds.). The stratigraphy, paleontology, depositional and diagenetic history of the Middle-Upper Devonian Cedar Valley Group of Central and Eastern Iowa: Iowa Department of Natural Resources Guidebook Series 16: 27-34.

Popp, B. N., Anderson, T. F. and Sandberg, P. A., 1986. Brachiopods as indicators of original isotopic compositions in some Paleozoic limestones. Geol. Soc. Amer., Bull., 97: 11262-1269.

Predtechensky, N. N., Koren, T. N., Modzalevskaya, T. L., Nikiforova, O. I., Berger, A. YA. and Abushik, A. F., 1983. Sedimentation cycles and changes of ecological faunal assemblages in the Silurian of Podolia. *In:* Trudy paleont. Inst., 194: 61-74. (In Russian)

Qing, H. and Veizer, J., 1994. Oxygen and carbon isotope composition of Ordovician brachiopods: Implications for coeval seawater. Geochim. Cosmochim. Acta, 58: 1501-1509.

Quinn, T. M., Lohmann, K. C. and Halliday, A. N., 1991. Sr isotopic variation in shallow water carbonate sequences: Stratigraphic, chronostratigraphic, and eustatic implications of the record at Enewetok Atoll. Paleoceanography, 6: 371-385.

Railsback, L. B., 1990. Influence of changing deep ocean circulation on the Phanerozoic oxygen isotopic record. Geochim. Cosmochim. Acta, 54: 1501-1509.

Railsback, L. B., Akerly, S. C., Anderson, T. F. and Cisne, J. L., 1990. Paleontological and isotope evidence for warm saline deep waters in Ordovician oceans. Nature, 243: 156-159.

Richardson, J., 1857. Report for 1856. Geological Survey of Canada, Reports of Progress 1853-6: 191-245.

Richter, F. M., Rowley, B. D., and DePaolo, D. J., 1992. Sr isotope evolution of seawater: The role of tectonics. Earth Planet. Sci. Lett., 109 (1/2): 11-23.

Rickards, R. B., 1989. Exploitation of graptoloid cladogenesis in Silurian Stratigraphy. *In*: C. H. Holland and M. G. Bassett (eds.). A global standard for the Silurian System. National Museum of Wales, Cardiff, Geological Series no. 9: 267-274.

Riding, R., 1981. Composition, structure and environmental setting of Silurian bioherms and biostromes in northern Europe. *In*: D. F. Toomey (ed.). European fossil reef models. Spec. Publs. SEPM Tulsa, 30: 41-83.

Riding, R., 1993. Phanerozoic patterns of marine $CaCO_3$ precipitation. Naturwissenschaften, 80: 513-516.

Rudwick, M. J. S., 1959. Growth and form of brachiopod shells. Geol. Mag., 96: 1-24.

Ruppel, S. C., James, E. W., Barrick, J. E., Nowlan, G. and Uyeno, T. T., 1996. High-resolution $^{87}Sr/^{86}Sr$ chemostratigraphy of the Silurian: implications for event correlation and strontium flux. Geology, 24: 831-834.

Rush, P. F. and Chafetz, H. S., 1990. Fabric-retentive, non-luminescent brachiopods as indicators of original $\delta^{13}C$ and $\delta^{18}O$ composition: A test. J. Sed. Petrol., 60: 968-981.

Sadler, P. M., 1981. Sedimentation rates and the completeness of stratigraphic sections. Geology, 89: 569-584.

Sami, T. and Deroshers, A., 1992. Episodic sedimentation on an early Silurian, storm dominated carbonate ramp, Becscie and Merrimack Formations, Anticosti Island, Québec. Sedimentology, 39: 355-381.

Samtleben, C., Munneke, A., Bickert, T. and Pätzold, J., 1996. The Silurian of Gotland (Sweden): Facies interpretation based stable isotopes in brachiopod shells. Geol. Rundsch., 85: 278-292.

Sapel'nikov, V. P., 1985. Sistema i Stratigraficheskoe Znachenie Brakhiopod Podotryada Pentameridin. Nauka, Moscow, 207 pp.

Schidlowski, M and Aharon, P., 1992. Carbon cycle and carbon isotope record: geochemical impact of life over 3.8 Ga of Earth history. *In*: M. Schidlowski, S. Golubic, M. M. Kimberley, D. M. McKirdy and P. A. Trudinger (eds.). Early organic evolution: Implications for mineral and energy resources. Springer-Verlag Berlin Heidelberg, p. 147-175.

Schidlowski, M., Eichmann, R. and Junge, C. E., 1975. Precambrian sedimentary carbonates: Carbon and oxygen isotope geochemistry and implications for the terrestrial oxygen budget. Precambrian Res., 2: 1-69.

Schönlaub, H. P., 1986. Significant geological events in the Paleozoic record of the Southern Alps (Austrian part). *In*: O. H. Walliser (ed.). Global Bio-events. Springer, Berlin, p.

163-167.

Schuchert, C. and Twenhofel, W. H., 1910. Ordovicic-Siluric section of the Mingan and Anticosti Islands, Gulf of St. Lawrence. Geol. Soc. Amer. Bull., 21: 677-716.

Scrutton, C. T. and McCurry, J. A., 1987. The derivation, biostratigraphy and palaeobiogeographic significance of corals from Silurian deep-sea turbidite facies in the south-west Southern Uplands. Scottish Journal of Geology, 23: 49-64.

Scotese, C. R. and McKerrow, W. S., 1990. Revised world maps and introduction to memoir. *In*: W. S. McKerrow and C. R. Scotese (eds.). Palaeozoic palaeogeography and biogeography. Geol. Soc. Lond. Memoir, 12: 1-21.

Scotese, C. R., Van der Voo, R. and Barrett , S. F., 1985. Silurian and Devonian base maps. *In*: W. G. Chaloner and J. D. Lawson (eds.). Shelf sands and sandstone reservoirs, SEPM. Short Course Notes, 13: 133-241.

Shergold, J. H. and Bassett, M. G., 1970. Facies and faunas at the Wenlock/Ludlow boundary of the Wenlock Edge, Shropshire. Lethaia, 3: 113-142.

Siveter, D. J., Owens, R. M. And Thomas, A. T., 1989. The northern Wenlock Edge area: shelf muds and carbonates on the Midland Platform. *In*: M. G. Bassett (ed.). Silurian field excursions, A geotraverse across Wales and the Welsh Borderland. National Museum of Wales, Cardiff, Geological Series no. 10: 23-35.

Skinner, B. J. and Porter, S. C., 1987. Physical geology. John Wiley & Sons, Inc.,p. 574.

Talent, J. A., Berry, W. B. N. and Boucot, A. J., 1975. Correlation of the Silurian rocks of Australia, New Zealand, and New Guinea. Spec. Pap., Geol. Soc. Amer., 150: 1-108.

Talent, J. A., Mawson, R., Andrew, A. S., Hamilton, P. J. and Whitford, D. J., 1993. Middle Paleozoic extinction events: faunal and isotopic data. Palaeogeog., Palaeoclimatol., Palaeoecol., 104: 139-152.

Thirwall, M. F., 1991. Long-term reproducibility and multicollector Sr and Nd isotope ratio analysis. Chem. Geol. (Isotope Geoscience Section), 94: 85-104.

Tipper, J., 1983. Rates of sedimentation and stratigraphical completeness. Nature, 302: 696-698.

Tucker, R. D., Krogh, T. E., Ross, R. J. and Williams, S. H., 1990. Time-scale calibration by high-precision U-Pb zircon dating of interstratified volcanic ashes in the Ordovician and Lower Silurian stratotypes of Britain. Earth Planet. Sci. Lett., 100: 51-58.

Turner, J.V., 1982. Kinetic fractionation of ^{13}C during calcium carbonate precipitation: Geochim. Cosmochim. Acta, 46: 1183-1192.

Twenhofel, W. H., 1914. The Anticosti Island faunas. G. S. C., Museum Bull. 3, Geological Series 19, 35 p.

Twenhofel, W. H., 1928. Geology of Anticosti Island. G. S. C., Memoir 154, 481 p.

Uyeno, T. T. and Barnes, C. R., 1983. Conodonts of the Jupiter and Chicotte formations (Lower Silurian), Anticosti Island, Québec. G. S. C. Bull., 355: 1-49, pls. 1-9.

Veizer, J., 1983a. Chemical diagenesis of carbonates: Theory and application of trace element technique. *In*: M. A. Arthur, T. F., Anderson, I. R. Kaplan, J. Veizer and L. S. Land (eds.), Stable Isotopes in Sedimentary Geology. SEPM Short Course, 10: III-1-III-100.

Veizer, J., 1983b. Trace elements and isotopes in sedimentary carbonates. Rev. Mineral., 11 :265-300.

Veizer, J., 1989. Strontium isotopes in seawater through time. Ann. Rev. Earth Planet. Sci. Lett., 17: 141-167.

Veizer, J., 1995. Reply to comment by L. S. Land on "Oxygen and carbon isotopic composition of Ordovician brachiopods: Implications for coeval seawater". Geochim. et Cosmochim. Acta, 59: 2845-2846.

Veizer, J., Bruckschen, P., Pawellek, F., Podlaha, O., Jasper, T., Korte, C., Strauss, H., Azmy, K. and Ala, D., in press. Oxygen isotope evolution of Phanerozoic seawater. Palaeogeogr., Palaeoclimatol., Palaeoecol.

Veizer, J. and Compston, W., 1974. $^{87}Sr/^{86}Sr$ in Precambrian carbonates as an index of crustal evolution. Geochim. Cosmochim. Acta, 40: 905-915.

Veizer, J. and Fritz, P., 1976. Possible control of post-depositional alteration in oxygen paleotemperature determinations. Earth Planet Sci. Letters, 33: 255-260.

Veizer, J., Fritz, P. and Jones, B., 1986. Geochemistry of brachiopods: oxygen and carbon isotopic records of Paleozoic oceans. Geochim. Cosmochim. Acta, 50: 1679-1996.

Veizer, J. and Hoefs, J., 1976. The nature of $^{18}O/^{16}O$ and $^{13}C/^{12}C$ secular trends in sedimentary carbonate rocks. Geochim. Cosmochim. Acta, 40: 1387-1395.

Wadleigh, M. A. and Veizer, J. 1992. $^{18}O/^{16}O$ and $^{13}C/^{12}C$ in Lower Paleozoic articulate brachiopods: implications for the isotopic composition of seawater. Geochim. Cosmochim. Acta, 56: 431-443.

Wang, Y., Boucot, A. J., Rong, J. Y. and Yang, X. C., 1987. Community paleoecology as a geologic tool: the Chinese Ashgillian-Eifelian (latest Ordovician through early Middle Devonian) as an example. Geol Soc. Amer., Spec. Pap., 211: 1-100.

Weber, J. N., 1965. The $^{18}O/^{16}O$ ratio in ancient oceans. Geokhimija, 6: 674-680.

Weber, J.N. and Raup, D.N., 1968. Comparison of $^{13}C/^{12}C$ and $^{18}O/^{16}O$ in skeletal calcite of recent and fossil echinoids. J. Paleontology, 42: 37-50.

Wefer, G. and Berger, W. H., 1991. Isotope paleontology: growth and composition of extant calcareous species. Marine Geology, 100: 207-248.

Wenzel, B. and Joachimski, M. M., 1996. Carbon and oxygen isotopic composition of Silurian brachiopods (Gotland/Sweden)- palaeoceanographic implications. Palaeogeogr., Palaeoclimatol., Palaeoecol., 122: 143-166.

Wilde, P. and Berry, W. B. N., 1986. The roles of oceanographic factors in the generation of global bio-events. *In*: Walliser, O H. (Ed.) Global Bio-events. Springer-Verlag, Berlin, Heidelberg, New York, London, Paris, Tokyo, 75-91.

Wilde, P., Berry, W. B. N. and Quinby-Hunt, M. S., 1991. Silurian oceanic and atmospheric circulation and chemistry. Spec. Pap. Palaeontol., 44: 123-143.

Williams, A., 1968. Evolution of the shell structure of articulate brachiopods. Spec. Pap. Palaeontology 2(2): 1-55.

Williams, A., 1970a. Comments on the growth of the shell of articulate brachiopods. Smithsonian Contributions to Palaeontology, 3: 47-67.

Williams, A., 1970b. Origin of laminar-shelled articulate brachiopods. Lethaia, 3: 392-342.

Williams, A., Rowell, A. J., Muir-Wood, H. M., Pitrat, C. W., Schmidt, H. Stehli, F. G., Ager, D. V., Wright, A. D. Elliott, G. F., Amsden, T. W., Rudwick, M. J. S., Hatai, K., Biernat, G., McLaren, D. J., Boucot, A. J., Johnson, J. G., Staton, R. D., Grant, R. E. and Jope, H. M., 1965. Morphology. Treatise on invertebrate palaeontology (Brachiopoda). Part

H., V1, University of Kansas Press. R. C. Moore (ed.), H56-H155.

Worsley, D. (ed.), 1982. Field meeting Oslo Region 1982. IUGS, Subcommission on Silurian Stratigraphy. Paleont. Contr. Univ. Oslo, 278: 1-175.

Worsley, D., 1989. The Llandovery Series in the Oslo Region. *In*: C. H. Holland and M. G. Bassett (eds.). A global standard for the Silurian System. National Museum of Wales, Cardiff, Geological Series no. 9: 108-116.

Worsley, D., Aarhus., N, Bassett, M. G., Howe, M. P. A. and Olaussen, S., 1983. The Silurian succession of the Oslo Region. Norg. Geol. Unders., 384: 1-57.

Ziegler, A. M., 1965. Silurian marine communities and their environmental significance. Nature, Lond., 207: 270-272.

Ziegler, A. M., Cocks, L. R. M. and Bambach, R. K., 1968. The composition and structure of Lower Silurian marine communities. Lethaia, 1: 1-27.

Ziegler, A. M., Hansen, K. S., Johnson, M. E., Kelly, M. A., Scotese, C. R. and Van der Voo, R., 1977. Silurian continental distributions, paleogeography, climatology, and biogeography. Tectonophysics, 40: 31-51.

Ziegler, W. and Lane, H. R., 1987. Cycles in conodont evolution from Devonian to mid-Carboniferous. *In*: R. J. Aldridge (ed.). Palaeobiology of conodonts. Br. Micropalaeontol. Soc. Ser., p. 147-164.]

Ziegler, A. M., Rickards, R. B. and McKerrow, W. S., 1974. Correlation of the Silurian rocks of the British Isles. Geol. Soc. Amer., Spec. Pap., 154: 1-154.

Ziegler, A. M., Scotese, C. R., McKerrow, W. S., Johnson, M. E. and Bambach, R. K., 1979. Paleozoic paleogeography. Ann. Rev. Earth planet. Sci., 7: 473-502.

APPENDIX 1

METHODOLOGY

A1.1. SAMPLING AND SEPARATION TECHNIQUES

Some of the brachiopods examined in this study were collected from exposed successions (Podolia, Ukraine) and from borehole materials (Lithuania and Latvia). Others were selected from collections at the Natural Museum of Wales (Britain, Norway and Sweden) and at the Department of Geology, Laurentian University (Anticosti Island, Québec). In addition to brachiopods, samples included some carbonate cements and matrix. The selection of the samples aimed to cover the entire Silurian Period with a resolution of some 200,000 years.

A1.1.1. Separation Techniques

The separation technique must usually be adjusted to the purpose for which the brachiopod samples are being used. Diagenetic alteration of the brachiopod shells is a significant problem because it can destroy the original isotopic signature of the shell. Identification of the well preserved parts of the shell and careful sampling can minimize this problem (Popp et al., 1986; Grossman et al., 1993). For each of the brachiopods selected, the following procedure was applied:

1- The apparently well preserved brachiopod shell was identified.

2- Two identical slabs passing through the umbo (each about 1.5 mm-thick) were cut using a microsaw cutting machine (ISOMET- low speed saw). The cutting was intended to pass through the umbo area because the thickness of the secondary layer reaches there the maximum and

because the secondary layer is usually well preserved in that area due to the dense microstructure of the shell that isolates calcite crystals from diagenetic fluids (Grossman et al., 1991; Grossman, 1994).

3-The inner side of each slab was gently polished on a glass plate using Al_2O_3 powder (size 9.5 μm).

4- The two slabs were checked under the luminoscope to identify the non-luminescent parts of the secondary layer of the shell. Usually, both slabs exhibited identical CL features. Shells with a brightly luminescent secondary layer were excluded.

5- One of the slabs was prepared as a thin section and the other was placed under a binocular microscope for microsampling. The carbonate material, from the non-CL parts of the secondary layer, was microsampled by smashing the shell with a stainless steel dental pick. The produced fragments were picked up by forceps. A sample of about 6 to 8 mg was separated.

6- For large brachiopods, samples were taken not only from the shell posterior, but also from the anterior in order to examine the possible effect of seasonality on the $\delta^{18}O$ and elemental composition of the brachiopod shells (Mii and Grossman, 1994).

7- The fragments were submerged in about 10 ml deionized water and cleaned in an ultrasonic bath for 2 minutes. Subsequently, they were rinsed with deionized water by filtration using a clean funnel and the no. 4 or 41 filter paper. Filter paper was previously rinsed with deionized water 4 or 5 times in order to wash out any possible contaminants.

8- The samples were dried overnight at room temperature.

9- A fragment of the dry sample was taken for examination by the Scanning Electron Microscope and the rest was ground in a previously acid-washed small agate mortar. The powder was kept

in small sealed plastic vials. About 4 mg of the powdered sample was analysed for oxygen and carbon isotopes and approximately 1 mg was used for Sr isotope measurements. The solution remaining after digestion of sample for liberation of CO_2 gas for O and C isotope analysis was used for trace element determinations.

A1.2 PETROGRAPHIC EXAMINATION

The preliminary assessment of the preservation of brachiopod shells is usually made by examining thin sections under the transmitted light polarizing microscope and in the luminoscope, using the cathodoluminescence technique. Both techniques allow the recognition of diagenetic changes in the fabric and mineralogy of the shell.

A1.2.1. Transmitted Light Microscopy

The studied thin sections were examined under a Nikon OPTIPHOT-POL polarizing microscope. Diagenetic alteration, involving dissolution-precipitation processes, usually causes deformation of the calcite prisms of the shell. Also, diagenetic dolomitization and silicification can be recognized as replacement criteria.

A1.2.2. Cathodoluminescence Petrography (CL)

A1.2.2.1. Theory

Luminescence is the temporary emission of light from a solid when it is excited by some form of energy such as an electron beam. The electron beam (β-rays), produced by an electron gun, bombards the atoms of the solid to excite their electrons and cause them to jump to higher energy

levels (orbitals). After a short delay time (10^{-8} s), the electrons in the excited atoms return to their original ground state and radiate the acquired energy (quanta) (Nickel, 1978; Miller, 1988).

This phenomenon was utilized in geology to study the petrography of rocks. In carbonates, the intensity and characteristics of the luminescence emitted are influenced by two main categories of factors, intrinsic and extrinsic.

The intrinsic factors depend on the mineral itself, such as the sites of imperfect lattice planes that were formed during growth. These sites absorb more energy from the bombarding beam and, as a result, they luminescence brightly.

The extrinsic factors depend on the nature of the environment in which the mineral was formed, such as: (1) Concentration and distribution of ions of impurities incorporated in the mineral from the surrounding medium. These ions usually replace Ca^{2+} in the lattice of calcite. Mn^{2+} is an important activator of the CL in calcite and dolomite. Other potential sensitizers of Mn-activated luminescence are Sm, Dy, Eu, Er, Ce and Pb. In contrast, Fe^{2+}, Fe^{3+}, Co^{2+} and Ni^{2+} are quencher elements that inhibit luminescence. Generally speaking, the Mn/Fe ratio in the mineral is an important factor that controls the CL type (cf. Bruhn et al., 1994); (2) Current intensity and voltage of the electron beam used; and (3) The smoothness and the level of the irradiated surface where points of high relief catch the oblique beam which increases the contrast (Machel, 1985; Choquette and James, 1987; Machel et al., 1991; Machel and Burton, 1991).

A1.2.2.2. Apparatus

Samples were examined utilizing a Technosyn cold cathode luminoscope, model 8200 MK II, which was attached to a Nikon OPTIPHOT-POL microscope and Nikon FX-35A Camera using

Nikon UFX-II exposure unit. The operating conditions were maintained at about 10 to 11 kv, gun current 350 to 400 mamp and a vacuum of ~ .03 Torr.

A1.2.2.3. Preparation Techniques

Samples were examined as either polished thin sections or polished slabs (chips). The preparation techniques are described in detail above.

A1.2.2.4. Luminescence Types

The three main kinds of luminescence that can be visually recognized in calcite are bright, dull and non-luminescence (Machel and Burton, 1991). Some recent studies correlated the concentrations of Fe and Mn in carbonates, detected by the proton microprobe (PIXE) technique, with their corresponding luminescence and, as a result, two additional types of luminescence were recognized, moderate and intrinsic. The latter is a dark blue CL caused not by ions, but by lattice defects in pure calcite (Bruhn et al., 1994). Note, however, that personal visual ability may contribute to the perception as to the type of luminescence.

The studied brachiopod shells were scanned therefore for only three types of luminescence, non-CL, dull CL and bright CL. Bright CL veinlets were occasionally observed associated with the first two types. In punctate shells, bright CL punctae can sometimes be recognized.

A1.2.3. Scanning Electron Microscopy (SEM)

SEM is a very useful technique for examining the preservation of the calcite prisms that form the secondary layer of the brachiopod shells and for recognition of any dissolution or

replacement features caused by diagenetic pore fluids.

Samples were studied using the SEM at the Department of Biology, Carleton University. A small clean portion from each sampled shell was taken and put on a double sided sticking strip which was already adhered to a regular-size glass slide. The fragments were coated under vacuum with gold film using ANATEC Limited Sputter Coater (100 Ångstrom, Au-Pd sputter coater). The slide with coated fractions was examined using a JOEL-6400 Digital Scanning Electron Microscope. Pictures were taken utilizing Polaroid 665 Positive / Negative Film (3 1/4" X 4 1/4" B/W Print / Neg.).

The state of preservation of the studied shells was graded as excellent, good, fair, poor and destroyed.

A1.3. ISOTOPE ANALYSIS

A1.3.1. Carbon and Oxygen Isotope Measurements

The measurement of C and O isotopic compositions for the studied brachiopods was based on reacting the carbonate shells with 100% orthophosphoric acid under vacuum at 25 °C (McCrea, 1950) and using the produced CO_2 gas for determination of $\delta^{13}C$ and $\delta^{18}O$ ratios of the carbonate.

A1.3.1.1. Glassware Cleaning Procedure

The trace element analysis was carried out using the solution remaining from the isotope reaction. Consequently, all the glassware used was acid-washed with aqua regia (HCl / HNO_3 = 3 / 1 by volume), then rinsed with deionized water several times and dried for 2 hrs. at 150 °C or overnight at 50 °C.

A1.3.1.2. Preparation of Ultrapure Orthophosphoric Acid

The H_3PO_4 used in the reaction had to be ultrapure to minimize as much as possible any contamination, since the acid solution left after the isotope reaction was used for trace element analysis. The acid was prepared as follows:

1- In 1-litre beaker, 500 g of ultrapure P_2O_5 (99.998% pure) was added to 500 ml of ultrapure H_3PO_4 (85%).

2- The solution was stirred with a glass rod and heated at 180 °C overnight.

3- 1 ml of H_2O_2 (30%) was added and heating was continued for 4.5 hrs. at 220 °C.

4- Heating was stopped and the acid was left to cool to 100 °C, then poured into clean bottle and sealed.

5- The acid was stored for 2 weeks to be homogenized before use.

A1.3.1.3. Extraction of the CO_2 Gas and Measuring the Isotope Ratios

Isotope analysis of the samples was performed at the Stable Isotope Laboratory, Department of Geology, University of Ottawa. The procedure used for the analysis was as follows:

1- About 3 mg of the powdered sample (see A1.1.1) was weighed in a clean acid-washed reaction vessel and reacted under vacuum overnight with ~1.5 ml of the already prepared ultrapure orthophosphoric acid at 25 °C in a water bath. Samples with observed dolomitization of the host rock were reacted only for 4 hrs.

2- The reaction vessels were connected to an on-line extraction system and CO_2 was extracted, cleaned of non-condensible gases and H_2O vapour using liquid N_2 and cool ethanol bath at -80 °C, and trapped in glass break-seals.

3- The break-seals containing the gas were loaded onto the VG Isogas SIRA-12 triple collecting mass spectrometer for measuring the isotope ratios.

The laboratory standards were NBS-18 ($\delta^{18}O$ = -23.00‰ and $\delta^{13}C$ = -5.00‰ PDB) and NBS-19 ($\delta^{18}O$ = -2.20‰ and $\delta^{13}C$ = +1.95‰ PDB). The routine precision (2σ) for a pure carbonate sample was 0.1‰.

All data were corrected for ^{17}O according to the procedure of Craig (1957) and Friedman and O'Neil (1977), using the fractionation factor α = 1.01025. Values for O and C isotopes are expressed in δ-notation and given in per mil (‰) relative to the PDB standard.

A1.3.2. Strontium Isotope Analysis

The main technical concept of the Sr-isotope analysis of a rock is based on the conversion of the solid sample into an acid solution, elution of Sr from coexisting elements and measuring the Sr-isotope ratio using the mass spectrometer. The Sr-isotope analysis of the studied brachiopod samples was performed at the Isotope Laboratory, Department of Earth Sciences, Carleton University. The procedure used for the analysis was as follows:

A1.3.2.1. Washing Procedure

All the vessels used for separation of Sr for analysis were teflonware, except for the separation columns.

1- Vessels were washed with soap and water in an ultrasonic cleaner for an hour.

2- Vessels were rinsed several times and soaked in 50% HNO_3 (v/v) for 48 hrs. at 150 °C.

3- The acid-washed vessels were rinsed with deionized water and soaked in deionized water for

at least 12 hrs. (or overnight).

4- Vessels were taken from water, rinsed again with deionized water and left covered to dry out at room temperature.

A1.3.2.2. Separation Procedure for Sr

1- The powdered sample aliquot (~ 1 mg) of the shell (see A1.1.1) is dissolved for 30 minutes in 1.5 ml of 2.5N HCl.

2- Sample is added carefully to a clean 10 ml separation (chromatography) column using a pipette. The drops should not drain the inside walls of the column. The column was a BIO-RAD Econo-Column filled with clean (acid-washed) 1.5 ml of Dowex AG50-X8 cation resin.

4- Wash the column inside walls with 1 ml 2.5N HCl to get all sample down into the resin and let that 1 ml drain through.

5- Add 18 ml of 2.5N HCl to wash all other elements through the column and let them drain. This portion is then discarded.

6- Put labelled sample collection 5 ml-beaker under column and add 6 ml 2.5N HCl to the column to be collected.

7- Evaporate the collected sample at 125 °C for 2 hrs.

8- The dried sample in the teflon vial is dissolved in 0.25 ml of 0.01N HCl for few minutes and added to a clean 10 ml separation column filled with teflon resin to separate Ca from Sr.

9- Add 1 ml of 0.01N HCl to wash the inside walls of the column and let it drain.

10- Add 3 ml of 0.01N HCl and collect them in the same teflon vial.

11- Evaporate the collected sample at 125 ^{0}C for 2 hrs. to be ready for running on the mass

spectrometer.

Blank samples were frequently run and spiked using ^{84}Sr-spike to control any contamination that might occur during the process of separation.

A1.3.2.3. Cleaning the Separation Columns

The columns with the Dowex AG50-X8 cation resin are constantly cleaned after running each sample by:

1- Adding 20 ml 6N HCl to the column, resin shrinks.

2- To re-expand resin, add 1 ml deionized H_2O and 5 ml 2.5N HCl.

3- Add 10 ml 2.5N HCl to re-equilibrate column and drain.

4- Block the column at the bottom using a parafilm, add 2 to 3 ml 2.5N HCl and put cap on top to restore column, with resin soaked in acid, for next use. Make sure that the parafilm does not leak.

The same procedure is used to clean the columns of teflon resin, except for the equilibration which is done by using 15 ml of 0.01N HCl instead of 2.5N HCl.

A1.3.2.4. Measuring the $^{87}Sr/^{86}Sr$ Ratio

The sample was dissolved in 0.4 ml of 1M H_3PO_4 for 2 minutes and about half of it was loaded on tantalum filament. The strontium isotope ratio was measured using the FINNIGAN MAT 261 multicollector thermal ionization mass spectrometer.

The laboratory standard used was NBS 987 ($^{87}Sr/^{86}Sr = 0.710256$) and routine precision (2σ) was calculated to be $\pm$ 0.000017.

A1.4. INDUCTIVELY COUPLED ARGON PLASMA SOURCE SPECTROMETRY

A1.4.1. Trace Element Analysis

The concentration of some of the major and trace elements in carbonates is an indication of the degree of preservation, where diagenetic alteration increases the concentration of some elements in calcite (such as Mn and Fe) and decreases the concentrations of others (such as Sr and Na). The measurement of concentrations of Ca, Mg, Sr, Mn and Fe in the studied brachiopod shells was carried out at the Geochemistry Laboratory of the Department of Geology, University of Ottawa, using a Thermo Jarrell Ash-AtomScan 25 Inductively Coupled Plasma Source Spectrometer. The residual H_3PO_4 left after the preparation of CO_2 gas for C and O isotope measurements was analysed using the method of Coleman et al. (1989) as follows:

1- The remaining solution in the reaction vessel was pipetted, as much as it was possible, using a small clean acid-washed glass pipette and transferred into a graduated 15 ml-plastic vial.

2- The volume was made up to about 10 ml by adding deionized water.

3- The vial was closed tightly and shaken well several times and the solution was analysed.

4- A set of similar solutions of a local standard limestone (LMS) was prepared in the same way and run together with the unknown samples. A second calibration and standardization procedure was applied by running liquid standards with known concentrations. These standards were made up from mixtures of standard solutions with different concentrations of the elements measured.

5- For control of any unexpected contamination, sets of blanks were similarly treated and were run along with the regular samples.

The advantage of this method is that the analysis was done on the carbonate material from the same spot for which the C and O isotope values were measured. This may minimize the effect

of heterogeneity on distribution of trace elements within the brachiopod shells.

The standards and blank acid solutions were run with almost every set of ten unknowns in order to control contamination. The chemical data were recalculated on an insoluble residue-free basis (100% soluble carbonate).

A1.4.1.1. Calculation of Element Concentrations

Calculation of the concentrations of elements in the analysed solution is programmed in the software of the spectrometer and based on the following steps:

Intensity of sample = I_s

Calibration curve equation $y = m x + a$

$I = m * conc + a$

$Conc_s = (I_s - a) / m$ µg/ml

The concentration of elements as ppm in the solid sample is calculated as:

(Conc$_s$ in µg/ml * sample volume in ml * 10^3) / sample weight in mg.

A1.4.1.2. Analytical Precision and Accuracy

Analytical precision was calculated using an internal limestone standard (LMS). A total of twenty two aliquots of the powdered LMS were weighed, treated as regular samples and run. Mean precision, in percent, for each analysed element is shown in Table 1 and is calculated as $(\sigma_{n-1}/X)*100$ where (n) is the number of determinations of (X) of the standard (LMS) and (σ_{n-1}) is the standard deviation.

Accuracy (Table A1) was calculated using the x-ray fluorescence (XRF) measurements of the

LMS as recommended values, following the equation $(X - X_{XRF})^* 100 / X_{XRF}$, where X is the average concentration of the element measured by wet chemistry and $X_{(XRF)}$ is the concentration measured by XRF.

Element	Ca	Mg	Mn	Sr
X	39.10	0.20	323	497
σ_{n-1}	0.16	0.02	26	28
$(\sigma_{n-1}/X)^*100$	0.4	10	8	5.6
X_{XRF}	38.99	0.18	286	436
Accuracy (%)	0.3	11.1	12.9	14

Table A1. Means, standard deviations, precisions in (relative %) and accuracy for replicate analyses of the standard LMS.

Appendix 2. Samples, descriptions, localities, stratigraphy, isotopic composition ($\delta^{18}O$ and $\delta^{13}C$ in ‰ PDB) and trace element contents.

Field No.	Formation	Member	Unit/Core	Species	Locality	Graptolite Biozone	$\delta^{18}O$	$\delta^{13}C$	$^{87}Sr/^{86}Sr$	2σ	Ca%	Mg%	Mn(ppm)	Sr(ppm)	Age (Ma)
A084	Ellis bay			*Parastrophinella* sp.	Anticosti Is.	*Ord./Sil. boundary*	-2.72	1.34	0.707951	0.000008	38.56	0.25	65	1137	438.7
A094	Becscie	Fox Point		*Eospirigerina* sp.	Anticosti Is.	[2] *avatus*	-3.37	1.83			39.62	0.10	38	707	438.2
A096	Becscie	Chabot		*Virgiana barrandii*	Anticosti Is.	[2] *avatus*	-3.93	0.02			39.56	0.31	22	1081	438.2
A150(a)	Merrimack		1	*Fenestrirostra primaeva*	Anticosti Is.	[4] *cyphus*	-4.85	0.85	0.708050	0.000007	40.87	0.24	214	1298	437.2
A172(4)	Jupiter	Pavillon	4	*Gotatrypa* sp.	Anticosti Is.	[12] *griestoniensis*	-5.15	1.07	0.708222	0.000008	37.54	0.11	24	1189	431.2
A225	Gun River	Sandtop		*Mendacella* sp.	Anticosti Is.	[7] *leptotheca*	-4.74	1.06			39.46	0.38	38	1127	434.8
A236	Gun River	Innommée		*Mendacella* sp.	Anticosti Is.	[5] *triangulatus*	-3.75	0.96	0.708095	0.000015	39.34	0.47	79	1013	436.5
A262	Chicotte	Brisantes		*Gotatrypa gibbosa*	Anticosti Is.	[12] *griestoniensis*	-5.59	1.14			39.75	0.18	35	1027	431.2
A317	Merrimack		13	*Fenestrirostra glacialis*	Anticosti Is.	[5] *triangulatus*	-4.96	0.53	0.708083	0.000009					436.5
A317	Merrimack		6	*Fenestrirostra glacialis*	Anticosti Is.	[4] *cyphus*	-5.38	0.07	0.708080	0.000007	37.76	0.25	150	1213	437.2
A356(4)	Merrimack		12	*Rhynchotrema fringilla*	Anticosti Is.	[5] *triangulatus*	-4.67	1.40	0.708063	0.000007	38.38	0.16	97	1140	436.5
A510	Gun River	Macgilvray		*Atrypa* sp. ?	Anticosti Is.	[7] *leptotheca*	-5.19	1.25	0.708161	0.000007	39.28	0.13		435	434.8
A740	Jupiter	Ferrum	18	*Gotatrypa* sp.	Anticosti Is.	[12] *griestoniensis*	-5.10	0.21			39.02	0.15	30	1217	431.2
A740	Jupiter	Ferrum	± 14	*Gotatrypa* sp.	Anticosti Is.	[11] *crispus*	-5.00	0.41	0.708207	0.000006	42.17	0.10	19	1147	431.7
A754	Gun River	Innommée		*Mendacella* sp.	Anticosti Is.	[5] *triangulatus*	-3.95	0.54	0.708052	0.000017	38.98	0.73	66	997	436.5
A757	Gun River	Sandtop		*Brachyprion robustum*	Anticosti Is.	[7] *leptotheca*	-4.96	1.47	0.708079	0.000009	39.13	0.62	57	1147	434.8
A800	Jupiter	Ferrum	C13	*Gotatrypa* sp. ?	Anticosti Is.	[11] *crispus*	-4.86	0.59	0.708197	0.000008	39.68	0.11	29	1067	431.7
A806	Jupiter	Ferrum	8-9	*Gotatrypa* sp.	Anticosti Is.	[11] *crispus*	-5.01	0.68	0.708192	0.000007	35.88	0.09	79	1153	431.7
A829	Jupiter	Ferrum	21-22	*Gotatrypa* sp.	Anticosti Is.	[12] *griestoniensis*	-5.19	0.19			39.02	0.13	22	1309	431.2
A830	Chicotte	Brisantes			Anticosti Is.	[12] *griestoniensis*	-3.74	1.76	0.708210	0.000011	39.80	0.14	17	1000	431.2
A832	Chicotte	Galiote		*Stegerhynchus* sp.	Anticosti Is.	[13] *crenulata*	-5.23	1.55	0.708292	0.000012	39.58	0.30	29	935	430.7
A846	Jupiter	Goéland	± 6	*Joviatrypa* sp.	Anticosti Is.	[8] *convolutus*	-5.18	0.94	0.708163	0.000007	40.98	0.11	44	1170	433.9
A848	Jupiter	Richardson	± 4	*Gotatrypa* sp.	Anticosti Is.	[5] *turriculatus*	-4.41	1.24	0.708167	0.000007	36.51	0.21	26	1183	432.3
A852a	Jupiter	Goéland	4-5	*Gotatrypa* sp.	Anticosti Is.	[8] *convolutus*	-5.29	1.71	0.708151	0.000010	38.33	0.08	9	1141	433.9
A854	Jupiter	Goéland	7-8	*Fardenia* sp.	Anticosti Is.	[8] *convolutus*	-5.52	1.00	0.708170	0.000007	35.90	0.26	85	1200	433.9
A862	Jupiter	Richardson	2	*Gotatrypa* sp.	Anticosti Is.	[9] *sedgwickii*	-4.41	2.05	0.708179	0.000008	34.20	0.15	52	1147	433.0
A868b	Jupiter	Cybèle	5	*Gotatrypa* sp.	Anticosti Is.	[11] *crispus*	-5.98	0.64	0.708188	0.000006	38.43	0.13	23	1129	431.7
A888a	Jupiter	Goéland	9	*Hercotrema* sp.	Anticosti Is.	[9] *sedgwickii*	-4.59	1.20	0.708124	0.000010	38.55	0.37	81	1510	433.0
A889	Jupiter	Goéland	8	*Joviatrypa* sp.	Anticosti Is.	[8] *convolutus*	-5.29	1.45			39.42	0.14	50	1408	433.9
A900	Jupiter	Goéland	2	*Hercotrema* sp.	Anticosti Is.	[8] *convolutus*	-5.05	1.45			39.17	0.28	28	1474	433.9
A916	Jupiter	Goéland	8	*Joviatrypa brabyla*	Anticosti Is.	[8] *convolutus*	-5.29	0.69			39.42	0.15	70	1226	433.9
A919	Jupiter	Richardson	3	*Gotatrypa* sp.	Anticosti Is.	[5] *turriculatus*	-4.84	1.60			39.40	0.19	23	1275	432.3
A922	Jupiter	Cybèle	8	*Gotatrypa* sp.	Anticosti Is.	[11] *crispus*	-4.84	1.21	0.708128	0.000010	39.51	0.12	16	1269	431.7
A924a	Jupiter	Cybèle	± 9		Anticosti Is.	[11] *crispus*	-4.02	2.93			39.45	0.15	131	1178	431.7
A931	Jupiter	Richardson	3	*Stegerhynchus* sp.	Anticosti Is.	[9] *sedgwickii*	-4.11	1.95			38.98	0.27	51	1266	433.0
A943a	Jupiter	Ferrum	±10	*Gotatrypa* sp.	Anticosti Is.	[11] *crispus*	-4.82	0.73			39.29	0.10	12	1082	431.7
A950a	Jupiter	Goéland	13	*Hercotrema* sp.	Anticosti Is.	[9] *sedgwickii*	-4.64	0.56	0.708127	0.000009	39.19	0.28	22	1389	433.0
A960	Jupiter	Ferrum	20	*Gotatrypa* sp.	Anticosti Is.	[12] *griestoniensis*	-5.50	-0.20			39.42	0.19	27	1148	431.2

Appendix 2 (cont.)

Field No.	Formation	Member	Unit/Core	Species	Locality	Graptolite Biozone	$\delta^{18}O$	$\delta^{13}C$	$^{87}Sr/^{86}Sr$	2σ	Ca%	Mg%	Mn(ppm)	Sr(ppm)	Age (Ma)
A967a	Jupiter	Richardson	14	*Gotatrypa* sp.	Anticosti Is.	[5] *turriculatus*	-4.50	1.14			38.98	0.12	154	951	432.3
A1085	Chicotte	Brisantes		*Eospirifer* sp.	Anticosti Is.	[12] *griestoniensis*	-5.26	2.12	0.708321	0.000014	39.64	0.26	20	1092	431.2
BLT1	Merrimack			*Ancillotoechia* sp.	Anticosti Is.	[5] *triangulatus*	-5.05	1.03	0.708061	0.000007					436.5
BLT3	Jupiter	Goéland		*Atrypa* sp.	Anticosti Is.	[8] *convolutus*	-5.41	1.18	0.708151	0.000009					433.9
BLT4	Jupiter	Goéland		*Mendacella* sp.	Anticosti Is.	[8] *convolutus*	-5.38	0.68	0.708159	0.000007					433.9
BLT5	Gun River	Innommée		*Ancillotoechia* sp.	Anticosti Is.	[5] *triangulatus*	-4.50	1.18	0.708108	0.000008					436.5
C716	Becscie	Fox Point	5	*Eospirigerina* sp.	Anticosti Is.	[1] *acuminatus*	-3.16	1.46	0.707930	0.000011	39.25	0.16	56	698	438.7
B01	Much Wenlock			*Anastrophia deflexa*	Britain	[22] *ludensis*	-5.02	0.59			38.39	0.33	234	1647	424.4
B03	Much Wenlock			*Dolerorthis rigida*	Britain	[22] *ludensis*	-5.47	2.45	0.708451	0.000010	38.41	0.44	214	1718	424.4
B04	Buildwas			*Whitfieldella* sp.	Britain	[15] *murchisoni*	-4.00	3.44	0.708328	0.000010	38.98	0.12	42	1530	429.3
B05	Much Wenlock			*Atrypa reticualris*	Britain	[21] *nassa*	-5.06	-0.30	0.708414	0.000014	38.83	0.19	299	1779	425.1
B06	Much Wenlock			*Spirigerina marginalis*	Britain	[22] *ludensis*	-4.33	2.96			39.09	0.12	94	957	424.4
B07	Much Wenlock			*Atrypa reticularis*	Britain	[22] *ludensis*	-5.16	0.81			38.78	0.15	286	1787	424.4
B08	Much Wenlock			*Atrypa reticularis*	Britain	[22] *ludensis*	-5.97	0.73			38.78	0.18	283	1797	424.4
B09	Much Wenlock			*Atrypa reticularis*	Britain	[22] *ludensis*	-4.85	1.21			38.89	0.16	190	1694	424.4
B10	Much Wenlock			*Atrypa reticularis*	Britain	[22] *ludensis*	-4.90	1.24	0.708474	0.000015	38.89	0.16	110	1676	424.4
B11	Coalbrookdale			*Plectatrypa imbricata*	Britain	[21] *nassa*	-1.95	2.39			38.64	0.18	120	1683	425.1
B12	Coalbrookdale			*Atrypa reticularis*	Britain	[21] *nassa*	-4.20	1.26	0.708468	0.000015	38.90	0.13	91	1900	425.1
B13	Coalbrookdale			*Microsphaeridiorhynchus* sp.	Britain	[21] *nassa*	-5.23	0.23			38.79	0.23	201	1691	425.1
B14	Farley			*Atrypa reticularis*	Britain	[21] *nassa*	-5.27	-0.06	0.708433	0.000009	38.91	0.14	158	1882	425.1
B15	Much Wenlock			*Atrypa reticularis*	Britain	[22] *ludensis*	-4.45	1.28	0.708448	0.000012	38.91	0.10	182	1792	424.4
B16	Buildwas			*Meristina obtusa*	Britain	[15] *murchisoni*	-6.32	2.57	0.708466	0.000015	38.93	0.14	41	1849	429.3
B17	Coalbrookdale			*Resserella whitfieldensis*	Britain	[16] *riccartonensis*	-4.40	4.41	0.708382	0.000012	38.73	0.27	200	1657	428.6
B18	Coalbrookdale			*Whitfieldella* sp.	Britain	[16] *riccartonensis*	-4.38	3.80	0.708367	0.000016	38.80	0.21	162	1645	428.6
B19	Much Wenlock			*Anasrophia deflexa*	Britain	[22] *ludensis*	-5.08	1.14			38.76	0.27	68	1686	424.4
B20	Much Wenlock			*Atrypa reticularis*	Britain	[22] *ludensis*	-5.81	0.67	0.708484	0.000012	38.78	0.25	402	1710	424.4
B21	Much Wenlock			*Atrypa reticularis*	Britain	[22] *ludensis*	-4.75	1.04			38.84	0.21	67	1820	424.4
B22	Much Wenlock			*Atrypa reticularis*	Britain	[22] *ludensis*	-5.10	0.98			38.88	0.12	95	1811	424.4
B23	Elton			*Atrypa reticularis*	Britain	[23] *nilssoni*	-5.01	1.23	0.708435	0.000010	38.86	0.18	52	1943	423.1
B24	Much Wenlock			*Atrypa reticularis*	Britain	[22] *ludensis*	-5.37	1.80			38.97	0.12	196	1868	424.4
B26	Much Wenlock			*Sphaerirhynchia wilsoni*	Britain	[22] *ludensis*	-5.37	0.37	0.708437	0.000009	38.72	0.19		1836	424.4
B27	Much Wenlock			*Isorthis amplificata*	Britain	[22] *ludensis*	-5.50	0.39			38.40	0.45	307	1934	424.4
B30	Much Wenlock			*Atrypa reticularis*	Britain	[21] *nassa*	-5.50	0.16			38.90	0.12	148	1936	425.1
B31	Much Wenlock			*Atrypa reticularis*	Britain	[22] *ludensis*	-5.25	1.25			38.93	0.15	79	1795	424.4
B34	Much Wenlock			*Atrypa reticularis*	Britain	[21] *nassa*	-5.65	2.24	0.708428	0.000010	38.84	0.16	39	1988	425.1
B37	Much Wenlock			*Atrypa reticularis*	Britain	[22] *ludensis*	-4.60	0.06			38.72	0.23	250	1837	424.4
B38	Much Wenlock			*Sphaerirhynchia* sp.	Britain	[22] *ludensis*	-6.56	-0.11			38.86	0.16	149	1805	424.4
B41	Coalbrookdale			*Atrypa reticularis*	Britain	[20] *lundgreni*	-5.00	0.73	0.708457	0.000009	38.86	0.17	234	1672	425.8

Appendix 2 (cont.)

Field No.	Formation	Member	Unit/Core	Species	Locality	Graptolite Biozone	$\delta^{18}O$	$\delta^{13}C$	$^{87}Sr/^{86}Sr$	2σ	Ca%	Mg%	Mn(ppm)	Sr(ppm)	Age (Ma)
B43	Much Wenlock			*Isorthis amplificata*	Britain	[22] *ludensis*	-6.13	1.04			38.62	0.37	175	1881	424.4
E16	Slite			*Anastrophia deflexa*	Gotland	[19] *ellesae*	-4.94	-0.57	0.708347	0.000016	38.68	0.28	101	1545	426.5
E17	Slite			*Atrypa* sp.	Gotland	[20] *lundgreni*	-4.64	-0.83			38.82	0.27	119	1664	425.8
G01	Slite			*Rhipidium tenuistriatum*	Gotland	[20] *lundgreni*	-4.48	1.00			39.06	0.14	14	1828	425.8
G02	Mulde			*Atrypa reticularis*	Gotland	[21] *nassa*	-3.85	2.16	0.708427	0.000014	38.81	0.18	41	1996	425.1
G03	Hamra			*Homoeospira* sp.	Gotland	[33] *kozlowskii*	-5.00	4.71			38.33	0.40	184	1567	412.3
G04	Slite			*Stegerhynchus* sp.	Gotland	[20] *lundgreni*	-4.11	2.38			38.56	0.32	67	1609	425.8
G05	Slite			*Atrypa reticularis*	Gotland	[20] *lundgreni*	-3.83	2.52	0.708442	0.000014	38.94	0.15	44	1978	425.8
G06	Lower Visby			*Eoplectodonta duvalii*	Gotland	[14] *centrifugus*	-5.38	2.04	0.708392	0.000250	38.61	0.34	120	1688	430.0
G07	Hemse			*Leptaena depressa*	Gotland	[25] *scanicus*	-5.70	-0.46			38.50	0.43	105	2143	419.6
G08	Hemse			*Cyrtia exporrecta*	Gotland	[25] *scanicus*	-5.58	0.34	0.708548	0.000010	38.70	0.33	208	1509	419.6
G09	Hemse			*Atrypa reticularis*	Gotland	[25] *scanicus*	-5.37	-0.22	0.708546	0.000010	38.85	0.23	41	1898	419.6
G11	Hemse			*Atrypa reticularis*	Gotland	[25] *scanicus*	-5.32	0.02	0.708519	0.000010	38.90	0.17	46	1857	419.6
G12p	Mulde				Gotland	[21] *nassa*	-4.46	1.70			38.60	0.37	116	2651	425.1
G14	Mulde			*Atrypa reticularis*	Gotland	[21] *nassa*	-4.13	1.75	0.708438	0.000012	38.82	0.17	88	1925	425.1
G15	Upper Visby			*Atrypa reticularis*	Gotland	[15] *murchisoni*	-4.81	4.09	0.708339	0.000015	38.83	0.22	129	1728	429.3
G16	Upper Visby			*Resserella cf. basalis*	Gotland	[15] *murchisoni*	-5.15	3.52	0.708363	0.000009	38.59	0.42	61	1737	429.3
G17	Hogklint			*Atrypa cf. reticularis*	Gotland	[16] *riccartonensis*	-5.24	4.36	0.708334	0.000013	38.93	0.16	137	1403	428.6
G18	Hogklint			*Resserella cf. basalis*	Gotland	[16] *riccartonensis*	-5.03	4.30	0.708380	0.000013	38.68	0.42	156	1487	428.6
G19	Hogklint			*Eospirifer radiatus*	Gotland	[16] *riccartonensis*	-4.75	4.37	0.708397	0.000017	38.85	0.25	128	1697	428.6
G20	Hogklint			*Leptaena rhomboidalis*	Gotland	[16] *riccartonensis*	-5.74	4.28			38.92	0.30	240	1134	428.6
G24	Hemse			*Didymothyris didyma*	Gotland	[28] *leintwardinensis*	-5.70	-0.38	0.708622	0.000010	38.98	0.22	48	1301	414.8
G25	Hemse			*Atrypa reticularis*	Gotland	[28] *leintwardinensis*	-5.69	0.66	0.708680	0.000012	38.97	0.12	37	1679	414.8
G26	Mulde			*Meristina obtusa*	Gotland	[21] *nassa*	-4.25	1.56	0.708423	0.000011	38.62	0.20	46	1870	425.1
G27	Slite			*Atrypa reticularis*	Gotland	[19] *ellesae*	-4.48	-0.57	0.708342	0.000012	38.99	0.22	28	1682	426.5
G29	Slite			*Eoplectodonta duvalii*	Gotland	[19] *ellesae*	-4.21	-0.53	0.708350	0.000013	38.70	0.38	48	1745	426.5
G34	Eke			*Leptaena depressa*	Gotland	[29] *bohemicus*	-4.32	4.93			38.59	0.44	166	1481	414.2
G35	Hogklint			*Rhynchtreta cf. cuneata*	Gotland	[16] *riccartonensis*	-4.63	5.30			38.87	0.30	88	1237	428.6
G37	Hemse			*Microsphaeridiorhynchus* sp.	Gotland	[28] *hemiaversus*	-5.43	-0.02	0.708558	0.000013	38.65	0.38	149	1329	416.0
G38a	Mulde			*Atrypa reticularis*	Gotland	[21] *nassa*	-3.45	1.40			38.93	0.22	53	1928	425.1
G38p	Mulde			*Atrypa reticularis*	Gotland	[21] *nassa*	-3.76	1.49			38.84	0.22	59	2017	425.1
G39	Klinteberg			*Ptychopleurella bouchardi*	Gotland	[22] *ludensis*	-5.04	2.29			38.77	0.43	123	851	424.4
G40	Klinteberg			*Rhynchotreta cuneata*	Gotland	[22] *ludensis*	-4.91	1.86	0.708462	0.000013	38.67	0.39	102	1059	424.4
G42	Lower Visby			*Howellella elegans*	Gotland	[15] *murchisoni*	-4.67	6.37			37.51	0.40	227	1121	429.3
G45	Slite			*Eoplectodonta duvalii*	Gotland	[20] *lundgreni*	-4.41	-0.40	0.708438	0.000010	38.32	0.61	322	1683	425.8
G48	Lower Visby			*Stegerhynchus borealis*	Gotland	[13] *crenulata*	-5.56	1.35			38.93	0.25	66	1664	430.7
G51	Slite			*Stegerhynchus* sp.	Gotland	[20] *lundgreni*	-5.21	-0.21	0.708488	0.000009	38.99	0.25	133	1343	425.8
G54	Eke			*Microsphaeridiorhynchus* sp.	Gotland	[29] *bohemicus*	-3.90	5.37	0.708740	0.000009	38.78	0.29	197	1531	414.2

Appendix 2 (cont.)

Field No.	Formation	Member	Unit/Core	Species	Locality	Graptolite Biozone	$\delta^{18}O$	$\delta^{13}C$	$^{87}Sr/^{86}Sr$	2σ	Ca%	Mg%	Mn(ppm)	Sr(ppm)	Age (Ma)
G56	Eke			*Atrypa ex. gr. reticularis*	Gotland	[29] *bohemicus*			0.708707	0.000012	38.74	0.25	170	1295	414.2
G57	Lower Visby			*Dalejina phaseola*	Gotland	[13] *crenulata*	-5.54	1.04			38.53	0.48	178	1503	430.7
G59a	Lower Visby			*Hesperorthis* sp. ?	Gotland	[13] *crenulata*	-6.12	1.13	0.708403	0.000013	38.81	0.33	457	1308	430.7
G59p	Lower Visby			*Hesperorthis* sp. ?	Gotland	[13] *crenulata*	-5.71	1.30			38.86	0.35	163	1542	430.7
G60a	Lower Visby			*Atrypa reticularis*	Gotland	[13] *crenulata*	-5.29	1.38	0.708342	0.000013	39.05	0.16	131	1674	430.7
G60p	Lower Visby			*Atrypa reticularis*	Gotland	[13] *crenulata*	-5.94	1.49			38.75	0.27	351	1448	430.7
G62	Hemse			*Stegerhynchus diodonta*	Gotland	[28] *leintwardinensis*	-6.03	-0.17	0.708616	0.000013	38.71	0.40	131	1339	414.8
G64	Eke			*Howellella elegans*	Gotland	[29] *bohemicus*	-3.85	5.11	0.708735	0.000016	38.31	0.47	108	1579	414.2
G66a	Mulde			*Atrypa reticularis*	Gotland	[21] *nassa*	-3.91	1.68			39.08	0.15	52	1717	425.1
G66p	Mulde			*Atrypa reticularis*	Gotland	[21] *nassa*	-3.98	1.71			38.84	0.24	60	1961	425.1
G67	Mulde			*Resserella elegantula*	Gotland	[21] *nassa*	-3.83	1.65	0.708425	0.000012	38.62	0.45	78	1957	425.1
G68	Mulde			*Atrypa reticularis*	Gotland	[21] *nassa*	-3.85	2.01	0.708460	0.000015	39.08	0.20	30	2042	425.1
G70	Mulde			*Resserella elegantula*	Gotland	[21] *nassa*	-3.68	1.92	0.708459	0.000012	38.70	0.36	81	1969	425.1
G73	Klinteberg			*Conchidium biloculare*	Gotland	[22] *ludensis*	-5.23	1.20			38.93	0.24	83	1607	424.4
G74a	Lower Visby			*Atrypa reticularis*	Gotland	[13] *crenulata*	-5.29	1.38			39.03	0.14	91	1575	430.7
G74p	Lower Visby			*Atrypa reticularis*	Gotland	[13] *crenulata*	-5.80	1.42			38.55	0.25	251	1431	430.7
G75	Lower Visby			*Eoplectodonta transversalis*	Gotland	[13] *crenulata*	-5.14	1.54			38.49	0.54	156	1788	430.7
G78	Hamra			*Boucotinskia sulcata*	Gotland	[33] *kozlowskii*	-4.55	7.43	0.708757	0.000010	38.64	0.35	198	1591	411.6
G80	Klinteberg			*Atrypa reticularis*	Gotland	[22] *ludensis*	-5.76	1.69	0.708497	0.000007	38.98	0.19	83	1258	424.4
G81	Lower Visby			*Desquamatia* sp. ?	Gotland	[13] *crenulata*	-5.44	1.61	0.708362	0.000016	39.15	0.10	75	1402	430.7
G82	Lower Visby			*Atrypa reticularis*	Gotland	[13] *crenulata*	-7.24	1.11	0.708439	0.000012	38.73	0.14	472	1206	430.7
G85a	Mulde			*Atrypa reticularis*	Gotland	[21] *nassa*	-3.51	1.60	0.708433	0.000011	38.99	0.15	25	1804	425.1
G85p	Mulde			*Atrypa reticularis*	Gotland	[21] *nassa*	-3.45	1.70			38.96	0.17	33	1885	425.1
G86a	Slite			*Atrypa reticularis*	Gotland	[20] *lundgreni*	-5.08	-0.76	0.708436	0.000012	38.99	0.18	64	1721	425.8
G86p	Slite			*Atrypa reticularis*	Gotland	[20] *lundgreni*	-5.47	-0.25			38.23	0.19	46	1606	425.8
G88	Mulde			*Atrypa reticularis*	Gotland	[21] *nassa*	-4.09	1.41	0.708440	0.000013	38.93	0.20	59	2094	425.1
G90	Upper Visby			*Atrypa reticularis*	Gotland	[15] *murchisoni*	-4.89	3.67			38.51	0.16	129	1345	429.3
G91	Upper Visby			*Atrypa reticularis*	Gotland	[15] *murchisoni*	-4.68	3.90	0.708377	0.000010	38.93	0.20	52	1633	429.3
G94	Slite			*Atrypa reticularis*	Gotland	[18] *flexilis*	-4.85	-0.60	0.708393	0.000009	38.77	0.19	36	1785	427.2
G97	Klinteberg			*Conchidium biloculare*	Gotland	[22] *ludensis*	-5.76	1.69	0.000007	0.708497	38.98	0.19	83	1258	424.4
G98	Klinteberg			*Hesperorthis martinssoni*	Gotland	[22] *ludensis*	-4.32	1.54	0.708457	0.000012	38.69	0.35	48	1355	424.4
EK32-2	Kaugatuma		Kaugatuma Cliff	*Delthyris magna*	Estonia	[36] *ultimus*	-6.00	-0.27							
EK34-3	Ohesaare		Ohesaare Cliff	*Delthyris magna*	Estonia	[41] *transgrediens*	-6.26	-0.79							410.2
EK36-5	Ohesaare		Ohesaare Cliff	*Microsphaeridiorhynchus* sp.	Estonia	[40] *perneri*	-5.99	-0.23			38.30	0.30		1212	408.7
EK37-6	Ohesaare		Ohesaare Cliff	*Delthyris elevata*	Estonia	[40] *perneri*	-5.11	-0.58			37.85	0.43	275	1207	409.0
EK38-7	Ohesaare		Ohesaare Cliff	*Delthyris elevata*	Estonia	[40] *perneri*	-5.50	-0.50			38.80	0.36	174	1351	409.0
EK40-9	Ohesaare		Ohesaare Cliff	*Homoeospira baylei*	Estonia	[40] *perneri*	-5.57	-0.10			38.95	0.31	104	1328	409.0
EK42-11	Ohesaare		Ohesaare Cliff	*Microsphaeridiorhynchus* sp.	Estonia	[39] *bouceki*	-5.95	-0.93			38.60	0.26	210	1215	409.0
											38.99	0.25	344	834	409.3

Appendix 2 (cont.)

Field No.	Formation	Member	Unit/Core	Species	Locality	Graptolite Biozone	$\delta^{18}O$	$\delta^{13}C$	$^{87}Sr/^{86}Sr$	2σ	Ca%	Mg%	Mn(ppm)	Sr(ppm)	Age (Ma)
EK03	Kaugatuma		Kolka 54	*Delthyris magna*	Latvia	[35] *parultimus*	-5.38	-0.52	0.708685	0.000012	38.61	0.31	48	1744	410.5
EK06	Kaugatuma		Kolka 54	*Atrypa* sp.	Latvia	[35] *parultimus*	-5.36	-0.28			38.88	0.16	82	1759	410.5
EK08	Kaugatuma		Kolka 54	*Atrypa* sp.	Latvia	[35] *parultimus*	-5.33	-0.06	0.708716	0.000012	38.92	0.18	43	1708	410.5
EK09	Kaugatuma		Kolka 54	*Isorthis* sp.	Latvia	[36] *ultimus*	-5.53	-0.22	0.708715	0.000011	39.19	0.30	105	1624	410.2
EK12	Ohesaare		Kolka 54	*Delthyris magna*	Latvia	[40] *perneri*	-6.42	-0.66			38.78	0.26	75	1832	409.0
EK14	Ohesaare		Kolka 55		Latvia	[41] *transgrediens*	-5.37	-0.22	0.708752	0.000011					408.7
EK16	Kaugatuma		Kolka 54	*Delthyris* sp.	Latvia	[40] *perneri*	-4.85	0.22	0.708709	0.000020	39.26	0.23	31	1828	409.0
EK18	Kaugatuma		Kolka 54	*Isorthis* sp.	Latvia	[37] *pridoliensis*	-5.36	-0.90			39.12	0.30	167	1764	409.9
EK22	Kaugatuma		Kolka 54	*Eospirifer* sp.	Latvia	[36] *ultimus*	-5.86	-1.10	0.708792	0.000017	39.22	0.26	168	1802	410.2
LK07	Paprieniai		Grauzai-105	*Leptaena depressa*	Lithuania	[15] *murchisoni*	-4.78	3.16	0.708322	0.000017	39.36	0.23	180	1764	429.3
LK08	Paprieniai		Grauzai-105	*Atrypina hedei*	Lithuania	[14] *centrifugus*	-3.79	4.21	0.708342	0.000012	38.87	0.20	89	1454	430.0
LK10	Paprieniai		Grauzai-105	*Atrypa reticularis*	Lithuania	[15] *murchisoni*	-3.37	3.71			39.51	0.12	71	1374	429.3
LK11	Paprieniai		Grauzai-105	*Atrypa reticularis*	Lithuania	[17] *rigidus*	-4.55	-0.82			38.76	0.30	122	1330	427.9
LK12	Paprieniai		Grauzai-105	*Atrypina barrandii*	Lithuania	[16] *riccartonensis*	-3.99	0.34	0.708356	0.000016	38.50	0.29	155	1382	428.6
LK13	Birstonas		Grauzai-105	*Atrypa* sp.	Lithuania	[17] *rigidus*	-4.39	-0.93	0.708365	0.000012	38.01	0.29	86	1320	427.9
LK14	Birstonas		Grauzai-105	*Atrypa reticularis*	Lithuania	[21] *nassa*	-4.25	-0.60	0.708381	0.000014	38.61	0.22	135	1578	425.8
LK15	Svencionys		Grauzai-105	*Atrypina hedei*	Lithuania	[12] *griestoniensis*	-5.93	1.14			39.66	0.07	27	1119	431.2
LK17	Paprieniai		Grauzai-105	*Cyrtia exporrecta*	Lithuania	[15] *murchisoni*	-3.44	2.41	0.708307	0.000013	39.38	0.18	27	1545	429.3
Lk18	Birstonas		Grauzai-105	*Cyrtia exporrecta*	Lithuania	[19] *ellesae*	-4.98	-1.05			36.76	0.39	124	1307	426.5
LK61	Riga		Vilkaviskis-129	*Plagiorhyncha analoga*	Lithuania	[15] *murchisoni*	-5.06	-1.54			35.28	0.19	114	1014	429.3
LK65	Geluva		Vilkaviskis-129	*Atrypa* sp.	Lithuania	[22] *ludensis*	-3.55	0.69			39.25	0.23	52	1828	424.4
LK66	Geluva		Vilkaviskis-129	*Atrypa reticularis*	Lithuania	[20] *lundgreni*	-3.92	1.20			39.34	0.19	37	1639	425.8
LK71	Riga		Vilkaviskis-129	*Cyrtia exporrecta*	Lithuania	[19] *ellesae*	-4.65	-0.50			39.29	0.18	10	2087	426.5
LK77	Geluva		Vilkaviskis-129	*Eospirifer radiatus*	Lithuania	[21] *nassa*	-4.02	0.48			38.71	0.18	51	1880	425.1
LK79	Riga		Vilkaviskis-129	*Atrypa reticularis*	Lithuania	[18] *flexilis*	-4.57	-0.99			38.64	0.27	55	1473	427.2
LK81	Riga		Vilkaviskis-129	*Atrypa reticularis*	Lithuania	[17] *rigidus*	-4.46	-0.81			38.47	0.26	72	1529	427.9
LK83	Svencionys		Vilkaviskis-129	*Atrypa* sp.	Lithuania	[12] *griestoniensis*	-5.80	1.21			39.64	0.10	11	1143	431.2
LK84	Riga		Vilkaviskis-129	*Cyrtia* sp.	Lithuania	[15] *murchisoni*	-4.01	-0.43			39.44	0.18	18	1594	429.3
LK23	Minija		Taurage-11		Lithuania	[35] *parultimus*	-4.83	0.19	0.708733	0.000010	39.69	0.25	52	1944	410.5
LK27	Minija		Taurage-11		Lithuania	[35] *parultimus*	-5.07	-0.08			39.65	0.25	49	1911	410.5
LK33	Dubysa		Taurage-11	*Isorthis* sp.	Lithuania	[34] *balticus/codatus*	-5.55	-0.90	0.708702	0.000009	39.30	0.25	36	1188	411.0
LK38	Jura		Taurage-11	*unidentified*	Lithuania	[38] *lochkovensis*	-5.70	-0.09	0.708713	0.000012	39.19	0.28	57	1710	409.6
LK39	Jura		Taurage-11	*Isorthis ovalis*	Lithuania	[38] *lochkovensis*	-6.34	-0.58	0.708772	0.000012	39.52	0.18	228	849	409.6
LK43	Minija		Taurage-11	*Delthyris* sp.	Lithuania	[37] *pridoliensis*	-5.50	-0.33	0.708694	0.000010	39.53	0.09	76	1521	409.9
LK47	Jura		Taurage-11	*Isorthis* sp.	Lithuania	[37] *pridoliensis*	-5.61	-0.29	0.708684	0.000015	39.20	0.26	160	1739	409.9

Appendix 2 (cont.)

Field No.	Formation	Member	Unit/Core	Species	Locality	Graptolite Biozone	$\delta^{18}O$	$\delta^{13}C$	$^{87}Sr/^{86}Sr$	2σ	Ca%	Mg%	Mn(ppm)	Sr(ppm)	Age (Ma)
N01	Skinnerbukta			*Atrypa ex gr. reticularis*	Norway	[13] *crenulata*	-12.50	1.37			39.02	0.14	77	1556	
N02	Solvik			*Protatrypa malmoeyensis*	Norway	[5] *triangulatus*	-8.03	1.24			39.29	0.11	51	826	
N03	Steinfjorden			*Eocoelia angelini*	Norway	[16] *riccartonensis*	-10.40	4.46			38.83	0.24	54	1773	
N04	Skinnerbukta			*Atrypa ex gr. reticularis*	Norway	[13] *crenulata*	-12.20	1.48			39.22	0.09	40	1426	
N05	Skinnerbukta				Norway	[16] *riccartonensis*	-10.90	2.64			38.88	0.12	57	1472	
N06	Solvik			*Howellella* sp.	Norway	[5] *triangulatus*	-11.20	0.11			38.57	0.43	115	1607	
N07	Solvik			*Eoplectodonta* sp.	Norway	[5] *triangulatus*	-11.80	0.52			38.64	0.44	100	1346	
N08	Solvik			*Protatrypa malmoeyensis*	Norway	[5] *triangulatus*	-13.70	1.02			39.05	0.13	154	1237	
N09	Malmoya				Norway	[17] *rigidus*	-20.70	4.06			39.00	0.12	63	1495	
N10	Solvik			*Protatrypa malmoeyensis*	Norway	[5] *triangulatus*	-11.60	1.13			38.90	0.14	364	1053	
N12	Steinfjorden			*Sphaerirhynchia* sp.	Norway	[21] *nassa*	-10.50	-1.38			38.33	0.19	52	1406	
N15	Steinfjorden			*Howellella cf. subinsignis*	Norway	[21] *nassa*	-6.85	-1.00			38.64	0.40	35	1819	
N16	Steinfjorden			*Costistricklandia lirata*	Norway	[21] *nassa*	-13.30	1.45			38.95	0.16	149	1596	
N19	Steinfjorden			*Howellella cf. subinsignis*	Norway	[21] *nassa*	-9.61	-0.47			38.76	0.30	30	1683	
N20	Steinfjorden			*Atrypa reticularis*	Norway	[21] *nassa*	-11.20	0.73			38.90	0.14	47	1713	
N22	Ryttaraker			*Atrypa reticularis*	Norway	[11] *crispus*	-9.01	1.18			38.88	0.22	195	1215	
PK15	Dwinogorod			*Atrypa cf. dzwinogorodensis*	Podolia	[39] *bouceki*	-5.82	0.13			39.19	0.11	69	1577	409.3
PK17	Dwinogorod			*Iridistrophia* sp. ?	Podolia	[40] *perneri*	-5.64	-0.38			38.90	0.35	119	1336	409.0
PK20	Dwinogorod			*Atrypa cf. dzwinogorodensis*	Podolia	[41] *transgrediens*	-5.74	-0.11	0.708728	0.000014	39.23	0.10	85	1457	408.7
PK22	Dwinogorod			*Atrypa cf. dzwinogorodensis*	Podolia	[40] *perneri*	-6.11	0.20	0.708720	0.000015	39.16	0.14	75	1476	409.0
PK24	Dwinogorod			*Delthyris* sp.	Podolia	[39] *bouceki*	-6.13	-0.35	0.708755	0.000018	38.99	0.25	74	1447	409.3
PK28	Rahskov			*Delthyris* sp.	Podolia	[38] *lochkovensis*	-6.38	-0.71	0.708772	0.000013	38.95	0.27	64	1147	409.6
PK33	Rahskov			*Atrypa* sp.	Podolia	[35] *parultimus*	-5.30	0.10	0.708730	0.000018	39.33	0.10	51	978	410.5
PK35	Rahskov			*Atrypa* sp.	Podolia	[35] *parultimus*	-5.91	-0.44	0.708740	0.000017	39.08	0.14	36	1417	410.5
21	Demshinie			*Atrypa ex gr. reticularis*	Podolia	[16] *riccartonensis*	-3.55	4.24			39.78	0.16	188	1411	428.6
22	Demshinie			*Atrypa ex gr. reticularis*	Podolia	[16] *riccartonensis*	-3.57	4.42	0.708371	0.000010	39.72	0.20	251	1585	428.6
23	Demshinie			*Atrypa sp.*	Podolia	[16] *riccartonensis*	-3.61	4.30			39.75	0.18	246	1391	428.6
25	Konovka			*? Septatrypa sp.*	Podolia	[23] *nilssoni*	-5.30	1.10			39.83	0.12	25	737	423.1
27	Konovka			*Atrypa ex gr. reticularis*	Podolia	[23] *nilssoni*	-4.77	1.76	0.708472	0.000012	39.60	0.29	192	1643	423.1
30	Sokol			*Atrypa ex gr. reticularis*	Podolia	[28] *hemiaversus*	-5.80	0.13			39.78	0.16	24	1372	416.0
33	Sokol			*Atrypa ex gr. reticularis*	Podolia	[28] *hemiaversus*	-5.88	-0.13	0.708568	0.000010	39.72	0.20	43	1424	416.0
36	Sokol			*Atrypa ex gr. reticularis*	Podolia	[28] *leintwardinensis*	-6.58	0.03	0.708684	0.000012	39.63	0.26	81	1060	414.8
39	Grinchuk			*Atrypa ex gr. reticularis*	Podolia	[28] *leintwardinensis*	-6.43	0.20			39.82	0.13	25	1400	414.8
40	Grinchuk			*Atrypa ex gr. reticularis*	Podolia	[28] *leintwardinensis*	-6.45	0.65	0.708698	0.000013	39.85	0.11	55	1621	414.8
CA172(4)	Jupiter	Pavillon	4	Cement	Anticosti Is.		-5.12	2.84			39.33	0.13	245	491	
CA848	Jupiter	Richardson	± 4	Cement	Anticosti Is.		-4.08	0.79			38.88	0.48	281	1395	
CA854	Jupiter	Goéland	7-8	Cement	Anticosti Is.		-4.01	1.08			39.25	0.25	208	628	

Appendix 2 (cont.)

Field No.	Formation	Member	Unit/Core	Species	Locality	Graptolite Biozone	$\delta^{18}O$	$\delta^{13}C$	$^{87}Sr/^{86}Sr$	2σ	Ca%	Mg%	Mn(ppm)	Sr(ppm)	Age (Ma)
CA916	Jupiter	Gotland	8	Cement	Anticosti Is.		-5.10	0.92			39.11	0.31	456	853	
CB05	Much Wenlock			Cement	England		-5.59	-0.59			38.65	0.97	1233	682	
CB15	Much Wenlock			Cement	England		-6.92	-1.17			39.82	0.13	395	176	
CB16	Buildwas			Cement	England		-7.37	1.46			39.45	0.39	485	1108	
CB26	Much Wenlock			Cement	England		-10.08	0.21			39.64	0.25	2794	1508	
CG14	Mulde			Cement	Gotland		-4.53	1.45			38.93	0.77	689	1337	
CG48	Slite			Cement	Gotland		-10.60	0.03			39.62	0.27	1020	91	
CG48	Slite			Cement	Gotland		-5.25	1.70			38.56	1.03	597	365	
CG60	Lower Visby			Cement	Gotland		-5.63	1.77			35.72	3.05	718	682	
CG69	Hemse			Cement	Gotland		-5.12	8.93			38.41	1.13	259	890	
CG74	Lower Visby			Cement	Gotland		-5.16	1.83			38.86	0.82	487	659	
CPK28	Rashkov			Cement	Podolia		-7.52	0.38			39.03	0.46	175	371	
MA94	Becscie	Fox Point		Matrix	Anticosti Is.		-2.95	1.55			38.38	0.65	624	1056	
MA172-4	Jupiter	Pavillon	4	Matrix	Anticosti Is.		-5.12	-0.50			38.89	0.38	673	475	
MA848	Jupiter	Richardson	± 4	Matrix	Anticosti Is.		-4.13	0.07			38.47	0.80	335	576	
MB10	Much Wenlock			Matrix	England		-7.61	1.11			39.10	0.64	728	873	
MB16	Buildwas			Matrix	England		-9.55	0.73			35.28	3.37	1257	868	
MB35				Matrix	England		-7.25	-0.83			36.01	2.85	1148	957	
MB41	Coalbrookdale			Matrix	England		-6.79	-0.91			36.18	2.73	2399	879	
MBLT1	Merrimack			Matrix	Anticosti Is.		-4.39	0.26			38.53	0.62	442	515	
MEK12	Kaugatuma		Kolka 54	Matrix	Latvia		-5.80	-0.59			33.58	3.81	913	536	
MEK16	Ohesaare		Kolka 54	Matrix	Latvia		-6.95	-1.55			30.30	5.38	889	542	
MEK8	Ohesaare		Kolka 54	Matrix	Latvia		-5.90	-0.70			31.44	4.04	859	484	
MG31	Upper Visby			Matrix	Gotland		-5.43	2.73			33.22	4.85	843	508	
MG53	Mulde			Matrix	Gotland		-4.39	2.90			37.17	2.02	623	863	
MG66	Mulde			Matrix	Gotland		-4.90	3.11			34.14	4.18	712	680	
MLK23	Minija		Taurage-11	Matrix	Lithuania		-6.30	0.34			33.53	3.14	950	679	
MLK28	Pagegia		Taurage-12	Matrix	Lithuania		-7.80	0.10			27.33	7.36	977	395	
MLK37	Minija		Taurage-13	Matrix	Lithuania		-6.58	-0.57			34.46	2.98	1008	406	
MPK22	Dwinogorod			Matrix	Podolia		-7.05	-0.67			35.02	2.81	599	409	
MPK24	Dwinogorod			Matrix	Podolia		-6.51	-1.11			28.14	6.79	692	366	

Appendix 3. Mean $\delta^{18}O$ and $\delta^{13}C$ values of Silurian brachiopods reproduced from Popp et al. (1986), Veizer et al. (1986) and Wadleigh and Veizer (1992).

Age (Ma)	$\delta^{18}O \pm 1\sigma$	$\delta^{13}C \pm 1\sigma$
410	-5.9 ± 0.7	3.2 ± 0.6
417	-4.2 ± 0.7	2.6 ± 1.4
421	-6.5 ± 0.4	0.2 ± 1.3
422	-3.8 ± 1.6	3.2 ± 1.9
423	-5.1 ± 1.2	1.6 ± 1.7
425	-4.4 ± 1.0	1.1 ± 0.9
427	-3.8 ± 0.6	3.0 ± 2.9
428	-4.2 ± 0.4	4.1 ± 2.1
431	-5.5 ± 0.4	2.1 ± 1.0
436	-4.2 ± 0.6	1.3 ± 1.6
437	-4.4 ± 0.3	1.0 ± 0.2
439	-4.6 ± 0.2	-0.2 ± 1.2

Appendix 4. Mean, standard deviation, maximum and minimum isotope values calculated for each graptolite biozone in the biocorrelation of Silurian Period.

Biozone	$n_{c,o}$	$\delta^{18}O_{mean} \pm 1\sigma$	Max.	Min.	$\delta^{13}C_{mean} \pm 1\sigma$	Max.	Min.	n_{Sr}	$^{87}Sr/^{86}Sr_{mean} \pm 1\sigma$	Max.	Min.
[41] *transgrediens*	3	-5.8 ± 0.5	-5.4	-6.3	-0.4 ± 0.4	-0.1	-0.8	2	0.708740	0.708752	0.708728
[40] *perneri*	8	-5.7 ± 0.5	-4.9	-6.4	-0.3 ± 0.3	-0.2	-0.7	2	0.708715	0.708720	0.708709
[39] *bouceki*	3	-6.0 ± 0.2	-5.8	-6.1	-0.4 ± 0.5	0.1	-0.9	1	0.708755		
[38] *lochkovensis*	3	-6.1 ± 0.4	-4.7	-6.4	-0.5 ± 0.3	0.1	-0.7	3	0.708779 ± 0.000005	0.708792	0.708772
[37] *pridoliensis*	3	-5.5 ± 0.1	-5.4	-5.6	-0.5 ± 0.3	-0.3	-0.9	2	0.708689	0.708694	0.708684
[36] *ultimus*	4	-5.8 ± 0.3	-5.5	-6.0	-0.5 ± 0.5	-0.2	-1.1	3	0.708716 ± 0.000007	0.708716	0.708715
[35] *parultimus*	7	-5.3 ± 0.3	-4.8	-5.9	-0.2 ± 0.3	0.2	-0.5	4	0.708719 ± 0.000023	0.708740	0.708685
[34] *balticus*	1	-5.6			-0.9			1	0.708752		
[33] *kozlowskii*	1	-4.6			7.4			1	0.708757		
[32] *inexpectatus*	1	-5.0			4.7						
[29] *bohemicus*	3	-4.0 ± 0.3	-3.9	-4.3	5.1 ± 0.2	5.4	4.9	3	0.708727 ± 0.000017	0.708740	0.708707
[28] *leintwardinensis*	6	-6.1 ± 0.4	-5.7	-6.6	0.2 ± 0.4	0.7	-0.4	6	0.708671 ± 0.000044	0.708728	0.708616
[27] *hemiavertus*	3	-5.7 ± 0.2	-5.4	-5.9	0.0 ± 0.1	0.1	-0.1	2	0.708563	0.708568	0.708558
[25] *scanicus*	4	-5.5 ± 0.2	-5.3	-5.7	-0.1 ± 0.3	0.3	-0.5	3	0.708538 ± 0.000016	0.708548	0.708519
[23] *nilssoni*	3	-5.0 ± 0.3	-4.8	-5.3	-1.4 ± 0.4	1.8	1.1	2	0.708454	0.708472	0.708435
[22] *ludensis*	26	-5.1 ± 0.7	-3.6	-6.6	1.2 ± 0.7	3.0	-0.1	8	0.708464 ± 0.000020	0.708497	0.708437
[21] *nassa*	24	-4.3 ± 0.7	-3.5	-5.7	1.4 ± 0.8	2.4	-0.3	13	0.708433 ± 0.000020	0.708468	0.708414
[20] *lundgreni*	10	-4.6 ± 0.6	-3.8	-5.5	0.4 ± 1.2	2.5	-0.8	5	0.708440 ± 0.000035	0.708488	0.708381
[19] *ellesae*	6	-4.6 ± 0.3	-4.2	-5.0	-0.6 ± 0.3	0.2	-1.1	4	0.708354 ± 0.000016	0.708378	0.708342

Appendix 4. (cont.)

Biozone	$n_{c,o}$	$\delta^{18}O_{mean} \pm 1\sigma$	Max.	Min.	$\delta^{13}C_{mean} \pm 1\sigma$	Max.	Min.	n_{Sr}	$^{87}Sr/^{86}Sr_{mean} \pm 1\sigma$	Max.	Min.
[18] *flexilis*	2	-4.7	-4.6	-4.9	-0.8	-0.6	-1.0	1	0.708393		
[17] *rigidus*	3	-4.5 ± 0.1	-4.4	-4.6	-0.9 ± 0.1	-0.8	-0.9	2	0.708368	0.708371	0.708365
[16] *riccartonensis*	11	-4.4 ± 0.7	-3.6	-5.7	4.0 ± 1.3	5.3	0.3	6	0.708369 ± 0.000022	0.708397	0.708334
[15] *murchisoni*	12	-4.6 ± 0.8	-3.4	-6.3	2.9 ± 2.1	6.4	-1.5	7	0.708339 ± 0.000020	0.708377	0.708307
[14] *centrifugus*	2	-4.6	-3.8	-5.4	3.1	4.2	2.0	2	0.708367	0.708392	0.708342
[13] *crenulata*	12	-5.6 ± 0.3	-5.1	-6.1	1.4 ± 0.2	1.6	1.0	4	0.708387 ± 0.000043	0.708439	0.708342
[12] *griestoniensis*	9	-5.3 ± 0.6	-3.7	-5.9	1.0 ± 0.8	2.1	-0.2	4	0.708261 ± 0.000053	0.708321	0.708210
[11] *crispus*	7	-4.9 ± 0.6	-4.0	-6.0	1.0 ± 0.9	2.9	0.4	5	0.708182 ± 0.000031	0.708207	0.708128
[10] *turriculatus*	3	-4.6 ± 0.2	-4.4	-4.8	1.3 ± 0.2	1.6	1.1	1	0.708167		
[9] *sedgwickii*	4	-4.4 ± 0.2	-4.1	-4.6	1.4 ± 0.7	2.1	0.6	3	0.708143 ± 0.000031	0.708179	0.708124
[8] *convolutus*	8	-5.3 ± 0.1	-5.1	-5.5	1.1 ± 0.4	1.7	0.7	5	0.708159 ± 0.000008	0.708170	0.708151
[7] *leptotheca*	3	-5.0 ± 0.2	-4.7	-5.2	1.3 ± 0.2	1.5	1.1	2	0.708120	0.708161	0.708079
[5] *triangulatus*	6	-4.5 ± 0.5	-3.8	-5.1	0.9 ± 0.4	1.4	0.5	6	0.708077 ± 0.000023	0.708108	0.708052
[4] *cyphus*	2	-5.1	-4.9	-5.4	0.5	0.9	0.1	2	0.708065	0.708080	0.708050
[2] *avatus*	2	-3.7	-3.4	-3.9	0.9	1.8	0.0				
[1] *acuminatus*	2	-2.9	-2.7	-3.2	1.4	1.5	1.3	2	0.707941	0.707951	0.707930